EPIDEMIOLOGICAL EVIDENCE OF COVID-19 AND POTENTIAL STRATEGIES FOR THE CONSTRUCTION INDUSTRY IN HONG KONG

YUAN ZIYUE

PhD

The Hong Kong Polytechnic University

2023

The Hong Kong Polytechnic University
Department of Civil and Environmental Engineering

Epidemiological Evidence of COVID-19 and Potential Strategies for the Construction Industry in Hong Kong

YUAN Ziyue

A thesis submitted in partial fulfilment of the requirements
for the degree of
Doctor of Philosophy

November 2022

CERTIFICATE OF ORIGINALITY

I hereby declare that this thesis is my own work and that, to the best of my knowledge and belief, it reproduces no material previously published or written, nor material that has been accepted for the award of any other degree or diploma, except where due acknowledgement has been made in the text.

YUAN Ziyue

Abstract

The first coronavirus disease 2019 (COVID-19) outbreak was reported in December 2019, developing into a global pandemic by March 2020 and producing shutdowns of business and industry across the world. In comparison with other industries, the disease produced particularly acute health crises and economic losses in the construction industry. This high vulnerability to COVID-19 was due in part to the unavoidable close proximity required during manual labour. In an attempt to mitigate these effects, the construction industry followed macro-level non-pharmaceutical interventions (NPIs), which were established based on transmission patterns at the city level. Since the pandemic, most recent research regarding the construction industry has investigated the effects and challenges of COVID-19 and the responses taken to address them. There is, however, still limited discussion of the specific and major transmission patterns within the construction industry and how a knowledge of such patterns can help decision-makers to align targeted NPIs proactively in order to mitigate such transmission.

In this dissertation, epidemiological evidence has been gathered in order to produce a comprehensive understanding of COVID-19 transmission within the construction industry, which has then been used to design targeted NPI response strategies. Primary data from confirmed cases and case clusters of COVID-19 in the construction industry in Hong Kong (including demographic information, epidemiological information regarding symptom onset date and date reported, and contact tracing data) are used. All cases were confirmed by the government and identified by the local authority of disease surveillance (Centre for Health Protection). Several epidemiological methods were used, including compartment models, spatiotemporal analysis, and K-shell decomposition analysis. There are four objectives of this study: 1) to explore the transmission dynamics of COVID-19 and the effectiveness of macro-level NPIs in Hong Kong; 2) to uncover the transmission patterns of COVID-19 in the construction industry in Hong Kong; 3) to estimate the effectiveness of contact restrictions and vaccinations for construction workers and their close contacts on a construction site; and 4) to investigate the feasibility of *a priori* identification of potential super-spreaders in a construction project. The present study contributes to the ongoing efforts to control and prevent the spread of COVID-19 in the construction industry in Hong Kong.

In this study, the transmission dynamics of COVID-19 and the effectiveness of macro-level NPIs (such as restrictions on gathering sizes and quarantine policies) are explored based on a modified Susceptible-Exposed-Infectious-Hospitalized-Recovered (SEIHR) model with nine-month data

from 2020 in Hong Kong. These phenomena indicate "pandemic fatigue," as demonstrated by lower and lower adherence to macro-level NPIs among people in Hong Kong. At the same time, from an epidemiological standpoint, the possibility of backward bifurcation makes it imperative for the construction industry to design targeted strategies for adapting to the post-pandemic environment. In order to identify the specific transmission pattern of COVID-19, a spatiotemporal analysis was used with data from five COVID-19 case clusters associated with construction sites in Hong Kong. In these cases, COVID-19 transmission diffused spatially from the workplace to the residential neighbourhoods in which the infected construction workers live, but not to the community surrounding the infected construction sites. Temporally, these outbreaks demonstrated three to five generations in 25.8 days. Several super-spreading events were identified, both at the workplace and within households. Around 18% of seed cases (those who can infect others) infected 79.6% of offspring cases (those who can be infected). It is estimated that, if super-spreaders were restricted before they infect others, it would be possible to eliminate at least half of the offspring cases.

Based on the transmission pattern found above, the feasibility and effectiveness of several response strategies, including contact restrictions, vaccinations, and *a priori* identification of potential super-spreaders, are discussed. A dual-community compartment model is developed to describe the transmission patterns of COVID-19 among construction workers and their close contacts, and to evaluate the effectiveness of contact restrictions. The best-performing scenario is found to be one in which the movements of the close contacts exposed to COVID-19 by infected construction workers are restricted. Such restrictions reduce the total attack rate (TAR) with 25% absolute efficiency (AE) and decrease the duration of an outbreak (DO) in the whole population by 1.8 days, according to the model. In addition to contact restrictions, the vaccination of all construction workers along with at least 67% of their close contacts can extinguish an ongoing wave. In order to identify potential super-spreaders, this study develops a network-based computational framework based on K-shell decomposition approach with the input of the topological interaction network of all project participants. The feasibility of the developed framework is evaluated by three numerical cases: one sample case with a hierarchical structure with an average accuracy of 98.45%, one sample case with a matrix structure with an average accuracy of 92.25%, and an empirical case related to a COVID-19 outbreak in a construction project in Hong Kong with an accuracy of over 80.13%. All potential super-spreaders, especially if they are employed by the main contractor, are suggested to take Rapid Antigen Tests (RATs) regularly. If all potential super-spreaders are detected through regular RATs and all potential

secondary cases were detected by contract tracing, up to 82.35% of infected cases could be prevented.

The main contribution of this study is threefold: (1) a comprehensive investigation of COVID-19 in the construction industry; (2) a more thorough understanding of the transmission dynamics of COVID-19 and super-spreading patterns; and (3) estimating the effectiveness of NPIs and vaccinations. The main epidemiological evidence includes the high infection risks demonstrated both at the workplace and in households, and the existence of super-spreaders. The proposed response strategies include contact restrictions between targeted groups (e.g., exposed individuals and their close contacts), vaccination plans, and the *priori* identification of potential super-spreaders.

Publications Arising from the Thesis

1. **Yuan, Z.**, Ye, Z., Zhang, Y. and Hsu, S. C.* (2023). Identifying potential superspreaders of airborne infectious diseases in construction projects. under review.

2. **Yuan, Z.**, Zhao, S., Hsu, S. C.* and Cheung, C. M. (2023). Uncovering Construction Site–Specific Transmission Patterns of COVID-19: A Spatiotemporal Connectivity Analysis in Hong Kong. *Journal of Management in Engineering*, 39(1), 04022067. DOI: 10.1061/(ASCE)ME.1943-5479.0001100.

3. **Yuan, Z.**, Musa, S. S., Hsu, S. C.*, Cheung, C. M., and He, D. (2022). Post pandemic fatigue: what are effective strategies?. *Scientific reports*, 12(1), 1-15. https://doi.org/10.1038/s41598-022-13597-0.

4. **Yuan, Z.**, Hsu, S. C.*, Cheung, C., and Asghari, V. (2022). Effectiveness of Interventions for Controlling COVID-19 Transmission between Construction Workers and Their Close Contacts. *Journal of Management in Engineering*, 38(3). DOI: 10.1061/(ASCE)ME.1943-5479.0001033.

Acknowledgements

I would like to express my deepest appreciation to my chief supervisor Dr. Mark Shu-Chien Hsu. His tremendous mentorship, constant guidelines and valuable suggestions have made my doctoral study a thoughtful and rewarding journey.

I am grateful to all members of my confirmation examination members, Prof. Yuhong Wang and Dr. Wei Ma from The Hong Kong Polytechnic University, for their insightful suggestions. Also, I would like to send my sincere appreciation to my dissertation committee members: Dr Zhen Leng from The Hong Kong Polytechnic University, Dr. Pin-Chao Liao from Tsinghua University and Dr. Xueqing Zhang from Hong Kong University of Science and Technology. I appreciate their inspiring suggestions for my study and future research.

I am deeply thankful to all co-authors in the publications arising from this study. I gratefully acknowledge Dr. Daihai He, Dr. Salihu Sabiu Musa and Dr. Shi Zhao for their patience and insightful comments. I own my appreciation to Mr. Zhongnan Ye, Dr. Clara Cheung and Dr. Vahid Asghari for their guidelines and encouragements. I am also really grateful to Mr. Yi Zhang from China State Construction Engineering (Hong Kong) Limited for his valuable suggestions and supports.

I would like to express my deepest appreciation to all colleagues and friends from Department of Civil and Environmental Engineering, Department of Building and Real Estate, Department of Logistic and Maritime Studies, and Department of Chinese and Bilingual Studies in The Hong Kong Polytechnic University. Also, I hereby intend to acknowledge the expert and encouragement received from Prof. Hai Yang from The Hong Kong University of Science and Technology, Dr. Weiya Chen, Prof. Yong Peng, and Prof. Hui Liu from Central South University.

Finally, I would like to express my love and deepest gratitude to my parents, Ms. Yajun Fan and Mr. Chaosong Yuan, my little sister Miss Moxuan Yuan, and grandparents, Ms Hongyan Wang and Mr. Mingliang Fan, for their love and unconditional supports.

Contents

Certificate of Originality ii

Abstract iii

Publications Arising from the Thesis vi

Acknowledgements vii

List of Figures xi

List of Tables xiv

List of Abbreviations xv

List of Symbols xvi

1 Introduction 1
- 1.1 Research Background . . . 1
- 1.2 Research Scope and Problem Statement . . . 2
- 1.3 Research Aims and Objectives . . . 3
- 1.4 Dissertation outline . . . 4

2 Literature Review 6
- 2.1 Studies relevant to COVID-19 . . . 6
  - 2.1.1 Epidemiological evidence of COVID-19 transmission . . . 6
  - 2.1.2 Response strategies to COVID-19 . . . 7
- 2.2 Studies relevant to COVID-19 in different industries . . . 8
- 2.3 Studies relevant to COVID-19 in the construction industry . . . 10
  - 2.3.1 Effects of COVID-19 on the construction industry . . . 10
  - 2.3.2 Response strategies to COVID-19 in the construction industry . . . 11
- 2.4 Summary and Research Gap . . . 12

3 Research Methodology 14
- 3.1 Transmission dynamics of COVID-19 . . . 14
  - 3.1.1 Compartment-based epidemic models . . . 14
  - 3.1.2 Network-based epidemic models . . . 16
- 3.2 Transmission patterns of COVID-19 . . . 18
  - 3.2.1 Retrospective and prospective cohort studies . . . 18
  - 3.2.2 Spatiotemporal connectivity analysis . . . 19
- 3.3 Super-spreading event identification . . . 19
  - 3.3.1 Spreading on a network-based epidemic model . . . 19
  - 3.3.2 K-shell decomposition analysis . . . 20

4 Transmission Dynamics of COVID-19 in Hong Kong 22
- 4.1 Introduction . . . 22
- 4.2 Materials and Methods . . . 23
  - 4.2.1 Data Collection . . . 23

4.2.2 Mathematical Model . . . 25
4.2.2.1 Model Formulation . . . 25
4.2.3 Mathematical Analysis . . . 27
4.2.3.1 Disease-free Equilibrium (DFE) . . . 28
4.2.3.2 Endemic Equilibrium (EE) . . . 30
4.2.3.3 Backward Bifurcation Analysis . . . 32
4.2.4 Fitting Analysis . . . 35
4.3 Results . . . 35
4.3.1 Modelling . . . 35
4.3.2 Mathematical Analysis . . . 36
4.3.2.1 Steady States . . . 36
4.3.2.2 Sensitivity Analysis . . . 37
4.3.3 Fitting Results . . . 38
4.3.3.1 Effective Contact Ratio . . . 42
4.4 Discussion . . . 44
4.5 Chapter Summary . . . 46

5 Transmission Patterns of COVID-19 in the Construction Industry in Hong Kong 47
5.1 Introduction . . . 47
5.2 Methods . . . 48
5.2.1 Data source and collection . . . 48
5.2.2 Transmission patterns . . . 49
5.2.3 Distribution of offspring cases . . . 53
5.3 Results and discussions . . . 57
5.4 Chapter Summary . . . 60
5.4.1 Conclusions and Implications . . . 60
5.4.2 Limitations and Directions for Future Research . . . 61

6 Non-pharmaceutical Interventions and Vaccine Program on Construction Sites 63
6.1 Introduction . . . 63
6.2 Methods . . . 65
6.2.1 Model Structure . . . 65
6.2.2 Basic Reproduction Number . . . 68
6.3 Sensitivity Analysis . . . 71
6.3.1 Global Sensitivity Analysis . . . 71
6.3.2 Local Sensitivity Analysis . . . 71
6.4 Effectiveness of Interventions . . . 72
6.4.1 Non-pharmaceutical Interventions (NPIs) . . . 72
6.4.1.1 Scenario Design . . . 75
6.4.2 Vaccination . . . 77
6.5 Results and discussion . . . 77
6.5.1 Sensitivity Analysis . . . 77
6.5.2 Effectiveness of NPIs . . . 79
6.5.3 Effectiveness of Vaccination . . . 80
6.6 Chapter Summary . . . 80
6.6.1 Conclusions and Implications . . . 81

6.6.2 Limitations and Directions for Future Research 82

7 A Priori Identification of Potential Superspreaders in Construction Projects 84
7.1 Introduction 84
7.2 Literature Review 85
7.3 Methods 86
7.3.1 K-shell decomposition method 86
7.3.2 Stochastic models in epidemiology 89
7.3.3 Performance measures 92
7.4 Case study of COVID-19 93
7.4.1 Numerical Cases modeled in a Hierarchical Network and Matrix Network 93
7.4.2 Empirical case of a construction project in Hong Kong 96
7.4.2.1 Data Description 96
7.4.2.2 Reproduction of the Interaction network 96
7.5 Results and discussions 98
7.5.1 Two numerical cases with sample networks 98
7.5.2 Empirical case of a construction project in Hong Kong 100
7.6 Chapter summary 107
7.6.1 Conclusions and Implications 107
7.6.2 Limitations and Directions for Future Research 108

8 Conclusion 109
8.1 Summary of major findings 109
8.2 Limitations and directions for future research 111

Bibliography 113

Supplementary Information 146
SI.1 Supplementary information in Chapter 4 146
SI.1.1 The Proof of the Existence of EE 146
SI.1.2 The initial variables and estimated parameters for four phases . . 148
SI.2 Supplementary information in Chapter 6 149
SI.3 Supplementary information in Chapter 7 150

List of Figures

1.1 Organization of studies in this dissertation 5

3.1 Research Methodology. 14
3.2 A non-directed network G of size $N = 6$ (with nodes $v_i \in V, 1 \leq i \leq 6$), consisting of $e_{\{v_1,v_2\}}$, $e_{\{v_1,v_3\}}$, $e_{\{v_1,v_5\}}$, $e_{\{v_3,v_5\}}$, $e_{\{v_4,v_5\}}$, and $e_{\{v_5,v_6\}}$. 17

4.1 Susceptible-Exposed-Infectious-Hospitalised-Recovered (SEIHR) Model. . . . 25
4.2 The partial rank correlation coefficient (PRCC) of the basic reproduction number $\mathcal{R}_0$ and infection attack rate with respect to model parameters. 39
4.3 Global sensitivity analysis. Inputs: (a) transmission rate (β_1 and β_2), (b)effective contact ratio (a_1-a_6), (c) transition rate [θ_1-θ_5 and $\theta_6 = (1-\theta_2-\theta_3)$], (d) recovery rate (γ_1-γ_5), (e) hospitalized rate (ϵ_1-ϵ_3), and (f) population size (S and N_q). Output: exposed individuals with outside movement (E_m), symptomatic infectious individuals (I_m) and asymptomatic infectious individuals (I_a). 40
4.4 Comparison between policy stringency index scores [82] and daily new cases [63] from 24th January to 4th December 2020. Yellow, orange, blue and green lines represent the periods from January 24 to March 24, from May 25 to July 19, from July 20 to 29, and from July 30 to October 30 respectively. Blue points show each inflection point of the grey line (policy stringency index). 42
4.5 Fitting results: (a) Jan. 24 to Mar. 24, (b) Mar. 25 to Jul. 19, (c) Jul. 20 to Jul. 29, and (d) Jul. 30 to Oct. 31. 42
4.6 Comparison between policy stringency index scores and effective contact ratios from Jan. 25 to Oct. 31 in 2020: (a) a_1 effective contact ratio between E_m and S, (b) a_2 effective contact ratio between I_m and S, (c) a_3 effective contact ratio between I_a and S, (d) a_4 effective contact ratio between E_m and N_q, (e) a_5 effective contact ratio between I_m and N_q and (f) comparison between domestic Mass Transit Railway (MTR) passengers flow and effective contact ratios [213]. 43

5.1 (a) Hypothesis transmission network based on the hypothesis information in Fig.1b: the arrow means the transmission relationship from an infector (i.e., seed case) to an infectee (i.e., offspring case). The transmission chain: case 0 is the primary case which infected 6 cases (i.e., case 1-6); case 6 infected 2 cases (i.e., case 7-8); and case 8 infected case 9. If the number of secondary cases is larger, the node is with deeper color and a larger size. If the weight of the edge (i.e., the transmission possibility under the setting) is with deeper color and becomes wider. (b)Collected data with hypothesis information for the transmission network in Fig.1a: "W"="Workplace", "RA"="Residential address", and "PP"="Public place". Notes: Case 6 is the only confirmed case that visited "PP 01" and "RA 08" and "RA 09" are close to each other. 49
5.2 (a) Transmission network: nodes with deeper color and bigger size have higher degrees of transmission (i.e., the number of secondary cases) and edges with deeper color have higher weights (i.e., the possibility of transmission); (b) Daily number of reported cases since the symptom onset date of the first case in each cluster. 51

5.3 (a) The number of offspring cases in each generation; Attack rate caused by workplace, household, and social activities in each cluster: (b) cluster at LOHAS Park/Kai Tak; (c) the first cluster at the TKO-LT Tunnel; (d) the second cluster at the TKO-LT Tunnel; (e) cluster at the Central Kowloon Route (Central Tunnel); and (f) cluster at Hong Kong International Airport Third Runway. 54
5.4 Spatial distribution of each cluster: (a) cluster at LOHAS Park/Kai Tak (orange points); (b) the first cluster at the TKO-LT Tunnel (black points); (c) the second cluster at the TKO-LT Tunnel (blue points); (d) cluster at the Central Kowloon Route (Central Tunnel) (yellow points); (e) cluster at Hong Kong International Airport Third Runway (green points). 55
5.5 Centrality Indices of each cluster: (a) Betweenness Centrality of cluster at LOHAS Park/Kai Tak; (b) Closeness Centrality of cluster at LOHAS Park/Kai Tak; (c) Betweenness Centrality of the first cluster at the TKO-LT Tunnel; (d) Closeness Centrality of the first cluster at the TKO-LT Tunnel; (e) Betweenness Centrality of the second cluster at the TKO-LT Tunnel; (f) Closeness Centrality of the second cluster at the TKO-LT Tunnel; (g) Betweenness Centrality of cluster at the Central Kowloon Route (Central Tunnel); (h) Closeness Centrality of cluster at the Central Kowloon Route (Central Tunnel); (i) Betweenness Centrality of cluster at Hong Kong International Airport Third Runway; (g) Closeness Centrality of cluster at Hong Kong International Airport Third Runway; (k) Betweenness Centrality of all nodes; and (l) Closeness Centrality of all nodes. . 56

6.1 Diagram of the dual-community model in Eq. (6.1) 68
6.2 Sobol indices of (a) transmission rate β_1 and β_2; and (b) transition rate between construction site and its connected community. 72
6.3 Sobol indices of (a) effective contact ratio a_{11} - a_{16}; and (b) effective contact ratio a_{21} - a_{26}. 73
6.4 Sensitivity analysis of (a) transmission rate β; (b) effective contact ratio a_{11} to a_{16}; (c) effective contact ratio a_{21} to a_{26}; (d) transition rate θ_1; (e) transition rate θ_2; (f) transition rate θ_3; and (g) transition rate θ_4 ranging from 0 to 1. 74
6.5 Scenario 1: baseline of (a) SEIARP model; (b) within the community; (c) on the construction site; and (d) attack rate. 74
6.6 Duration of Outbreak. 75
6.7 Vaccination effectiveness (a) when only construction workers vaccinated; (b) when only close contacts vaccinated; (c) when 100% construction workers vaccinated; (d) when 70% construction workers vaccinated; (e) when 50% construction workers vaccinated; and (f) when 30% construction workers vaccinated. 78

7.1 Workflow of the proposed network-based computational framework: (a) K-shell decomposition analysis; and (b) epidemic simulation. 87
7.2 The transition of epidemic spreading in (a) a SIR system of each node v_i; (b) an SEIR system of each node v_i; and (c) a SIRV system of each node v_i. 90
7.3 Organization chart view of a construction project: (a) hierarchical structure and (b) matrix structure. 95
7.4 Distribution of offspring cases generated by each seed case. 96
7.5 Interaction network including 315 participants from 12 subcontractors. Thick arrows indicate interactions across groups. Nodes with the same colour represent people from the same group. Nodes with bigger sizes have a higher degree. "GXnode$Y" represents the No. Y case in group GX. 98

7.6 Results of K-shell decomposition methods in the hierarchical network by (a) conventional K-shell decomposition analysis; (b) weighted K-shell decomposition analysis; and (c) generalized K-shell decomposition analysis. 101
7.7 Results of K-shell decomposition methods in the Matrix network by (a) conventional K-shell decomposition analysis; (b) weighted K-shell decomposition analysis; and (c) generalized K-shell decomposition analysis. 102
7.8 Cumulative number of infected cases on the 4th day predicted by stochastic epidemic models in the hierarchical network where nodes are analysed with: (a) conventional K-shell decomposition; (b) weighted K-shell decomposition; and (c) generalized K-shell decomposition. 103
7.9 Cumulative number of infected cases on the 4th day predicted by stochastic epidemic models in the matrix network where nodes are analysed with: (a) conventional K-shell decomposition; (b) weighted K-shell decomposition; and (c) generalized K-shell decomposition. 103
7.10 Cumulative number of infected cases on the 4th day predicted by stochastic epidemic models in the interaction network of the construction project in Hong Kong where nodes are analyzed with (a) conventional K-shell decomposition analysis; (b) weighted K-shell decomposition analysis; and (c) generalized K-shell decomposition analysis. 106

List of Tables

4.1 Local Situation of COVID-19 in Hong Kong(as of April 13, 2021) 24
4.2 Notation of a modified SEIHR model 27
4.3 Number of possible positive real roots of Eq. (4.21) 34
4.4 Interpretation of the basic reproduction number R_0 37
4.5 Parameter descriptions and values 41

5.1 Basic properties of each network 52
5.2 Transmission characteristics of each cluster 59

6.1 Notation of a dual-community model 67
6.2 Interpretation of the basic reproduction number $\mathcal{R}_0$ 70
6.3 Scenario 76

7.1 Three types of K-shell decomposition methods 89
7.2 Notation of epidemic models 91
7.3 Assumptions owing to different types of interactions 94
7.4 Demographic information of all COVID-19 confirmed cases 97
7.5 Information of the interaction network containing people from the 12 selected groups 99
7.6 Performance of the proposed network-based computational framework for identifying superspreaders 99
7.7 Predictive performance of K-shell methods and Stochastic Epidemic Models as compared to empirical results 104

SI.1.1 The initial variables and estimated parameters for four phases (Phase 1: 24th Jan.-24th Mar., Phase 2: 25th May.-19th Jul., Phase 3: 20th Jul.-29th Jul. and Phase 4: 30th Jul.-31st Oct.). 148
SI.2.1 Scenario Performance 149
SI.3.1 Description of actual superspreaders in the empirical case 150

List of Abbreviations

COVID-19	Coronavirus Disease 2019
SARS-CoV-2	Severe Acute Respiratory Syndrome Coronavirus 2
MERS	Middle East respiratory syndrome
SARS	severe acute respiratory syndrome coronavirus
DFE	Disease-free Equilibrium
EE	Endemic Equilibrium
FB	Forward Bifurcation
BB	Backward Bifurcation
NPI	Non-pharmaceutical Intervention/Non-pharmacological Intervention
SSE	Super-spreading event
OxCGRT	Oxford COVID-19 Government Response Tracker
SIR	Susceptible-Infectious-Recovered
SEIR	Susceptible-Exposed-Infectious-Recovered
SEIHR	Susceptible-Exposed-Infectious-Hospitalized-Recovered
SEI/AHR-P	Susceptible-Exposed-Infectious/Asymptomatic-Hospitalized-Recovered-Pathogen
SEIAHR	Susceptible-Exposed-Infectious/Asymptomatic-Hospitalized-Recovered
AR	Attack Rate
TAR	Total Attack Rate
DO	Duration of an outbreak
AE	Absolute Effectiveness
RE	Relative Effectiveness
WHO	World Health Organization

List of Symbols

$\mathcal{R}_0$	basic reproduction/reproductive number
R_t	effective reproduction/reproductive number
β	the transmission rate between S and I
$1/\gamma$	the average duration of incubation period
λ	the force of infection
S	the number of susceptible individuals
E	the number of exposed individuals
I	the number of infectious individuals
R	the number of recovered individuals
V	the number of vaccinated individuals with a life-long immunity
N	the total number of individuals
N_q	the number of quarantined inbound travellers
E_m	the number of exposed individuals with outside movement
E_q	the number of quarantined exposed individuals
I_a	the number of asymptomatic infectious individuals
I_m	the number of symptomatic infectious individuals with outside movement
I_q	the number of quarantined symptomatic infectious individuals
H_a	the number of hospitalized asymptomatic infectious individuals
H_s	the number of hospitalized symptomatic infectious individuals
R	the number of recovered individuals
m_N	the number of inbound travellers without quarantine
m_{N_q}	the number of quarantined inbound travellers
π	the number of new natural births
μ_H	the number of inbound travellers without quarantine
β_1	transmission rate contributed by the disease among S (in Chapter 4)
β_2	transmission rate contributed by the disease among N_q (in Chapter 4)
a_1	the effective contact ratio between E_m and S
a_2	the effective contact ratio between I_a and S

a_3	the effective contact ratio between I_m and S
a_4	the effective contact ratio between E_m and N_q
a_5	the effective contact ratio between I_a and N_q
a_6	the effective contact ratio between I_m and N_q
θ_1	The rate of susceptible individuals who self-quarantined according to the strict policy (in Chapter 4).
θ_2	The rate of quarantined individuals who remain susceptible after 14-day quarantine observation period and return back to the susceptible group (in Chapter 4).
θ_3	The rate of quarantined individuals who have been infected during the quarantine period and show the symptoms after the quarantine (in Chapter 4).
θ_4	The rate of exposed individual with outside movement who has been quarantined (in Chapter 4).
θ_5	The rate of infectious individual with outside movement who has been quarantined (in Chapter 4).
σ_1	the transition rate from exposed to asymptomatic infectious status (in Chapter 4)
σ_2	the transition rate from exposed to symptomatic infectious status (in Chapter 4)
σ_3	the transition rate from exposed to symptomatic infectious status under quarantine (in Chapter 4)
ϵ_1	the hospitalization rate of asymptomatic infectious individuals (in Chapter 4)
ϵ_2	the hospitalization rate of symptomatic infectious individuals (in Chapter 4)
ϵ_3	the hospitalization rate of quarantined symptomatic infectious individuals (in Chapter 4)
γ_1	the rate of asymptomatic infectious individuals who recovered without hospitalization (in Chapter 4)
γ_2	the rate of symptomatic infectious individuals who recovered without hospitalization (in Chapter 4)

γ_3	the rate of quarantined symptomatic infectious individuals who recovered without hospitalization (in Chapter 4)
γ_4	the rate of symptomatic infectious individuals who recovered after treatment in the hospital (in Chapter 4)
γ_5	the rate of asymptomatic infectious individuals who recovered after treatment in the hospital (in Chapter 4)
δ_m	the rate of death among symptomatic infectious individuals with outside movement I_m (in Chapter 4)
δ_q	the rate of death among quarantined symptomatic infectious individuals I_q (in Chapter 4)
δ_h	the rate of death among hospitalized symptomatic infectious individuals H_s (in Chapter 4)
ξ	the rate of reinfection based on no lifelong immunity
S_{hi}	the number of susceptible individuals on the construction site
E_{hi}	the number of exposed individuals on the construction site
A_{hi}	the number of asymptomatic infectious individuals on the construction site
I_{hi}	the number of symptomatic infectious individuals on the construction site
P_a	the pathogen concentration inhaled/infected per person on the construction site
S_{ho}	the number of susceptible individuals in its connected community
E_{ho}	the number of exposed individuals in its connected community
A_{ho}	the number of asymptomatic infectious individuals in its connected community
I_{ho}	the number of symptomatic infectious individuals in its connected community
H_h	the number of hospitalized infectious individuals
R_h	the number of recovered individuals
θ_1	the transition rate from S_{ho} to S_{hi} (in Chapter 6)
θ_2	the transition rate from S_{hi} to S_{ho} (in Chapter 6)
θ_3	the transition rate from E_{hi} to E_{ho} (in Chapter 6)
θ_4	the transition rate from E_{ho} to E_{hi} (in Chapter 6)

σ_1	the transition rate from E_{hi} to I_{hi} (in Chapter 6)
σ_2	the transition rate from E_{ho} to I_{ho} (in Chapter 6)
σ_3	the transition rate from E_{hi} to A_{hi} (in Chapter 6)
σ_4	the transition rate from E_{ho} to A_{ho} (in Chapter 6)
ϵ_1	the hospitalized rate of I_{hi} (in Chapter 6)
ϵ_2	the hospitalized rate of I_{ho} (in Chapter 6)
ϵ_3	the hospitalized rate of A_{hi} (in Chapter 6)
ϵ_4	the hospitalized rate of A_{ho} (in Chapter 6)
γ	the recovery rate of hospitalized individuals H_h
δ_i	the rate of death among symptomatic infectious individuals
δ_h	the rate of death among hospitalized population (in Chapter 6)
δ_r	the rate of death among recovered individuals
η_1	the rate of virus spread to environment by E_{hi}
η_2	the rate of virus spread to environment by I_{hi}
η_3	the rate of virus spread to environment by A_{hi}
μ	natural death rate of pathogens in the environment
β_1	the transmission rate between human to human in its connected community (in Chapter 6)
β_2	the transmission rate between human to human on the construction site (in Chapter 6)
β_3	the transmission rate between pathogen to human on the construction site (in Chapter 6)
a_{11}	effective contact ratio between E_{ho} and S_{ho}
a_{12}	effective contact ratio between I_{ho} and S_{ho}
a_{13}	effective contact ratio between A_{ho} and S_{ho}
a_{14}	effective contact ratio between E_{hi} and S_{ho}
a_{15}	effective contact ratio between I_{hi} and S_{ho}
a_{16}	effective contact ratio between A_{hi} and S_{ho}
a_{21}	effective contact ratio between E_{ho} and S_{hi}
a_{22}	effective contact ratio between I_{ho} and S_{hi}
a_{23}	effective contact ratio between A_{ho} and S_{hi}
a_{24}	effective contact ratio between E_{hi} and S_{hi}
a_{25}	effective contact ratio between I_{hi} and S_{hi}

a_{26}	effective contact ratio between A_{hi} and S_{hi}
S_i	When the node v_i is susceptible, S_i equals to 1; otherwise, it is 0.
E_i	When the node v_i is exposed, E_i equals to 1; otherwise, it is 0.
I_i	When the node v_i is infectious, I_i equals to 1; otherwise, it is 0.
R_i	When the node v_i is recovered, R_i equals to 1; otherwise, it is 0.
V_i	When the node v_i gets a life-long immunity, V_i equals to 1; otherwise, it is 0.
b_i^t	the value of the state of node v_i at time t, $b_i^t \in \mathbb{D}$ ($\mathbb{D} = \{\mathbb{S}, \mathbb{E}, \mathbb{I}, \mathbb{R}, \mathbb{V}\}$)
$1/\sigma_i$	the duration of incubation period of node v_i
$1/\gamma_i$	the duration of infection period of node v_i
$1/\xi_i$	the duration of immunity period of node v_i
$1/\omega_i$	the duration of vaccination period of node v_i
N_{v_i}	the set of close contacts of v_i whose state is infectious
$p_{\{u,v_i\}}$	transmission probability p_e between an infected node u and node v_i

Chapter 1

Introduction

1.1 Research Background

Since the first outbreak of coronavirus disease 2019 (COVID-19) was reported in December 2019, and a global pandemic declared in March 2020 [163], the disease has caused health crises around the world. By August 2022, the total number of COVID-19 cases worldwide exceeded 591.68 million, resulting in more than 6.44 million deaths [164]. It soon came to be understood that COVID-19 transmits via droplets and small airborne particles through close face-to-face contact with pre-symptomatic, asymptomatic, or symptomatic infectious individuals [237]. Governments struggled with instituting and enforcing various non-pharmaceutical intervention (NPI) measures (mask mandates [57], travel restrictions [202], quarantine orders [127], and contact tracing [50]) to slow down the spread of the virus. In addition to NPIs, COVID-19 vaccines were developed throughout 2020 and made available to the public through emergency use authorization by early 2021 [219]. As of August 2022, a total of 12.41 billion vaccine doses have been administered [164]. Owing to the frequent mutations and the decline in vaccine immunity over time, there is still much work to be done in order to achieve herd immunity (when enough people in the population have developed protective antibodies against future infection) [24, 38]. Given the economic shocks that followed the health crisis, there also remains an urgent need to improve resilience to the post-pandemic reality across every industry.

The construction industry represents a large proportion of the economic productivity of almost every country, comprising approximately 13% of the global gross domestic product [45, 162]. During the COVID-19 pandemic, the significant rise in unemployment throughout the construction industry triggered financial recessions globally [28]. Due to the integral nature of the industry, many countries tried to resume construction even in the face of repeated waves of infections [67]. These attempts, however, frequently conflicted with the objectives of public health and disease prevention. In the face of macro-level NPIs in response to COVID-19, many construction projects were delayed, suspended, or even cancelled [28]. Construction sites were forced to shut down during city lockdowns, even if no construction workers were infected [18]. Even on active construction sites, when a case was confirmed at the workplace, all of the infected person's colleagues might have to accept a quarantine order [139]. Due to physical distancing,

many construction workers were unable to complete their tasks onsite [70, 83]. To complicate matters still further, the implementation of work from home required greater cooperation between construction companies and local residents [96]. These restrictions have produced a number of negative impacts, most notably a shortage of workers [165]. Going forward, the construction industry must be able to establish a targeted response to epidemics if it wishes to successfully navigate between the objectives of controlling disease and continuing construction activities.

In comparison to other industries, construction industry is particularly vulnerable to COVID-19. The unavoidable reality of the close proximity of manual labourers on construction sites provides ample opportunity for droplet transmission of COVID-19. The prevalence of smoking among onsite workers further increases the risk of COVID-19 infections [169]. During the COVID-19 pandemic, construction employees demonstrated a hospitalization rate nearly five-fold higher than for other occupational categories [107]. The frequency of COVID-19 cases in the construction industry has been noted consistently across different countries and cities (e.g., Singapore [118], the United States [10], and Hong Kong [178]), even in the face of interventions (such as mask wearing and physical distancing). Most recent studies have discussed the effects of COVID-19 on the construction industry without considering its transmission dynamics [5, 18]. Several studies have investigated response strategies but have so far not proposed any targeted strategies for the construction industry [15, 191]. A comprehensive investigation of COVID-19 based on epidemiological evidence is thus required to help the construction industry to coordinate their continued response to COVID-19.

1.2 Research Scope and Problem Statement

By August 2022, the densely populated metropolitan area of Hong Kong had endured at least five epidemic waves, with 367,537 confirmed cases and 9,580 deaths [64]. One component of the waves included at least five COVID-19 case clusters (comprising 221 total confirmed cases) associated with construction sites [178]. Based on the work of Adam et al. (2020), the super-spreading potential of COVID-19 throughout Hong Kong was also expected to pose serious challenges to active construction workers [1]. In order to mitigate the severity of the COVID-19 outbreak, the construction industry complied with several NPIs introduced by the municipal government of Hong Kong, which policies were classified as moderately stringent by the Oxford COVID-19 Government Response Tracker (OxCGRT) [82]. Meanwhile, the construction industry in Hong Kong also tried to implement several more specific strategies aimed at safeguarding workers. For example, each construction worker was assigned to specific

locations for changing, resting, and dining so as to maintain physical distancing [42]. Even in the face of a volatile and complex epidemic, the construction industry in Hong Kong showed a high degree of resilience in response to COVID-19. In December 2020, the Hong Kong Construction Industry Council (HKCIC) announced that there were 103,000 workers working on construction sites on a daily basis, which was a 5.2% increase over 2019 [249]. The response of this vital industry to the novel coronavirus provides insight into the spread and mitigation of COVID-19 in construction industry in other densely populated international metropolises.

In the discussion of disease prevention and control, researchers usually explore the epidemiological evidence of a disease (transmission dynamics [102], transmission patterns [132], and super-spreading potential [136]) before designing response strategies such as NPIs and vaccination plans on the basis of the epidemiological evidence [51, 127, 242]. During the COVID-19 pandemic, many industries have explored this epidemiological evidence in order to build a comprehensive understanding of the disease's spread and to construct effective response strategies. Health care providers [138, 158, 239] and the restaurant industry [17, 137, 184] have, unsurprisingly, been at the forefront of this push. Compared with other industries, the studies associated with the construction industry have mostly investigated the impacts and challenges [18] presented by COVID-19, and have mostly neglected the epidemiological element. Response strategies in the construction industry, meanwhile, were designed based on the tactical strategies announced by local governments [56, 58, 162]. During the pandemic, policy makers tried to maintain construction activities via several generally mandated NPIs, including face masks and shift work [172, 191]. The efficacy of cross-applying epidemic mitigation strategies from one industry to another, however, is ambiguous [19]. In addition, given the lack of attention to epidemiological evidence regarding the spread of COVID-19, it is difficult to design strategies tailored specifically for the construction industry. This study addresses this research gap through an exploration of the epidemiological evidence (transmission dynamics and patterns), which provides the basis for several strategies targeted at epidemic mitigation in the construction industry in Hong Kong.

1.3 Research Aims and Objectives

The aims of this study are twofold: 1) to explore the epidemiological evidence of the spread of COVID-19 as it relates to Hong Kong's construction industry, and 2) to design response strategies based on this epidemiological evidence. In order to attain the aims, this study establishes the following objectives:

1. To estimate the transmissibility of COVID-19 from the first three waves in Hong Kong;
2. To determine the industry-specific transmission patterns of COVID-19 in the construction industry in Hong Kong;
3. To explore NPIs (i.e., contact restrictions, a ban on visitors onsite and onsite disinfection) and vaccine programs on construction sites;
4. To investigate *a priori* identification of potential super-spreader in construction projects.

1.4 Dissertation outline

Based on the research background, research scope, problem statement, and research aims and objectives described above, the rest of the dissertation is organized as follows:

Chapter 2 summarizes the literature relevant to COVID-19 epidemiological investigations and response strategies, studies of COVID-19 in different industries, and studies of the particular response of the construction industry.

Chapter 3 presents the research methods used in this study to explore the transmission dynamics of COVID-19 (compartment models), the transmission patterns of COVID-19 (retrospective cohort studies and spatiotemporal connectivity analysis), and the identification of potential super-spreaders (network-based epidemic models and K-shell decomposition analysis).

Chapter 4 describes the transmission dynamics of COVID-19 in Hong Kong via a modified Susceptible-Exposed-Infectious-Hospitalised-Recovered (SEIHR) model, and estimates the effectiveness of municipally mandated NPIs (especially gathering restrictions and quarantine orders). This chapter indicates the necessity of designing targeted strategies for individual industries to adapt to the post-pandemic environment.

Chapter 5 explores the transmission pattern of COVID-19 via construction sites in Hong Kong, which offers the epidemiological foundation for the response strategies presented in later chapters.

Chapter 6 investigates the effectiveness of several response strategies (e.g., contact restrictions and vaccinations) for controlling COVID-19 transmission among construction workers and their close contacts on construction sites.

Chapter 7 proposes a network-based computational based on K-shell decomposition methods and stochastic network-based epidemic models to identify potential super-spreaders on construction projects.

Chapter 8 concludes the study with a discussion of the major findings, their implications, their limitations, and specific directions for future research arising from this study. The outline of the studies arising from this dissertation is also provided in visual form below in Figure 1.1.

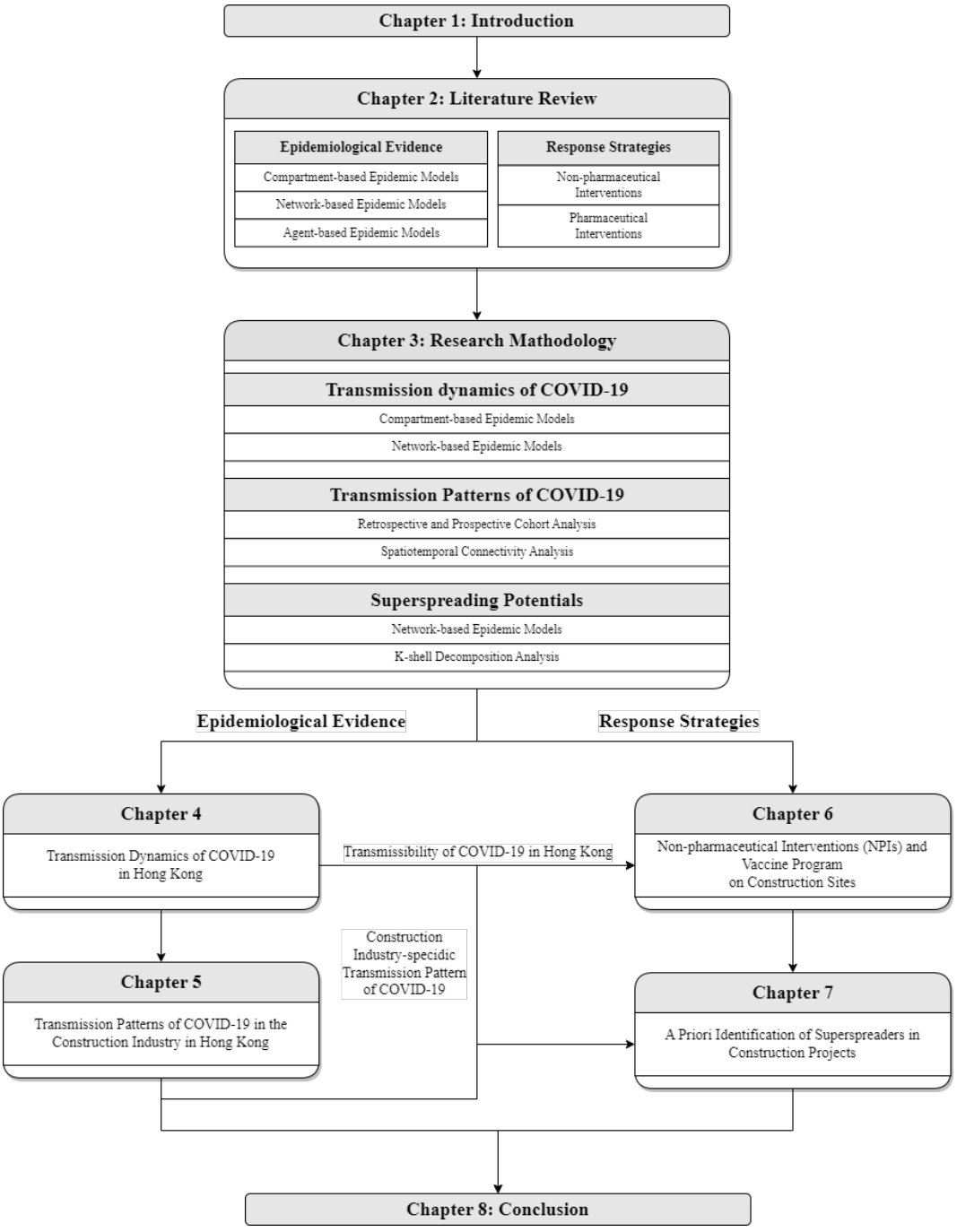

Figure 1.1: Organization of studies in this dissertation

Chapter 2

Literature Review

2.1 Studies relevant to COVID-19

2.1.1 Epidemiological evidence of COVID-19 transmission

For the purposes of both determining the severity and scale of the disease and designing appropriate interventions and responses, it is necessary to first explore the transmission dynamics of COVID-19. Numerous epidemiological studies have been conducted to understand the transmission dynamics of COVID-19 and to estimate the basic reproduction number (i.e., the average number of secondary infections caused by a single infection when a population is wholly susceptible, $\mathcal{R}_0$) [202]. The $\mathcal{R}_0$ values of a given illness are usually estimated from compartment models in which the transmission dynamics of the disease are formulated by dividing the populations into mutually-exclusive compartments representing disease status [102, 227]. When the basic reproduction number $\mathcal{R}_0$ is less than one, the disease is likely to die out by itself. When Ro is larger than one, the disease has the potential to start spreading within a population [127]. Since December 2019, many studies have estimated the $\mathcal{R}_0$ values of COVID-19 in different countries. Tang et al. (2020) employed a deterministic, Susceptible-Exposed-Infectious-Recovered (SEIR) compartmental model to determine a mean reproduction number of 6.39 for mainland China [202]. D'Arienzo and Coniglio et al. (2020) estimated $\mathcal{R}_0$ values ranging from 2.43 to 3.10 in Italy [51]. In addition to compartment models, several quantitative methods were also available. Wu et al. (2020) calculated $\mathcal{R}_0$ in mainland China as 2.68 through the use of a Markov chain Monte Carlo (MCMC) method [242]. Zhao et al. (2020) estimated that the $\mathcal{R}_0$ ranges from 2.24 to 5.71 for mainland China by modelling the epidemic curve in accordance with exponential growth [259]. In Hong Kong, Cowling et al. (2020) used a branching process model to estimate the time-varying intensity of transmission, with a daily effective reproduction number R_t that ranged from 0.72 to 1.28 [49]. In South Korea, the $\mathcal{R}_0$ values were estimated at 2.3 to 3.5 via a maximum likelihood estimation approach [260]. A recent systematic review and meta-analysis of 85 studies by Alimohamadi [9] reported that the mean $\mathcal{R}_0$ was calculated as 3.38 ± 1.40, with a range of 1.90 to 6.49. Such a high $\mathcal{R}_0$ indicates that COVID-19 is capable of transmission across at least three to four generations [202], which provoked the global panic in March 2020.

After analyzing the data regarding laboratory-confirmed, positive COVID-19 cases, many studies

explored the epidemiological characteristics of COVID-19, such as incubation period, infection period, and transmission heterogeneity. Given the possibility of human-to-human transmission between pairs of COVID-19 patients, many secondary cases were determined to have become infected during the pre-symptomatic stage of an infected case [87, 196]. Asymptomatic and mild COVID-19 cases, it was discovered, were also able to infect others [69]. Alene et al. (2021) concluded, based on a systematic review and meta-analysis, that the mean serial interval (that is, the time delay between the onset of symptoms of a primary case and the presentation of symptoms in one or more secondary cases) ranged from 4.2 to 7.5 days, and that the mean incubation period ranged from 4.8 to 9 days [8]. At the same time, many countries (including Hong Kong) announced several reinfection cases [95]. Many super-spreading events were also found globally, provoking speculation that such events might be the main catalyst of the pandemic [74]. In an attempt to determine the risks of super-spreading event, many studies have evaluated the dispersion parameter (k) as having a value less than 1, which indicates an over-dispersed transmission pattern of COVID-19 [232]. Compared with other respiratory diseases (such as Middle East Respiratory Syndrome (MERS) and Severe Acute Respiratory Syndrome coronavirus (SARS)), COVID-19 makes more people (including pre-symptomatic, asymptomatic, and symptomatic individuals) available to infect others.

2.1.2 Response strategies to COVID-19

Faced with a lack of available vaccines and antiviral medication, many governments implemented highly restrictive NPIs in response to COVID-19 so as to delay and moderate the spread of the emerging pandemic [82, 85, 119]. The effectiveness of different NPIs has since been explored by many studies. Eikenberry et al. (2020) used a modified compartment model to determine that the use of face masks by the general public is highly effective in curtailing community transmission [57]. Tian et al. (2020) found that quantitative analysis indicated that city lockdown policies delayed the growth and limited the size of the COVID-19 pandemic in Wuhan, China [222]. Chinazzi et al. (2020) used a global metapopulation disease transmission model to highlight the positive impact of international travel restrictions in Wuhan on delaying the global dispersion of COVID-19 [46]. The lockdown policy also had large effects on reducing transmission in 11 European countries (Italy, France, Spain, the UK, Belgium, Germany, Sweden, Switzerland, Austria, Norway, and Denmark) [61]. By means of an age-structured, susceptible-exposed-infected-removed (SEIR) model, Prem et al. (2020) evaluated the effectiveness of physical distancing in preventing transmission for different groups, and focused

particularly on workers and school children [174]. Gatto et al. (2020) identified the importance of identifying and isolating pre-symptomatic infected individuals in Italy through a metacommunity, Susceptible–Exposed–Infected–Recovered (SEIR)-like transmission model [72]. In light of the limited capacity of the US health care system, Moghadas et al. (2020) discussed the effectiveness of self-isolation and contact tracing for symptomatic individuals through a modified compartment model [146] [50]. Thanks to studies such as these, mask mandates, city lockdowns, travel restrictions, physical distancing, and contact tracing became the major NPIs implemented globally.

After the genetic sequence of the virus SARS-CoV-2 became available through the Global Initiative on Sharing Avian Influenza Data (GISAID) in early January 2020, the development of vaccines against COVID-19 was initiated [108]. There are four major vaccine types: whole virus vaccines (CoronaVac-Sinovac), subunit vaccines (EpiVacCorona-FBRI), viral vector vaccines (Ad5-nCoV-CanSino), and nucleic acid vaccines (BNT162b2-Pfizer/BioNTech) [44], with different vaccine efficacy levels. For example, the nucleic acid vaccine (the BNT162b2 mRNA COVID-19 vaccine) was found to confer 95% protection against COVID-19 in persons 16 years of age or older [173]. In an attempt to optimize the allocation of limited vaccine supplies in the early stages of the rollout, the prioritization of vaccination for the elderly (> 60 years old) was found to reduce deaths significantly [65]. It was then determined based on occupations, that concentrated essential workers (such as health care workers) should receive priority for vaccination, followed by clustered essential workers (including construction workers) [34]. Before the achievement of herd immunity, authorities tried to stress, a high level of compliance with NPIs remained crucial, as an early relaxation of safe behaviours might trigger a disease resurgence [75]. In addition, it was expected that the vaccine's efficacy against COVID-19 might wane naturally over time or decline in the face of a still-evolving virus [104, 224]. Even after the eventual mass uptake of the vaccines, a combination of vaccination and NPIs might remain necessary to control future transmission risks.

2.2 Studies relevant to COVID-19 in different industries

As the most important sector for any response to emerging diseases, the emergence of COVID-19 provoked immediate concerns about the overloading of the global health care system [107, 215]. In an effort to improve the resilience of health care provision in the face of epidemics, studies related to this sector included 1) estimations of the infection risk of different people (such as front-line medical providers) and/or settings (such as hospital wards); 2) protection methods for at-risk

people and/or settings; and, 3) optimizations of the system's overall capacity [239, 246]. Front-line health care workers were found in one prospective study to have an infection risk of COVID-19 at least three times greater than the public [158]. Given these risks, it was recommended to prioritize the provision of both face masks [226] and vaccines [252] so as to protect them from COVID-19 infections. During the pandemic, some COVID-19 patients were infected in hospital wards or in an open cubicle of a general ward before their diagnosis [239], a phenomenon known as "nosocomial transmission". Some health care workers were afraid of getting infected by these patients and refused to work [192]. In order to prevent nosocomial transmissions in hospital wards, ventilation systems were specially designed in response to simulations of airborne transmission [138]. In another effort to prevent nosocomial transmissions, the implementation of traffic control bundling (TCB) was recommended in Taiwan, which involved triage outside of hospitals, the classification of patients based on their symptoms, and separate zones (including contamination, transition, and clean zones) [188]. A similar triage system was also proposed by Wake et al. (2020), which combined clinical assessments with rapid SARS-CoV-2 testing [229]. In terms of system capacity optimization, Moghadas et al. (2020) used a modified compartment model to predict the potential of severe cases and maximize the effective utilization of intensive care units (ICUs) [146]. Before designing any response strategies in the health-care sector, researchers focused on an analysis of relevant epidemiological data from existing patients. Their response strategies were mostly designed to reduce the infection risk of vulnerable people and settings.

Restaurants have also proved highly vulnerable to many respiratory diseases over the years (including influenza, SARS, and COVID-19). Many COVID-19 outbreaks were associated with air conditioning in restaurants in both China [137] and Korea [115], as well as across the globe. After conducting case studies of the existing outbreaks, several researchers conducted an experimental study that simulated the airborne transmission route of COVID-19 [90, 123]. Mounting evidence also indicated airborne transmission of particles RNA material from the SARS-CoV-2 virus was detected and its survival in air estimated [17, 133]. The infection distribution reported in these studies was consistent with a spread pattern representative of long-range transmission via exhaled, virus-laden aerosols. Hence, the prevention of airborne transmission in restaurants became a major challenge over the course of the pandemic response. Tang et al. (2020) suggested a reduction of the use of central air conditioning [203], while Mohanmmadi et al. (2021) indicated the importance of educating restaurant staff regarding mitigation measures [147]. Takeaway and food delivery services were also widely promoted

[184]. In response to the dining restrictions implemented during the pandemic, a number of new strategies have since been proposed, including the elimination of certain menu items and the redesigning of dining rooms [161].

The difference in epidemiological evidence across different industries (in this case, health care and restaurant) influenced the varying response strategies that they eventually adopted. The basic strategy of analysis in the case of these two industries was to determine the infection risks of a group of people by analyzing the data of laboratory-confirmed COVID-19 infections. For groups that demonstrated a higher risk of infection (i.e., front-line, health care providers), their protection was usually prioritized in mitigation strategies. For scenarios where the infection risk was significantly high in general (i.e., hospital wards and restaurant dining rooms), more targeted strategies were likely to be designed. Throughout the epidemic, a combination of epidemiological research and response strategy development contributed to different disease response efforts in each industry.

2.3 Studies relevant to COVID-19 in the construction industry

2.3.1 Effects of COVID-19 on the construction industry

During the COVID-19 pandemic, researchers have focused on investigating the effects of the disease and the practical challenges it poses, and on developing effective response strategies. In the absence of vaccines and antiviral medication in early 2020, NPIs were implemented globally as the major anti-epidemic strategy [85]. The Chinese government initially implemented several extreme measures, including citywide lockdowns, travel restrictions, and quarantine orders, which effectively mitigated further transmission in Wuhan [46, 127]. In Hong Kong, early government interventions contributed to a reduction in COVID-19 infections carried by cross-border travellers [113]. As a result of this tactical strategy, many industries (including the construction industry) were also required to comply with these government-mandated NPIs in response to COVID-19 [19].

Given the general lack of scientific evidence regarding the risk of COVID-19 infection in the construction industry, it is informative to first quantify the effects of the outbreak on the industry and to discuss ongoing challenges. Several studies have relied on interviews, surveys, and questionnaires in order to quantify the impact of COVID-19 on the construction industry in different countries. Significant negative effects, including low business turnover, job loss, and difficulty working from home, have been reported in both developing and highly industrialized

countries [18, 56, 162]. In South Africa, the lack of compliance with COVID-19 safety measures among construction workers proved to be a major and continuous safety management challenge [11]. In Ghana, disease control strategies (such as social distancing) caused a decrease in the work rate, which had deleterious consequences for the construction industry overall [2]. In Egypt, due to the suspension of multiple construction projects, half of the respondents reported temporarily changing their employment to other industries [58]. In Malaysia, only 30% of workers were allowed onsite, which led to slow progress and project delays [70]. The Iraqi construction industry faced an acute labour shortage due to a lack of safety and risk management [5]. In the United Kingdom, as some construction workers were forced to work from home, management and coordination of projects became increasingly difficult [96]. In the United States [10], the construction industry implemented social distancing and the wearing of masks to protect the workforce, but this also resulted in additional costs and productivity losses. In Singapore, meanwhile, a high infection rate of COVID-19 among migrant workers contributed to a labour shortage [128]. Globally, COVID-19 mitigation efforts tended to restrict onsite construction activities, obstructing progress and exacerbating labour issues.

2.3.2 Response strategies to COVID-19 in the construction industry

The pandemic has had a variety of effects on the construction industry at different stages of its progress. Multiple studies have proposed a variety of reliable measures with which to monitor the dynamic impact of COVID-19 on the construction industry. Kanno (2021) used dynamic conditional correlation multivariate GARCH models to asses the dynamic impacts of COVID-19 on a number of industries (including construction) [100]. Chih et al. (2022) examined the magnitude and severity of the impact of COVID-19 on construction organizations via an examination of the longitudinal daily stock prices and indices [45]. Joen et al. (2022) proposed the Purdue Index for Construction (Pi-C) and observed continuous fluctuations in construction employment in the US [98]. These observations of the difficulties produced by the response to COVID-19 suggest that further response strategies should be flexible in order to compensate for the dynamic nature of the pandemic.

During the early stages of COVID-19, the construction industry was restricted by NPIs implemented by public authorities. Construction workers were forced to stay at home due to lockdowns and quarantine ordinances [62]. Supply chain disruptions further delayed construction projects, leading eventually to their suspension or even cancellation [18]. When confronted with an outbreak, healthy workers were rendered unable to participate in any productive activity. In terms

of the effectiveness of these NPIs, Araya (2021) used a simulation of COVID-19 transmission to consider the possibility of a tiered response for construction workers, in which a two-week quarantine restriction was implemented for sick workers alongside a physical distancing policy for healthy onsite workers [15]. Man et al. (2021) confirmed the importance of a climate of safety through an examination of the acceptance of personal protective equipment (PPE) among construction workers [143]. Kim et al. (2021) also analyzed the feasibility of a disinfection process for workers before and after their shifts [105]. This research has taken the need for flexibility in response seriously, but has done so largely within the response framework already established by governments and civil authorities.

As the acute crisis produced by COVID-19 has started to abate, more studies have begun to explore the possibilities of designing a response strategy specifically tailored to the construction industry. Araya and Sierra (2021) indicated that different stakeholders in construction projects (engineers, management, workers, etc.) should have different response strategies tailored to their level of risk and exposure [16]. Pamidimukkala and Kermanshachi (2021) further discussed the varied response strategies among field and office workforces, respectively [165]. Liang et al. (2022) addressed the needs of decision-makers trying to make choices in the face of an uncertain response environment to COVID-19 for workers on a construction project with varying levels of education and experience [126]. Seresht (2022) evaluated the efficiency with which COVID-19 spread through different sections of a construction project [191]. He et al. (2022) addressed the challenges of social distancing on construction sites by evaluating the effectiveness of the Takt-time planning method, which they then used to reduce the overlap in workspace between different construction operations [86]. In practice, in addition to the larger scale NPIs implemented by governing authorities, more health and safety (H&S) technologies have been promoted by construction companies in conjunction with public health officials, including the adoption of the health quick response (QR) code system, artificial intelligence (AI)-powered fever monitoring, and site access control systems [250].

2.4 Summary and Research Gap

As the studies surveyed here attest, COVID-19 posed a significant challenge to the construction industry in a number of different dimensions, particularly in regard to labour shortages [5, 18]. A number of existing studies have explored some of the different response strategies like disinfection [105] and social distancing, but few studies have explored the epidemiological patterns of COVID-19 transmission within the construction industry, or its super-spreading potential. Current

response strategies were largely established based on the adoption and adjustment of NPIs announced by local governments [62]. Because of the lack of an epidemiological foundation, the effectiveness of these NPIs as implemented in the construction industry is ambiguous [19]. Hence, limited research considered both transmission characteristics of a disease (COVID-19) and industry-specific characteristics of the population in the construction industry. Few studies explored the targeted response strategies at different scopes for the construction industry. A serious consideration of the epidemiological paths by which COVID-19 spreads would allow a full analysis of the effectiveness of response methods that is currently lacking in the available literature.

In contrast to the construction industry, health care providers and restaurants invested in developing a full understanding of the epidemiological evidence of COVID-19's spread in order to design targeted response strategies. On the other hand, although construction workers have exhibited a great deal of vulnerability to COVID-19 infection, a full picture of the spread of COVID-19 has yet to be drawn. In the meantime, construction workers have reported a nearly five-fold hospitalization rate over other occupational categories [166]. Cases of COVID-19 have continued to occur frequently in the construction industry globally (as shown in, for example, reports from Singapore [118] and the United States [10]). In this regard, Hong Kong is of particular interest because there were at least five significant COVID-19 outbreaks associated with construction sites [178]. Several of the individual construction sites even experienced multiple outbreaks of COVID-19 [209]. Given this context, this study aims to explore the epidemiological evidence of the spread of COVID-19 related to the construction industry in Hong Kong, as shown in Chapters 4 and 5, and then design targeted response strategies based on the epidemiological evidence, as shown in Chapters 6 and 7.

Chapter 3

Research Methodology

This chapter introduces the research methods applied in this study, which include compartment-based epidemic models and network-based epidemic models for describing the transmission dynamics of COVID-19, retrospective and prospective cohort studies (including spatiotemporal connectivity analysis) for investigating the transmission patterns of COVID-19, and K-shell decomposition analysis for identifying super-spreaders on a network-based epidemic model. Research methodology has been summarized in 3.1

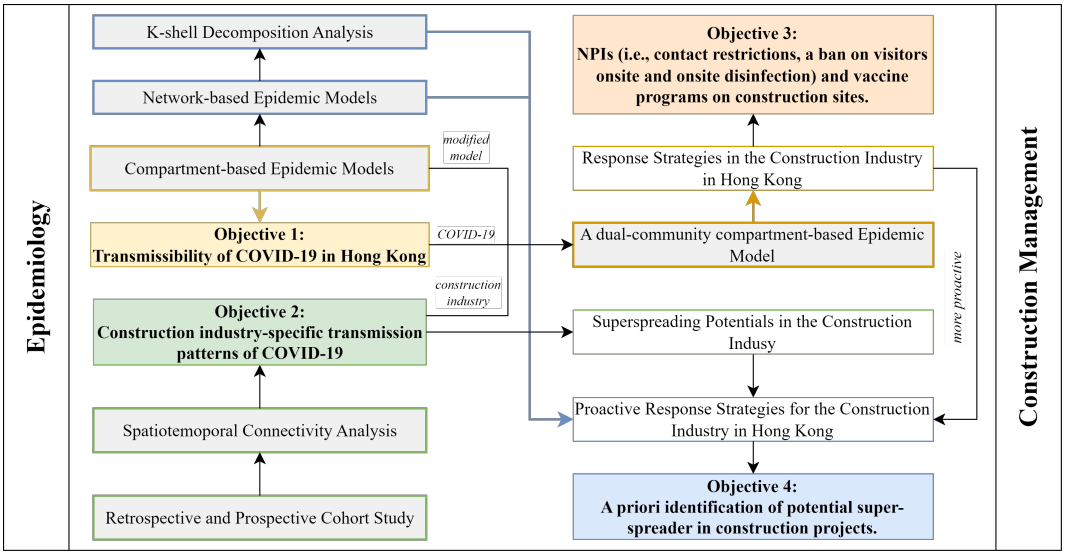

Figure 3.1: Research Methodology.

3.1 Transmission dynamics of COVID-19

3.1.1 Compartment-based epidemic models

Epidemic models have rested at the core of all comprehensive investigations of infectious disease since 1760 [27], and compartment models have come to be the most prevalent of these [102]. Compartment-based Epidemic Models have been widely applied to describe the transmission dynamics of infectious diseases, and have been employed during the COVID-19 pandemic to estimate the basic reproduction number $\mathcal{R}_0$ of the novel coronavirus [245]. It is important to note that the model assumes well-mixed homogeneous populations [102]. The transmission dynamics of a given disease are then formulated based on dividing the populations into mutually

exclusive compartments. The population within each compartment is assigned different definitions. For example, the classical Susceptible-Infectious-Recovered (SIR) model classifies people into three compartments based on their epidemic characteristics [89]. This can be formulated mathematically as follows:

$$\begin{cases} \dfrac{dS}{dt} = -\dfrac{\beta IS}{N}, \\ \dfrac{dI}{dt} = \dfrac{\beta IS}{N} - \gamma I, \\ \dfrac{dR}{dt} = \gamma I, \end{cases} \tag{3.1}$$

$$N(t) = S(t) + I(t) + R(t), \tag{3.2}$$

$$\lambda = \frac{\beta I}{N}, \tag{3.3}$$

$$\mathcal{R}_0 = \rho(FV^{-1}) = \frac{\beta}{\gamma}, \tag{3.4}$$

where

β is the transmission rate between S and I; $1/\gamma$ is the average duration of the incubation period; λ is the force of infection; $N(t)$ is the total population at time t, which is assumed to remain constant; $S(t)$ is the number of people susceptible to infection at time t; $I(t)$ is the number of infectious individuals at time t; $R(t)$ is the number of recovered people (in this group, individuals are either immune or deceased) at time t; F is the matrix of the new infection terms. The matrices of the remaining individuals transferring out of (or into) the various compartments are represented as V^- and V^+; and the transition term V is the difference between V^- and V^+.

In the SIR model, the total population N remains constant, and only infectious people I can shed the virus and infect others. As shown in Eq. (3.3), the force of infection λ describes the transition rate of individuals from the susceptible compartment S to the infectious compartment I. The basic reproduction number $\mathcal{R}_0$ is then defined as the spectral radius of the next generation matrix under a disease-free equilibrium (DFE) [227]. The DFE is locally asymptotically stable when $\mathcal{R}_0 < 1$, and unstable when $\mathcal{R}_0 > 1$. In Eq. (3.1), $\mathcal{R}_0$ is estimated as $\mathcal{R}_0 = \frac{\beta}{\gamma}$. When $\mathcal{R}_0$ is greater than one, and when $\beta > \gamma$ in Eq. (3.1), the disease will persist; otherwise, the disease will die out. The SIR model is a classical approach to studying the the severity and size of a given disease. In addition to the disease-free equilibrium discussed here, researchers have devoted attention to the relative stability of other equilibria, such as the endemic equilibrium and backward bifurcation [13]. This study conducts the mathematical analysis using compartment models, more detailed descriptions of which are provided in Chapters 4 and 6.

During the early phase of COVID-19, the compartment model was mostly used for calculating the $\mathcal{R}_0$ values of COVID-19 and evaluating the effectiveness of different NPIs (as mentioned in Section 2.1). Based on the calculation of $\mathcal{R}_0$, it follows that the at-risk group that contributes most to $\mathcal{R}_0$ should be prioritized for infection control. For example, by simulating the spread of COVID-19 with compartment models, Gatto et al. (2020) found that pre-symptomatic individuals contributed the most to the spread in Italy [72]. Moghadas et al. (2020) also indicated that mildly symptomatic individuals contributed the most to the spread in the United States [146]. Prem et al. (2020) identified the significance of workers and school children in the spread of COVID-19 in China [174]. In addition to its basic information-gathering properties (e.g., the identification of disease-free and endemic equilibria), the compartment model also provides important information for generating epidemic prevention and control strategies, including travel restrictions, lockdowns, and quarantine orders [127].

3.1.2 Network-based epidemic models

In the real world, epidemic spread is heterogeneous among individuals. Individuals may contact a given disease in a specific interaction pattern, or they may come into contact with only a small section of the population [167]. In contrast to compartment models, which are based on a well-mixed population, network-based epidemic models have been developed to compute epidemic dynamics at the general population level from the individual behaviours of infectious persons [101]. Networks are mostly described as graphs, consisting of points (vertices) and edges. Each point represents an individual. The edge represents an interaction between two individuals. The weight of an edge can represent the transition rate, transmission possibility, contact rate, or infection probability [152]. If there is a graph G of size N (with nodes $v_i \in V, 1 \leq i \leq n$), an adjacency matrix A summarizes all connections within the network with elements a_{ij}. Most networks are non-directed, as the virus can pass in either direction across an interaction; thus, $A_{ij} = A_{ji}$ and the adjacency matrix A are symmetric. If a_{ij} is equal to one, nodes v_i and v_j are connected. If a_{ij} is equal to zero, nodes v_i and v_j are not connected. As for the edge $e_{\{v_i,v_j\}}$, when considering contact heterogeneity, $e_{\{v_i,v_j\}}$ is defined as the contact rate between individuals v_i and v_j. In epidemiology, the infection risk can be increased through a higher contact rate [152]. Figure 3.2, depicts a non-directed network G of size $N = 6$ (with nodes $v_i \in V, 1 \leq i \leq 6$), consisting of $e_{\{v_1,v_2\}}$, $e_{\{v_1,v_3\}}$, $e_{\{v_1,v_5\}}$, $e_{\{v_3,v_5\}}$, $e_{\{v_4,v_5\}}$, and $e_{\{v_5,v_6\}}$. There is a connection between individuals v_1 and v_2, so $a_{12} = 1$. The weight of edge $e_{\{v_1,v_2\}}$ shows how frequent or close their contact is with each other, and thus the possibility of shedding the virus

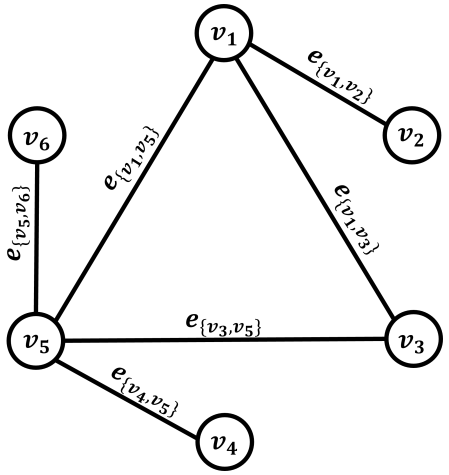

Figure 3.2: A non-directed network G of size $N = 6$ (with nodes $v_i \in V, 1 \leq i \leq 6$), consisting of $e_{\{v_1,v_2\}}$, $e_{\{v_1,v_3\}}$, $e_{\{v_1,v_5\}}$, $e_{\{v_3,v_5\}}$, $e_{\{v_4,v_5\}}$, and $e_{\{v_5,v_6\}}$.

as a result of this interaction.

By using a network to represent the epidemic spread, knowledge of every individual in a population and every relationship between individuals is required. In many cases, it is not clear how to define such relationships of how much contact is necessary to have with an infected individual. As a result, much research has been devoted to understanding how the topology of a network affects the epidemic spreading process [167]. Newman et al. (1999) described disease propagation as an imitation of the infection of individuals in the network [156]. The Watts and Strogatz network [234] also described disease propagation based on small-world network properties, emphasising short average path lengths and high clustering. In this study, a high-dimensional, small-world network has been used, which allows a consideration of the mean degree, dimension, and rewiring rate [231]. Given the number of nodes N, the mean degree of nodes $\langle k \rangle$, and a rewiring probability p, a non-directed graph is constructed with N nodes and $\frac{N\langle k \rangle}{2}$ edges, satisfying $0 \leq p \leq 1$ and $N \gg \langle k \rangle \gg \ln N \gg 1$. Dimensions determine the location of a node. Rewiring makes isolated nodes impossible and disconnections unlikely. The mean network distance $\langle d \rangle$ between distinct nodes is $\frac{1}{N(N-1)} \sum_{i=1}^{N} \sum_{j=1}^{N} d_{ij}, i \neq j$. The number of edges in the shortest path between nodes i and j is represented by d_{ij}. In a small-world network, two individuals may not contact each other via a direct connection, but can contact each other within the shortest path distance across other individuals.

3.2 Transmission patterns of COVID-19

The transmission patterns of infectious disease have been used on several occasions to design targeted control strategies. The frequent hospital-associated outbreaks of MERS-CoV [47] led to strict isolation requirements for patients with MERS-CoV, and the adoption of personal protective equipment by health care professionals in contact with such patients [7]. More recently, the awareness of super-spreading events of SARS-CoV also drove the implementation of a variety of prevention measures (quarantining of close contacts, increased hand washing after sneezing, or coughing [176], among others). Compared to MERS-CoV and SARS-CoV, SARS-CoV-2 has demonstrated a higher viral load in the upper respiratory tract at an earlier stage of infection, ensuring a higher proportion of transmission competent individuals (including pre-symptomatic, asymptomatic, and symptomatic infectious individuals) [244] and leading to greater difficulties in screening infectors [60]. The expeditious human-to-human transmission pattern of COVID-19 quickly became evident during the early stage of the outbreak [183], supporting decision-making by governments to implement a variety of control strategies (such as the wearing of masks [91] and travel restrictions [127]). The degree to which super-spreading events (SSEs) were involved in SARS-CoV-2 transmission [128] also informed the coordination of current screening and containment strategies. The labour-intensive nature of industries such as construction rendered workers more vulnerable to COVID-19 infection through SSEs [166], necessitating further discussion of the specific transmission patterns of the virus.

3.2.1 Retrospective and prospective cohort studies

Generally speaking, a cohort study records the clinical symptoms and COVID-19 nucleic acid test results of each close contact approximately every 24 hours [139, 225]. By assessing the second attack rate (i.e., the ratio of the number of cases occurring within the incubation period following exposure to a primary case to the total number of susceptible contacts), the riskiest contact setting can be identified [189]. Both retrospective and prospective studies can be conducted for the analysis of confirmed cases. When it is unclear whether or not each close contact had been infected, a prospective cohort study is used [144]. When data on the number of secondary cases generated by each primary case is available, a retrospective cohort study can be performed [144]. Kwok et al. (2021) depicted COVID-19 transmission based on age assortativity and the different types of social settings for the first two epidemic waves of COVID-19 in Hong Kong [114]. Adam et al. (2020) further identified 7 SSEs across 51 clusters in Hong Kong [1]. Liu et al. (2021) found a connector (a confirmed case that sheds the virus from one cluster to another), which

linked two large clusters [132]. Both prospective and retrospective cohort studies are intended to determine the risk factors of infection based on the transmission relationship between each pair of confirmed cases.

3.2.2 Spatiotemporal connectivity analysis

Spatiotemporal connectivity analysis is conducted as part of a retrospective cohort study [132, 144]. An event in a spatiotemporal dataset describes a spatial and temporal phenomenon that exists at a certain time t and location x. In epidemiology, the temporal phenomenon represents the time when an infector passed the virus to an infectee. The spatial phenomenon represents the place in which an infector transmitted the disease to an infectee. The transmission relationship between each pair of confirmed cases was reconstructed in accordance with temporal and/or spatial connectivity [132]. According to available data, when the onset date of a second case was within 14 days [178] of the onset date of the first case, the transmission relationship between the first and second cases are characterized by temporal connectivity. People who visited the same building within 14 days of their symptom onset are referred to as spatially connected cases. The categories for the spatial connectivity of these cases include a variety of settings, and are based on the type of activities most closely associated with the venues where the source cases were identified [48]. When there is more than one seed case identified due to temporal connectivity, the case that is also connected spatially will be regarded as the primary seed case. The priority of sources when determining the transmission relationship between each pair of confirmed cases is as follows: both spatial and temporal connectivity, only spatial connectivity, and only temporal connectivity. This approach is described in further detail in Chapter 5.

3.3 Super-spreading event identification

3.3.1 Spreading on a network-based epidemic model

Super-spreading is explicitly influenced by both the quantity and quality of interactions between individuals [194]. The impact of interaction heterogeneity on individual infectiousness has been described by compartment models [255], network-based models [185], and agent-based models [15]. Compartment models, as the core approach to describing the dynamics of disease transmission, are limited by a well-mixed population assumption [223]. The other two methods were developed to correct the assumptions of the standard transmission dynamics described in compartmental models, and bring them into closer alignment with the observed course of a disease. The heterogeneous epidemic spreading processes can be simulated by agent-based

models and network-based models. While agent-based models can mimic individual interactions within well-defined parameters [197], their performance can be marred by poor data quality [228]. A network-based structure, on the other hand, enables models to compute epidemic dynamics at the general population level from information about individual infections [101]. Similar to the spread of human sexual diseases via sexual partnership networks [76], airborne infectious diseases spread through interpersonal interaction [22]. A large number of close contacts thus increases the risk of SSEs [201], the likelihood of which can be estimated via network theory [106]. Hence, network-based epidemic models have tended to dominate research into individual infectiousness [167].

Network-based models describe interactions as a cluster of nodes (individuals), edges (contacts between persons) and the weights of edges (the probability of infections). These models can be constructed as random networks, scale-free networks [234], small-world networks [23], and heavy-tailed networks [251]. The spread and control of the disease throughout the network are each highly affected by a small number of influential nodes distinguished by degree centrality (the number of the immediate neighborhood of the node) [6, 23], betweenness centrality (a measure of how many shortest paths cross through this node) [29, 66], or K-shell decomposition analysis (a measure to locate a node in the network [39]. The K-shell index helps to predict the outcome of spread more reliably than either degree or betweenness centrality [106] and is adopted for the purposes of this study.

3.3.2 K-shell decomposition analysis

K-shell decomposition analysis was introduced as a tool for investigating the topology in a network. Many recent studies of Internet topology [135] and social networks [39] have used it to identify the most influential spreader within a complex network. This method has also found application in the study of the spread of epidemics throughout human contact systems [134]. The identification of the most influential spreaders within complex networks is essential for controlling the spread of any infectious disease. K-shell decomposition analysis decomposes a network into hierarchically ordered shells, which are labelled according to the k-shell index k_s. The k-shell decomposition algorithm works by recursively pruning all nodes with a degree less than the current shell index in the following manner: First, all nodes with degree $k = 1$ are removed. Then, nodes of $k = 1$ are successively eliminated until all are removed. The removed nodes now belong to the $k_s = 1$ k-shell index. Second, nodes with degree $k = 2$ are removed in a similar manner until all nodes with $k = 2$ are excluded. This produces the $k_s = 2$ shell. The

procedure ends when all nodes of the network are removed. This approach is described in greater detail in Chapter 7.

Chapter 4

Transmission Dynamics of COVID-19 in Hong Kong

4.1 Introduction

The COVID-19 outbreak led to a global pandemic in early 2020 [163]. The disease has reached almost every country in the world. Since then, many countries such as the USA, England, and Italy have experienced several waves of the epidemic [210]. By March 2021, the total number of COVID-19 cases exceeded 119.2 million, including more than 2.64 million deaths globally [163]. Its spread has also left economies and businesses counting the costs as governments struggle with instituting and enforcing various NPI measures (e.g. social distancing, face coverings, and mandatory quarantine of inbound travellers) to slow down the spread of the virus. Although the recent rollout of SARS-CoV-2 vaccines has raised hopes that the pandemic is nearing an end, identifying the duration of immunity, i.e., how long a person is protected after being vaccinated, could take several years of monitoring and research [31]. If immunity declines before herd immunity—when a large portion of the population of an area achieves immunity—previously vaccinated individuals will become susceptible to infection again. Under these circumstances, implementing effective NPIs remains critical to controlling the spread of COVID-19 [221].

Yet according to the World Health Organisation (WHO), as the pandemic has continued to persist, the NPIs implemented in many countries have caused an increase in "pandemic fatigue", that is, demotivation about following recommended or required measures to protect themselves and others from the virus [124]. It becomes a growing challenge for governments to find effective ways to handle this fatigue and reinvigorate public vigilance. To guide governments in the planning and implementing NPIs, WHO developed a framework of policy recommendations in late 2020 with four key strategies [221]. One of the strategies highlighted the importance of collecting and using evidence for targeted, tailored, and effective policies, interventions, and communication. In line with this strategy, infectious disease modelling techniques, aptly named compartment models, have been used to provide insights into creating more targeted NPIs to control COVID-19 transmission.

Indeed, compartment models have been used for a long time to study disease transmission

dynamics and gain insight into how diseases spread, which can help in devising prevention and control measure. Compartment models are formulated based on dividing populations into mutually-exclusive compartments representing disease status using the Kermack-McKendrick framework [102]. For example, Wu et al. (2020) calculated the reproduction number, $\mathcal{R}_0$, of COVID-19 as 2.68 via the use of the Susceptible-Exposed-Infectious-Removed (SEIR)-based model [242]. Tang et al. (2020) employed a dynamic model to assess the efficiency of travel restrictions [202], and Lin et al. (2020) examined transmission trends and the effects of NPIs on the dynamics of COVID-19 spread by using an SEIR-based model [127].

Many previous studies have found that human mobility by transportation such as air [116], rail [93], or public transit [145] have contributed to epidemic diffusion. The use of quarantines for members of the general public has been studied to combat the spread of respiratory diseases [154, 157, 187, 242]. By employing a modified SEIHR model to assess the transmission dynamics of SARS-CoV-2, this study extends previous work by incorporating inbound travellers with and without quarantine into the studied population in order to better understand how those NPIs affect transmission. Some basic qualitative properties of the model are analyzed, such as the basic reproduction number $\mathcal{R}_0$ and stability of the equilibria. The model is fitted using data on Hong Kong to show the trends characterizing the spread of the disease. Hong Kong was selected because it is a densely populated city with a higher risk and speed of COVID-19 transmission [238].

During this pandemic, a government policy stringency assessment system, which was developed by Oxford University and partners, and uses 20 indicators to generate scores ranging from 0 to 100, gave Hong Kong an average score of 56 in terms of its response to COVID-19 [82]. As of 14^th April 2021, Hong Kong has implemented strict quarantine policies for travellers and close contacts of infected persons, during which time it recorded 11612 cases and 209 deaths and still met a fourth wave of COVID-19 infections [63]. As a highly densely-populated city, it is especially critical for Hong Kong to be able to implement feasible measures for controlling the spread of COVID-19.

4.2 Materials and Methods

4.2.1 Data Collection

The time-series data of COVID-19 confirmed cases were obtained from Hong Kong Centre for the Health Protection (CHP) in the period between 24th January 2020 and 13th April 2021

[63], i.e., the period during which Immigration Department recorded the Statistics on Passenger Traffic [211]. From the demography related data in Table 4.1, the transmission dynamics of SARS-CoV-2 is not gender or age dependent [99]. We assume that every individual should have an identical possibility of getting infected with the same risk of death.

The median of the generation interval (GI) for COVID-19 was estimated as five days [77], but it can be longer than seven days [205]. We notice about three percent of confirmed cases in Hong Kong have an exceeded-14-day time-delay between symptom onset and reporting, reflecting the possibility of indirectly showing the symptom after quarantine. Additionally, more than 30 percent of infectious individuals are asymptomatic. This study considers both asymptomatic cases and people who onset after quarantine.

Table 4.1: Local Situation of COVID-19 in Hong Kong(as of April 13, 2021)

Symptom Type	**Subtotal**	**Percentage**
Symptomatic	8087	69.75
Asymptomatic	3508	30.25
Gender Distribution	**Subtotal**	**Percentage**
Female	6008	50.88
Male	5587	49.12
Age Distribution	**Subtotal**	**Percentage**
$(0,10]$	548	4.96
$(10,20]$	762	6.90
$(20,30]$	1752	15.86
$(30,40]$	2073	18.77
$(40,50]$	1891	17.12
$(50,60]$	1852	16.76
$(60,70]$	1649	14.93
$(70,80]$	683	6.18
$(80,90]$	316	2.86
$(90,120]$	69	0.62
Distribution of Time-delay between Symptom Onset and Reporting	**Subtotal**	**Percentage**
$(-3,0]$	21	0.26
$(0,5]$	5628	69.77
$(5,10]$	1889	23.42
$(10,15]$	404	5.01
$(15,20]$	100	1.24
$(20,30]$	33	0.41
$(30,40]$	9	0.11
$(40,100]$	3	0.04
Fatality Rate distributed based on Age	**Subtotal**	**Percentage**
$(0,35]$	0	0.00
$(35,60]$	17	0.35
$(60,70]$	30	1.82
$(70,80]$	56	8.20
$(80,85]$	42	22.34
$(85,90]$	40	31.25
$(90,120]$	22	31.88

4.2.2 Mathematical Model

4.2.2.1 Model Formulation

The epidemic model used in this study follows the compartment model from Kermack and McKendrick [102]. COVID-19 has a wide range of the targeted susceptible group and various complications (e.g., fever and cough) [80]. Considering implemented anti-epidemic strategies, the diagram is shown as Figure 4.1. The modified SEIHR model is presented in ordinary differential equations (4.1). All variables and parameters are described in Tables 4.5 and 4.2. We split the total human population at time t , denoted by susceptible individuals $S(t)$, quarantined inbound travellers $N_q(t)$, exposed individuals with outside movement $E_m(t)$, quarantined exposed individuals $E_q(t)$, asymptomatic infectious individuals $I_a(t)$, symptomatic infectious individuals with outside movement $I_m(t)$, quarantined symptomatic infectious individuals $I_q(t)$, hospitalized asymptomatic infectious individuals $H_a(t)$, hospitalized symptomatic infectious individuals $H_s(t)$ and recovered individuals $R(t)$.

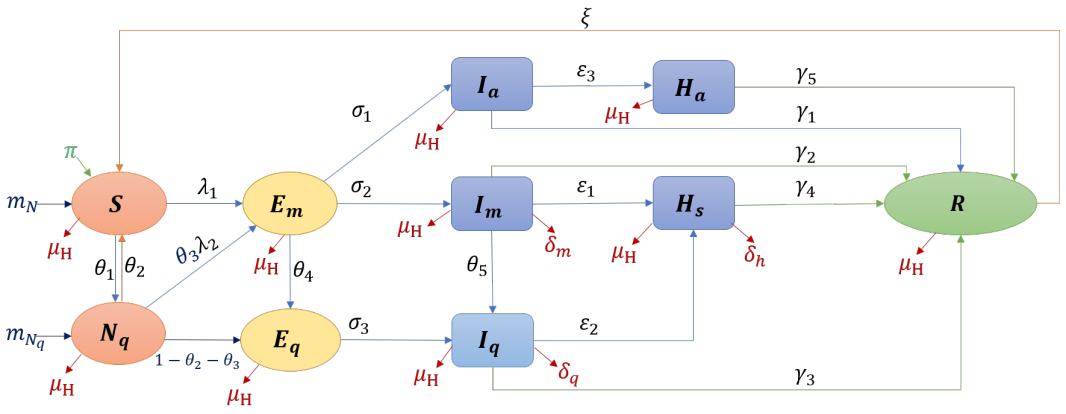

Figure 4.1: Susceptible-Exposed-Infectious-Hospitalised-Recovered (SEIHR) Model.

The labels q, m, a and s represent “quarantined", “with movement", “asymptomatic" and “symptomatic" respectively. Given that the life expectancy in Hong Kong is 84.89, this study considers the daily natural birth π as "225" and the natural death rate μ_H as "0.00003" [141]. Rare reinfections of COVID-19 caused by various viral isolates have been reported [95]. We assumed the reinfected probability to be a constant parameter ξ with a value of "0.0001". δ_k $(k = m, q, h)$, is the death rate among I_m, I_q and H_s. In Figure 4.1, all arrows are labelled with the transition rates between compartments. θ_k $(k = 1, 2, 3, 4, 5)$, is the percentage rate of a given population in one compartment transferring to another compartment. A positive term $(1 - \theta_2 - \theta_3)$ represents the probability of a quarantined inbound traveller being infected before the quarantine. $\frac{1}{\sigma_k}$ $(k = 1, 2, 3)$ is the average duration of the latency period, i.e., the time

between when an individual is exposed to the virus and when the individual starts to infect others. ϵ_k $(k = 1,2,3)$ represents the hospitalization rate and γ_k $(k = 1,2,3,4,5)$ is the mortality among each group I_k $(k = a,m,q)$ or H_k $(k = a,s)$. Each parameter ranges from 0 to 1. The force of infection λ_1 and λ_2 contain the transmission rates β_1 and β_2 due to the characteristics of the disease itself and due to interactions between members of the population as indicated through the effective contact ratio a_i $(i = 1,2,3,4,5,6)$. The initial population equals the number of local residents at the end of 2019: 7,520,800 [207].

$$
\begin{cases}
\frac{dS}{dt} = \pi + m_N + \xi R + \theta_2 N_q - (\theta_1 + \mu_H + \lambda_1) S, \\
\frac{dN_q}{dt} = m_{N_q} + \theta_1 S - (\theta_2 + \mu_H + (1 - \theta_2 - \theta_3) + \theta_3 \lambda_2) N_q, \\
\frac{dE_m}{dt} = \lambda_1 S + \theta_3 \lambda_2 N_q - (\sigma_1 + \sigma_2 + \theta_4 + \mu_H) E_m, \\
\frac{dE_q}{dt} = (1 - \theta_2 - \theta_3) N_q + \theta_4 E_m - (\sigma_3 + \mu_H) E_q, \\
\frac{dI_a}{dt} = \sigma_1 E_m - (\gamma_1 + \epsilon_3 + \mu_H) I_a, \\
\frac{dI_m}{dt} = \sigma_2 E_m - (\gamma_2 + \epsilon_1 + \delta_m + \theta_5 + \mu_H) I_m, \\
\frac{dI_q}{dt} = \sigma_3 E_q + \theta_5 I_m - (\gamma_3 + \epsilon_2 + \delta_q + \mu_H) I_q, \\
\frac{dH_a}{dt} = \varepsilon_3 I_a - (\gamma_5 + \mu_H) H_a, \\
\frac{dH_s}{dt} = \varepsilon_1 I_m + \varepsilon_2 I_q - (\gamma_4 + \delta_h + \mu_H) H_s, \\
\frac{dR}{dt} = \gamma_1 I_a + \gamma_2 I_m + \gamma_3 I_q + \gamma_4 H_s + \gamma_5 H_a - (\xi + \mu_H) R
\end{cases}
\tag{4.1}
$$

where the force of infection is given by:

$$
\lambda_1 = \frac{\beta_1 (a_1 E_m + a_2 I_a + a_3 I_m)}{N}, \; \lambda_2 = \frac{\beta_2 (a_4 E_m + a_5 I_a + a_6 I_m)}{N}, \tag{4.2}
$$

with N representing the total population at time t given by $N(t) = S(t) + N_q(t) + E_m(t) + E_q(t) + I_a(t) + I_m(t) + I_q(t) + H_a(t) + H_s(t) + R(t)$.

The force of infection λ_1 and λ_2 are driven by E_m, I_a and I_m. As for the quarantined group, N_q may transition to one of three groups, including back to susceptible group S, with symptom onset during quarantine E_q or after quarantine as E_m. We assume that if a quarantined individual is

Table 4.2: Notation of a modified SEIHR model

Notation	Description
Variables	
S	the number of susceptible individuals
N_q	the number of quarantined inbound travellers
E_m	the number of exposed individuals with outside movement
E_q	the number of quarantined exposed individuals
I_a	the number of asymptomatic infectious individuals
I_m	the number of symptomatic infectious individuals with outside movement
I_q	the number of quarantined symptomatic infectious individuals
H_a	the number of hospitalized asymptomatic infectious individuals
H_s	the number of hospitalized symptomatic infectious individuals
R	the number of recovered individuals
Parameters	
m_N	the number of inbound travellers without quarantine
m_{N_q}	the number of quarantined inbound travellers

infected during the quarantine period, symptoms would appear after the quarantine. In addition, the government will ask the individual's close contacts to comply with a 14-day compulsory quarantine. E_q is made up of individuals who were exposed to the virus through contact with quarantined inbound travellers or other close contacts. The specific moment when an exposed individual becomes exposed and pre-symptomatic is unknown. In this study, we assume the average latency period is three days. All exposed individuals are also assumed to be pre-symptomatic and can transmit the virus, and all quarantined infectious individuals are assumed to be symptomatic. Owing to their obvious symptoms, I_m cannot be regarded as a related individual who can take care of the quarantined people: $a_6 = 0$.

4.2.3 Mathematical Analysis

In this section, a brief summary of the mathematical analysis underlying this study is provided. The equations in the model (4.1) are defined as a positive dynamical system with the domain Ω. The stability of equilibria is formulated in terms of the next generation method [227] and bifurcation theory [13]. Firstly, we consider solutions to (4.1), which is given by

$$\Omega = \{(S, N_q, E_m, E_q, I_a, I_m, I_q, H_a, H_s, R) \in \mathbb{Z}_+^{10} : N > 0\}.$$

Thus, simplifying N from model (4.1) i.e., $N^{'} = S^{'} ... + R^{'}$, one can clearly see that all solutions to the model that start in Ω will remain in Ω for all $t \geq 0$. Hence, Ω is positive-invariant, and it

is sufficient to determine solutions that are restricted to Ω. Therefore, for the model (4.1), the existence, uniqueness, and continuation results hold provided the solutions that are restricted to Ω hold [94, 152].

4.2.3.1 Disease-free Equilibrium (DFE)

The DFE showed a locally asymptotic stablility with the initial condition [227]: only $S(0)$ and $N_q(0)$ are not equal to zero, and other variables should be equal to zero or much less than $S(0)$ and $N_q(0)$.

$$\begin{aligned}\Omega_1 &= [S(0), N_q(0), E_m(0), E_q(0), I_a(0), I_m(0), I_q(0), H_a(0), H_s(0), R(0)] \\ &= [S_0, N_{q0}, 0, 0, 0, 0, 0, 0, 0, 0].\end{aligned}$$

The matrix for the new infection terms is designated as F. The matrices of the remaining individuals transferring out of (into) compartments are represented as V^- and V^+. The transition term V is the difference between V^- and V^+. Based on the equations in model (4.1), the DFE of S is as follows:

$$S_0^* = \frac{(\pi + m_N)\mu_H + (\pi + m_N)(1-\theta_3) + m_{N_q}\theta_2}{{\mu_H}^2 + (1+\theta_1-\theta_3)\mu_H + \theta_1(1-\theta_2-\theta_3)}. \tag{4.3}$$

Substituting Eq. (4.3) into (4.1),we obtain

$${N_{q0}}^* = \frac{(\pi + m_N + m_{N_q})\theta_1 + m_{N_q}\mu_H}{(1+\mu_H-\theta_2-\theta_3)\theta_1 + \mu_H(\mu_H+1-\theta_3)}. \tag{4.4}$$

where $0 < \theta_2 + \theta_3 < 1$ and $0 < \theta_1 < 1$.

Hence, S_0^* and ${N_{q0}}^*$ are both positive.

Applying the next generation method [227] to the equations in (4.1), the new infections F and transition terms V are as follow:

To analyze the interplay between different groups, we defined a_1, a_2, a_3, a_4, a_5 and a_6 as the effective contact ratio between E_m and S, I_a and S, I_m and S, E_m and N_q, I_a and N_q and I_m and N_q. The transmission rates for S and N_q are assumed as β_1 and β_2 respectively. Thus, F can be

rewritten as:

$$F = \begin{bmatrix} \beta_1 a_1 + \theta_3 \beta_2 a_4 & 0 & \beta_1 a_2 + \theta_3 \beta_2 a_5 & \beta_1 a_3 + \theta_3 \beta_2 a_6 & 0 & 0 & 0 \\ 0 & 0 & 0 & 0 & 0 & 0 & 0 \\ 0 & 0 & 0 & 0 & 0 & 0 & 0 \\ 0 & 0 & 0 & 0 & 0 & 0 & 0 \\ 0 & 0 & 0 & 0 & 0 & 0 & 0 \\ 0 & 0 & 0 & 0 & 0 & 0 & 0 \\ 0 & 0 & 0 & 0 & 0 & 0 & 0 \end{bmatrix}.$$

The transition terms V is as follows:

$$V = \begin{bmatrix} q_1 & 0 & 0 & 0 & 0 & 0 & 0 \\ -\theta_4 & q_2 & 0 & 0 & 0 & 0 & 0 \\ -\sigma_1 & 0 & q_3 & 0 & 0 & 0 & 0 \\ -\sigma_2 & 0 & 0 & q_4 & 0 & 0 & 0 \\ 0 & -\sigma_3 & 0 & -\theta_5 & q_5 & 0 & 0 \\ 0 & 0 & -\varepsilon_3 & 0 & 0 & q_6 & 0 \\ 0 & 0 & 0 & -\varepsilon_1 & -\varepsilon_2 & 0 & q_7 \end{bmatrix}.$$

The basic reproduction number, $\mathcal{R}_0$, is given by

$$\mathcal{R}_0 = \rho(FV^{-1}) = \frac{(a_4\beta_2\theta_3 + a_1\beta_1)q_3q_4 + (a_6\beta_2\theta_3 + a_3\beta_1)\sigma_2 q_3 + (a_5\beta_2\theta_3 + a_2\beta_1)\,\sigma_1 q_4}{q_1 q_3 q_4}, \quad (4.5)$$

where

$$q = \theta_1 + \mu_H, \quad q_0 = 1 - \theta_3 + \mu_H, \quad q_1 = \sigma_1 + \sigma_2 + \theta_4 + \mu_H, \quad q_2 = \theta_3 + \mu_H,$$
$$q_3 = \gamma_1 + \epsilon_3 + \mu_H, \quad q_4 = \gamma_2 + \epsilon_1 + \delta_m + \theta_5 + \mu_H, \quad q_5 = \gamma_3 + \epsilon_2 + \delta_q + \mu_H,$$
$$q_6 = \gamma_5 + \mu_H, \quad q_7 = \gamma_4 + \delta_h + \mu_H \quad \text{and} \quad q_8 = \xi + \mu_H.$$

Theorem 4.1. *The DFE in the model* (4.1) *is locally-asymptotically stable when* $\mathcal{R}_0 < 1$*, and unstable when* $\mathcal{R}_0 > 1$.

Proof The proof of Theorem 4.1 can be deducted following [227].

The basic reproduction number ($\mathcal{R}_0$) represents the average number of secondary infections caused by a single infection when a population is wholly susceptible [227]. The interpretation of $\mathcal{R}_0$ is shown in Table 4.4. Based on the initial values estimated from [33, 127, 202], the basic reproduction number $\mathcal{R}_0$ is larger than one. In addition, E_m contributed the most infections, which exceeded 80%.

4.2.3.2 Endemic Equilibrium (EE)

In this subsection, for mathematical convenience, we assumed that λ_1 and λ_2 are the same:

$$\lambda_1 = \lambda_2 = \lambda = \frac{\beta(a_1 E_m + a_2 I_a + a_3 I_m)}{N}. \tag{4.6}$$

The EE is a scenario where a disease persists in a population. The globally asymptotic stability of the EE exists when $\mathcal{R}_0 > 1$ and the infected compartments are non-empty. Suppose Ω_2 is given as

$$\Omega_2 = [S^*, N_q^*, E_m^*, E_q^*, I_a^*, I_m^*, I_q^*, H_a^*, H_s^*, R^*].$$

Given the Eqns. (4.1), we obtain

$$E_q^* = \frac{(\theta_4 - (h_1 q_6 + h_2)\xi t_2 \omega^{-1}) E_m^* - (\xi t_4 t_3 \theta_1 + m_{N_q} q_0 t_4) t_2 \omega^{-1}}{q_2}, \tag{4.7}$$

$$I_a^* = \frac{\sigma_1 E_m^*}{q_3}, \tag{4.8}$$

$$I_m^* = \frac{\sigma_2 E_m^*}{q_4}, \tag{4.9}$$

$$I_q^* = \frac{(q_2\sigma_2\theta_5 + \theta_4 t_2 \omega^{-1} \sigma_3 q_4 - \xi t_2 \omega^{-1} \sigma_3 q_4 (h_1 q_6 + h_2)) E_m^* + (t_3\theta_1\xi + m_{N_q} q_0) t_2 t_4 \sigma_3 q_4 \omega^{-1}}{q_2 q_4 q_5}, \tag{4.10}$$

$$H_a^* = \frac{\epsilon_3 \sigma_1 E_m^*}{q_3 q_6}, \tag{4.11}$$

$$H_s^* = \frac{(\sigma_2\epsilon_1 q_2 q_5 + \sigma_2\theta_5 q_2\epsilon_2 - ((h_1 q_6 + h_2)\xi - \theta_4)\sigma_3 t_2 q_4 \omega^{-1})E_m^* - \epsilon_2 t_4 q_4(\xi t_3\theta_1 + m_{N_q} q_0)}{q_2 q_4 q_5 q_7}, \tag{4.12}$$

where

$$t_1 = \lambda\theta_3 + q, \qquad t_2 = \theta_2 + \theta_3 - 1, \qquad t_3 = \pi + m_N,$$

$$t_4 = q_8 q_4 q_6 q_7 q_3 q_2 q_5, \qquad t_5 = \gamma_2 q_5 + \gamma_3\theta_5, \qquad t_6 = q_5\epsilon_1 + \theta_5\epsilon_2,$$

$$t_7 = -\theta_1\theta_2 + q_0(\lambda\theta_3 + q), \qquad t_8 = \epsilon_2\gamma_4 + \gamma_3 q_7, \qquad t_9 = (\gamma_2 q_5 + \gamma_3\theta_5)q_7 + \gamma_4(q_5\epsilon_1 + \theta_5\epsilon_2),$$

$$\omega = q_4((\xi(\theta_2 + \theta_3 - 1)(\epsilon_2\gamma_4 + \gamma_3 q_7)\sigma_3 - q_7 q_8\theta_2 q_2 q_5)\theta_1 + q_5 q_7 q_8 q_0 q_2(\lambda\theta_3 + q))q_6 q_3,$$

$$h_1 = h_{11} + h_{12} + h_{13} = q_7\gamma_1\sigma_1 q_2 q_4 q_5 + \sigma_3\theta_4 q_3 q_4(\epsilon_2\gamma_4 + \gamma_3 q_7) + (q_2 q_3\sigma_2((\gamma_2 q_5 + \gamma_3\theta_5)q_7 + \gamma_4(q_5\epsilon_1 + \theta_5\epsilon_2))),$$

$$h_2 = \gamma_5\sigma_1\epsilon_3 q_2 q_4 q_5 q_7, \qquad h_3 = (\theta_2 + \theta_3 - 1)(\epsilon_2\gamma_4 + \gamma_3 q_7)\sigma_3 q_3 q_4 q_6(m_{N_q} q_0 + (\pi + m_N)\theta_1).$$

Simplify the model (4.1) by substituting Eq. (4.7) to (4.12), the EE of S^*, N_q^* and R^* can be rewritten as follows:

$$S^* = \frac{((h_1 + h_2)\xi E_m^* t_1 - h_3\xi m_{N_q} + t_4(m_{N_q}\theta_2 + t_1 t_3))}{\omega}, \tag{4.13}$$

$$N_q^* = \frac{((h_1 q_6 + h_2)\xi E_m^* + \xi t_4 t_3\theta_1 + m_{N_q} q_0 t_4)}{\omega}, \tag{4.14}$$

$$R^* = \frac{((h_{11}(q_0 t_1 - \theta_1\theta_2) + (h_{12} + h_{13})t_7)E_m^* - h_3)}{\omega}, \tag{4.15}$$

and

$$E_m^* = \frac{B_2\lambda^2 + B_1\lambda}{\lambda^2 A_2 + \lambda A_1 + A_0}, \tag{4.16}$$

where

$$B_1 = -(((q_5q_8(q_0\theta_3+\theta_2)q_2-\gamma_3\sigma_3\xi t_2)m_{N_q}+q_8q_2q_5t_3(\theta_1\theta_3+q))q_7-\gamma_4\sigma_3\epsilon_2 m_{N_q}\xi t_2)q_3q_6q_4,$$

$$B_2 = -q_6q_4q_3q_2q_5q_7q_8\theta_3t_3,$$

$$A_0 = -q_6q_4q_3((\xi t_2t_8\sigma_3-q_7q_8\theta_2q_2q_5)\theta_1+qq_0q_2q_5q_7q_8)q_1,$$

$$A_1 = (\theta_1\theta_3+q)(((\sigma_2t_9q_3+q_7\gamma_1\sigma_1q_4q_5)q_2+\sigma_3\theta_4q_3q_4t_8)q_6+q_7\gamma_5\sigma_1\epsilon_3q_2q_4q_5)\xi-q_0q_1t_4\theta_3,$$

$$A_2 = \theta_3\xi(((\sigma_2t_9q_3+q_7\gamma_1\sigma_1q_4q_5)q_2+\sigma_3\theta_4q_3q_4t_8)q_6+q_7\gamma_5\sigma_1\epsilon_3q_2q_4q_5).$$

From above, we express other variables in terms of E^*, which is difficult to adjust whether the variables are always positive or not. This study proves the existence of EE in Section SI.1.1.

Substituting Eq. (4.16), (4.8) and (4.9) into (4.6), we obtain

$$\lambda^* = \frac{\beta(a_1E_m^*+a_2I_a^*+a_3I_m^*)}{N^*}, \tag{4.17}$$

and

$$N^* = S^*+N_q^*+E_m^*+E_q^*+I_a^*+I_m^*+I_q^*+H_a^*+H_s^*+R^*. \tag{4.18}$$

Now, substituting the endemic equilibrium points (SI.1.1) and Eq. (4.17) into Eq. (4.18), we have

$$S^*+N_q^*+(1-\frac{\beta a_1}{\lambda^*})E_m^*+E_q^*+(1-\frac{\beta a_2}{\lambda^*})I_a^*+(1-\frac{\beta a_3}{\lambda^*})I_m^*+I_q^*+H_a^*+H_s^*+R^*=0. \tag{4.19}$$

Simplifying this equation may point towards the existence of the existence of the backward bifurcation phenomenon, which will be discussed in the subsequent section.

4.2.3.3 Backward Bifurcation Analysis

When the disease cannot develop into an epidemic, $\mathcal{R}_0$ is less than unity which is a necessary condition. In considering the possibility of the coexistence of stable DFE and EE, the backward bifurcation (BB) phenomenon is discussed in this section. Here, we simplify the Eq. (4.5) with " $\beta_1=\beta_2$", "$a_1=a_4$","$a_2=a_5$" and "$a_3=a_6$" as follows:

$$R_0 = R_{E_m}+R_{I_a}+R_{I_m}, \tag{4.20}$$

with

$$R_{E_m} = \beta(1+\theta_3)\,\frac{a_1}{q_3 q_4},$$
$$R_{I_a} = \beta(1+\theta_3)\,\frac{a_2\sigma_1}{q_1 q_3},$$
$$R_{I_m} = \beta(1+\theta_3)\,\frac{a_3\sigma_2}{q_1 q_4}.$$

Substituting Eq. (4.17) and (4.18) into Eq. (4.19),

$$C_4\lambda^{*4} + C_3\lambda^{*3} + C_2\lambda^{*2} + C_1\lambda^{*} + C_0 = 0, \tag{4.21}$$

where

$$\begin{aligned}
C_0 =& q_3(-\epsilon_2 t_4 q_4(\xi t_3\theta_1 + m_{N_q} q_0) + c_0(((((\theta_2+q_0)m_{N_q} + t_3(\xi\theta_1+q))q_2 - t_2(\xi t_3\theta_1 + m_{N_q} \\
& q_0))q_5 + t_2\sigma_3(\xi t_3\theta_1 + m_{N_q} q_0))t_4 - q_5 h_3 q_2(\xi m_{N_q}+1))q_4 q_7)q_6 A_0 + \frac{-B_1 q_2 q_5 q_6 q_7}{1+\theta_3}(q_3^2 q_4^2 R_{E_m} \\
& + q_1 q_3 q_4 R_{I_a} + q_1 q_3 q_4 R_{I_m}), \\
C_1 =& (-q_3 q_6 t_4 \epsilon_2 A_1 q_4(\xi t_3\theta_1 + m_{N_q} q_0) + \xi q_3 h_1(((q_2 - t_2)q_5 - t_2\sigma_3)q_7 - t_2\sigma_3)B_1 q_4 c_0 {q_6}^2 + \\
& (((((((((qh_1 + h_2(q+1))\xi + h_1(q\,q_0 - \theta_1\theta_2))B_1 + (\xi t_3\theta_1 A_1 + ((\theta_2+q_0)m_{N_q} + qt_3)A_1 \\
& + t_3\theta_3 A_0)t_4 - h_3 A_1(\xi m_{N_q}+1))c_0 + B_1 + (c_1 t_3\theta_1 A_0\xi + ((\theta_2+q_0)c_1 m_{N_q} + q c_1 t_3)A_0)t_4 \\
& - \xi A_0 c_1 h_3 m_{N_q} - A_0 c_1 h_3)q_2 - (h_2\xi B_1 + t_4 A_1(\xi t_3\theta_1 + m_{N_q} q_0))t_2 c_0 + B_1\theta_4 - t_2 t_4 A_0(\xi \\
& t_3\theta_1 + m_{N_q} q_0)c_1)q_5 + (((-\xi h_2 + \theta_4)B_1 + t_4 A_1(\xi t_3\theta_1 + m_{N_q} q_0))c_0 + t_4 A_0(\xi t_3\theta_1 + m_{N_q} \\
& q_0)c_1)t_2\sigma_3)q_7 - B_1 t_2\sigma_3 c_0(\xi h_2 - \theta_4))q_4 - q_2\sigma_2((-B_1 q_5 - \theta_5 B_1)q_7 - B_1(q_5\epsilon_1 + \theta_5\epsilon_2) \\
&))q_3 + q_2 q_4 q_5 q_7\sigma_1 B_1)q_6 + q_2 q_4 q_5 q_7\sigma_1\epsilon_3 B_1 + \frac{-B_2 q_2 q_5 q_6 q_7}{1+\theta_3}({q_3}^2 {q_4}^2 R_{E_m} + q_1 q_3 q_4 R_{I_a} \\
& + q_1 q_3 q_4 R_{I_m}), \\
C_2 =& -q_3 q_6 t_4 \epsilon_2 A_2 q_4(\xi t_3\theta_1 + m_{N_q} q_0) + (((q_2 - t_2)q_5 - t_2\sigma_3)q_7 - t_2\sigma_3)q_3\xi h_1 q_4(B_1 c_1 + B_2 c_0) \\
& {q_6}^2 + ((((((((((qh_1 + h_2(q+1))B_2 + A_2 t_3 t_4\theta_1 + \theta_3(h_1+h_2)B_1 - h_3 m_{N_q} A_2)c_0 + (A_1 t_3 t_4\theta_1 \\
& + (qh_1 + h_2(q+1))B_1 - h_3 m_{N_q} A_1)c_1)\xi + (h_1(qq_0 - \theta_1\theta_2)B_2 + (t_3\theta_3 A_1 + ((\theta_2+q_0)m_{N_q} + \\
& qt_3)A_2)t_4 + \theta_3 q_0 h_1 B_1 - h_3 A_2)c_0 + ((((\theta_2+q_0)m_{N_q} + qt_3)A_1 + t_3\theta_3 A_0)t_4 + h_1(qq_0 - \theta_1\theta_2) \\
& B_1 - h_3 A_1)c_1 + B_2)q_2 - ((A_2 t_3 t_4\theta_1 + B_2 h_2)c_0 + c_1(A_1 t_3 t_4\theta_1 + B_1 h_2))t_2\xi - c_1 t_2 t_4 m_{N_q} q_0 A_1 \\
& - t_2 t_4 m_{N_q} q_0 A_2 c_0 + B_2\theta_4)q_5 - \sigma_3 t_2(((-A_2 t_3 t_4\theta_1 + B_2 h_2)c_0 + c_1(-A_1 t_3 t_4\theta_1 + B_1 h_2))\xi + (- \\
& t_4 m_{N_q} q_0 A_2 - B_2\theta_4)c_0 - c_1(t_4 m_{N_q} q_0 A_1 + B_1\theta_4)))q_7 - t_2\sigma_3(\xi h_2 - \theta_4)(B_1 c_1 + B_2 c_0))q_4 + \\
& B_2((q_5+\theta_5)q_7 + q_5\epsilon_1 + \theta_5\epsilon_2)q_2\sigma_2)q_3 + q_2 q_4 q_5 q_7\sigma_1 B_2)q_6 + q_2 q_4 q_5 q_7\sigma_1\epsilon_3 B_2,
\end{aligned}$$

$$C_3 = (((((((((q+q_6)h_1+h_2(q+1))B_2+(t_3\theta_1t_4-h_3m_{N_q})A_2+\theta_3(h_1+h_2)B_1)\xi+h_1(qq_0-\theta_1\theta_2)$$
$$B_2+(((\theta_2+q_0)m_{N_q}+qt_3)t_4-h_3)A_2+\theta_3(A_1t_3t_4+B_1h_1q_0))q_2-(((h_1q_6+h_2)B_2+A_2t_3t_4$$
$$\theta_1)\xi+t_4m_{N_q}q_0A_2)t_2)q_5-(((h_1q_6+h_2)B_2-A_2t_3t_4\theta_1)\xi-t_4m_{N_q}q_0A_2-B_2\theta_4)\sigma_3t_2)c_1+\theta_3$$
$$q_2q_5(B_2(h_1+h_2)\xi+q_0h_1B_2+t_3t_4A_2)c_0)q_7-B_2((h_1q_6+h_2)\xi-\theta_4)\sigma_3c_1t_2)q_6q_4q_3,$$

and

$$C_4 = q_2(((\xi+q_0)h_1+\xi h_2)B_2+t_3t_4A_2)q_7q_5\theta_3q_3q_6c_1q_4.$$

To be more specific and discuss the possible of roots of Eq. (4.21), we used Descartes' rule of sign changes [73] and showed 32 possible results in Table 4.3.

Table 4.3: Number of possible positive real roots of Eq. (4.21)

Case	C_4	C_3	C_2	C_1	C_0	$\mathcal{R}_0$	**No. of possible changes**	**Positive Real Roots**
1	−	−	−	−	−	$\mathcal{R}_0>1$	0	0
2	−	+	+	+	+	$\mathcal{R}_0<1$	1	1
3	−	−	−	−	+	$\mathcal{R}_0<1$	1	1
4	−	−	−	+	+	$\mathcal{R}_0<1$	1	1
5	−	−	−	+	+	$\mathcal{R}_0<1$	1	1
6	−	−	+	+	+	$\mathcal{R}_0<1$	1	1
7	−	+	+	+	−	$\mathcal{R}_0>1$	2	0,2
8	−	+	−	−	−	$\mathcal{R}_0>1$	2	0,2
9	−	−	+	−	−	$\mathcal{R}_0>1$	2	0,2
10	−	−	−	+	−	$\mathcal{R}_0>1$	2	0,2
11	−	+	+	−	−	$\mathcal{R}_0>1$	2	0,2
12	−	−	+	+	−	$\mathcal{R}_0>1$	2	0,2
13	−	−	+	−	+	$\mathcal{R}_0<1$	3	1,3
14	−	+	+	−	+	$\mathcal{R}_0<1$	3	1,3
15	−	+	−	+	+	$\mathcal{R}_0<1$	3	1,3
16	−	+	−	+	−	$\mathcal{R}_0>1$	4	0,2,4
17	+	+	+	+	+	$\mathcal{R}_0<1$	0	0
18	+	+	+	+	−	$\mathcal{R}_0>1$	1	1
19	+	−	−	−	−	$\mathcal{R}_0>1$	1	1
20	+	+	−	−	−	$\mathcal{R}_0>1$	1	1
21	+	+	+	−	−	$\mathcal{R}_0>1$	1	1
22	+	−	−	−	+	$\mathcal{R}_0<1$	2	0,2
23	+	−	−	+	+	$\mathcal{R}_0<1$	2	0,2
24	+	−	−	+	+	$\mathcal{R}_0<1$	2	0,2
25	+	+	+	−	+	$\mathcal{R}_0<1$	2	0,2
26	+	+	−	+	+	$\mathcal{R}_0<1$	2	0,2
27	+	−	+	+	+	$\mathcal{R}_0<1$	2	0,2
28	+	−	+	−	−	$\mathcal{R}_0>1$	3	1,3
29	+	−	−	+	−	$\mathcal{R}_0>1$	3	1,3
30	+	+	−	+	−	$\mathcal{R}_0>1$	3	1,3
31	+	−	+	+	−	$\mathcal{R}_0>1$	3	1,3
32	+	−	+	−	+	$\mathcal{R}_0<1$	4	0,2,4

4.2.4 Fitting Analysis

We inputted into the model the data from 24 January to 31 October 2020 in Hong Kong by employing the Pearson's Chi-squared test and the least square method via **R** statistical software version 3.4.1 [186]. The demographic related data includes π as natural birth 225 and μ_H as the crude death rate 0.00003 [141]. The initial S_0 is set as 7,181,657 on 24th January 2020, which equals the summation of the net growth of inbound travellers [211], initial local population 7,520,800 [207] and released quarantined inbound travellers. With reference to the epidemic model in Eqns. (4.1) and local data, we assume m_N as zero since the number of inbound travellers without quarantine is unknown. All inbound travellers are assumed to follow quarantine rules since 24 January 2020. During the first 13 days, no quarantined visitor is released: $m_{N_q}(1) = \ldots = m_{N_q}(13) = 0$. All initial values of parameters are shown in Table 4.5.

The Hong Kong government announced a quarantine policy on 25 March 2020. All inbound travellers are required to quarantine for 14 days after arriving in Hong Kong. During quarantine, people are not allowed to have any close contact with others. If an inbound traveller becomes symptomatic, the traveller will be hospitalized by the government. If the latency period exceeds 14 days, the released quarantine people can still transmit the virus to others as asymptomatic infectious individuals; owing to the absence of symptoms, it is difficult to screen them from the public. As a result, the Hong Kong government has imposed various restrictions designed to reduce the risk of transmission among the whole population, such as one-meter social distancing [179], wearing masks, a ban on restaurant dining, and restrictions on the maximum number of people gathering. The proposed 'effective contact ratio' helps describe the degree of adherence to these restrictions among the public. Based on six types used by the Hong Kong government [63], we subdivide confirmed cases based on the infection sources and symptoms. Imported cases and cases epidemiologically linked with imported cases are from or caused by quarantined individuals. The other four types related to local cases are divided into asymptomatic or symptomatic cases. Infection control policies enacted by the Hong Kong government are indicated in Figure 4.4.

4.3 Results

4.3.1 Modelling

A modified compartmental model is developed to overcome the limitations of only considering well-mixed homogeneous populations in the previous well-established compartment model.

The newly proposed model can divide the population into ten groups based on transmission characteristics (shown in Figure 4.1). An individual may progress from being susceptible (S) to being exposed (E_m) to being asymptomatic/symptomatic (I_a or I_m) to being hospitalized (H_a or H_s) to having recovered (R), and can be quarantined while being susceptible (N_q), exposed (E_q) or infectious (I_q). Pre-symptomatic, symptomatic and asymptomatic individuals are all contagious to susceptible individuals under effective contact, i.e., when an already infected individual is in contact with another individual who thus may become infected as well. In our model, the duration of the transmission spans from being pre-symptomatic to being hospitalized. The amount of virus in the bodies of infected individuals during incubation increases over several days (which is assumed in our study to be three days) before symptom onset [87]. It is often not easy to study the transmission onset time, as it is difficult to know who infected whom exactly when. This study assumed that each exposed individual was pre-symptomatic and contagious. Due to a lack of symptoms, both exposed individuals E_m and asymptomatic infectious individuals I_a may come in contact with both susceptible individuals with (N_q) and without (S) quarantine through outside movement, in household settings, or during provision of daily necessities by volunteers. The force of infection, which is the rate at which individuals become infected per unit time [88], is shown in Eqns. (4.2). Each COVID-19 confirmed case can continue to shed the virus to others up to and including during hospitalized. Owing to reinfection [204] and virus mutations [37], an infected individual's convalescence period may end without lifelong immunity—a recovered individual transfer from R to S by a reinfection rate xi. Considering that many countries suffered from several waves due to imported cases and frequent virus mutations, and that COVID-19 might become a seasonal disease [151], the proposed model is designed with a dynamic population by natural birth and death, mortality from COVID-19, and cross-boundary (in and out of a given territory or country) human mobility.

4.3.2 Mathematical Analysis

4.3.2.1 Steady States

Disease extinction and persistence [140] are determined by the stability of the disease-free equilibrium (DFE) and the endemic equilibrium (EE) of the model (4.1). Under the locally asymptotical stability in this system (i.e., DFE), applying the next-generation method [227] to the equations in the model (4.1) (see Section 4.2.3.1), the basic reproduction number $\mathcal{R}_0$ (i.e., the average number of secondary cases caused by each infectious individual) in Eq. (4.5) is contributed by three groups ($\mathcal{R}_0 = R_{E_m} + R_{I_m} + R_{I_a}$). The interpretation of $\mathcal{R}_0$ is shown in Table 4.4.

To be more specific, $R_{E_m} = (a_4\beta_2\theta_3 + a_1\beta_1)/q_1$, which is caused by exposed individuals with outside movement, $R_{I_m} = (a_6\beta_2\theta_3 + a_3\beta_1)\sigma_2/q_1q_4$, which is caused by symptomatic infectious individuals with outside movement, and $R_{I_a} = (a_5\beta_2\theta_3 + a_2\beta_1)\,\sigma_1/q_1q_3$, which is caused by asymptomatic individuals with outside movement, can be explained by the force of infection Eqns. (4.2).

Table 4.4: Interpretation of the basic reproduction number R_0

Section	Equation	Interpretation
R_{E_m}	$\frac{a_4\beta_2\theta_3+a_1\beta_1}{q_1}$	Numerator: the infections produced by E_m; Denominator: the population transferring out of E_m.
R_{I_m}	$\frac{(a_6\beta_2\theta_3+a_3\beta_1)\,\sigma_2}{q_1q_4}$	$a_6\beta_2\theta_3 + a_3\beta_1$: the infections produced by I_m; σ_2/q_1q_4: the net population left in I_m among population from E_m .
R_{I_a}	$\frac{(a_5\beta_2\theta_3+a_2\beta_1)\,\sigma_1}{q_1q_3}$	$a_5\beta_2\theta_3 + a_2\beta_1$: the infections produced by I_a; σ_1/q_1q_3: the net population left in I_a among population from E_m.

The pandemic is still evolving with several resurgences globally. The possible coexistence of DFE with a stable EE is explored. A global asymptotic stability exists, which corresponds to positive solutions to Eq. (4.19) (proven in SI.1.1). The backward bifurcation (BB) phenomenon has been shown to exist when the classical epidemiological requirement of having $\mathcal{R}_0 < 1$ is no longer sufficient for effective control of COVID-19 infections. Substituting the force of infection Eq. (4.17) and global asymptotically points (in SI.1.1) into the total population at EE Eq. (4.18), there are 32 scenarios that reflects the plausibility of BB phenomenon (see Table 4.3).

4.3.2.2 Sensitivity Analysis

Sensitivity analysis was conducted to explore the impacts of the mutations in infectiousness, gathering restrictions, and quarantine policies on the dynamical system described in the model (4.1). The basic reproduction number $\mathcal{R}_0$, also known as a threshold quantity, is used to assess whether the disease can spread or will die out, though it is not the only factor. Meanwhile, the severity of an outbreak is reflected by the infection attack rate [243]. This paper used Partial Rank Correlation Coefficients (PRCCs) [68] to investigate the impacts of each parameter on the overall dynamics, with $\mathcal{R}_0$ and the infection attack rate as response functions (see Figure 4.2). Furthermore, using the tool SimBiology in MATLAB [216], this paper adopted a global sensitivity analysis (shown in Figure 4.3) between parameters and variables related to the force of infection (i.e., E_m, I_a and I_m).

In Figure 4.2, the outputs include the basic reproduction number $\mathcal{R}_0$ (i.e., an epidemiologically key parameter for determining whether the disease will persist) and the infection attack rate (i.e.,

the severity of an outbreak). The results of the analysis show that four parameters are most significant in their sensitivity:β_1, β_2, θ_3 and a_6. The transmission rate among susceptible people β_1 and transfer rate θ_3 from quarantined people N_q to exposed individuals with outside movement E_m ranked as the most sensitive parameters. The transmission rate β_2 among quarantined people, which significant, is less sensitive than that among susceptible people (i.e., β_1). The effective contact ratio a_6 between asymptomatic infectious individuals I_a and quarantined individuals N_q is the most sensitive parameter among all effective contact ratios. The four significant parameters should especially be taken into consideration by decision-makers in designing and enacting measures for timely and effective infection control.

In Figure 4.3, transmission rate β_1 is more sensitive to three outputs (i.e., E_m, I_m and I_a) than β_2. When any mutated variant attacks susceptible people in the absence of restrictions on movement, its transmission risk will be almost double that of quarantined people. Exposed individuals E_m is the most sensitive group among all infectors. Effective contact ratio a_1 between E_m and S ranked as having the most significant effect on the outputs. Meanwhile, all effective contact ratios $(a_1, ..., a_6)$ have a greater impact on E_m compared to the other two outputs I_m and I_a. In addition, E_m is also affected by transfer rates between disease status compartments (i.e., θ_1, θ_4, $\theta_6 = 1 - \theta_2 - \theta_3$), thus E_m implicitly indicates the effectiveness of quarantine policies. Recovery rate γ_4 of hospitalized symptomatic individuals H_s shows significant impacts on all outputs, especially E_m. The hospitalization rates of I_q (i.e., ϵ_2) and I_a (i.e., ϵ_3) both show an obvious sensitivity to themselves (i.e., I_q or I_a) respectively. As shown in 4.3(f), the sharp increase in the infected population might be triggered by the influx of inbound travellers who do not quarantine. A quarantine policy for cross-boundary travellers is still suggested.

4.3.3 Fitting Results

This study used time-series data on confirmed COVID-19 cases [63] and data on cross-boundary travellers [211] in Hong Kong to populate the proposed model. Table 4.5 provides the descriptions, the initial values, and ranges for each parameter according to reasonable assumptions and previous studies [33, 127, 141, 230]. Demographic information on the studied population is shown in Table 4.1. Policy stringency index scores [82], specific policies implemented at each inflexion point, and the number of new daily cases from 24th January to 4th December 2020 are compared in Figure 4.4. The full Eqns. in the model (4.1) are fitted to symptomatic cases with outside movement I_m as shown in Figure 4.5. The "R-squared" R^2 ranges from 0.69 to 0.98, specifically 0.82 (Phase 1: 24th Jan.-24th Mar.), 0.96 (Phase 2: 25th May.-19th Jul.), 0.98 (Phase

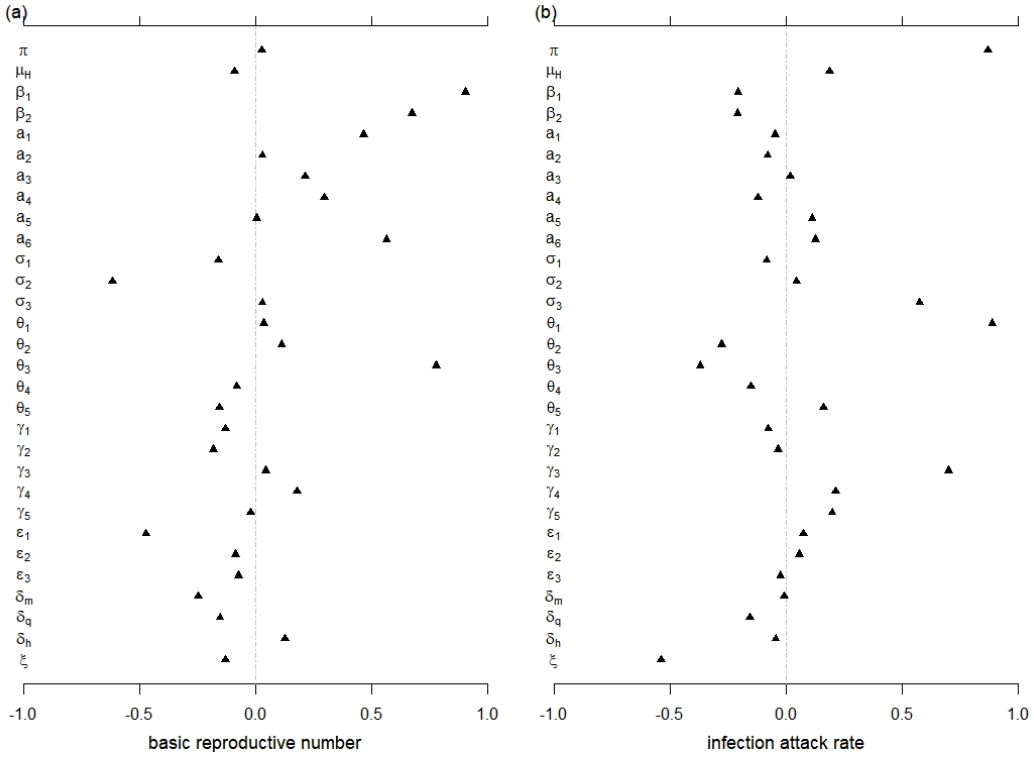

(a)

Figure 4.2: The partial rank correlation coefficient (PRCC) of the basic reproduction number $\mathcal{R}_0$ and infection attack rate with respect to model parameters.

3: 20th Jul.-29th Jul.) and 0.69 (Phase 4: 30th Jul.-31st Oct.) respectively. Model simulations well fitted both the cumulative and daily data. After the quarantine policy was announced on 24th March 2020, the government relaxed, then tightened, then once again relaxed gathering restrictions on 29th May, 19th July and 11st September 2020, respectively. This study separated the study period (282 days) into four subsections because the pandemic in Hong Kong occurred in four waves. At the same time, the government adjusted gathering restrictions or/and quarantine rules every time the daily confirmed cases increased significantly, as shown in Figure 4.4. All data can be found on GitHub [254] and all initial values of variables and estimated parameters (i.e., a_1-a_5, β_1, $beta_2$ and θ_3) are shown in SI.1.2.

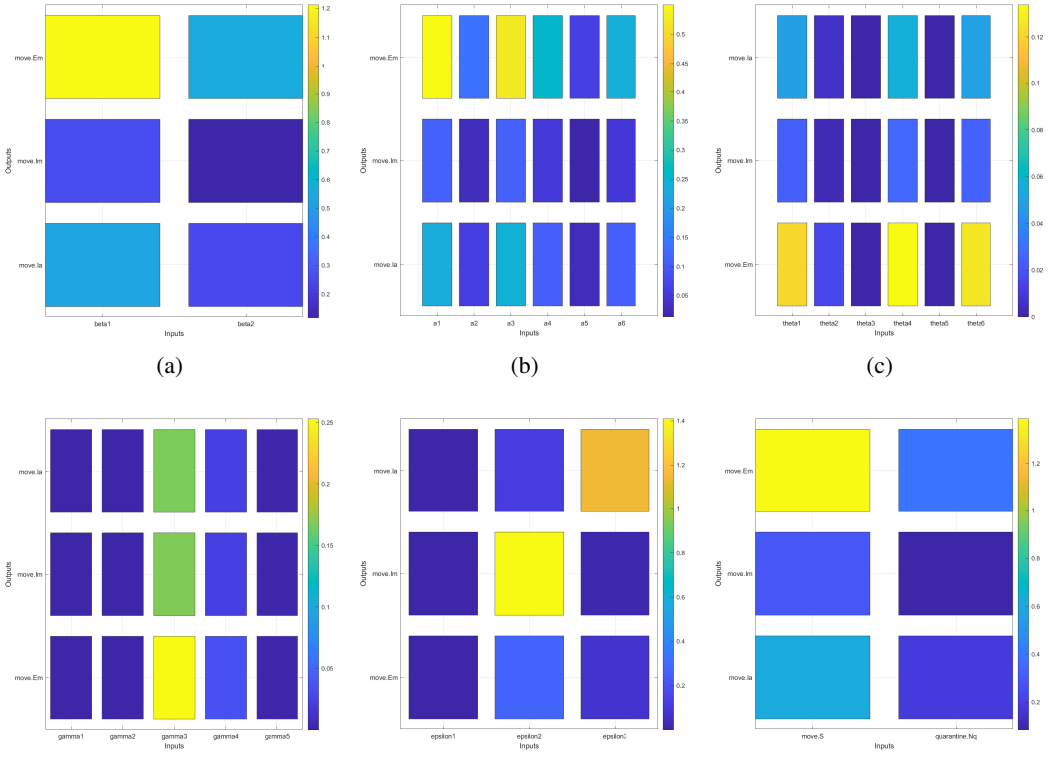

(a) (b) (c)

(d) (e) (f)

Figure 4.3: Global sensitivity analysis. Inputs: (a) transmission rate (β_1 and β_2), (b)effective contact ratio (a_1-a_6), (c) transition rate [θ_1-θ_5 and $\theta_6 = (1-\theta_2-\theta_3)$], (d) recovery rate (γ_1-γ_5), (e) hospitalized rate (ϵ_1-ϵ_3), and (f) population size (S and N_q). Output: exposed individuals with outside movement (E_m), symptomatic infectious individuals (I_m) and asymptomatic infectious individuals (I_a).

Table 4.5: Parameter descriptions and values

Parameter	Description	Initial Value	Range	Citation
π	the number of new natural births	225	100, 1000	[141]
μ_H	the number of inbound travellers without quarantine	0.00003	0.00001, 0.00005	[141]
β_1	transmission rate contributed by the disease among S	0.745	0.36, 1.2	[127]
β_2	transmission rate contributed by the disease among N_q	0.745	0.54, 1.7	[127]
a_1	the effective contact ratio between E_m and S	0.18	0.11, 0.18	estimated from [33] and [230]
a_2	the effective contact ratio between I_a and S	0.12	0.05, 0.17	estimated from [33] and [230]
a_3	the effective contact ratio between I_m and S	0.15	0.1, 0.19	estimated from [33] and [230]
a_4	the effective contact ratio between E_m and N_q	0.13	0.05, 0.18	estimated from [33] and [230]
a_5	the effective contact ratio between I_a and N_q	0.09	0.09, 0.16	estimated from [33] and [230]
a_6	the effective contact ratio between I_m and N_q	0	0, 1	assumed
θ_1	The rate of susceptible individuals who self-quarantined according to the strict policy.	0.069	0.01, 0.18	validated
θ_2	The rate of quarantined individuals who remain susceptible after 14-day quarantine observation period and return back to the susceptible group.	0.084	0.002, 0.1	validated
θ_3	The rate of quarantined individuals who have been infected during the quarantine period and show the symptoms after the quarantine.	0.44	0.075, 0.5	validated
θ_4	The rate of exposed individual with outside movement who has been quarantined.	0.084	0.002, 0.1	validated
θ_5	The rate of infectious individual with outside movement who has been quarantined.	0.09	0.001, 0.3	validated
σ_1	the transition rate from exposed to asymptomatic infectious status	0.025	0.001, 0.07	estimated from [33]
σ_2	the transition rate from exposed to symptomatic infectious status	0.187	0.1, 0.255	validated
σ_3	the transition rate from exposed to symptomatic infectious status under quarantine	0.289	0.1, 0.3	validated
ϵ_1	the hospitalization rate of asymptomatic infectious individuals	0.8	0.025, 0.95	assumed
ϵ_2	the hospitalization rate of symptomatic infectious individuals	0.85	0.05, 0.975	assumed
ϵ_3	the hospitalization rate of quarantined symptomatic infectious individuals	0.96	0.02, 0.99	assumed
γ_1	the rate of asymptomatic infectious individuals who recovered without hospitalization	0.008	0.01, 0.45	assumed
γ_2	the rate of symptomatic infectious individuals who recovered without hospitalization	0.133	0.0714, 0.3333	[33]
γ_3	the rate of quarantined symptomatic infectious individuals who recovered without hospitalization	0.134	0.0714, 0.3333	[33]
γ_4	the rate of symptomatic infectious individuals who recovered after treatment in the hospital	0.116	0.0714, 0.3333	validated
γ_5	the rate of asymptomatic infectious individuals who recovered after treatment in the hospital	0.005	0.001, 0.5	assumed
δ_m	the rate of death among symptomatic infectious individuals with outside movement I_m	0.1275	0.01, 0.345	assumed
δ_q	the rate of death among quarantined symptomatic infectious individuals I_q	0.1275	0.01, 0.345	assumed
δ_h	the rate of death among hospitalized symptomatic infectious individuals H_s	0.1275	0.01, 0.345	assumed
ξ	the rate of reinfection based on no lifelong immunity	0.0001	0, 1	assumed

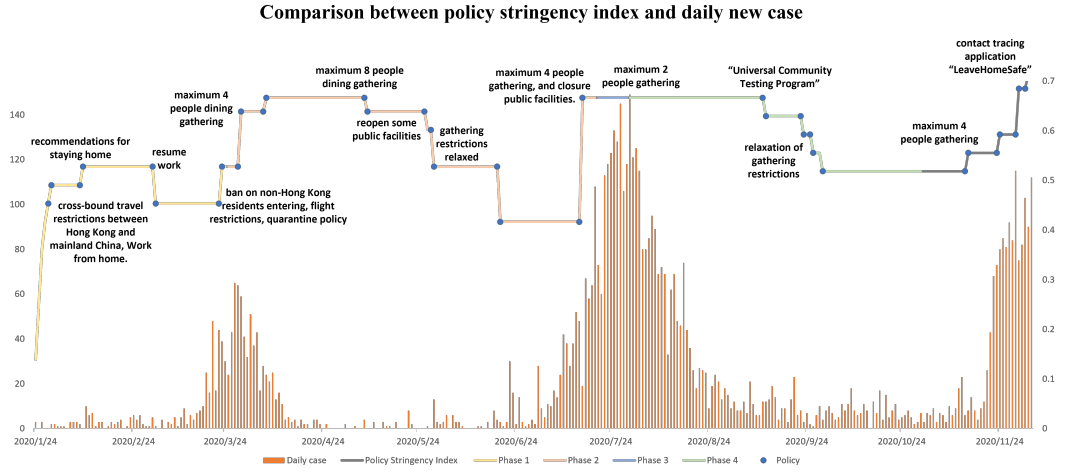

Figure 4.4: Comparison between policy stringency index scores [82] and daily new cases [63] from 24th January to 4th December 2020. Yellow, orange, blue and green lines represent the periods from January 24 to March 24, from May 25 to July 19, from July 20 to 29, and from July 30 to October 30 respectively. Blue points show each inflection point of the grey line (policy stringency index).

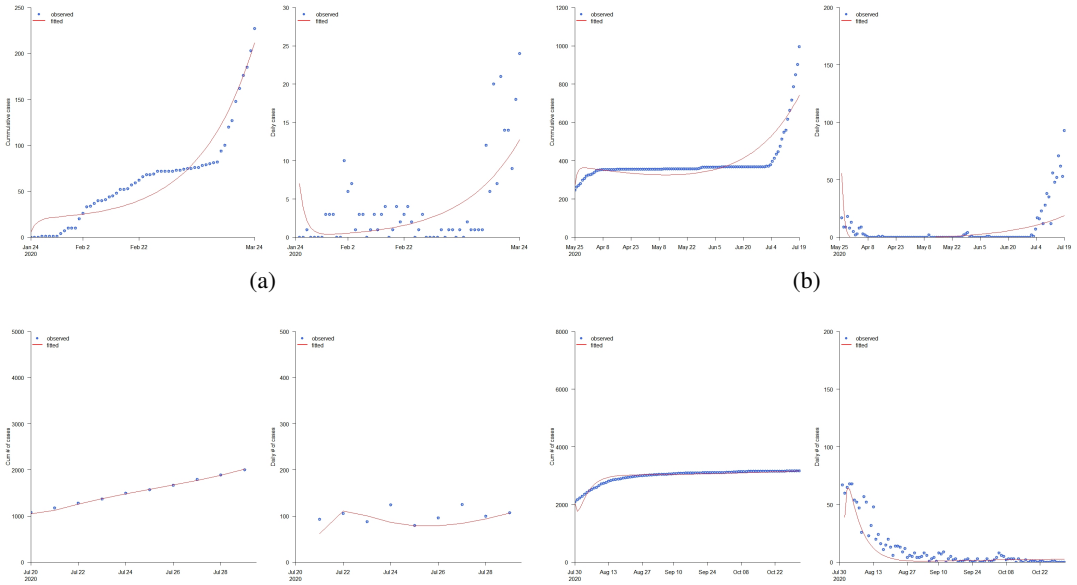

Figure 4.5: Fitting results: (a) Jan. 24 to Mar. 24, (b) Mar. 25 to Jul. 19, (c) Jul. 20 to Jul. 29, and (d) Jul. 30 to Oct. 31.

4.3.3.1 Effective Contact Ratio

Individuals are highly likely to get infected by other pre-symptomatic, asymptomatic or symptomatic individuals through effective contact. Some large-scale studies indicate that greater human mobility may lead to higher infection probability [127, 150], but these studies have failed to assess the influence of this mobility on a heterogeneous population from both epidemiology

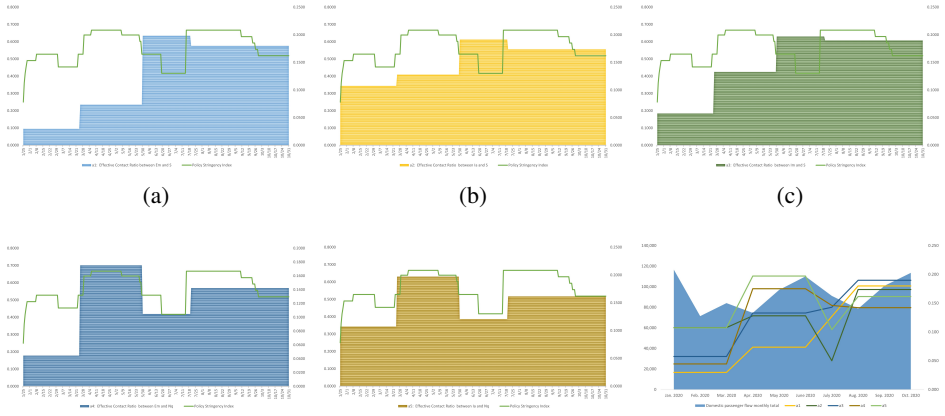

(a) (b) (c)

(d) (e) (f)

Figure 4.6: Comparison between policy stringency index scores and effective contact ratios from Jan. 25 to Oct. 31 in 2020: (a) a_1 effective contact ratio between E_m and S, (b) a_2 effective contact ratio between I_m and S, (c) a_3 effective contact ratio between I_a and S, (d) a_4 effective contact ratio between E_m and N_q, (e) a_5 effective contact ratio between I_m and N_q and (f) comparison between domestic Mass Transit Railway (MTR) passengers flow and effective contact ratios [213].

and policy perspectives. This study explored the effective contact between different groups based on the proposed model.

In Figure 4.6, all effective contact ratios (i.e., $a_1 - a_5$) were at the lowest level before March 2020. After quarantine rules were announced in March 2020, the daily number of cross-boundary travellers gradually decreased from 228 to 1 on average [213]. Two effective contact ratios (i.e., a_4 and a_5) related to quarantined people did not decrease, suggesting that quarantined people may become infected during the quarantine. Meanwhile, when the transfer rate θ_3 from N_q to E_m grew, the severity of infections during the quarantine became more serious. Owing to the relaxation of gathering restrictions during the gap between the second and third wave, a_1, a_2 and a_3 increased by 0.1245, 0.0632, and 0.0639, respectively. a_4 and a_5 decreased by 0.0703 and 0.0763 due to tighter quarantine restrictions. When the third wave came and peaked in mid-July, a restaurant dine-in ban after 6 pm did not curb gatherings among citizens or mitigate the ongoing wave. One week later on 29th July, a stricter gathering restriction was announced and decreased a_1, a_2 and a_3 by 8% on average. Meanwhile, a_4 and a_5 increased by 25% in total. Compared to the effective contact ratios in March, all effective contact ratios had a twofold increase even with the implementation of stricter measures, and domestic passenger flows increased as well in late July 2020.

4.4 Discussion

The modified SEIHR model (4.1) describes the transmission dynamics of SARS-CoV-2 by incorporating heterogeneous effective contact ratios between different groups. Via mathematical analysis, we computed the basic reproduction number, $\mathcal{R}_0$ (which determines whether the disease persists or dies out) and stability of equilibria. We find that the model exhibits the phenomenon of backward bifurcation, which increases the difficulty of SARS-CoV-2 control since the dynamics do not depend solely on $\mathcal{R}_0$. The existence of a BB means that when a stable endemic equilibrium co-exists with a stable disease-free equilibrium, even if the basic reproduction number is less than unity, the disease may persist. The epidemiological consequence of the backward bifurcation phenomenon makes the controlling or eliminating the disease more difficult. Potential epidemiological mechanisms of continued transmission may include exogenous re-infection as frequently observed for COVID-19 and imperfect vaccine efficacy due to virus mutations [81]. These and other possible mechanisms require further study.

The main impact factors of $\mathcal{R}_0$ shown in Eq.(4.5) are effective contact ratios a_1, a_2 and a_3 controlled by gathering restrictions, and effectiveness contact ratios between quarantined inbound travellers and infectious individuals outside (i.e., a_4 and a_5) and the transition rate θ_3 from N_q to I_m which reflect potential infection during quarantine. This study assumed the effective contact ratio a_6 between I_m and N_q to be zero since people visiting N_q are assumed to be without symptoms. In Figure 4.2, a_6 showed high sensitivity to $\mathcal{R}_0$ and the infection attack rate, a result that indicates the contact between I_m and N_q should be emphasised for overall control. As for quarantined individuals, incomplete adherence to quarantine recommendations could potentially accelerate and prolong infectious disease outbreaks. Transition rate θ_3 was validated to be greater than zero, which confirms the existence of infections during quarantine. There are at least two transmission links. Some inbound travellers are susceptible before being quarantined and get infected by their close contacts. In addition, inbound travellers still have the possibility of infecting their close contacts due to the high frequency of secondary infections from imported cases [63]. Given the lesson from Australia [214], if any infection is passed from quarantined individuals to their close contacts, the virus may spread into the community, resulting in an outbreak.

Additional evidence of infections possibly occurring during quarantine includes the increases in a_4 and a_5 in late March and late July 2020. A higher effective contact ratio increases the possibility of shedding the virus in the population and infecting others. Up until the end of July

2020, the policy stringency index score is almost 2 times higher than that in late January 2020 [82]. Contrary to the expected change shown in Figure 4.6, even the best performance, i.e., the effective contact ratio a_1 between E_m and S, increased by 0.15 in total. Owing to no symptoms and delayed recognition by decision makers of the relative transmissibility of asymptomatic infection, effective contact ratios related to I_a indicate low adherence to gathering restrictions, exhibiting the second highest increase of all the effective contact ratios between January and October 2020.

After implementing a stricter restriction, a_1, a_2 and a_3 decreased only 8% on average while the third wave reached its peak. After gathering restrictions were relaxed in September 2020 to allow a maximum of four people together, the effective contact ratios, with an average increase of 0.0475, were approximately six times greater than that in July 2020. The synchronized effective contact ratio didn't change with the stringency of gathering restrictions. This implies that people practiced lower and lower adherence to policies. Hong Kong may have experienced pandemic fatigue in their populations in July 2020, with the most severe resurgence occurring in September 2020.

The occurrence of backward bifurcation, infection during quarantine, and pandemic fatigue may be reasons why Hong Kong experienced multiple waves of infection during the COVID-19 pandemic. Pandemic fatigue was expressed through an increasing number of people not sufficiently following recommendations and restrictions, as reflected in effective contact ratios. Already infected individuals who volunteer to provide daily necessities to quarantined individuals may, despite the very quarantine policy, infect the quarantined individuals who, after quarantine and when initially asymptomatic, interact with and infect other community members, triggering an outbreak. According to guidance from WHO [221], we need to apply more tailored measures to allow people to live their lives but reduce risks.

In February 2021, the Hong Kong government announced sewage tests for COVID-19 and promoted the "LeaveHomeSafe" mobile application to record citizens' social activities. With these measures in place, the government also implemented a policy such that if one or more new confirmed cases with unknown sources are found in buildings, or there are sewage samples that test positive and thus imply possible infection risks, the buildings will be included in a mandatory test notice [177]. The sewage tests detected nine infections in two blocks [217]. Using data collected through the "LeaveHomeSafe" application, the Hong Kong government was able to efficiently identify close contacts traceable to an infection cluster that occurred in

the K11 Musea shopping center [199]. More cross-cutting measures and their efficacy need to be explored. Finally, this study can be extended by examining the time-varying effective contact ratios using more detailed data, incorporating heterogeneous data to gain further insight on the contacts between different groups, and exploring more tailored policies and their efficacy.

4.5 Chapter Summary

Recurrent updates in NPIs aim to control successive waves of the COVID-19 but are often met with low adherence by the public. This chapter evaluated the effectiveness of gathering restrictions and quarantine policies based on a modified SEIHR model by incorporating cross-boundary travellers with or without quarantine to study the transmission dynamics of COVID-19 with data spanning a nine-month period during 2020 in Hong Kong. The asymptotic stability of equilibria reveals that the model exhibits the phenomenon of backward bifurcation, which in this study is a co-existence between a stable disease-free equilibrium (DFE) and an endemic equilibrium (EE). Even if the basic reproduction number ($\mathcal{R}_0$) is less than unity, this disease cannot be eliminated.

The effect of each parameter on the overall dynamics was assessed using Partial Rank Correlation Coefficients (PRCCs). Transmission rates (i.e., β_1 and β_2), effective contact ratio a_6 between symptomatic individuals and quarantined people, and transfer rate θ_3 related to infection during quarantine were identified to be the most sensitive parameters. The effective contact ratios between the infectors and susceptible individuals in late July were found to be over twice as high as that in March of 2020, reflecting pandemic fatigue and the potential existence of infection during quarantine. People showed a lower and lower adherence to macro-level NPIs in Hong Kong. Each industry should put effort into the investigation of its specific transmission patterns of COVID-19 and design its targeted response strategies.

Chapter 5

Transmission Patterns of COVID-19 in the Construction Industry in Hong Kong

5.1 Introduction

Pandemic fatigue is caused by macro-level NPIs (e.g., gathering restrictions), resulting in demotivation to follow recommended protective behaviors [221]. In addition, with the gradual relaxations of COVID-19 restrictions [142, 218], all of the above factors contributed to epidemic resurgences (i.e., repetitive outbreaks). Meanwhile, the uneven distribution of COVID-19 vaccination rates [206], insufficiency of vaccine efficacy, and frequent virus mutations [37, 110] hinder herd immunity globally. As a result, COVID-19 may likely persist and become a recurrent seasonal disease [151]. To recover the productivity of each industry but protect people from health crises, wide-ranging restrictions may not be feasible in the long run. Against this backdrop, more sector-specific and individual-level NPIs (e.g., face covering for certain work settings) may still be needed.

The different transmission patterns in each industry influence the effectiveness of anti-epidemic strategies. Understanding transmission patterns can help decision-makers take appropriate actions to reduce infection risks. For example, controlling airborne transmission has been regarded as part of an overall strategy to limit infection risk indoors [149] (e.g., in restaurants, hotels, hospitals, etc.). As people cannot wear masks while eating and drinking, the restaurant sector redesigned sitting arrangements [55] to alter contaminated airflow patterns between people. In a quarantine hotel, aerosols containing the virus can flow into the opposite room with the door open. Diagonal rooms are recommended for hotel guests to reduce the risk of door-to-door transmission [240]. The existing specialized ventilation systems of hospitals [43, 138], have reduced infection risk in hospital wards. During the pandemic, hospitals developed temporary triage systems [229] to reduce infection risk during patient consultations.

There is limited discussion on what the major specific transmission pattern is in the construction industry and how to align targeted NPIs to mitigate such transmission [5, 45, 98, 128]. Compared to other sectors, the construction industry has exhibited a higher vulnerability to COVID-19 infection. The unavoidable need for manual labour within a close proximity among construction

employees during work activities [255] and the prevalence of smoking among workers [169] increased the possibility of exposure to virus. Nearly five-fold hospitalization rate higher than that of other occupational categories [107] showed a greater number of severe and fatal outcomes from infection. Frequent COVID-19 cases have been found in the construction industry globally [e.g., Singapore[118], the United States[10], and Hong Kong [178]], although some specific NPIs have been in place (e.g., arranging each worker to a designated location for changing, resting, and dining [42], disinfecting construction sites [105], etc.). Due to a moderate stringency of policies in Hong Kong [159], the information on COVID-19 outbreaks is ideal for identifying a transmission relationship between each pair of confirmed cases. Therefore, this study aims to explore the transmission patterns in the construction industry by analyzing COVID-19 cases clusters associated with construction sites in Hong Kong, thereby providing key intelligence for more effective interventions and infectious disease control.

5.2 Methods

5.2.1 Data source and collection

We collected data on COVID-19 case clusters associated with construction sites, as publicly released by the Government of Hong Kong Special Administrative Region's Department of Health [178]. As of November 2021, there have been 12,369 confirmed cases of COVID-19 in Hong Kong, including 54 large clusters (those with 10 or more cases). A total of 5 COVID-19 case clusters sourced on construction sites consisting of 221 cases are identified, including construction sites at LOHAS Park/Kai Tak (74 cases), Tseung Kwan O-Lam Tin (TKO-LT) Tunnel (first and second clusters, 29 and 50 cases), a cluster related to the Central Kowloon route (Central Tunnel, 37 cases), and a construction site at the third runway of Hong Kong International Airport (31 cases). A list of all confirmed cases in each cluster is announced by the government. The transmission chain of each cluster is unclear. The demographic information, classification of the case ("Local case" [L] or "Epidemiologically linked with local case" [Epi-L]), symptom onset date, reported date, the residential address, and venues they visited 14 days before their symptom onset were collected. The only one local case in each cluster is regarded as the primary case (e.g., Case 0 in Fig.5.1(a)). Each case was identified by a unique identification number assigned by the local authority of disease surveillance, and thus their real-world identities were masked.

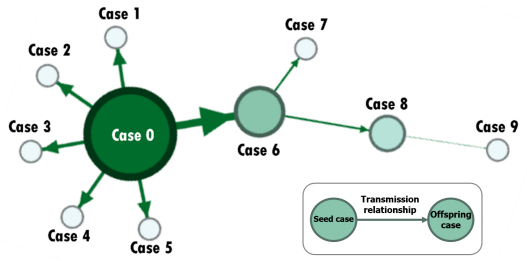

(a)

Case	Type	Symtom Onset	Report Date	Residential address	Visiting venues				Settings	Connectivity
					Place1	Date1	Place2	Date2		
0	L	Day1	Day2	RA 01	W 01	Day1	RA 01	Day1-3	Workplace	both spatial and temporal connectivity
1	Epi-L	Day2	Day2	RA 02	W 01	Day1			Workplace	both spatial and temporal connectivity
2	Epi-L	Asymptomatic	Day3	RA 03	W 01	Day1			Workplace	both spatial and temporal connectivity
3	Epi-L	Day2	Day3	RA 04	W 01	Day1			Workplace	both spatial and temporal connectivity
4	Epi-L	Asymptomatic	Day3	RA 05	W 01	Day1			Workplace	both spatial and temporal connectivity
5	Epi-L	Day3	Day4	RA 06	W 01	Day1			Workplace	both spatial and temporal connectivity
6	Epi-L	Asymptomatic	Day6	RA 01	PP 01	Day2	PP 02	Day4	Household	both spatial and temporal connectivity
7	Epi-L	Asymptomatic	Day7	RA 07	PP 01	Day3			Social activities	temporal connectivity
8	Epi-L	Asymptomatic	Day8	RA 08	PP 02	Day4			Social activities	both spatial and temporal connectivity
9	Epi-L	Day3	Day9	RA 09	PP 03	Day1			Social activities	spatial connectivity

(b)

Figure 5.1: (a) Hypothesis transmission network based on the hypothesis information in Fig.1b: the arrow means the transmission relationship from an infector (i.e., seed case) to an infectee (i.e., offspring case). The transmission chain: case 0 is the primary case which infected 6 cases (i.e., case 1-6); case 6 infected 2 cases (i.e., case 7-8); and case 8 infected case 9. If the number of secondary cases is larger, the node is with deeper color and a larger size. If the weight of the edge (i.e., the transmission possibility under the setting) is with deeper color and becomes wider. (b)Collected data with hypothesis information for the transmission network in Fig.1a: "W"="Workplace", "RA"="Residential address", and "PP"="Public place". Notes: Case 6 is the only confirmed case that visited "PP 01" and "RA 08" and "RA 09" are close to each other.

5.2.2 Transmission patterns

This study used a spatiotemporal connectivity analysis [132], which is part of a retrospective cohort study [144], to identify the transmission relationship between each pair of confirmed cases. Figure 5.1 presents a diagram of the process. According to available data, the onset dates of asymptomatic infectious individuals, owing to no symptoms, are estimated according to when they contacted an infector directly or indirectly. In Fig.5.1(b), the onset date of Case 2 is assumed to be "Day1" when Case 2 met Case 0 at the workplace "W1". When the onset date of a second case was within 14 days [178] after the onset date of the first case with the same or close visiting venues, the transmission relationship between the first and second cases is characterized by temporal connectivity shown as indicated with Cases 6 and 7 in Fig.5.1(b). People who visited the same or a nearby building on different dates but within 14 days before their symptom onset are referred to as spatially connected cases, indicated for Cases 8 and 9 in Fig.5.1(b). Residential addresses "RA 08" and "RA 09" are assumed to be located nearby. When the first and second cases visited the same place on the same date, they are connected by

the spatial and temporal connectivity, such as for Cases 0 and 6 in Fig.5.1(b). The categories for the spatial connectivity of these cases include workplace, household, and social activities, on the basis of the type of activities most closely associated with the venues where the source cases were identified [48]. When there is more than one seed case (which infected offspring cases) generated due to temporal connectivity, the case that is also associated with the spatial connectivity will be regarded as the seed case of the offspring case (the individual who gets infected by the seed case). The priority of sources in determining the transmission relationship between each pair of confirmed cases is as follows: both spatial and temporal connectivity, only spatial, and only temporal connectivity.

Illustrations of the transmission networks were created by Gephi (version 0.9.2) [25], as shown in Fig.5.2(a). Each node represents a COVID-19 confirmed case associated with construction sites as reported by the Hong Kong government [178]. The directed graph is determined by the spatial and/or temporal connectivity of any two nodes. Each network is rooted from the primary case (i.e., the first case in each cluster) labeled as cases 6346, 7139, 8955, 9152, and 9928 according to the official COVID-19 surveillance system in Hong Kong. All offspring cases are classified into five generations. The difference between the first-, second-, third-, fourth-, and fifth-generation spreaders mainly lies in the distance (the number of interval generations) between the generation where the spreader (an infected person) was located and the primary case of each cluster [92]. The weight of each edge represents the possibility of exposure under different environments, ranging from 0 to 1, which is set based on the secondary attack rates in light of certain data regarding the place of contact between different groups. The household secondary attack rates for contacts who were spouses, other adult members, or children were 27.8%, 17.3%, 4%, respectively [120]. Assuming that a single primary case generated all confirmed cases on the construction site through brief exposure events (e.g., dining or smoking), the secondary attack rate among close contacts was inferred to be 35% [131]. In our model, the secondary attack rate of close contact excluding home settings and co-worker proximity was assumed to be 11.3% [3].

The transmission network of all nodes is ranked by the number of degrees, i.e., the number of connections it has to other nodes. We calculated the basic properties of each network (as shown in Table. 5.1), including average degree, average weighted degree, graph density, modularity, average path length, and centrality. Average degree is the average number of edges per node in the graph, and average weighted degree is the average sum of weights of the edges of nodes. By comparing average degree and average weighted degree, we quantify the closeness of the

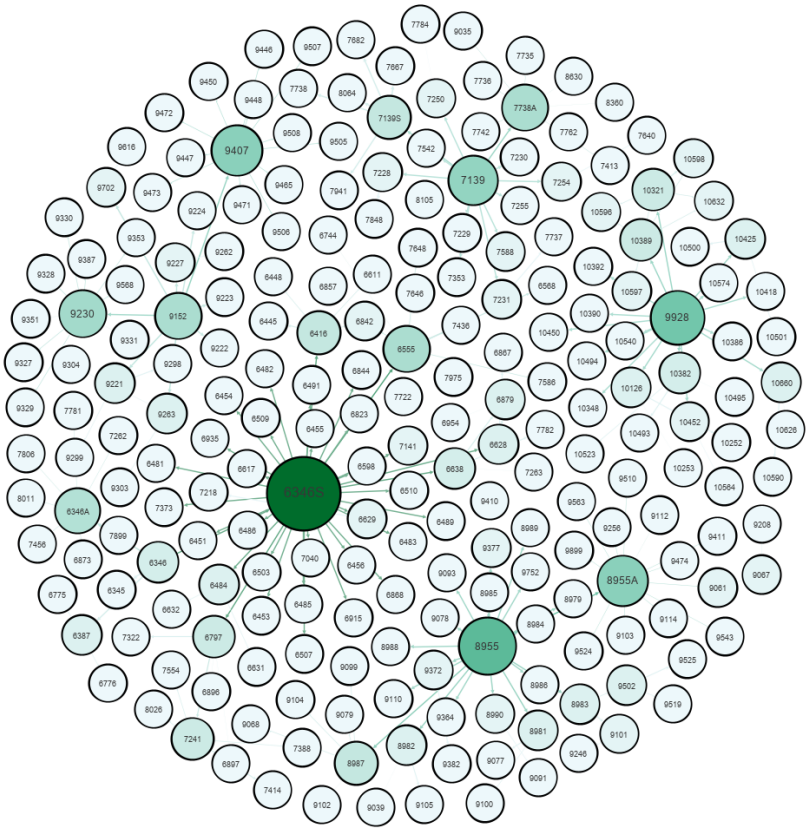

(a)

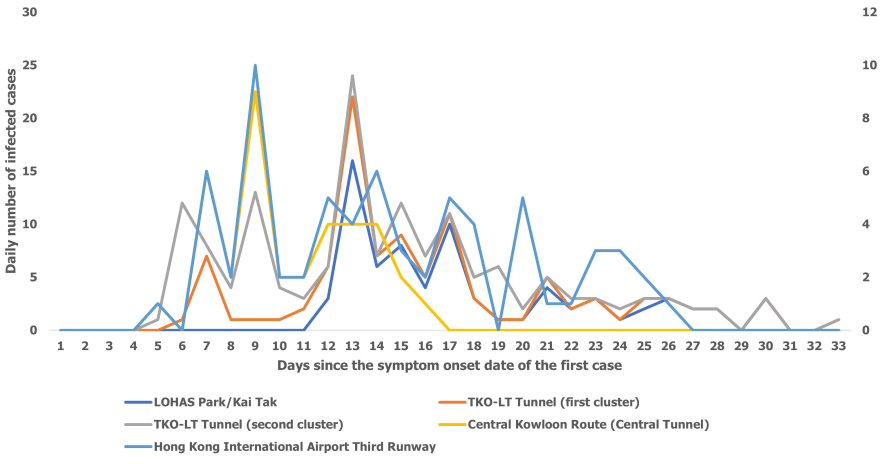

(b)

Figure 5.2: (a) Transmission network: nodes with deeper color and bigger size have higher degrees of transmission (i.e., the number of secondary cases) and edges with deeper color have higher weights (i.e., the possibility of transmission); (b) Daily number of reported cases since the symptom onset date of the first case in each cluster.

relationship between the primary case and offspring cases. Graph density measures how close the network is to complete. Modularity measures the strength of the division of a network into modules. Networks with high modularity have dense connections between the nodes within modules but sparse connections between nodes in different modules. The average path length is the average number of steps along the shortest paths for all possible pairs of network nodes, which measures the efficiency of epidemic diffusion in each cluster. The network structure was characterized by network centrality indices, which encompasses where each node is placed within a weighted network, e.g., betweenness centrality $C_B(v)$ and closeness centrality $C_C(v)$ of a node v.

Table 5.1: Basic properties of each network

ID	Average Degree	Avg. Weighted Degree	Graph Density	Modularity	Avg. Path Length
LOHAS Park/Kai Tak	1.013	0.254	0.014	0.463	1.792
TKO-LT Tunnel (first cluster)	1.097	0.279	0.037	0.372	1.292
TKO-LT Tunnel (second cluster)	0.973	0.205	0.027	0.522	1.429
Central Kowloon Route (Central Tunnel)	0.938	0.235	0.030	0.495	1.302
Hong Kong International Airport Third Runway	0.980	0.220	0.020	0.468	1.506
Five clusters	1.004	0.240	0.004	0.806	1.578

$$C_B(v) = \sum_{s \neq v \neq t \in V} \frac{\sigma_{st}(v)}{\sigma_{st}} \tag{5.1}$$

$$C_C(v) = \frac{1}{\sum_{v \neq u \in V} d(v,u)} \tag{5.2}$$

where V is the set of all nodes, σ_{st} is the number of the shortest paths between nodes s and t, $\sigma_{st}(v)$ is the number of the shortest paths between nodes s and t through node v, and $d(v,u)$ is the distance between u and v.

Indicators of centrality assign numbers or rankings to nodes within a graph corresponding to their network position, identifying the most influential person(s) in the network, namely, super-spreaders of this disease. Specifically, closeness centrality is intended to evaluate the average distance from one node to each other node and measures how close the case is linked to other cases [233]. Betweenness centrality is the number of times that the shortest path between any

two nodes passes through another node and measures the importance of the case in linking to other cases [233].

5.2.3 Distribution of offspring cases

To classify all offspring cases into different generations, the serial interval of COVID-19 is set as 6 days [1, 8] in this study. The serial interval refers to the time interval from illness onset in a primary case (i.e., an infector) to the onset of a secondary case (i.e., infectee) [60]. People whose symptom onset date is within 6 days after the symptom onset date of the primary case are identified as the first generation. In the chronological order of their symptom onset date, the offspring cases in the k^{th} generation are secondary cases caused by one infectious individual in the $(k-1)^{th}$ generation via direct or indirect contacts. The number of offspring cases in each generation is shown in Fig.5.3(a).

The severity of an outbreak is described by attack rate as shown in Eq. (5.3). The attack rates caused by each setting in each cluster are shown in Fig.5.3(b)-5.3(f). The case terminal to the inferred chain of transmission and sporadic cases were considered to have zero secondary cases. The distribution of the area in which a confirmed case was located was collected using ArcGIS Online Map Viewer Classic; this information describes the spatial transmission in Fig. 5.4. To explore the significance of controlling the super-spreading events, the super-spreading threshold is defined as 4, 5, or 6 secondary cases of each seed case, according to 90%, 95%, or 99% percentile of a Poisson distribution with the reproduction number of 2 [1]. As such, we estimated the betweenness centrality $C_B(v)$ and closeness centrality $C_C(v)$ of each node v to identify the super spreader candidates (illustrated in Fig.5.5).

$$\text{attack rate} = \frac{\text{the number of infected cases}}{\text{the initial number of susceptible individuals}} \tag{5.3}$$

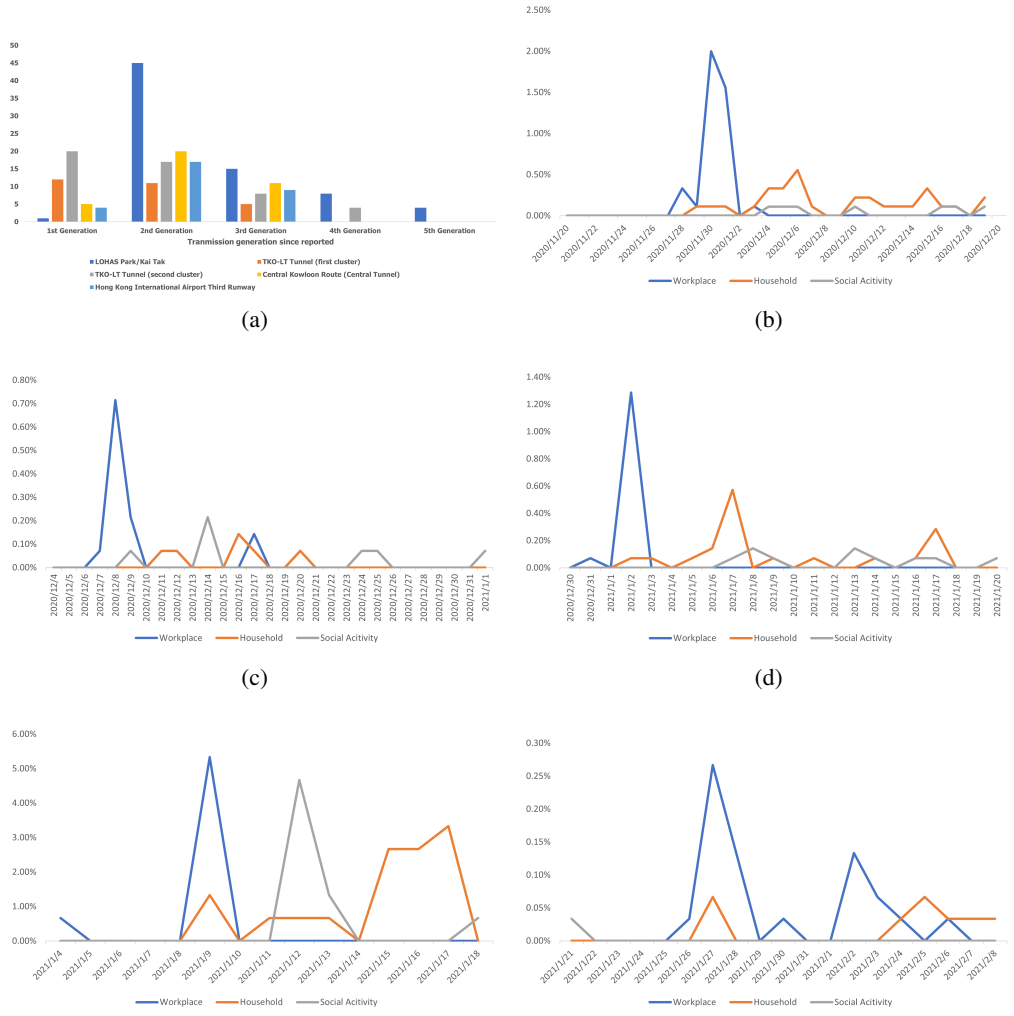

(a) (b)

(c) (d)

(e) (f)

Figure 5.3: (a) The number of offspring cases in each generation; Attack rate caused by workplace, household, and social activities in each cluster: (b) cluster at LOHAS Park/Kai Tak; (c) the first cluster at the TKO-LT Tunnel; (d) the second cluster at the TKO-LT Tunnel; (e) cluster at the Central Kowloon Route (Central Tunnel); and (f) cluster at Hong Kong International Airport Third Runway.

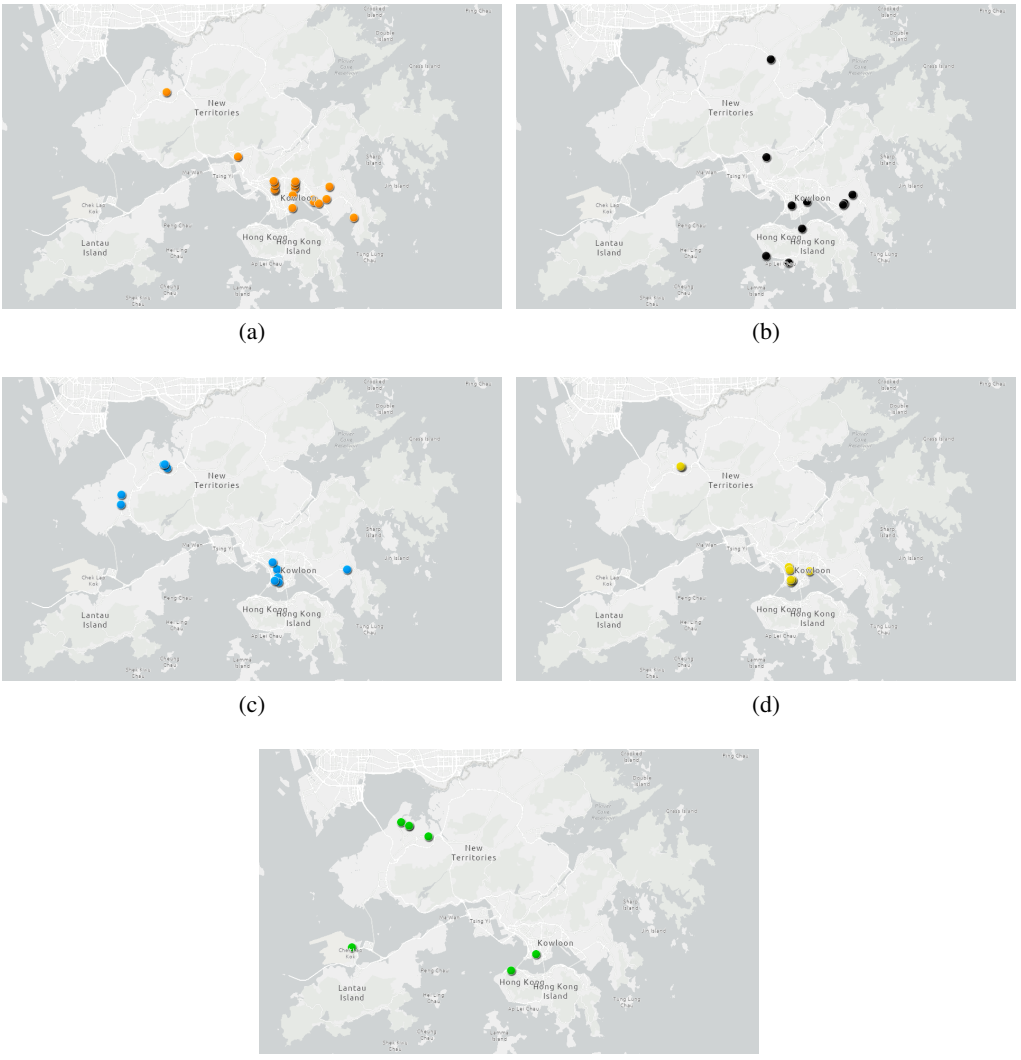

Figure 5.4: Spatial distribution of each cluster: (a) cluster at LOHAS Park/Kai Tak (orange points); (b) the first cluster at the TKO-LT Tunnel (black points); (c) the second cluster at the TKO-LT Tunnel (blue points); (d) cluster at the Central Kowloon Route (Central Tunnel) (yellow points); (e) cluster at Hong Kong International Airport Third Runway (green points).

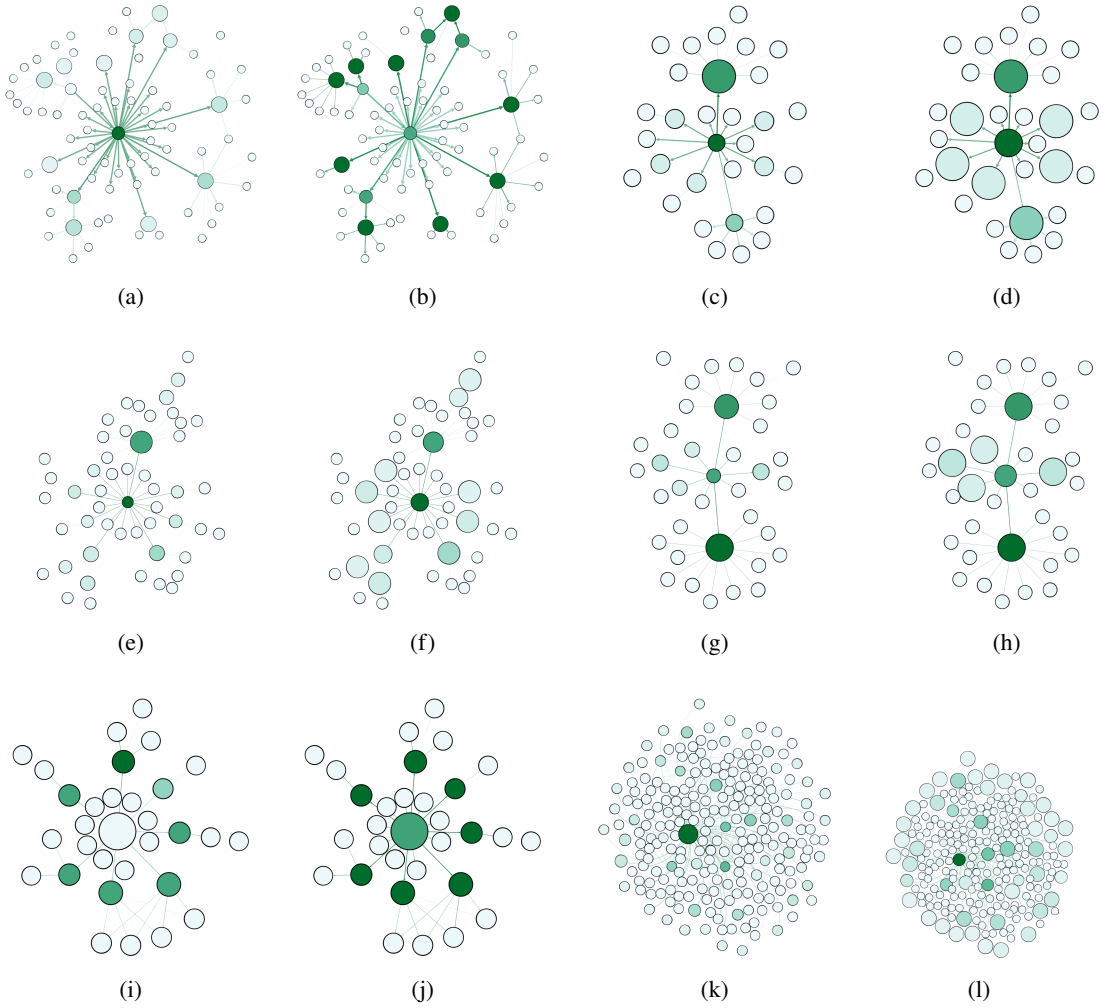

Figure 5.5: Centrality Indices of each cluster: (a) Betweenness Centrality of cluster at LOHAS Park/Kai Tak; (b) Closeness Centrality of cluster at LOHAS Park/Kai Tak; (c) Betweenness Centrality of the first cluster at the TKO-LT Tunnel; (d) Closeness Centrality of the first cluster at the TKO-LT Tunnel; (e) Betweenness Centrality of the second cluster at the TKO-LT Tunnel; (f) Closeness Centrality of the second cluster at the TKO-LT Tunnel; (g) Betweenness Centrality of cluster at the Central Kowloon Route (Central Tunnel); (h) Closeness Centrality of cluster at the Central Kowloon Route (Central Tunnel); (i) Betweenness Centrality of cluster at Hong Kong International Airport Third Runway; (g) Closeness Centrality of cluster at Hong Kong International Airport Third Runway; (k) Betweenness Centrality of all nodes; and (l) Closeness Centrality of all nodes.

5.3 Results and discussions

In Fig.5.2(a), the transmission network of all confirmed cases is depicted. Among the 221 cases in all 5 selected case clusters, 68% are male cases. The minimum, maximum, and average ages are 14-day-old, 83, and 37.6 years, respectively. Compared to the demographics data reported by the Construction Industry Council [41], more females were reported, including not only female employees working for the construction sites but also close contacts of male workers. 10% of the cases were infected by male infected construction workers, especially their family members. Fig.5.2(b) shows the daily number of infected cases since the symptom onset date of the first case in each cluster. The duration of an outbreak is 30 (LOHAS PARK/Kai Tak), 33 (TKO-LT Tunnel (first cluster)), 24 (TKO-LT Tunnel (second cluster)), 16 (Central Kowloon Route (Central Tunnel), and 26 (Hong Kong International Airport Third Runway) days respectively.

Each cluster has three to five generations (as shown in Fig.5.3(a)). The average number of secondary cases caused by each infectious individual in each generation is 7.6, 26.3, 10.6, 3.6, and 1.3, respectively. The major transmission in the first and second generations is among the construction workers. The third generation is among the workers and their family members. The fourth and fifth generations are driven by social activities, which may lead to community transmission. In this study, 53.36% of infected cases were in the community. As contact tracing was strictly implemented in Hong Kong, the risk of further transmission has been eliminated. However, many construction workers live in poor housing conditions globally [e.g., in China [103], the United States [53], and India [97]],with risks of a severe outbreak when many construction workers gather without NPIs, [e.g., at dormitories of construction workers [107]]. In some cities [e.g., central Texas [166]], the continuation of construction works nearly quadrupled the risk of community transmission. An outbreak in the construction industry poses significant risks to the community. More detailed research is needed on transmission chains from the construction industry to communities, such as transmission caused by their housing conditions.

Around averages of 46.61%, 37.56%, and 15.84% of offspring cases were infected at the workplace, in a household, and through social activities, respectively. The workplace posed the greatest infection risk. This study suggests that the construction site should be shut down within 2 working days after the primary case is identified. The intervals between the date when the first case visited the workplace and the shutdown date of each cluster are 3, 3, 1, 2, and 4 working days. As shown in Fig.3b-f, after suspending onsite work, the largest reductions in the attack

rate caused by the workplace in each cluster were 1.89%, 0.5%, 1.29%, 5.33%, and 0.13%.

If infected construction workers' household members follow a self-quarantine policy or take protective measures when going out, 15.84% of cases can be reduced on average. Infected construction workers' household members should be reminded to be monitored. Transmission through household settings was found to extend the outbreak duration by 7.8 days on average, which was around 2.5 times greater than transmission at the workplace. As shown in Fig.5.3(b)-5.3(f), the household attack rates are 3.33%, 0.43%, 1.50%, 12.00%, and 0.27%, which occupied 40.54%, 20.69%, 42.00%, 48.65%, and 25.81% of all infected cases in each cluster. The attack rates caused by social activities were 9.46%, 24.24%, 20.00%, 27.03%, and 3.23% in each cluster. For outbreaks at construction sites, control strategies should pay more attention on family members of infected construction workers.

The percentage of potential super-spreaders (with over 5 offspring cases) of each cluster is 6.76%, 3.45%, 4.00%, 8.11%, and 9.68%, respectively (as shown in Table 2). We found that among all 221 cases, 6 (2.7%) of them are associated with over 10 secondary cases, while over 75% of cases are not associated with any offspring cases. This means that 18% of seed cases generated 79.6% of offspring cases. It may be common to see super-spreading events in high-risk settings (e.g., the workplace). Among all case clusters, the cluster at the TKO-LT Tunnel has the highest modularity as some secondary cases were caused by the same infected individual, i.e., a super spreader (e.g., a confirmed case that generated at least 6 offspring cases [99% percentile]). Airborne transmission in the tunnel construction site environment might be the potential reason, a topic for further investigation.

Identifying the most influential 'spreaders' in a network is an important step toward optimizing the use of available resources and hindering the epidemic infection transmission spreading [106]. In Fig.5, the network structure was characterized by network centrality indices, i.e., closeness and betweenness centrality [29]. Nodes with higher betweenness centrality also have a higher degree, which means they are more likely to be a super spreader. Around 54% of nodes whose closeness centrality is between 0.4 to 0.8 are potential super-spreading candidates. Around 13% of the nodes whose betweenness centrality equals 1 are potential super-spreading candidates. Hence, while using centrality indices to explore the potential super spreaders, a node with higher betweenness centrality may have a higher contribution to disease transmission. When the super-spreading threshold is 6, 106 cases could be screened out, with only 50.7% of cases remaining. If the operating threshold of a super spreader is lowered (e.g., 5 secondary cases [95% percentile] or

4 secondary cases [90% percentile]), the total number of confirmed cases could be decreased by 56.1% and 63.8%, respectively. To adapt to a post-pandemic era, it is recommended that a social contact network describing the relationships between each person and his/her close contacts be established, which can help find potential super-spreaders [159, 197].

As depicted in Fig.5.4, the spatial distribution of each cluster is scattered. The majority of confirmed cases were not located in areas immediately near the primary case (i.e., surrounding the construction sites), but in residential areas where infected construction workers live. In an unstable labour market with project-by-project pay, it is difficult to collect construction workers' addresses. To establish an infectious disease surveillance system for the construction industry, high-density residential areas where workers live, such as dormitories of construction workers with poor housing conditions [107] should be monitored. In this study, Sai Kung, which has a lower population density but a high construction worker density, is regarded as a high-risk district that should also be prioritized for controlling COVID-19 case clusters associated with construction sites. Meanwhile, some workers in high contacts have a high probability of becoming a super spreader. For example, some infected construction worker cases, those who work for multiple construction sites might especially drive epidemic diffusion between construction sites, such as case 6879 bringing the virus from the construction site at LOHAS Park to another construction site at Kai Tak. This study suggests that construction workers with poor housing conditions and high contacts should be traced.

Table 5.2: Transmission characteristics of each cluster

Name of clusters	**Duration of an outbreak (days)**	**Percentage of COVID-19 case infected by different settings**			**Number of potential super-spreaders (with over 5 offspring cases)**
		workplace	household	social activities	
LOHAS Park/ Kai Tak	30	50.00%	40.54%	9.46%	6.76%
TKO-LT Tunnel (first cluster)	33	55.17%	20.69%	24.14%	3.45%
TKO-LT Tunnel (second cluster)	24	38.00%	42.00%	20.00%	4.00%
Central Kowloon Route (Central Tunnel)	16	24.32%	48.65%	27.03%	8.11%
Hong Kong International Airport Third Runway	26	70.97%	25.81%	3.23%	9.68%
Average	25.8	46.61%	37.56%	15.84%	6.33%

5.4 Chapter Summary

To adapt to the prolonged pandemic, the construction industry, which has a high vulnerability to COVID-19 infection, has sought more sector-specific and individual-level NPIs. Understanding infection transmission patterns can determine what, when, and how NPIs should be implemented. This study examined infection transmission proceeding from construction sites by using spatiotemporal analysis with COVID-19 case cluster data from construction sites in Hong Kong. The study revealed that COVID-19 transmission diffuses from the workplace to residential neighborhoods where infected construction workers live, but not to the surrounding the infected construction sites. The average number of offspring cases infected by each seed case in the first to fifth transmission generations are 7.8, 26.1, 10.6, 3.6, and 1.3, respectively. Around 18% of cases were responsible for 79.6% of all COVID-19 transmission, driven mainly by workplace and household settings. This study found that closing workplace within two working days after the primary case is identified can help reduce the attack rate by 5.33%. Encouraging household members of infected construction workers to follow quarantines can reduce 15.84% of offspring cases on average. A priori identification of super-spreaders can help remove half of COVID-19 cases.

5.4.1 Conclusions and Implications

To design targeted COVID-19 control strategies for the construction industry, it is critical to match it with the transmission pattern on a construction site. This study analyzed five COVID-19 case clusters associated with construction sites in Hong Kong (including 221 confirmed cases) by the spatiotemporal analysis, from an epidemiological perspective. In comparison with other sectors, the diffusion of COVID-19 transmission occurs from the workplace to residential neighborhoods where infected construction workers live instead of surrounding the construction site where the primary case was found. Driven by social activities, the outbreak in the construction industry poses significant risks to the community.

Workplace and household settings contributed around 85% of offspring cases. Transmission at the workplace can generate three to five generations. The average number of secondary cases caused by each infectious individual in each generation is 7.6, 26.3, 10.6, 3.6, and 1.3 respectively. The outbreak is mostly delayed by household transmission (7.8 days on average). Social activities account for around 16% of offspring cases, also posing significant risks to the community. This study found that closing workplace within two working days after the primary

case is identified can help reduce the attack rate by 5.33%. Encouraging household members of infected construction workers to follow quarantines can reduce 15.84% of offspring cases on average.

In terms of super-spreading events, 18% of cases were responsible for 79.6% of all SARS-CoV-2 transmission in summary. Super-spreading events are mainly driven by the workplace and household settings. Owing to substantial heterogeneity in the transmissibility of SARS-CoV-2 infection and the significant infection force by super-spreading events, identifying the most influential spreaders in the heterogeneous contact interaction networks is also recommended. When the operating threshold of a super spreader is lowered (e.g., 6 secondary cases [99% percentile], 5 secondary cases [95% percentile], or 4 secondary cases [90% percentile]), the total number of confirmed cases could be decreased by 50.7%, 56.1%, and 63.8%, respectively.

5.4.2 Limitations and Directions for Future Research

Many uncertainties might influence the results caused by the limited dataset. The symptom onset date of each asymptomatic infectious individual cannot be identified. There was potential recall bias regarding symptom onset among patients with COVID-19. The COVID-19 surveillance system for tracing close contacts in Hong Kong is based on the application "LeaveHomeSafety", which does not collect geographic information system (GIS) data automatically. The spatial connectivity is mostly driven by highly frequented locations (e.g., residential buildings, workplaces, and restaurants), and may miss some random contacts. The weight of each edge in the transmission network (as shown in Fig.5.3) was classified into five groups based on the relationship between each pair of confirmed cases, which may in actuality be more heterogeneous. If more specific relationship data can be collected, the weight (i.e., the possibility of getting infected) of each edge may be more heterogeneous.

As of November 2021, the TKO-LT Tunnel construction site with a poorly ventilated work environment met two outbreaks. Its highest modularity also showed a higher possibility of super-spreading events in the tunnel construction site. During the fifth wave of COVID-19 with omicron variants in 2022 in Hong Kong, the TKO-LT Tunnel construction site experienced its third outbreak in February with 170 cases. Meanwhile, the Ho Man Tin construction site of the Central Kowloon Route and the T2 Trunk Road construction site have experienced outbreaks as well [209]. Due to data limitations, this study did not explore these outbreaks and the transmission risks in different work environment, which needs to be further researched by other methods [e.g., Computational Fluid Dynamics (CFD) analysis [149]].

To responsibly adapt to a post-pandemic era, further research should be conducted. The importance of mitigating super-spreading events underlines the need for additional research, such as exploring the efficacy of regular testing among workers who join multiple projects and establishing a social contact network that can help screen out potential super spreaders. Variation in individual transmission numbers arises due to a combination of host, pathogen, and environment effects [136], such as unrecognized or misdiagnosed illness, heterogeneous contact rates, co-infections, hygiene habits, and crowded or confined settings. To prevent indirect transmission within enclosed or confined construction sites, consistently followed disinfection practices [105] can be an effective method. In addition, the efficacy of installing and/or improving ventilation systems in response to COVID-19 is advised to be explored. Flexible work schedules should also be optimized while balancing project productivity with minimizing the possibility of triggering an epidemic outbreak.

Chapter 6

Non-pharmaceutical Interventions and Vaccine Program on Construction Sites

6.1 Introduction

Since the initial COVID-19 outbreak in December 2019 [122], this pandemic has spread globally, causing unprecedented fatalities. COVID-19 vaccines offer hope in ending this pandemic if enough of the population (i.e. at least 75–90%) gets vaccinated to attain the basic reproduction number $\mathcal{R}_0$ (2.5-3.5) [12]), in turn achieving herd immunity. More than six vaccines have been approved for emergency or full use by the World Health Organization (WHO) [219]. As of August 30 2021, a total of 5,019,907,027 vaccine doses have been administered [163], which accounts for around 60% of the global population. This implies that there is still a long journey ahead in achieving herd immunity. Even if all eligible people have been vaccinated (assumed vaccine efficacy: 88%), the $\mathcal{R}_0$ may not be reduced to below one [148] because the effect of a given vaccine on SARS-CoV-2 is highly contingent on the specific properties of each vaccnine and the degree of population uptake. Meanwhile, the frequent mutations of SARS-CoV-2 also pose challenges to vaccines' continual efficacy [24]. For example, the SARS-CoV-2 Delta variant has increased the secondary attack rate by 42 to 55% higher than the Alpha variant [38]. Therefore, vaccination alone may not be sufficient to contain the outbreak. A combination of vaccination and non-pharmaceutical interventions (NPIs) is probably necessary to control the transmission risks.

NPIs, including mask wearing, lockdowns, and social distancing , have been widely used at the city and country level since the beginning of the pandemic, which did achieve some great successes in containing the virus [57, 127, 242]. In addition, the majority of these macroscopic NPIs were studied using well-established compartment models (e.g., Susceptible-Infectious-Susceptible(SIS), Susceptible-Infectious-Recovered (SIR), and Susceptible-Exposed-Infectious-Recovered(SEIR)). The fundamental assumption of these models is that the macroscopic NPIs are circumscribed by well-mixed and homogeneous populations, which is an assumption that may oversimplify the reality. Meanwhile, as the pandemic has continued to persist over a prolonged period, the public has shown signs of pandemic fatigue in relation to macroscopic NPIs [221]

since the second half of 2020 (as shown in Chapter 4), meaning that the public has become demotivated in following these NPIs. To reinvigorate public support, many governments and researchers have shifted from advocating and implementing macroscopic NPIs to promoting microscopic NPIs at individual levels, such as indoor pedestrians [247], students in universities [235], consumers in restaurants [123], and passengers in cruise ships [20]. At this a smaller scale of intervention, microscopic NPIs are generally easier to implement. Moreover, studies on microscopic NPIs overcome the limitations of macroscopic NPI' studies because the former ones could be more effectively considering transmission heterogeneity and the characteristics of people in a specific scenario [20, 123, 235, 247]. Furthermore, as an infected individual may participant in both work and non-work scenarios, focusing solely on one setting is likely to not account for the entire transmission process, and thus leading to increased transmission risks. To address this methodological limitation, it is essential to analyze the effectiveness of microscopic NPIs in different settings with consideration of vaccination rates.

Construction sites are characterized by heterogeneous work types, changeable work environments, and tiers in the labor force. Such complexities could make the implementation of microscopic NPIs on sites together with vaccination a challenging task. It is not surprising that numerous construction site-associated COVID-19 clusters have been recorded globally [28] (e.g., Singapore [118, 220], the United States [10, 212], and Hong Kong [208]). However, the most of COVID-19 related studies in the construction literature concentrate on the severity of the economic losses and health crises brought about by this pandemic [10] or the efficacy of NPIs (e.g., social distancing, PPE, and sanitization) by collecting feedback from construction companies [195] or employees [52]. Few studies have depicted the transmission dynamics of SARS-CoV-2 on the construction site, which form the basis of enhancing anti-epidemic strategies. To narrow such knowledge gaps and address methodological hurdles in predicting transmission risks, this study investigates how different combinations of microscopic NPIs and vaccination plans could affect the transmission dynamics of SARS-CoV-2 among construction workers and their close contacts so as to predict the effectiveness of various interventions. A dual-community compartment model was developed, including a SEI/AHR-P model for construction workers and a SEIAHR model for their close contacts. Mathematical modeling approaches were chosen because they offer insights into the importance of multiple transmission routes of SARS-CoV-2 and how different intervention scenarios can reduce transmissibility through comparison of the respective attack rate (AR) with absolute/relative effectiveness (AE/RE) and the duration of the outbreak (DO) associated with each scenario.

6.2 Methods

6.2.1 Model Structure

This study modified the SEIR model by incorporating direct and indirect transmission routes to simulate SARS-CoV-2 transmission dynamics at a construction site, within its connected community, and between each of these. All those designated in this study as close contacts of construction workers in the connected community are not employed by the construction site. All construction employees working on the construction site are designated construction workers. The total human population at time t, denoted as $N(t)$, has been split into ten mutually exclusive compartments as follows: susceptible individuals (who can get infected) on the construction site $S_{hi}(t)$, susceptible individuals in its connected community $S_{ho}(t)$, exposed individuals (who are under incubation period) on the construction site $E_{hi}(t)$, exposed individuals in its connected community $E_{ho}(t)$, asymptomatic infectious individuals (who get infected and show no symptom) on the construction site $A_{hi}(t)$, asymptomatic infectious individuals in its connected community $A_{ho}(t)$, symptomatic infectious individuals (who get infected and show symptoms) on the construction site $I_{hi}(t)$, symptomatic infectious individuals in its connected community $I_{ho}(t)$, hospitalized infectious individuals $H_h(t)$ (who are hospitalized) and recovered individuals $R_h(t)$ (who are recovered or die). The pathogen concentration inhaled/infected per person on the construction site is represented as $P_a(t)$. The model is given by nonlinear ordinary differential equations (ODEs) as Eqs. (6.1) and depicted in Fig. 6.1. All variables and parameters are

described in Table 6.1.

$$
\begin{cases}
\frac{dS_{ho}}{dt} = \theta_2 S_{hi} - (\lambda^c_{hh} + \theta_1) S_{ho}, \\
\frac{dS_{hi}}{dt} = \theta_1 S_{ho} - (\lambda^s_{hh} + \lambda^s_{ha} + \theta_2) S_{hi}, \\
\frac{dE_{ho}}{dt} = \lambda^c_{hh} S_{ho} + \theta_3 E_{hi} - \alpha_1 E_{ho}, \\
\frac{dE_{hi}}{dt} = (\lambda^s_{hh} + \lambda^s_{ha}) S_{hi} + \theta_4 E_{ho} - \alpha_2 E_{hi}, \\
\frac{dI_{ho}}{dt} = \sigma_2 E_{ho} - \alpha_3 I_{ho}, \\
\frac{dI_{hi}}{dt} = \sigma_1 E_{hi} - \alpha_4 I_{hi}, \\
\frac{dA_{ho}}{dt} = \sigma_4 E_{ho} - \epsilon_4 A_{ho}, \\
\frac{dA_{hi}}{dt} = \sigma_3 E_{hi} - \epsilon_3 A_{hi}, \\
\frac{dH_h}{dt} = \epsilon_1 I_{hi} + \epsilon_2 I_{ho} + \epsilon_3 A_{hi} + \epsilon_4 A_{ho} - \alpha_5 H_h, \\
\frac{dR_h}{dt} = \gamma H_h - \delta_r R_h, \\
\frac{dP_a}{dt} = \eta_1 E_{hi} + \eta_2 I_{hi} + \eta_3 A_{hi} - \mu P_a,
\end{cases}
\tag{6.1}
$$

The force of infection is written as:

$$
\begin{aligned}
\lambda^c_{hh} &= \frac{C_{11}E_{ho} + C_{12}I_{ho} + C_{13}A_{ho} + C_{14}E_{hi} + C_{15}I_{hi} + C_{16}A_{hi}}{N^c}, \\
\lambda^s_{hh} &= \frac{C_{21}E_{ho} + C_{22}I_{ho} + C_{23}A_{ho} + C_{24}E_{hi} + C_{25}I_{hi} + C_{26}A_{hi}}{N^s}, \\
\lambda^s_{ha} &= \frac{\beta_3 P_a}{N^s},
\end{aligned}
\tag{6.2}
$$

where

$$
\begin{aligned}
&\alpha_1 = \theta_4 + \sigma_2 + \sigma_4, \quad \alpha_2 = \theta_3 + \sigma_1 + \sigma_3, \quad \alpha_3 = \epsilon_2 + \delta_i, \quad \alpha_4 = \epsilon_1 + \delta_i \quad \alpha_5 = \gamma + \delta_h. \\
&C_{11} = \beta_1 a_{11}, \quad C_{12} = \beta_1 a_{12} \quad C_{12} = \beta_1 a_{13}, \quad C_{12} = \beta_1 a_{14}, \quad C_{12} = \beta_1 a_{15}, \quad C_{12} = \beta_1 a_{16}, \\
&C_{21} = \beta_2 a_{21}, \quad C_{22} = \beta_2 a_{22} \quad C_{22} = \beta_2 a_{23}, \quad C_{22} = \beta_2 a_{24}, \quad C_{22} = \beta_2 a_{25}, \quad C_{22} = \beta_2 a_{26},
\end{aligned}
\tag{6.3}
$$

with N^s and N^c representing the total population at time t within the construction site and its connected community formulated as $N^s(t) = S_{hi}(t) + E_{hi}(t) + A_{hi}(t) + I_{hi}(t)$, $N^c(t) = S_{ho}(t) + E_{ho}(t) + A_{ho}(t) + I_{ho}(t) + H_h(t) + R_h(t)$ and $N(t) = N^s(t) + N^c(t)$.

Table 6.1: Notation of a dual-community model

Notation	Description
Variables	
S_{hi}	the number of susceptible individuals on the construction site
E_{hi}	the number of exposed individuals on the construction site
A_{hi}	the number of asymptomatic infectious individuals on the construction site
I_{hi}	the number of symptomatic infectious individuals on the construction site
P_a	the pathogen concentration inhaled/infected per person on the construction site
S_{ho}	the number of susceptible individuals in its connected community
E_{ho}	the number of exposed individuals in its connected community
A_{ho}	the number of asymptomatic infectious individuals in its connected community
I_{ho}	the number of symptomatic infectious individuals in its connected community
H_h	the number of hospitalized infectious individuals
R_h	the number of recovered individuals
Parameters	
θ_1	the transition rate from S_{ho} to S_{hi}
θ_2	the transition rate from S_{hi} to S_{ho}
θ_3	the transition rate from E_{hi} to E_{ho}
θ_4	the transition rate from E_{ho} to E_{hi}
σ_1	the transition rate from E_{hi} to I_{hi}
σ_2	the transition rate from E_{ho} to I_{ho}
σ_3	the transition rate from E_{hi} to A_{hi}
σ_4	the transition rate from E_{ho} to A_{ho}
ϵ_1	the hospitalized rate of I_{hi}
ϵ_2	the hospitalized rate of I_{ho}
ϵ_3	the hospitalized rate of A_{hi}
ϵ_4	the hospitalized rate of A_{ho}
γ	the recovery rate of hospitalized individuals H_h
δ_i	the rate of death among symptomatic infectious individuals
δ_h	the rate of death among hospitalized population
δ_r	the rate of death among recovered individuals
η_1	the rate of virus spread to environment by E_{hi}
η_2	the rate of virus spread to environment by I_{hi}
η_3	the rate of virus spread to environment by A_{hi}
μ	natural death rate of pathogens in the environment
β_1	the transmission rate between human to human in its connected community
β_2	the transmission rate between human to human on the construction site
β_3	the transmission rate between pathogen to human on the construction site
a_{11}	effective contact ratio between E_{ho} and S_{ho}
a_{12}	effective contact ratio between I_{ho} and S_{ho}
a_{13}	effective contact ratio between A_{ho} and S_{ho}
a_{14}	effective contact ratio between E_{hi} and S_{ho}
a_{15}	effective contact ratio between I_{hi} and S_{ho}
a_{16}	effective contact ratio between A_{hi} and S_{ho}
a_{21}	effective contact ratio between E_{ho} and S_{hi}
a_{22}	effective contact ratio between I_{ho} and S_{hi}
a_{23}	effective contact ratio between A_{ho} and S_{hi}
a_{24}	effective contact ratio between E_{hi} and S_{hi}
a_{25}	effective contact ratio between I_{hi} and S_{hi}
a_{26}	effective contact ratio between A_{hi} and S_{hi}

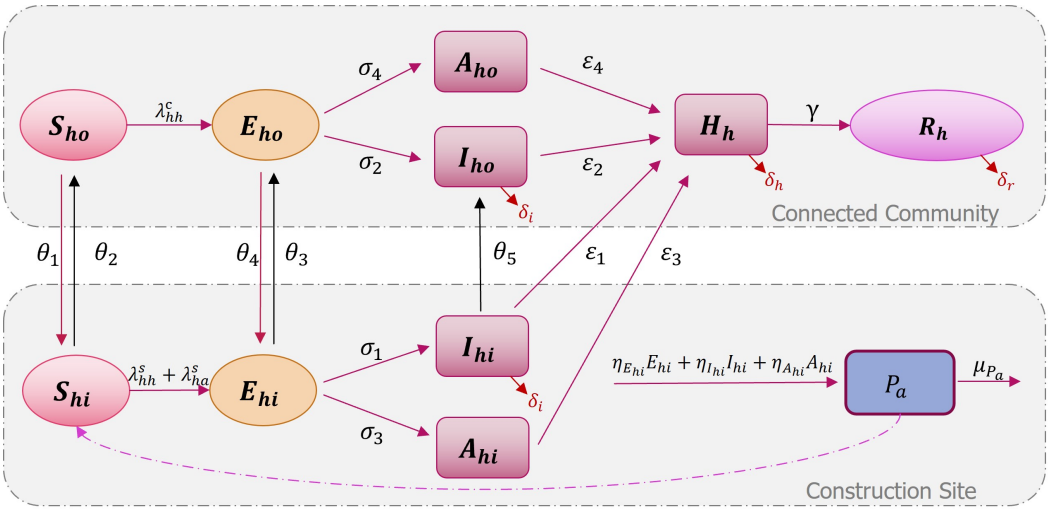

Figure 6.1: Diagram of the dual-community model in Eq. (6.1)

6.2.2 Basic Reproduction Number

First of all, we consider solutions of Eqs. (6.1), formulated as

$$\Omega = \{(S_{hi}, E_{hi}, A_{hi}, I_{hi}, P_a, S_{ho}, E_{ho}, A_{ho}, I_{ho}, H_h, R_h) \in \mathbb{Z}^{11}_{+} : N > 0\}.$$

All solutions of the model that start in Ω will remain in Ω for all $t \geq 0$. The existence, uniqueness, and continuation results hold provided restricted solutions in Ω hold [153]. The basic reproduction number $\mathcal{R}_0$ is defined as the average number of secondary infections caused by an individual in an entirely susceptible population [155]. The Disease-free Equilibrium (DFE) is a state in which a disease is absent from a population ahd locally asymptotically stable [227]: only $S_{hi}(0)$ and $S_{ho}(0)$ are not equal to zero, other variables should equal zero or much less than $S_{hi}(0)$ and $S_{ho}(0)$ as shown in Ω_1.

$$\begin{aligned}\Omega_1 =& [S_{hi}(0), E_{hi}(0), A_{hi}(0), I_{hi}(0), P_a(0), S_{ho}(0), E_{ho}(0), A_{ho}(0), I_{ho}(0), H_h(0), R_h(0)] \\ =& [S_{hi}(0), 0, 0, 0, 0, S_{ho}(0), 0, 0, 0, 0, 0].\end{aligned}$$

Based on a next generation matrix [227], let
$x = (E_{ho}, E_{hi}, I_{ho}, I_{hi}, A_{ho}, A_{hi}, H_h, P_a)^T$, the model (6.1) can be represented as $\frac{dx}{dt} = F(x) -$

$V(x)$.

$$F(x) = \begin{pmatrix} \frac{C_{11}E_{ho}+C_{12}I_{ho}+C_{13}A_{ho}+C_{14}E_{hi}+C_{15}I_{hi}+C_{16}A_{hi}}{N^c} \\ \frac{C_{21}E_{ho}+C_{22}I_{ho}+C_{23}A_{ho}+C_{24}E_{hi}+C_{25}I_{hi}+C_{26}A_{hi}}{N^s} \\ 0 \\ 0 \\ 0 \\ 0 \\ 0 \\ \eta_1 E_{hi} + \eta_2 I_{hi} + \eta_3 A_{hi} \end{pmatrix} \tag{6.4}$$

and

$$V(x) = \begin{pmatrix} \alpha_1 E_{ho} - \theta_3 E_{hi} \\ \alpha_2 E_{hi} - \theta_4 E_{ho} \\ \alpha_3 I_{ho} - \sigma_2 E_{ho} \\ \alpha_4 I_{hi} - \sigma_1 E_{hi} \\ \epsilon_4 A_{ho} - \sigma_4 E_{ho} \\ \epsilon_3 A_{hi} - \sigma_3 E_{hi} \\ \alpha_5 H_h - \epsilon_1 I_{hi} - \epsilon_2 I_{ho} - \epsilon_3 A_{hi} - \epsilon_4 A_{ho} \\ \mu P_a \end{pmatrix}. \tag{6.5}$$

The basic reproduction number $\mathcal{R}_0$ is represented as follows:

$$\mathcal{R}_0 = \rho(FV^{-1}) = \frac{1}{6}\sqrt[3]{g_1 + 12\sqrt{g_2}} - 6\frac{g_3}{\sqrt[3]{g_1 + 12\sqrt{g_2}}} + \frac{D_8}{3} + \frac{D_1}{3}. \tag{6.6}$$

where

$$g_1 = 8{D_1}^3 - 12{D_1}^2 D_8 + 36 D_1 D_2 D_7 - 12 D_1 {D_8}^2 - 72 D_{15} D_{13} D_1 + 36 D_2 D_7 D_8 + 108 D_{14} D_2 D_{13} + 8{D_8}^3 + 36 D_{15} D_8 D_{13},$$

$$g_2 = -12{D_{13}}^3 {D_{15}}^3 + [24{D_1}^2 {D_{15}}^2 + (-108 D_2 D_{14} D_{15} - 24 D_8 {D_{15}}^2) D_1 + 81{D_2}^2 {D_{14}}^2 + (-36 D_7 {D_{15}}^2 + 54 D_8 D_{14} D_{15}) D_2 - 3{D_8}^2 {D_{15}}^2]{D_{13}}^2 + [-12{D_1}^4 D_{15} + (12 D_2 D_{14} + 24 D_8 D_{15}){D_1}^3 + ((-60 D_7 D_{15} - 18 D_8 D_{14}) D_2 - 6{D_8}^2 D_{15}){D_1}^2 + (54{D_2}^2 D_7 D_{14} + (6 D_7 D_8 D_{15} - 18{D_8}^2 D_{14}) D_2 - 6{D_8}^3 D_{15}) D_1 + (-36{D_7}^2 D_{15} + 54 D_7 D_8 D_{14}){D_2}^2 + (-6 D_7 {D_8}^2 D_{15} + 12{D_8}^3 D_{14}) D_2]D_{13} - 3({D_1}^2 - 2 D_8 D_1 + 4 D_7 D_2 + {D_8}^2)(D_8 D_1 - D_7 D_2)^2,$$

$$g_3 = \frac{D_8 D_1}{9} - \frac{D_7 D_2}{3} - \frac{D_{15} D_{13}}{3} - \frac{{D_1}^2}{9} - \frac{{D_8}^2}{9},$$

$$D_1 = \frac{C_{11}\alpha_2}{\alpha_6} + \frac{C_{14}\theta_4}{\alpha_6} + \frac{C_{12}\sigma_2\alpha_2}{\alpha_6\alpha_3} + \frac{C_{15}\sigma_1\theta_4}{\alpha_6\alpha_4} + \frac{C_{13}\sigma_4\alpha_2}{\alpha_6\epsilon_4} + \frac{C_{16}\sigma_3\theta_4}{\alpha_6\epsilon_3}$$

$$D_2 = \frac{C_{11}\theta_3}{\alpha_6} + \frac{C_{14}\alpha_1}{\alpha_6} + \frac{C_{12}\sigma_2\theta_3}{\alpha_6\alpha_3} + \frac{C_{15}\sigma_1\alpha_1}{\alpha_6\alpha_4} + \frac{C_{13}\sigma_4\theta_3}{\alpha_6\epsilon_4} + \frac{C_{16}\sigma_3\alpha_1}{\alpha_6\epsilon_3}$$

$$D_7 = \frac{C_{21}\alpha_2}{\alpha_6} + \frac{C_{24}\theta_4}{\alpha_6} + \frac{C_{22}\sigma_2\alpha_2}{\alpha_6\alpha_3} + \frac{C_{25}\sigma_1\theta_4}{\alpha_6\alpha_4} + \frac{C_{23}\sigma_4\alpha_2}{\alpha_6\epsilon_4} + \frac{C_{26}\sigma_3\theta_4}{\alpha_6\epsilon_3}$$

$$D_8 = \frac{C_{21}\theta_3}{\alpha_6} + \frac{C_{24}\alpha_1}{\alpha_6} + \frac{C_{22}\sigma_2\theta_3}{\alpha_6\alpha_3} + \frac{C_{25}\sigma_1\alpha_1}{\alpha_6\alpha_4} + \frac{C_{23}\sigma_4\theta_3}{\alpha_6\epsilon_4} + \frac{C_{26}\sigma_3\alpha_1}{\alpha_6\epsilon_3}$$

$$D_{14} = \frac{\eta_1\theta_4}{\alpha_6} + \frac{\eta_2\sigma_1\theta_4}{\alpha_6\alpha_4} + \frac{\eta_3\sigma_3\theta_4}{\alpha_6\epsilon_3}, \quad D_{15} = \frac{\eta_1\alpha_1}{\alpha_6} + \frac{\eta_2\sigma_1\alpha_1}{\alpha_6\alpha_4} + \frac{\eta_3\sigma_3\alpha_1}{\alpha_6\epsilon_3},$$

$$D_{13} = \frac{\beta_3}{\mu}, \quad \text{and} \quad \alpha_6 = \alpha_2\alpha_1 - \theta_4\theta_3.$$

$\mathcal{R}_0$ is determined by human-related factors (D_1, D_2, D_7 and D_8) and pathogen-related factors (D_{13}, D_{14} and D_{15}), representing two modes of transmission of this disease as shown in Table 6.2.

Table 6.2: Interpretation of the basic reproduction number $\mathcal{R}_0$

Term	**Interpretation**
$\alpha_6 = \alpha_2\alpha_1 - \theta_4\theta_3$	the remaining exposed individuals in the whole system.
$D_n\,(n = 1, 2, 7, 8)$	D_n has six terms representing the contributions to $\mathcal{R}_0$ from E_{ho},E_{hi},I_{ho},I_{hi},A_{ho} and A_{hi} respectively.
D_{13}	β_3 is the infectious rate transmitting from pathogen to human and μ shows the emigration rate of pathogens. Hence, D_{13} represents the remaining pathogens.
$D_{14}\,(m = 14, 15)$	D_m has three terms representing contributions to $\mathcal{R}_0$ from E_{hi},I_{hi} and A_{hi} respectively.

6.3 Sensitivity Analysis

Both global and local sensitivity analyses are conducted in this study. As Eqs. (6.1) are nonlinear ODEs with non-monotonic input-output relationships, global sensitivity analysis by the Sobol method [258] can reveal the influences of parameter interaction. Local sensitivity is designed to explore the effects of every single parameter in response to the outputs when other parameters are constant, which directly provides insights on the efficacy of various control strategies.

6.3.1 Global Sensitivity Analysis

The Sobol method was performed using **SimBiology** via **Matlab** software version **R2021a** [216]. First-order and total-order sensitivity indices are intended to show how every single parameter and the interaction between parameters contribute to the output variance over a full range of parameter space [198]. According to the basic reproduction number $\mathcal{R}_0$ and previous studies [125, 130], the inputs include human-to-human transmission rates (β_1, β_2), transition rate between the construction site and its connected community (θ_1 - θ_4) and effective contact ratio (a_{11} - a_{26}). This section excludes transmission rate from pathogens β_3 owing to the model complexity, which will be discussed in the following subsection. Since symptomatic and asymptomatic infectious individuals are generated in the latency period by exposed individuals [227], the exposed individuals within the connected community $x(1)$ and the exposed individuals within the construction site $x(2)$ contribute the most to determining $\mathcal{R}_0$. Hence, the output includes exposed individuals on the construction site ($[constructionsite].E_{hi}$) and in its connected community ($community.E_{ho}$) as shown in Figures 6.2 and 6.3.

6.3.2 Local Sensitivity Analysis

Given the results found of previous studies described above, this section sets 0.1 as the interval and tests transmission rate, effective contact ratio and transition rate ranging from 0 to 1, as shown in Fig. 6.4. The transmission rates are assumed to be equal: $\beta_1 = \beta_2 = \beta_3 = \beta$. The outputs include total attack rate (TAR) and attack rate (AR) in each area. TAR is defined as the proportion of being infected (including pre-symptomatic, asymptomatic and symptomatic) among the whole susceptible population during the simulation period [130]. Attack rate on the construction site (AR^s) and in its connected community (AR^c) reflect the severity of the outbreak in each area respectively. Another criterion is the duration of an outbreak (DO). All results are shown in Fig. 6.4.

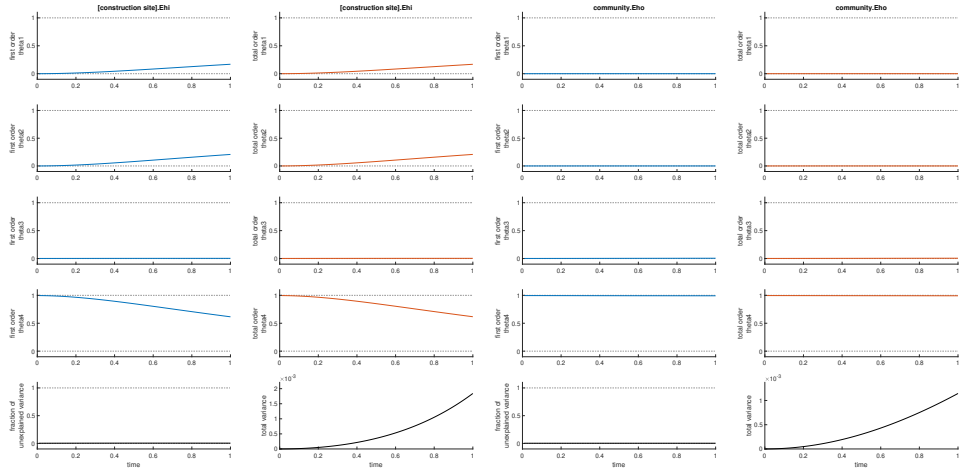

(a)

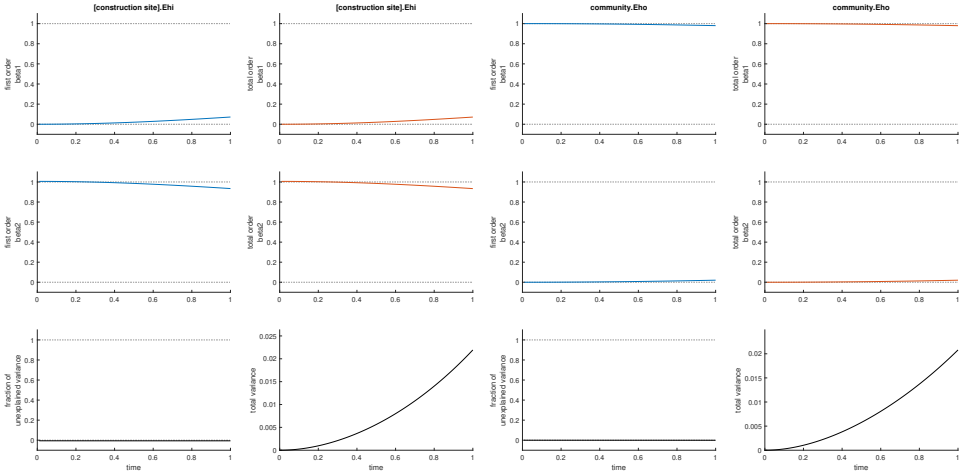

(b)

Figure 6.2: Sobol indices of (a) transmission rate β_1 and β_2; and (b) transition rate between construction site and its connected community.

6.4 Effectiveness of Interventions

6.4.1 Non-pharmaceutical Interventions (NPIs)

"Scenario 1" is set as a baseline with all effective contact ratios kept as one and $\beta_1 = \beta_2 = \beta_3 = 0.54$ as depicted in Fig. 6.5, representing no intervention in the whole population. Globally, the average household size is 4.0 [40]. The close contact size is assumed to be 5 which is larger than 4. The initial population N^s is assumed to be 40 which is one-fifth of the population in its connected community N^c. Absolute effectiveness (AE) and relative effectiveness (RE) [130] are defined to

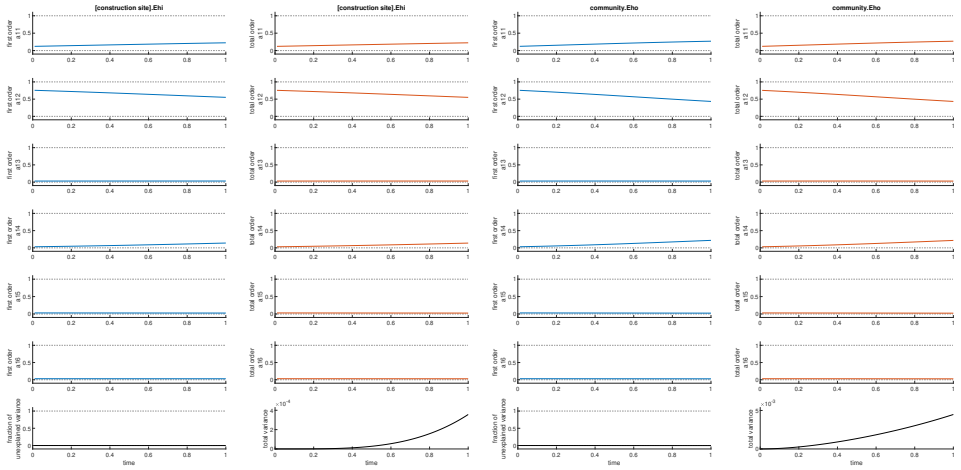

(a)

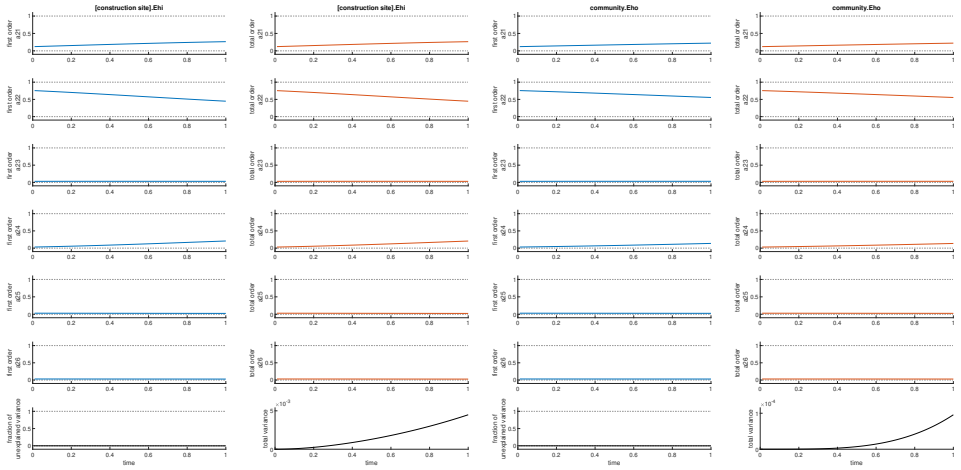

(b)

Figure 6.3: Sobol indices of (*a*) effective contact ratio a_{11} - a_{16}; and (*b*) effective contact ratio a_{21} - a_{26}.

assess the efficiency of different interventions.

$$
\begin{aligned}
TAR &= \frac{\text{the number of confirmed cases}}{\text{the total population}}, \\
AE_i &= TAR_i - TAR_{baseline}, \\
RE_i &= AE_i / TAR_i.
\end{aligned}
\tag{6.7}
$$

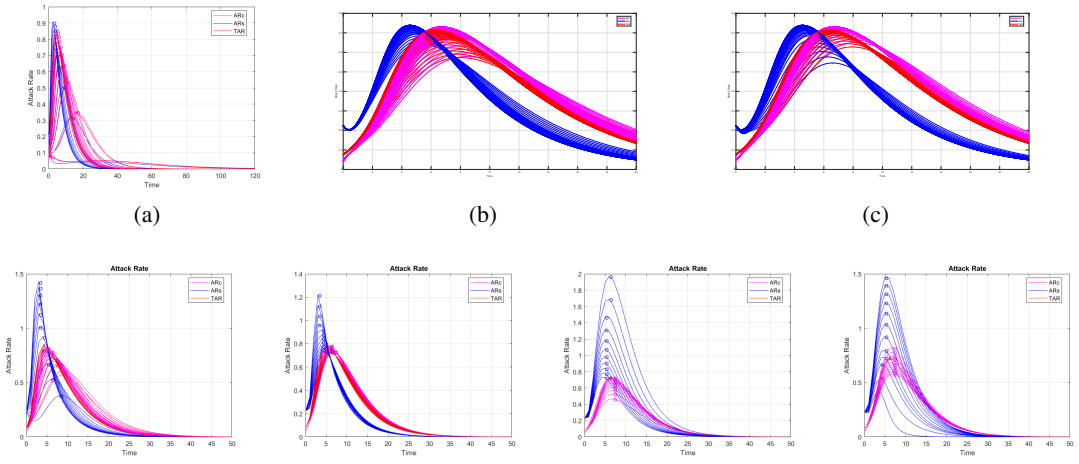

Figure 6.4: Sensitivity analysis of (a) transmission rate β; (b) effective contact ratio a_{11} to a_{16}; (c) effective contact ratio a_{21} to a_{26}; (d) transition rate θ_1; (e) transition rate θ_2; (f) transition rate θ_3; and (g) transition rate θ_4 ranging from 0 to 1.

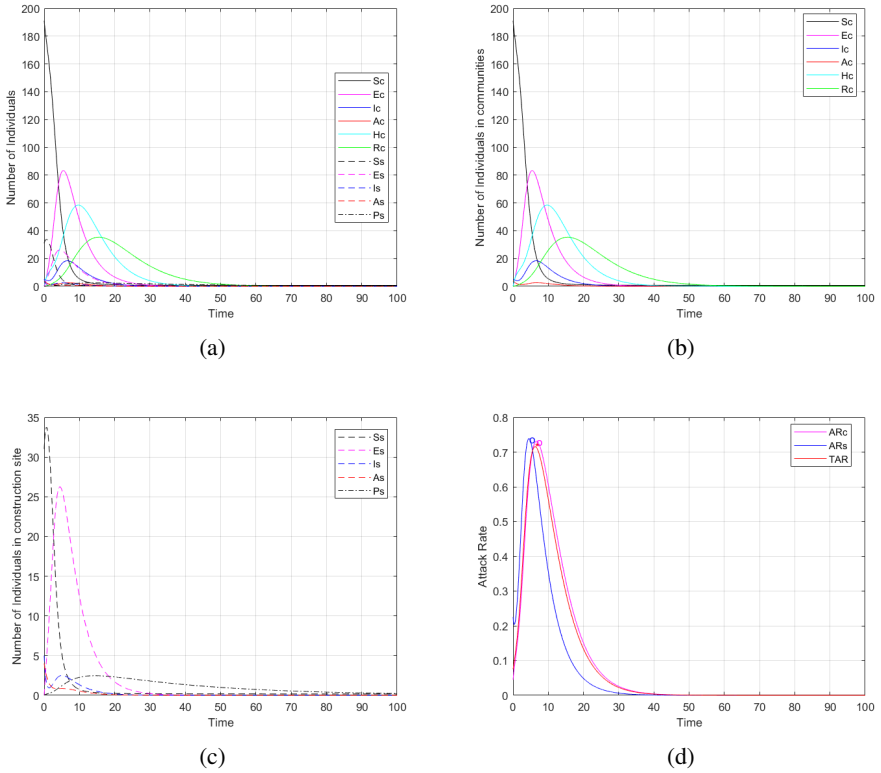

Figure 6.5: Scenario 1: baseline of (a) SEIARP model; (b) within the community; (c) on the construction site; and (d) attack rate.

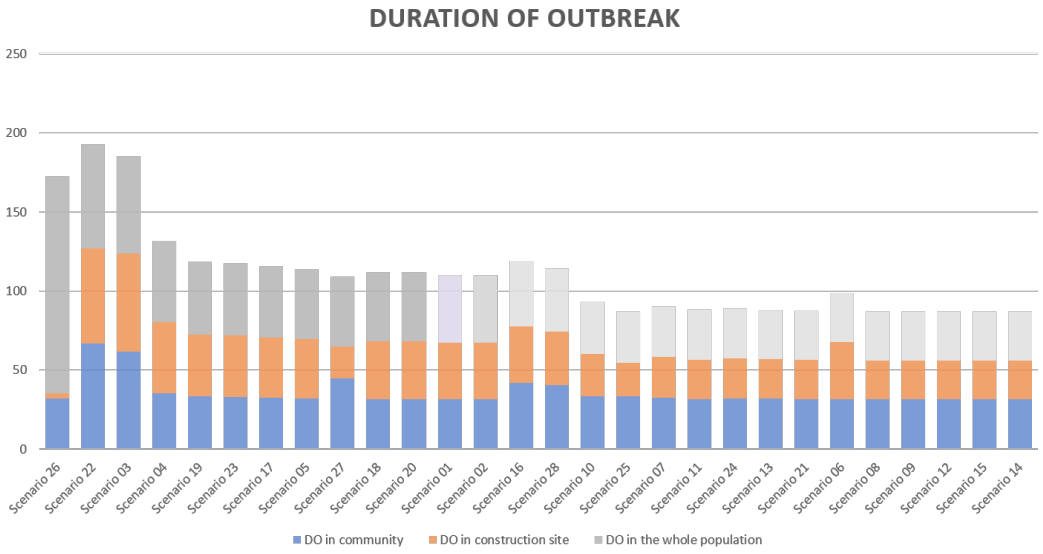

Figure 6.6: Duration of Outbreak.

6.4.1.1 Scenario Design

The transmissibility between populations and transmission pathways in under varying scopes of reducing effective contact is investigated in this section. Parameters elicited in the sensitivity analyses were organized into 28 scenarios of interventions and TAR and DO were constructed to quantitatively evaluate each of these scenarios. The effective contact ratio $a_{ij}, (i = 1,2$ and $j = 1,2,...,6)$ between different populations, human-related (i.e., direct) transmission rate (β_1, β_2), pathogen-related (indirect) transmission rate β_3 and transition rate θ_k, $(k = 1,2,3,4)$, which are considered as key elements in designing different NPIs, has a range from 0 to 1. The interval is set as 0.1 following the conditions in local sensitivity analysis. As mentioned, Scenario 1 is the baseline without any intervention. Scenario 2 is intended to prevent pathogen-related transmission. Scenarios 4 – 15 are single parameter targeted. Scenarios 16 – 21 aim to control two parameters from the same infectious resources in one community. Scenarios 22 – 24 consider four parameters from the same origins in both communities. Scenarios 3, 27, and 28 represent interventions for different scopes for controlling effective contact. Scenario 25 prohibits physical interaction between these two communities. Scenario 26 protects the whole population from risks through a more complete control of both effective contact and connection between the two communities. All scenarios are described in Table 6.3.

The three criteria for evaluating the performance of all scenarios are AE, RE and DO. All 28 scenarios are ranked by their DO as shown in Fig. 6.6. Scenario 16 was identified to be the best one.

Table 6.3: Scenario

Scenario No.	Conditions	Description
Scenario 1	$a_{11} = ... = a_{16} = 1$ $a_{21} = ... = a_{26} = 1$	Baseline: No intervention.
Scenario 2	β_3	Controlling pathogen on the construction site.
Scenario 3	$a_{11}, ..., a_{16}$ $a_{21}, ..., a_{26}$	Controlling effective contact among the whole population.
Scenario 4	a_{11}	Controlling effective contact between E_{ho} and S_{ho}.
Scenario 5	a_{12}	Controlling effective contact between I_{ho} and S_{ho}.
Scenario 6	a_{13}	Controlling effective contact between A_{ho} and S_{ho}.
Scenario 7	a_{14}	Controlling effective contact between E_{hi} and S_{ho}.
Scenario 8	a_{15}	Controlling effective contact between I_{hi} and S_{ho}.
Scenario 9	a_{16}	Controlling effective contact between A_{hi} and S_{ho}.
Scenario 10	a_{21}	Controlling effective contact between E_{ho} and S_{hi}.
Scenario 11	a_{22}	Controlling effective contact between I_{ho} and S_{hi}.
Scenario 12	a_{23}	Controlling effective contact between A_{ho} and S_{hi}.
Scenario 13	a_{24}	Controlling effective contact between E_{hi} and S_{hi}.
Scenario 14	a_{25}	Controlling effective contact between I_{hi} and S_{hi}.
Scenario 15	a_{26}	Controlling effective contact between A_{hi} and S_{hi}.
Scenario 16	a_{11}, a_{21}	Controlling effective contact between E_{ho} and S in both construction site and its close contact community.
Scenario 17	a_{12}, a_{22}	Controlling effective contact between I_{ho} and S in both construction site and its close contact community.
Scenario 18	a_{13}, a_{23}	Controlling effective contact between A_{ho} and S in both construction site and its close contact community.
Scenario 19	a_{14}, a_{24}	Controlling effective contact between E_{hi} and S in both construction site and its close contact community.
Scenario 20	a_{15}, a_{25}	Controlling effective contact between I_{hi} and S in both construction site and its close contact community.
Scenario 21	a_{16}, a_{26}	Controlling effective contact between A_{hi} and S in both construction site and its close contact community.
Scenario 22	$a_{11}, a_{14}, a_{21}, a_{24}$	Controlling effective contact between all E and S.
Scenario 23	$a_{12}, a_{15}, a_{22}, a_{25}$	Controlling effective contact between all I and S.
Scenario 24	$a_{13}, a_{16}, a_{23}, a_{26}$	Controlling effective contact between all A and S.
Scenario 25	$\theta_1, ..., \theta_4$	Controlling connection between construction site and its connected community.
Scenario 26	$a_{11}, ..., a_{26}$ $\theta_1, ..., \theta_5$	Controlling effective contact and connection among the whole population.
Scenario 27	$a_{11}, ..., a_{16}$	Controlling effective contact in community.
Scenario 28	$a_{21}, ..., a_{26}$	Controlling effective contact on the construction site.

6.4.2 Vaccination

Pharmacological intervention measures include effective medical treatments and available vaccinations. Many industries have encouraged their personnel to get vaccinated. For example, in Hong Kong's construction industry, construction workers have been asked to take regular PCR-RTC tests for COVID-19 since September 2020 [180] and encouraged to get vaccinated since May 2021 [181]. In this section, the vaccine efficacy is assumed as at least 60% [24]. This study simulates the effectiveness of different vaccination rates under different scenarios [24] and aims to identify how to best extinguish an ongoing wave of infection by reducing the attack rate on the construction site as shown in Fig. 6.7.

6.5 Results and discussion

6.5.1 Sensitivity Analysis

Comparing the results for first-order, total-order, fraction of unexplained variance, and total variance, this study analyzed the relationships between different parameters. The fraction of unexplained variance represents the amount of variance that is not captured by the proposed model, which is both close to zero in Figs. 6.2 and 6.3. Their total variances tend to increase but do not exceed 0.005 or 0.0001, meaning that the unexplained variance could be insignificant.

A local virus mutation represents more sensitivity than an imported virus mutation as indicated in Fig.6.2(a). Transmission rate β_1 is more sensitive in the connected community and so is β_2 on the construction site. Generally, when the Sobol indices of one parameter exceed 0.05 that implies an important input to the outputs. The contribution to the variance of E_{hi} from the interaction between β_1 and β_2 increases smoothly and becomes significant when β_1 and β_2 are larger than 0.8. Hence, due to the greater number of susceptible people in a larger community, virus mutations are especially impactful in such a population. Unexpected variances appear to increase as shown in Fig. 6.2(a). While this suggests that excluded factors do not have a significant impact, additional research could clarify potential relationships involving such factors.

In Fig. 6.2(b), transition rate θ_4 represents the most sensitivity indicating that intermingling of a higher percentage of contagious individuals with a wholly susceptible population increases the possibility of triggering an outbreak. Theoretically, the mobility of susceptible individuals cannot accelerate infection since only pre-symptomatic, asymptomatic, and symptomatic infectious individuals participate in transmitting SARS-CoV-2. The Sobol indices of θ_1 and θ_2

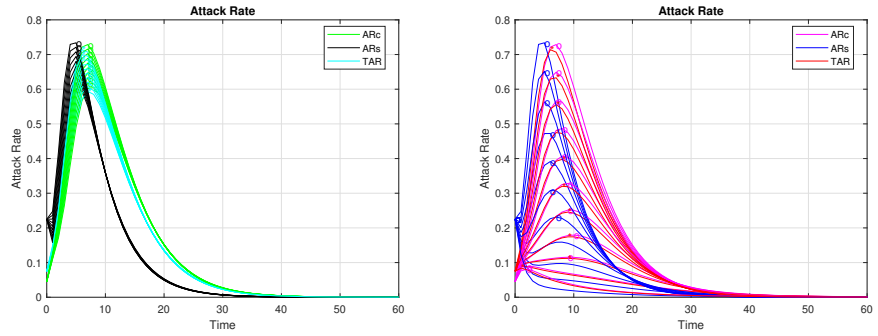

(a)

(b)

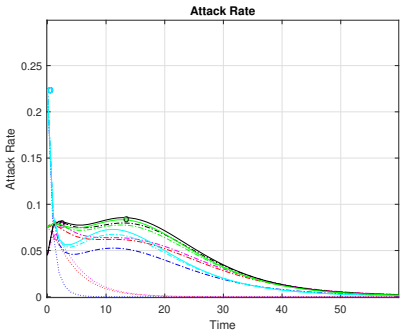

(c)

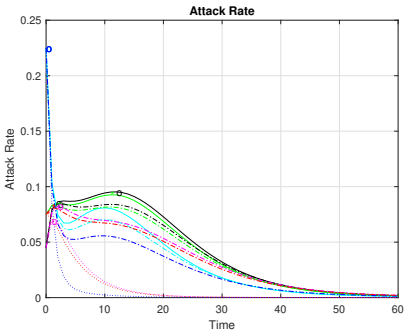

(d)

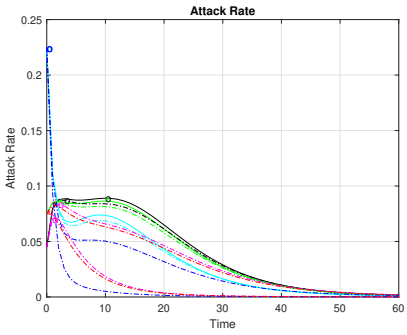

(e)

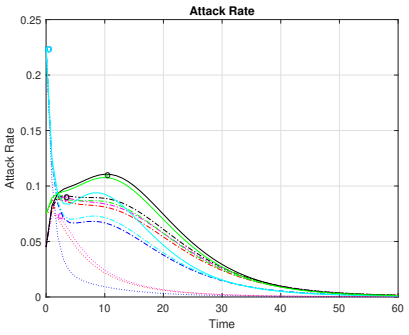

(f)

Figure 6.7: Vaccination effectiveness (a) when only construction workers vaccinated; (b) when only close contacts vaccinated; (c) when 100% construction workers vaccinated; (d) when 70% construction workers vaccinated; (e) when 50% construction workers vaccinated; and (f) when 30% construction workers vaccinated.

from susceptible individuals demonstrate increases over time, indicating that fully unrestricted population mobility is not feasible before herd immunity.

As shown in Fig. 6.3, the results within the construction site and its connected community exhibit similarities due to their analogous transmission dynamics. Sobol indices of a_{12} (0.55 - 0.756)/a_{22} (0.43 - 0.75), a_{11} (0.12 - 0.26)/a_{21} (0.12 - 0.22) and a_{14} (0.03 - 0.217)/a_{24} (0.03 - 0.2) rank as the top three to which I_{ho}, E_{ho} and E_{hi} especially contribute. Compared their impacts on the construction site and its connected community, higher effective contact ratios will contribute more to a large population. Although symptomatic individuals (a_{12}, a_{22}) is more sensitive to the variance of E_{hi} and E_{ho}, exposed people may more freely between different locations in the absence of symptoms and should be wll controlled owing to the high sensitivity of θ_3 and θ_4. Nevertheless, controlling exposed individuals is difficult due to the period of asymptomatic presentation that precedes and sometimes continues during infection, so vaccination remains a critical practice. For example, the Hong Kong government has encouraged more construction employees to get vaccinated and has exempted them from regular COVID-19 testing after 14 days upon his or her completion of the necessary doses of vaccine [181]. To help make optimal vaccination plans for the construction industry, the following section discusses their effectiveness.

In Fig. 6.4, the maximum AR (from 0.05 to 0.5) and average DO (from 120 to 50) changed sharply when the transmission rate β was less than 0.3. When β equals 0.7, AR and DO tend to be stable at 0.85 and 30 respectively due to a small proportion of the remaining susceptible people. Similarly as a_{ij} ($i = 1, 2; j = 1, 2, 4$ in Fig. 6.3 indicates high sensitivity. In Figs 6.4(d)-6.4(g), when θ_1, θ_3 and θ_4 exceed 0.5 and/or θ_2 exceeds 0.8, AR^s will be larger than 1, which may be attributable to human mobility leading to overall population increased on the construction site while the original number of construction workers remains unchanged.

6.5.2 Effectiveness of NPIs

Scenario 1 is the baseline (TAR: 51.55%, DO in the whole population: 42.93 days). Of all the 28 scenarios, Scenario 3 displays the greatest efficiency by reducing the attack rate up to 14 times RE but increasing DO by 18.75 days. Scenario 14 reduces DO the most, by 28% with a low RE of 1.305%. When controlling the effective contact ratio with wide-ranging restrictions, the AR can be reduced by at least 17% but will increase DO (Scenario 3, 19, 22, 23, and 27) in most cases. Hence, aiming for high-sensitivity effective contact ratios will lead to more significant efficiency. According to the sensitivity analysis, a_{ij} ($i = 1, 2; j = 1, 2, 4$) are the targeted elements. Compared to Scenario 4, 10, and 16, controlling both a_{11} and a_{21} from E_{ho} shows a better comprehensive

performance than separate controlling. Controlling I_{ho} extends DO with moderate effectiveness (around 5%). In terms of E_{hi}, Scenario 19 performed better than Scenarios 7 and 13 while increasing DO by three days. To reduce both TAR and DO, Scenario 16 demonstrates the best performance (25% AE and around 1.8 days DO reduction).

In terms of the pathogen, controlling indirect contacts can decrease the AR, though with low efficiency. Due to the limitation of this case study, the risk from indirect transmission pathways calls for more investigation. A visiting ban between the construction site and its connected community can only reduce AR by around 17.3% RE. The relationship between the pathogen in the environment and the severity of a pandemic in the construction industry was minimal and more empirical research is needed.

6.5.3 Effectiveness of Vaccination

A comparison of the results shown in Figs. 6.7(a) and 6.7(b) reveals that even if 100% of construction workers get vaccinated, the attack rates will still increase sharply within 10 days. Vaccination of all construction workers would lead to lower TAR in comparison to vaccination of merely 15% of both construction workers and their close contacts. Attack rates decreased as an outcome of vaccination during the simulation for a vaccine assumed to have at least a 60% vaccine efficacy in preventing infection compared to no vaccination, varying with a vaccination rate among close contacts shown in Figs. 6.7(c)-6.7(f). When 30%, 50%, 70%, and 100% of construction workers get vaccinated, 79%, 76%, 72%, and 67% respectively of their close contacts should be encouraged to also get vaccinated. Therefore, not only should construction workers be urged to get vaccinated but also their close contacts.

6.6 Chapter Summary

The insufficiency of continued NPIs and ongoing vaccination programs continue to pose challenges in recovering from the COVID-19 pandemic. Before herd immunity, controlling at-risk and vulnerable groups in combination with vaccination plans is strongly recommended. The construction industry is especially vulnerable to the negative impacts of COVID-19 as illustrated by frequent relevant clusters globally and given the manual labor performed by construction workers in close physical proximity. It increases the likelihood of exposure. To gain insights into the transmission dynamics COVID-19 to inform the establishment of effective, and targeted NPIs in the construction industry, a dual-community model was developed that includes the SEI/AHR-P model for construction workers and the SEIAHR model for their close contacts. The

results of our sensitivity analysis corroborate previous findings that close contacts are significant participants in the spread of the infection. However, the contributions of indirect transmission pathways at a construction site were found to be weak, suggesting the need for further study given conflicting results in other research. Based on the parameters identified as significant in the sensitivity analyses, 28 NPI scenarios were devised to analyze the total attack rate (TAR) and duration of an outbreak (DO). The scenario in which exposed individuals are controlled in terms of close contacts performs best, reducing the TAR with 25% absolute efficiency (AE) and decreasing the DO in the whole population by 1.8 days. In addition to NPIs, both construction workers and their close contacts are suggested to get vaccinated. Vaccination of all construction workers would lead to a lower TAR compared to vaccination of only 15% of both construction workers and their close contacts. Vaccination of all construction workers along with at least 67% of their close contacts can extinguish an ongoing wave.

6.6.1 Conclusions and Implications

The dual-community compartment model in this study is intended to examine how different combinations of targeted NPIs and vaccination plans could affect the transmission dynamics of SARS-CoV-2 among construction workers and their close contacts. The findings show that when the index case of SARS-CoV-2 is introduced to the construction industry, in the absence of any intervention, infection rapidly spreads among both construction workers and their close contacts, reaching its peak within 10 days. In addition, the SARS-CoV-2 in each community follows different transmissibility danamics. The construction site is impacted by both direct and indirect transmission pathways. Designed according to the sensitivity of significant parameters (i.e., effective contact ratios between different groups, transmission rates, etc.) from model (6.1), 28 customized NPI scenarios helped reduce the TAR and DO. In particular, controlling exposed individuals among their close contacts (Scenario 16) is recommended given the estimated ability of such control to reduce DO by 1.8 days and TAR with 25% AE as the primary measures. Limited by the insufficiency of screening technologies and frequent virus mutations, the NPIs combined with COVID-19 vaccines are strongly supported particularly in light of the diminishing public adherence to some existing NPIs. The results indicate the efficacy of having both construction workers and their close contacts become vaccinated. Otherwise, the vaccination of only construction workers will not be able to curb an outbreak. Around 67–79% of the close contacts of vaccinated construction workers should also be given a vaccine.This study supplements the limited literature addressing the epidemic spread of SARS-CoV-2 in the

construction industry considering the virus's transmission dynamics at the industry level. The macroscopic compartment model has been used to describe transmission dynamics at a city or country scale, but this model is hampered by its well-mixed and heterogeneous population assumptions. Designing an individual-based anti-epidemic strategy may prompt a discussion on transmission heterogeneity but cannot optimize misses the effectiveness of containing the epidemic explicitly. This study treats construction workers and their close contacts as part of the whole population in the construction industry due to their social activities. Thus, it balances the challenges faced in considering heterogeneous transmissibility microscopically and intervention planning macroscopically.

Targeted NPIs in combination with sufficient vaccination are recommended for implementation on construction sites. The vulnerability of construction workers is evident through their close physical proximity and the manual labor required. Given the objective of prioritizing the protection of construction worker health, controlling at-risk people (i.e. exposed individuals among their close contacts) and encouraging both construction workers and their close contacts to get vaccinated are the two most effective methods identified through this study.

6.6.2 Limitations and Directions for Future Research

This study did not distinguish indoor or outdoor construction sites. The majority of scenarios in prior studies are indoor settings since sharing indoor spaces with infected individuals has been confirmed to be the major infection risk origin of SARS-CoV-2 by many retrospective analyses [175]. However, there are significant gaps in our understanding of indoor and outdoor settings due to their vague definition [35]. Many outdoor risk sources (aerosolized particles emitted during wastewater treatment [190], respiratory droplets shedding from infected patients when gathering outside [118], etc.) can act as virus carriers as well. The significance of indirect pathogen transmission calls for more investigation and, will be influenced by whether the construction site is indoors or outdoors.

Theoretically, indirect pathogen transmission has been confirmed to be not as significant as human-related direct transmission, although the force of infections as shown in Eqs. (6.1) and the interpretation of $\mathcal{R}_0$ both point to a certain plausibility to the significance of pathogen-related transmission. Empirical and experimental evidence indicates that indirect transmission of the virus has occurred [10, 182, 248]. As for the construction industry, more empirical and observation studies are needed, which may include examining the possibility of construction workers shedding the virus into the environment or differing pathogen concentrations in indoor

or outdoor construction sites.

A longitudinal study to prevent other respiratory diseases is also needed for further researches, e.g., establishing a social-contact network [235]. The epidemiological justification for suspending face-to-face construction projects is that infected construction workers can spread a virus to others when sharing the same space through work or non-work activities. Co-working on the same construction site with someone who might shed the virus does not necessarily lead to an infection as workers may stand some distance away from each other or wear masks properly, but there can remain an increased risk. Management can facilitate responsibly resuming or continuing a construction project during an epidemic outbreak by supporting co-working networks for contact-tracing. Future research can further explore this topic by collecting construction workers' activity trajectories.

Chapter 7

A Priori Identification of Potential Superspreaders in Construction Projects

7.1 Introduction

Airborne infectious diseases typically spread through droplet nuclei with viruses that are transmitted via talking, coughing, and sneezing [112, 121]. Airborne infectious diseases have wrought adverse impacts on many sectors, especially construction sectors [30, 36, 162]. Poorly ventilated construction environments and the dynamic nature of construction activities construction workers greatly exacerbate the risk of infection, and can even trigger a super-spreading event, i.e. when a small fraction of highly contagious individuals disproportionately infect a large number of secondary cases [136, 257]. Infectious diseases have been found to be the second most common cause of absence in the construction industry [30]. Due to influenza-like illness, the average number of workdays missed is 1.30 days per episode of illness per person and the average work loss is valued at $137 per person [4]. Given their pivotal role in driving large outbreaks [117], superspreader individuals have been observed in connection with many airborne infectious diseases such as severe acute respiratory syndrome [SARS] [193], influenza [170], and coronavirus disease 2019 [COVID-19] [1]. Once a super-spreading event transpires, construction projects have to be delayed or suspended as the majority of workers cannot be present on site [28]. Construction site shutdowns owing to COVID-19 case clusters have occurred in many countries [e.g., the United Kingdom [96], the United States [10], Singapore [67] and Egypt [58]]. As a labour-intensive industry, it is crucial for the construction industry to understand the role of such superspreaders in determining the most effective ways to direct disease surveillance and controls [59, 257].

As for airborne infectious diseases, many industries have designed strategies for preventing and controlling super-spreading events, such as specialized ventilation systems in hospital wards [43], triage systems for patient consultations [229] and customized sitting arrangements in restaurants [55]. Due to the dynamic nature of construction activities, control strategies from other industries are not appropriate and difficult to implement in the construction industry. Previous studies in the construction industry mainly focused on the impacts and challenges caused by an outbreak, such

as economic losses and supply chain disruptions [5, 28], as well as response strategies to mitigate an outbreak [e.g., disinfection [105] and site access control systems [250]]. Only a few existing studies investigated the effectiveness of anti-epidemic interventions from an epidemiological perspective, such as interaction restrictions [15, 191, 255]. Few studies have explored strategies for preventing super-spreading events in the construction industry. Hence, this study aims to develop a method for identifying potential superspreaders of airborne infectious diseases in construction projects.

7.2 Literature Review

There is known heterogeneity between individuals in airborne infectious disease transmissions, leading to a general rule whereby 20% of cases cause 80% of transmission [159, 241, 257]. One of the sources of this heterogeneity is driven by interactions between individuals [78, 200]. Previous studies have discussed how heterogeneous interactions influence individual infectiousness through various models, such as compartmental epidemic models [255], agent-based epidemic models [15, 191], and network-based epidemic models [185]. Compartmental epidemic models describe heterogeneous interactions by different transmission probabilities between individuals across compartments, which is limited by a well-mixed population assumption [256]. Comparatively, agent-based epidemic models and network-based epidemic models refine the details of the assumptions in more realistic ways. For instance, the transmission probability could be nondeterministic, stochastic, and/or more heterogeneous. Agent-based epidemic models simulate individual-based interactions within defined rules from a microscopic perspective, while their performances rely more on the quality of the individual-level behaviour data, which raises a noticeable challenge for data collection [228]. Network-based epidemic models compute population-level epidemic dynamics in terms of individual-level interactions based on a network representing the interactions among all individuals [101]. Given their ability to model the complex interactions between individuals, network-based epidemic models have dominated research on individual infectiousness [168].

Network-based epidemic models describe the spread of infectious diseases according to nodes (i.e., individuals), edges (i.e., interactions between individuals) and weight of edges (i.e., the probability of infections). A small number of nodes (e.g., superspreaders) can have a major impact on the global spread of the disease. The importance of the nodes in disease spread can be quantified through various network-based performance measures, such as degree centrality [i.e., the number of edges that the node has] [6, 23], betweenness centrality [i.e., a measure of

how many shortest paths cross through this node] [29, 66], and K-shell index [i.e., a measure of the coreness of a node in the network] [39]. K-shell decomposition methods have been explored based on different algorithms to achieve enhanced performances [39, 134, 135]. In terms of identifying more influential spreaders in epidemiology, a K-shell index can help predict the progression of infection more reliably than an only degree or betweenness centrality [106, 135].

7.3 Methods

To explore the variance of individual infectiousness and the prevention of super-spreading events in the construction industry, this study aims to develop a network-based computational framework as a priori identification of potential superspreaders, consisting of K-shell decomposition approaches for analysing an interaction network and a stochastic network-based epidemic model for predicting infected cases. As shown in Figure 7.1, with data on the interactions of construction practitioners amongst themselves and others as input, the interaction network is established. In the interaction network $G(V,E)$, there are n nodes ($v_i \in V, 1 \leq i \leq n$). The edge between nodes v_i and v_j is represented as e_{ij} ($e \in E, i \neq j$). The value of e_{ij} is equal to 1 if v_i is connected to v_j; otherwise, e_{ij} is equal to 0. The transmission probability between individuals (P_e) is defined based on their interaction properties, organizational relationships, and contact ratios. The proposed framework is designed to estimate the K-shell index of each node and simulates the sequence of epidemic spread. According to the value of the K-shell index [$k_s(i)$] of the node v_i, if $k_s(i)$ is greater than the threshold of K-shell index [$k_{s,thr}$], the node v_i will be regarded as a K-shell based superspreader. During the stochastic epidemic spreading process within the interaction network, if the attack rate [$AR(i)$] of the node v_i (i.e., the number of secondary cases) within a serial interval (i.e., the duration of one generation) is larger than the threshold of attack rate [AR_{thr}], the node v_i will be regarded as a numerically certified superspreader. This study proposes to identify potential superspreaders who are included in both the K-shell based superspreader pool and the numerically certified superspreader pool. If the proposed framework were applied to a specific disease in a construction project, more detailed epidemiological parameters would be inputted according to the transmission characteristics of the particular disease.

7.3.1 K-shell decomposition method

K-shell decomposition methods can be used to identify the core and the periphery of a network. In this study, K-shell decomposition is carried out to measure the coreness of each node. After K-shell decomposition, each node v_i in the network is assigned a K-shell index $k_s(i)$ to represent

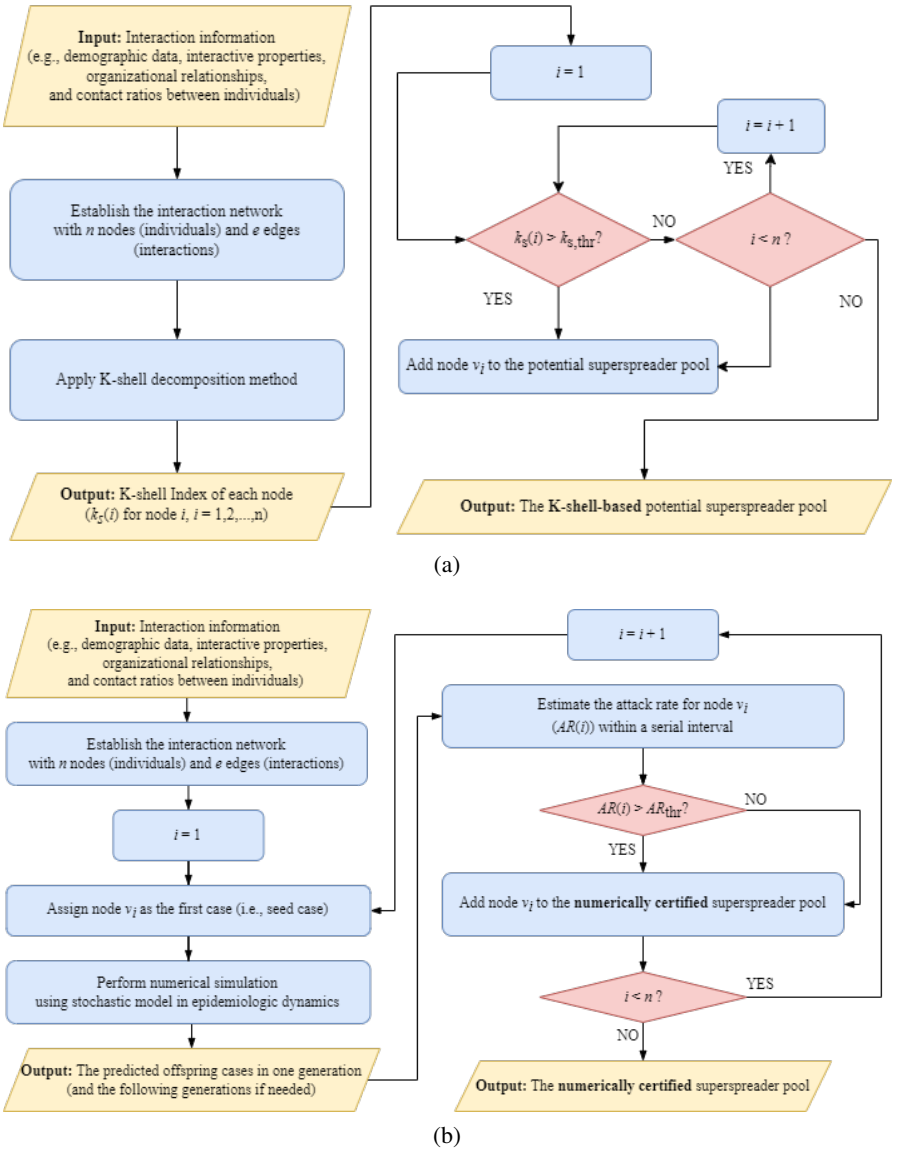

Figure 7.1: Workflow of the proposed network-based computational framework: (a) K-shell decomposition analysis; and (b) epidemic simulation.

its coreness in the network. A large k_s indicates a core position in the network, while a small k_s indicates a more peripheral position. The K-shell index of each node $k_s(i)$ is calculated based on its degree (k_i), which refers to the number of edges between the node v_i and its connected nodes. Generally, the K-shell index k_s provides more information on the role played by a node in the graph than the raw degree k, and thus k_s can be adopted as the indicator to determine whether a node is a potential superspreader [106].

$$K_i = \sum_{j}^{n} e_{ij} \tag{7.1}$$

The conventional K-shell decomposition algorithm is stated as follows: Firstly, all the nodes with degree $k_i = 1$ are removed. After such removal, the remaining nodes with $k_i = 1$ are also removed until all nodes with $k_i = 1$ are removed. All the these removed nodes are then clustered into the shell with $k_s = 1$. Secondly, we start to remove the nodes with $k_i = 2$ in a similar manner until all nodes with $k_i = 2$ are removed. Thus, the shell with $k_i = 2$ is established. This procedure continues until all nodes of this network are removed. Finally, each node in the network is assigned its corresponding k_s. In the above algorithm, the edges are treated equally. During the epidemic spreading process, the edges will have different values as the transmission probability of a specific disease for each contact is different [120, 160].

To further identify the node importance, a measure of potential edge weights in an unweighted network has been conducted [236]. The weighted K-shell decomposition analysis groups all nodes based on their weighted degrees (k_i^w).

$$k_i^w = \alpha k_i + (1-\alpha) \sum_{v_j \in V} (k_i + k_j) \tag{7.2}$$

In Eq.(7.2), k_i^w is a weighted degree of node v_i and α is a positive tuning parameter from 0 to 1. When α equals 1, the weighted degree of each node will equal its degree. When α equals 0, the weighted degree of each node will equal the sum of its degree and the degree of its connected nodes, which means that nodes with higher edge weights are more likely to be more influential. In this study, we set α as 0.5, which treats edge weights and degrees equally. Using the mentioned weighted degree k_i^w, the weighted K-shell decomposition algorithm follows a pruning route that is the same as the conventional K-shell decomposition algorithm except in that the former is based on the weighted degree (k_i^w) instead of the degree (k_i). Both conventional K-shell decomposition analysis and weighted K-shell decomposition analysis are capable of identifying potential superspreaders without considering edge weights. In reality, an individual may come into contact with many people, but they may all wear masks well (i.e., a node may have many connections, but each connection may have a small weight). In a weighted network, the weight of each edge w_{ij} can represent the transmission possibility between nodes v_i and v_j during the epidemic spreading process. To explore the impact of edge weights, a generalized K-shell decomposition analysis was also conducted [71]. In a weighted network, a generalized K-shell decomposition algorithm applies a pruning route that is the same as the conventional K-shell decomposition analysis but is based on an alternative node degree wk_i, as shown in Eq.(7.3)

[71].

$$wk_i = \left[k_i^{\sigma} \left(\sum_j^{k_i} w_{ij} \right)^{\rho} \right]^{\frac{1}{\sigma+\rho}} \tag{7.3}$$

In Eq.(7.3), there are two turning parameters: σ represents the impact from the degree of node v_i (k_i) and ρ represents the impact of the weight of edges (w_{ij}) associated with node v_i. In this study, we set $\sigma = \rho = 1$, which means that the node degree and the weight of edges have equivalent impacts while estimating the node influences. Hence, there are three types of K-shell decomposition methods in this study, which are compared in Table 7.1.

Table 7.1: Three types of K-shell decomposition methods

Methods	**Fundamental Indicators**	**Value of turning parameters**	**Considerations**		
			Degree of node v_i (k_i)	Degree of neighbour nodes (k_j)	Weight of edge e_{ij} (w_{ij})
Conventional K-shell decomposition analysis	$K_i = \sum_j^n e_{ij}$	N.A.	✓		
Weighted K-shell decomposition analysis	$k_i^w = \alpha k_i + (1-\alpha) \sum_{v_j \in V} (k_i + k_j)$	$\alpha = 0.5$	✓	✓	
Generalized K-shell decomposition analysis	$wk_i = \left[k_i^{\sigma} \left(\sum_j^{k_i} w_{ij} \right)^{\rho} \right]^{\frac{1}{\sigma+\rho}}$	$\sigma = \rho = 1$	✓	✓	✓

7.3.2 Stochastic models in epidemiology

To simulate the possible sequence of an epidemic spread, stochastic network-based epidemic models are used, in which the parameters and/or variables change with unit time. Figure 7.2 depicts three models for epidemic spread: a Susceptible-Infectious-Recovered (SIR) model (e.g., influenza), a Susceptible-Infectious-Recovered-Vaccinated (SIRV) model (e.g., measles), and a Susceptible-Exposed-Infectious-Recovered (SEIR) model (e.g., COVID-19).

A stochastic model for epidemiology is proposed that has including three components, namely a domain $\mathbb{D} = \{\mathbb{S}, \mathbb{E}, \mathbb{I}, \mathbb{R}, \mathbb{V}\}$, an underlying graph $G(V, E)$ with n nodes (i.e., individuals) and a collection $\mathcal{F} = \{f_1, f_2, \ldots, f_n\}$ of functions, where f_i is the local transmission function associated with nodes $v_i \in V, 1 \leq i \leq n$ [185]. A vector $(b_1^t, b_2^t, \ldots, b_n^t)$ consists of n elements, where $b_i^t \in \mathbb{D}$ is the value of the state of the node v_i at time t, $1 \leq i \leq n$. The unit interval t is measured in days. Due to the heterogeneity of intrinsic (i.e. properties of the individual) and extrinsic (environmental) factors that can affect transmission, let $\frac{1}{\sigma_i}$, $\frac{1}{\gamma_i}$, $\frac{1}{\xi_i}$ and $\frac{1}{\omega_i}$ denote the duration of incubation, infection, immunity, and vaccination period of each node v_i respectively. For $v \in V$, close contacts of v, denoted by N_v, contain each node u such that the edge $e = \{u, v\}$ is in E and associated with a transmission probability p_e. The transition of each system of each node v_i is depicted with the local transition function f_i synchronously (see Fig.7.2). Hence, each

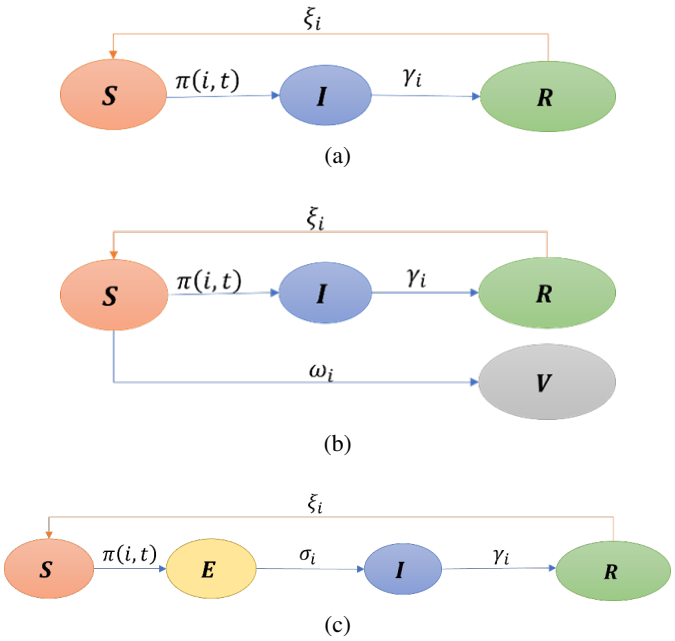

Figure 7.2: The transition of epidemic spreading in (a) a SIR system of each node v_i; (b) an SEIR system of each node v_i; and (c) a SIRV system of each node v_i.

node can be presented as $v_i \propto f_i(b_i^t, \sigma_i, \gamma_i, \xi_i, \omega_i, N_{v_i}, p_{\{u,v_i\}})$. The notation of all variables and parameters is shown in Table 7.2. If the state of v_i at time t is $\mathbb{S}$, the state of v_i at time $(t+1)$ is determined by the following stochastic process. Let $X_i(t) \subseteq N_{v_i}$ denote the set of close contacts of v_i whose state is infectious, such as $\mathbb{E}$ and $\mathbb{I}$ with an influenza A (H1N1) virus [79], at time t, and let the probability of becoming a confirmed case $\pi(i,t)$ be defines as follows:

$$\pi(i,t) = 1 - \prod_{u \in X_i(t)} (1 - p_{\{u,v_i\}}^{\max\{t-t_u,0\}}), \quad X_i(t) \neq \emptyset \tag{7.4}$$

For each node v_i, the immediate neighbour nodes u can infect v_i and start to infect v_i when pre-symptomatic, asymptomatic or symptomatic (which depends on the transmission characteristics of a specific disease) at the time (t_u+1). The transmission probability p_e is defined as $p_{\{u,v_i\}}^{\max\{t-t_u,0\}}$ and changes over time. If the states of v_i at the time $(t-1)$ is $\mathbb{S}$ and becomes infected by u at time t, the state of v_i at the time $(t+1/\sigma_i)$ is $\mathbb{E}$ and becomes $\mathbb{I}$ at the time $(t+1/\sigma_i+1)$. If the states of v_i at the time $(t-1)$ and t are $\mathbb{E}$ and $\mathbb{I}$ respectively, the state of v_i at the time $(t+1/\gamma_i)$ is $\mathbb{E}$ and becomes $\mathbb{I}$ at the time $(t+1/\gamma_i+1)$. If the states of v_i at the time $(t-1)$ and t are $\mathbb{I}$ and $\mathbb{R}$ respectively, the state of v_i at the time $(t+1/\xi_i)$ is $\mathbb{R}$ and becomes $\mathbb{S}$ at the time $(t+1/\xi_i+1)$. If the states of v_i at time t is $\mathbb{S}$, the state of v_i at the time $(t+1/\omega_i)$ is $\mathbb{V}$ with life-long immunity. To simplify the formulation, this study defined five dummy variables that can only take the value of 0 or 1 for a node v_i: when node v_i is susceptible at time t $(b_i^t = \mathbb{S})$, $S_i(t) = 1$; when this same node

v_i is exposed at time t ($b_i^t = \mathbb{E}$), $E_i(t) = 1$; when node v_i is infectious at time t ($b_i^t = \mathbb{I}$), $I_i(t) = 1$; when node v_i is recovered at time t ($b_i^t = \mathbb{R}$), $R_i(t) = 1$; and when node v_i gets vaccinated with a life-long immunity at time t ($b_i^t = \mathbb{V}$), $V_i(t) = 1$. Meanwhile, the sum of five dummy variables of node v_i equals 1 (i.e., $S_i(t) + E_i(t) + I_i(t) + R_i(t) + V_i(t) = 1$).

Table 7.2: Notation of epidemic models

Notation	Description
Variables	
S	the number of susceptible individuals
E	the number of exposed individuals
I	the number of infectious individuals
R	the number of recovered individuals
V	the number of vaccinated individuals with life-long immunity
N	the total number of individuals
Dummy Variables for node v_i	
S_i	When the node v_i is susceptible, S_i equals 1; otherwise, it is 0.
E_i	When the node v_i is exposed, E_i equals 1; otherwise, it is 0.
I_i	When the node v_i is infectious, I_i equals 1; otherwise, it is 0.
R_i	When the node v_i has recovered, R_i equals 1; otherwise, it is 0.
V_i	When the node v_i develops life-long immunity, V_i equals 1; otherwise, it is 0.
Local Transmission Function of node v_i	
b_i^t	the value of the state of node v_i at time t, $b_i^t \in \mathbb{D}$ ($\mathbb{D} = \{\mathbb{S}, \mathbb{E}, \mathbb{I}, \mathbb{R}, \mathbb{V}\}$)
$1/\sigma_i$	the duration of the incubation period of node v_i
$1/\gamma_i$	the duration of the infection period of node v_i
$1/\xi_i$	the duration of the immunity period of node v_i
$1/\omega_i$	the duration of the vaccination period of node v_i
N_{v_i}	the set of close contacts of v_i whose state is infectious
$p_{\{u,v_i\}}$	transmission probability p_e between an infected node u and node v_i

For example, as for the SIR model, the total population at time t $N(t)$ can be segmented into: susceptible individuals $S(t)$, infected individuals $I(t)$, and recovered individuals $R(t)$. Its transmission dynamic is shown as follows:

$$\begin{cases} \dot{S}(t) = \sum_{i=1}^{n} \xi_i(t)\, R_i(t) - \sum_{i=1}^{n} \pi(i,t)\, S_i(t), \\ \dot{I}(t) = \sum_{i=1}^{n} \pi(i,t)\, S_i(t) - \sum_{i=1}^{n} \gamma_i(t)\, I_i(t), \\ \dot{R}(t) = \sum_{i=1}^{n} \gamma_i(t)\, I_i(t) - \sum_{i=1}^{n} \xi_i(t)\, R_i(t). \end{cases} \tag{7.5}$$

$$S(t) + I(t) + R(t) = N(t) \tag{7.6}$$

In a SIRV model, the total population at time t $N(t)$ can be segmented into: susceptible individuals $S(t)$, infected individuals $I(t)$, recovered individuals $R(t)$, and vaccinated individuals

$V(t)$. The transmission dynamic of an SIRV system is shown as follows:

$$\begin{cases} \dot{S}(t) = \sum_{i=1}^{n} \xi_i(t)\, R_i(t) - \sum_{i=1}^{n} [\pi(i,t) + \omega_i(t)]\, S_i(t), \\ \dot{I}(t) = \sum_{i=1}^{n} \pi(i,t)\, S_i(t) - \sum_{i=1}^{n} \gamma_i(t)\, I_i(t), \\ \dot{R}(t) = \sum_{i=1}^{n} \gamma_i(t)\, I_i(t) - \sum_{i=1}^{n} \xi_i(t)\, R_i(t), \\ \dot{V}(t) = \sum_{i=1}^{n} \omega_i(t)\, S_i(t). \end{cases} \tag{7.7}$$

$$S(t) + I(t) + R(t) + V(t) = N(t) \tag{7.8}$$

In an SEIR model, the total population at time t $N(t)$ is segmented into: susceptible individuals $S(t)$, exposed individuals $E(t)$, infected individuals $I(t)$, and recovered individuals $R(t)$. The transmission dynamic of the SEIR system is shown as follows:

$$\begin{cases} \dot{S}(t) = \sum_{i=1}^{n} \xi_i(t)\, R_i(t) - \sum_{i=1}^{n} \pi(i,t)\, S_i(t), \\ \dot{E}(t) = \sum_{i=1}^{n} \pi(i,t)\, S_i(t) - \sum_{i=1}^{n} \sigma_i(t)\, E_i(t), \\ \dot{I}(t) = \sum_{i=1}^{n} \sigma_i(t)\, E_i(t) - \sum_{i=1}^{n} \gamma_i(t)\, I_i(t), \\ \dot{R}(t) = \sum_{i=1}^{n} \gamma_i(t)\, I_i(t) - \sum_{i=1}^{n} \xi_i(t)\, R_i(t). \end{cases} \tag{7.9}$$

$$S(t) + E(t) + I(t) + R(t) = N(t) \tag{7.10}$$

In epidemiology, the attack rate (AR) is the percentage of an at-risk population that contracts the disease during a specified time interval. In Eq.(7.11), the AR of COVID-19 is represented. As a result of a number of people getting infected at the workplace and having to be absent from work, a labour-intensive operation cannot be carried out properly. Operating thresholds can be set concerning the relationship between human resources and task allocations [26]. When the attack rate at time t is larger than the operation threshold AR_{thr}, the project will be suspended.

$$AR = \frac{\sum_{i=1}^{n} [E_i(t) + I_i(t)]}{n} \tag{7.11}$$

7.3.3 Performance measures

A confusion matrix is used to evaluate the performance of the proposed network-based computational framework in identifying superspreaders [253]. This study selects four metrics (i.e., *accuracy*, *precision*, *recall*, and F_1 score) and defines them in Eqns.(7.12)-(7.15). True Positive

(TP) is the number of actual superspreaders classified correctly as superspreaders. False Negative (FN) is the number of actual superspreaders classified incorrectly as non-superspreaders. False Positive (FP) is the non-superspreaders classified incorrectly as superspreaders, and True Negative (TN) is the non-superspreaders classified correctly as non-superspreaders.

$$Accuracy = \frac{TP+TN}{TP+FP+TN+FN} \tag{7.12}$$

$$Precision = \frac{TP}{TP+FP} \tag{7.13}$$

$$Recall = \frac{TP}{TP+FN} \tag{7.14}$$

$$F_1 = \frac{TP}{TP+(FN+FP)/2} \tag{7.15}$$

7.4 Case study of COVID-19

Given the repetitive waves of COVID-19 that had devastating effects on the construction industry [28], this study adopted COVID-19 as a case study to illustrate the feasibility and effectiveness of the framework on superspreader identification in construction projects. The epidemiologic characteristics of COVID-19 used in the case study follow the SEIR system as described in Eq.(7.9). All individuals are divided into four groups: susceptible, exposed, infectious, and recovered individuals. Susceptible individuals could get infected by pre-symptomatic, asymptomatic, or symptomatic individuals under effective contact as specified for each possible interactive activity. Each exposed individual is pre-symptomatic. Infectious individuals can be either asymptomatic or symptomatic, while their transmissibility is the same.

7.4.1 Numerical Cases modeled in a Hierarchical Network and Matrix Network

Networks with a matrix structure or a hierarchical structure are widely used to visualize cooperative and management behaviours among construction project practitioners [14, 111, 129]. This study generates one network with a hierarchical structure and another with a matrix structure. Each network has 43 nodes. The epidemic spreads according to the following assumptions:

1. Based on different activities between individuals, the transmission probability of each pair of interactions (P_e) is classified into five types [109]. The transmission probability of each interaction type (i.e., the weight of each edge) is assumed as shown in Table 7.3 according to the epidemiological features of COVID-19 and interactive characteristics of specific activities.

2. The node will transition to become an exposed individual when the value of $\pi(i,t)$ is larger than 0.5 and become an infectious individual when the value of $\pi(i,t)$ is larger than 0.7.
3. The duration of the immunity period ξ_i of each node v_i is set as 6 months [54, 171].
4. The serial interval (i.e., the duration of one generation) is assumed to be 4 days.
5. The operation threshold (AR_{thr}) is assumed as 20% [241]. Within one serial interval (assumed as 4 days), if the total attack rate becomes larger than 20%, the first case can be regarded as a potential superspreader.

Table 7.3: Assumptions owing to different types of interactions

Type of interaction	**Transmission probability P_e**
leadership between departments	0.1
leadership in the same department	0.2
regular interactions between departments	0.3
close interactions with colleagues	0.4
close interactions with other close contacts offsite (e.g., family members)	0.5

The scope of the interaction network of practitioners in a construction project in this study covers both interactions on-site and off-site (Yuan, Zhao, et al., 2022). As shown in Eq.(7.4), $\pi(i,t)$ describes the probability of a susceptible individual being infected after contacting an infected individual. In the proposed stochastic network-based epidemic model, when $\pi(i,t)$ is larger than 50%, the susceptible individual has a 50% possibility of becoming infected. As the viral load will increase during the incubation period, the exposed individual is assumed to show symptoms when $\pi(i,t)$ is larger than 0.7. The duration of immunity is assumed to be 6 months, as COVID-19 vaccines offer immunity against COVID-19 for at least six months [54, 171]. A serial interval is defined as the time from illness onset in the primary case to illness onset in the secondary cases. The mean serial interval of the alpha variant of severe acute respiratory syndrome coronavirus 2 (SARS-CoV-2) ranged from 4.2 to 7.5 days [8]. The serial interval of the delta variant is 4.7 days on average [84]. The omicron variant has the shortest serial interval (ranging from 2.2 to 3.5 days) [21]. In this study, the serial interval is assumed to be 4 days. As for many airborne infectious diseases (e.g., COVID-19), in a super-spreading event, the core 20% population are potentially highly contagious [241]. The operation threshold (AR_{thr}) is set as 20%. Hence, if the total attack rate is greater than 20% during the first 4 days, the first case can be regarded as a potential superspreader.

Two sample networks are shown in Figure 7.3. In this study three random nodes that have close interactions off-site were selected from each network [Nodes 7, 11, and 16 in Fig. 7.3(a); Node

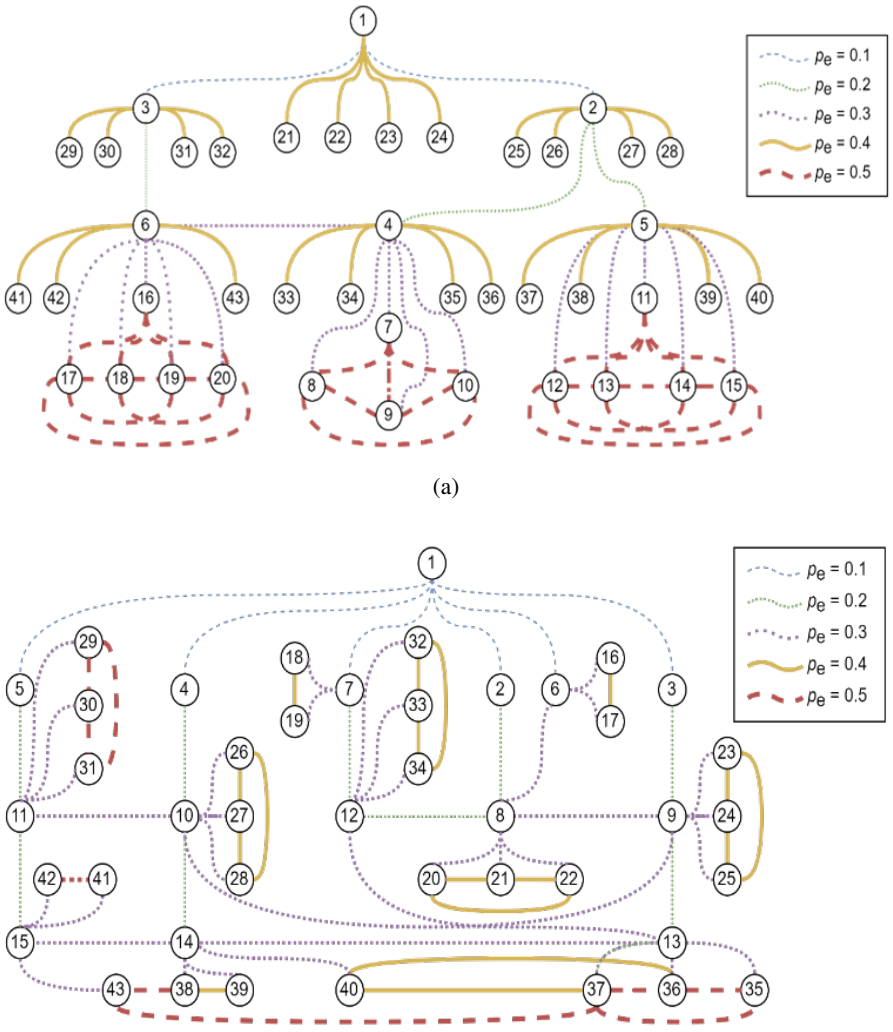

(a)

(b)

Figure 7.3: Organization chart view of a construction project: (a) hierarchical structure and (b) matrix structure.

29, 35, and 41 in Fig. 7.3(b)]. All edges in Figure 7.3 are set to different weights according to the appropriately corresponding assumption in Table 7.3. For example, in Fig. 7.3(a), the relationship between Node 1 and Node 2 is "leadership between departments". The leadership between Node 3 and Node 6 is in the same department. Node 4 and Node 6, which are from different departments, have regular interactions. The relationship between Node 4 and Node 33-36 is "close interactions with colleagues". Node 16 has close contact with Nodes 17-20 outside the workplace. After performing three types of K-shell decomposition analyses (as shown in Table 7.1) to classify all individual nodes into different shells, every node is considered to be the first infected case (i.e., the primary case) and the transmission dynamics are simulated using the SEIR model in Eq.(7.9). The results of the K-shell decomposition computations for two sample

networks are represented in Figures 7.6 and 7.7.

7.4.2 Empirical case of a construction project in Hong Kong

7.4.2.1 Data Description

This study collected information regarding 1846 participants' interactions with 123 sub-contractors (including 212 COVID-19 confirmed cases) from January 28 to March 24, 2022, in a construction project in Hong Kong. We obtained demographic information, the date of diagnosis, last working date, and employment relationship of each person. In total, 91.04% of infected cases are male and 8.96% of infected cases are female. Classified by their occupations in Table 7.4, there are 0.94%, 3.77%, 7.08%, 16.04%, 68.87%, and 3.30% of COVID-19 cases who work as managers, officers, foremen, engineers, on-site workers, and others respectively. As shown in Figure 7.4, three-quarters of cases generated less than 2 offspring cases, and 32.08% of cases didn't generate any offspring cases. Only 10.38% of seed cases generated 79.72% of the offspring cases (i.e., susceptible individuals who get infected by seed cases).

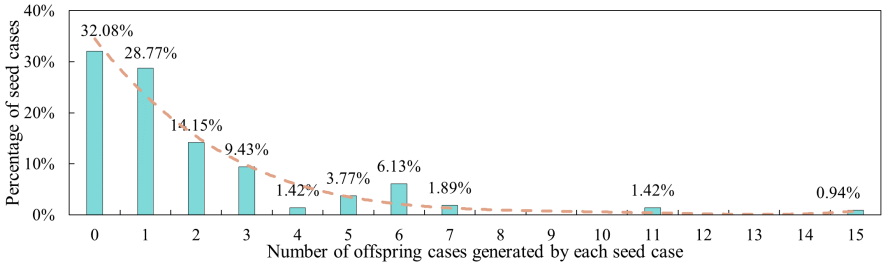

Figure 7.4: Distribution of offspring cases generated by each seed case.

7.4.2.2 Reproduction of the Interaction network

There are 27 subcontractors, among which have at least one confirmed case, labeled as G1 to G27 ("G" for Group). To explore the transmission dynamics based on interactions among these participants, this study considered their intra-subcontractor interactions (i.e., interactions among people who are hired by the same subcontractor) and inter-subcontractor interactions (i.e., interactions among people who are hired by different subcontractors) respectively. There are 41 pairs of intra-subcontractor interactions across 9 groups (i.e., G1, G2, G4, G8, G9, G12, G15, G17 and G25). This study selected these 9 groups as inputs of the interaction network. In addition, there are three pairs of groups (i.e., G2 & G3, G9 & G14, and G12 & G13) where they have the same number of employees, but one had a super-spreading event and one did not. This study also selected G3, G13 and G14 to explore why a super-spreading event occurred.

Table 7.4: Demographic information of all COVID-19 confirmed cases

Gender	**Number of cases**	**Percentage (%)**	**Attack Rate (%)**
Male	193	91.04	11.60
Female	19	8.96	10.44
Occupation	**Number of cases**	**Total Population**	**Attack Rate (%)**
Officer (e.g., office clerks)	8	10	80.00
Engineer	34	60	56.67
Others (e.g., drivers and securities)	7	18	38.89
Foreman	15	52	28.85
Manager	2	10	20.00
On-site Worker	146	1368	10.67
Scaffolder	6	6	100.00
Carpenter	11	13	84.62
Asphalter	1	5	20.00
Construction Materials Purchaser/ Storekeeper	2	14	14.29
Electrical Fitter	28	204	13.73
Electrician	3	24	12.50
Plumbers	11	117	9.40
General Worker	72	808	8.91
Builder's Lift Operator	3	36	8.33
Construction Plant operator	5	64	7.81
Refrigeration/ Air-conditioning/Ventilation Mechanic	2	29	6.90
Leveler	1	23	4.35
Bar Bender and Fixer	1	25	4.00

In conclusion, this study developed an interaction network containing 317 people from the 12 mentioned groups (i.e., G1-G4, G8-G9, G12-G15, G17, and G25) in terms of their demographic information (i.e., number of employees) and epidemic information (i.e., number of cases, attack rate, and number of superspreaders), as shown in Table 7.5.

The topology of the intra-subcontractor interaction network is assumed as a small-world network with a mean degree of 4 [231]. In a small-world network, most nodes are not neighbors of one another, but most nodes can be reached from every other node through a small number of steps. Each person is identified by a unique identification number assigned by the dataset (i.e., "GXnode$Y", the No. Y case in group GX), and thus their real-world identities were masked. As shown in Figure 7.5, all interactions from the 12 selected groups and between them are represented with 1309 edges. This study analyzes the interaction network by the proposed network-based computational framework. As 10.38% of the seed cases generated 79.72% of the offspring cases (as shown in Figure 7.4), this study assumed the AR_{thr} to be equal to 11%. Each node is assumed to be a primary case and this study conducted 100 simulations to estimate the

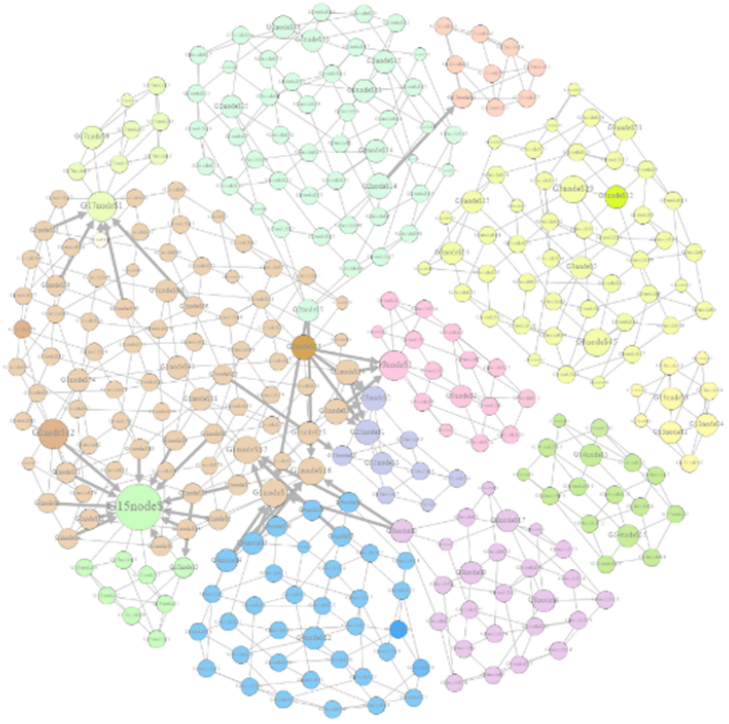

Figure 7.5: Interaction network including 315 participants from 12 subcontractors. Thick arrows indicate interactions across groups. Nodes with the same colour represent people from the same group. Nodes with bigger sizes have a higher degree. "GXnode$Y" represents the No. Y case in group GX.

possible sequence of the epidemic spread during the first 4 days. When AR on the 4^{th} day is larger than 11%, the primary node is regarded as a numerically certified superspreader. Through a comparison with the list of actual superspreaders in reality (as shown in Table SI.3.1, the performance is estimated by Eqns.(7.12)-(7.15) and shown in Table 7.6.

7.5 Results and discussions

7.5.1 Two numerical cases with sample networks

In these two sample networks, the total population is 43. ARthr is assumed as 20% as stated in Section 7.4.1, which means that the threshold number of confirmed cases on the 4^{th} day is 8.6. Following the workflow as shown in Fig.7.1(a), in the hierarchical network, the three K-shell decomposition methods (i.e., conventional, weighted, and generalized K-shell decomposition analysis) divided all nodes into 4, 6 and 2 groups respectively, as shown in Fig.7.6. In the matrix network, the three K-shell decomposition methods divided all nodes into 2, 4, and 4 groups respectively, as shown in Fig.7.7. In this study, people with k-shell index values in the top 50

Table 7.5: Information of the interaction network containing people from the 12 selected groups

No. (i)	Label	Number of employees	Number of cases	Number of Superspreaders (who generated over 6 offspring cases)	Attack rate(%)
1	G1	81	40	20	49.38
2	G2	49	24	4	48.98
3	G3	49	5	Nil	10.20
4	G4	36	16	3	44.44
5	G8	25	2	1	8.00
6	G9	16	6	1	37.50
7	G12	9	4	1	44.44
8	G13	9	1	Nil	11.11
9	G14	16	7	Nil	43.75
10	G15	9	5	5	55.56
11	G17	9	3	1	33.33
12	G25	9	8	2	88.89
	sum	317	121	38	38.17

Table 7.6: Performance of the proposed network-based computational framework for identifying superspreaders

Network	K-shell Decomposition Method	$k_{s,thr}$	Confusion Matrix		Precision	Recall	F1 Score	Accuracy
Hierarchical network	Conventional K-shell decomposition analysis	50%	21	1	95.45%	95.45%	95.45%	95.45%
			1	20				
	Weighted /generalized K-shell decomposition analysis	50%	22	0	100.00%	100.00%	100.00%	100.00%
			0	21				
Matrix network	Conventional/weighted K-shell decomposition analysis	50%	11	2	50.00%	84.62%	62.86%	69.77%
			11	19				
		26%	11	2	100.00%	85.62%	91.67%	95.35%
			0	30				
	Generalized K-shell decomposition analysis	50%	9	4	40.91%	69.23%	51.43%	60.47%
			13	17				
		26%	9	4	81.82%	69.23%	75.00%	86.05%
			2	28				

percent are identified as K-shell based superspreaders. This study validated the value of $k_{s,thr}$ in comparison with the results of the stochastic network-based epidemic models. The performance of the network-based computational framework is estimated with the AR^{thr} set to 20% and the default $k_{s,thr}$ set to 50%.

Following the workflow in Fig.7.1(b), the stochastic epidemic spreads were simulated. The average attack rate is 19.57% in the hierarchical network and 17.36% in the matrix network. There are 22 and 13 individuals who are numerically certified superspreaders in each network,

respectively. In comparison with the results of the K-shell based and the numerically certified superspreader pools, in the hierarchical structure 21 individuals are both K-shell based and numerically certified superspreaders. There is one FP node (i.e., 'n1') that is not a numerically certified superspreader but has a high k_s value, as shown in Fig.7.8(a). Both weighted K-shell decomposition analysis and generalized K-shell decomposition analysis successfully identified all 22 superspreaders. In the matrix network, conventional K-shell decomposition analysis and weighted K-shell decomposition analysis, successfully identified 11 numerically certified superspreaders. There are 2 individuals (i.e., 'n15' and 'n43') who are numerically certified superspreaders but have low ks values, as shown in Fig.7.9(a-b). Meanwhile, there are 4 FN nodes (i.e., 'n14', 'n15', 'n40' and 'n43') from the results of generalized K-shell decomposition analysis, as shown in Fig.7.9(c). The performance results for the two sample networks are summarized in Fig.7.6. After comparing two superspreader pools, the value of $k_{s,thr}$ remains as 50% in the hierarchical network and the value of $k_{s,thr}$ is found to be 26% in the matrix network. The proposed network-based computational framework can help identify superspreaders from the hierarchical network with an average accuracy of 98.45% $\left(AR_{thr} : 20\%;\ k_{s,thr} : 50\%\right)$ and the matrix network with an average accuracy of 92.25% $\left(AR_{thr} : 20\%;\ k_{s,thr} : 26\%\right)$.

In the hierarchical network, 'n1' has been classified incorrectly as an 'FP' node. Node 'n1' has 6 connected nodes and two of them (i.e., 'n2' and 'n3') are numerically certified superspreaders. Once 'n2' or 'n3' was infected by 'n1', a super-spreading event was triggered. In terms of the results of the K-shell decomposition methods, 'n1' was given a relatively high ks value. After considering the impacts contributed by its connected nodes and the weight of edges, accuracy is significantly improved.

In terms of the matrix network, 'n14', 'n15', 'n40' and 'n43' are numerically certified superspreaders but have low ks values. These four nodes have contacts with three superspreaders (i.e., 'n10', 'n11', and 'n13') that are identified correctly. Similarly, once the aforementioned 4 'FN' nodes infect or are infected by three superspreaders (i.e., 'n10', 'n11' or 'n13'), a super-spreading event would be triggered. Hence, the network-based computational network can help identify both superspreaders and individuals who can trigger a super-spreading event.

7.5.2 Empirical case of a construction project in Hong Kong

All nodes in the interaction network are divided into 3, 6, and 2 groups by the three K-shell decomposition methods applied in this study, respectively, as shown in Figures7.10(a)-7.10(c). According to Table SI.3.1, 38 actual superspreaders are listed. Compared with the empirical

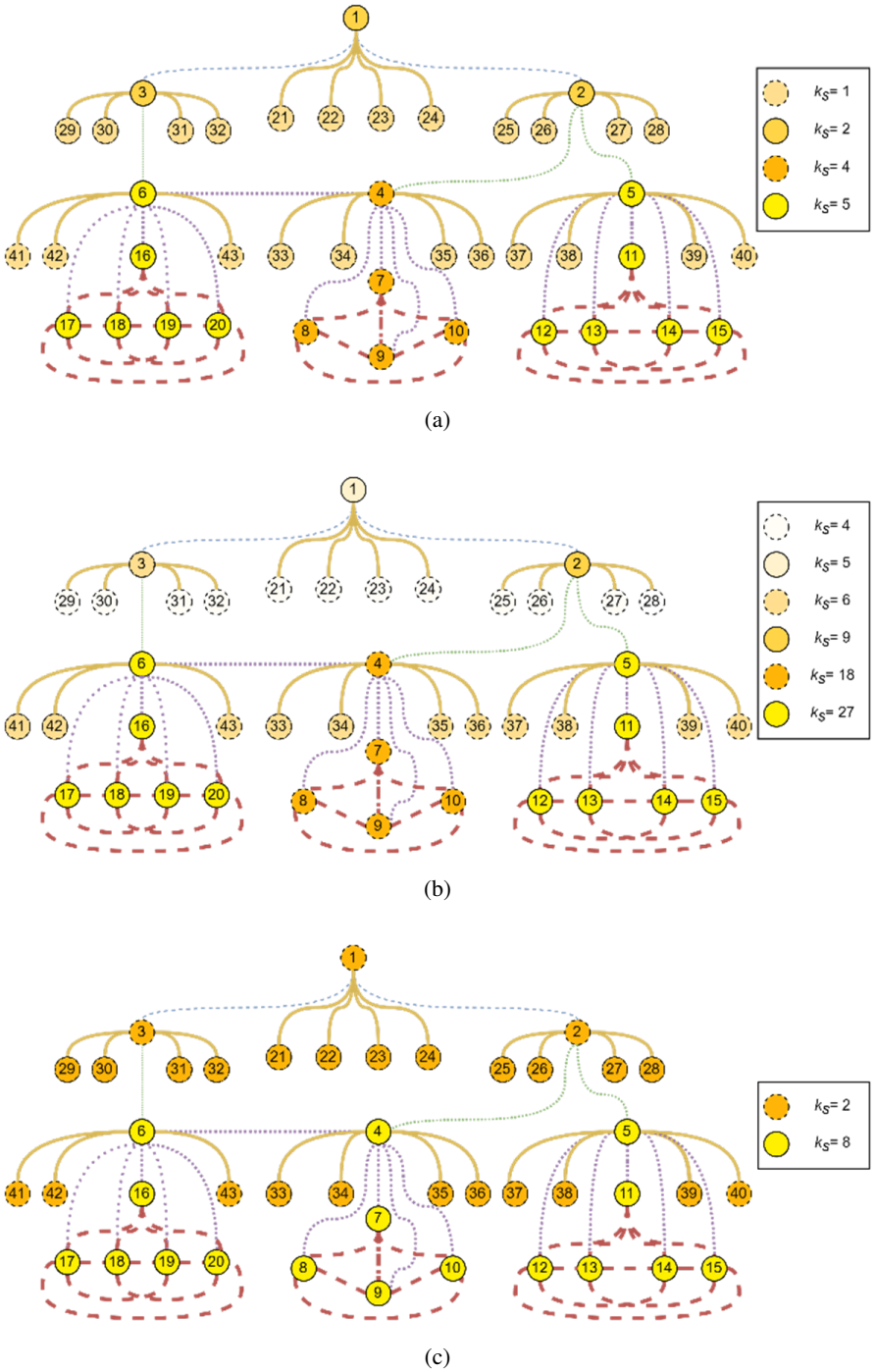

Figure 7.6: Results of K-shell decomposition methods in the hierarchical network by (a) conventional K-shell decomposition analysis; (b) weighted K-shell decomposition analysis; and (c) generalized K-shell decomposition analysis.

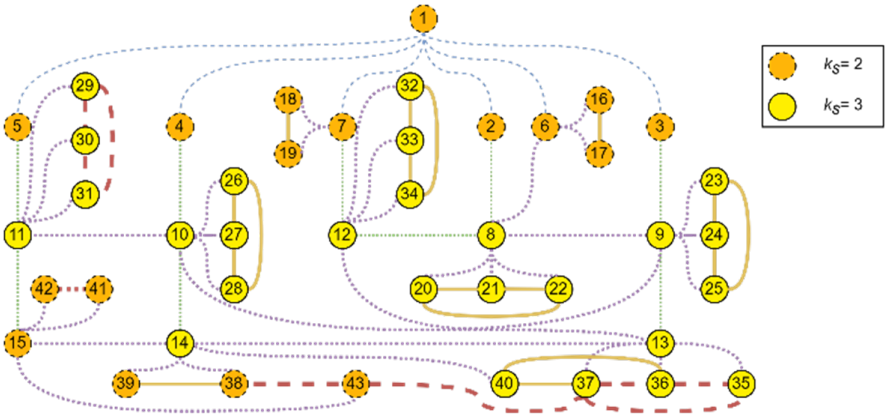

(a)

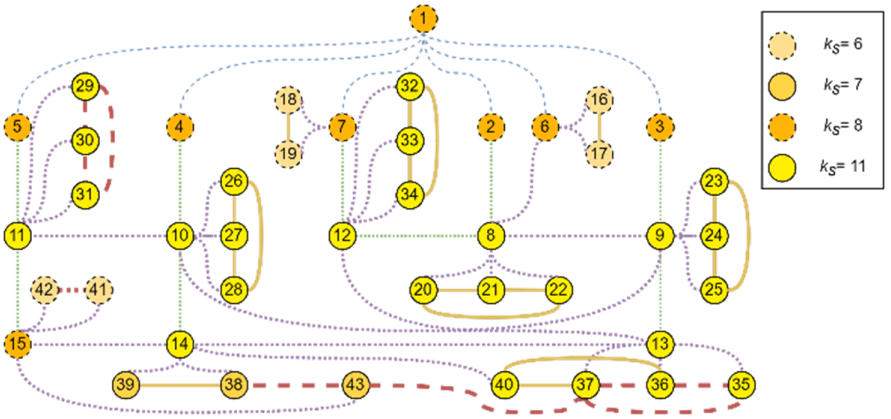

(b)

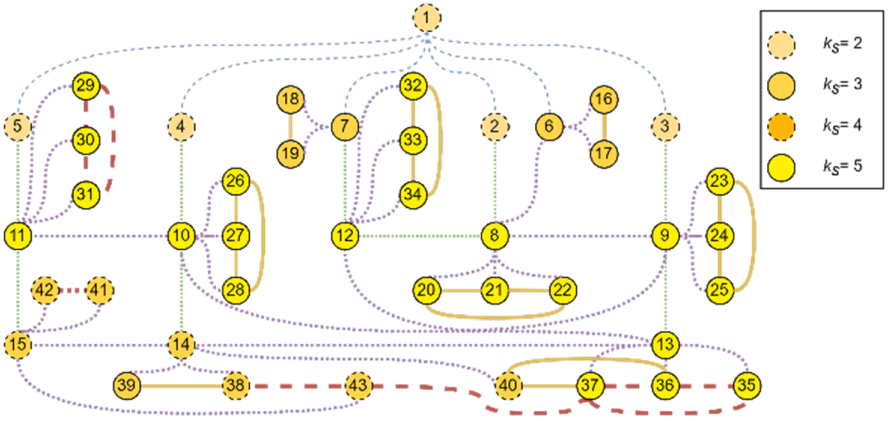

(c)

Figure 7.7: Results of K-shell decomposition methods in the Matrix network by (a) conventional K-shell decomposition analysis; (b) weighted K-shell decomposition analysis; and (c) generalized K-shell decomposition analysis.

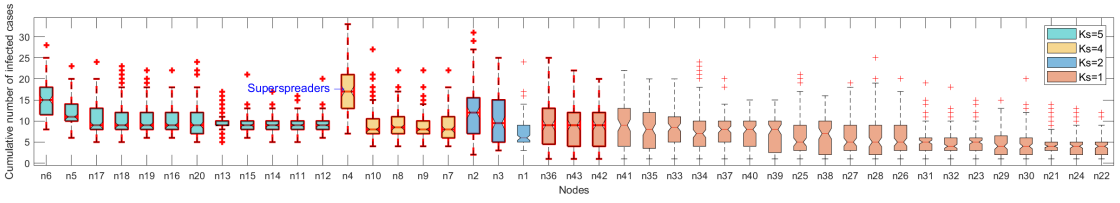

(a)

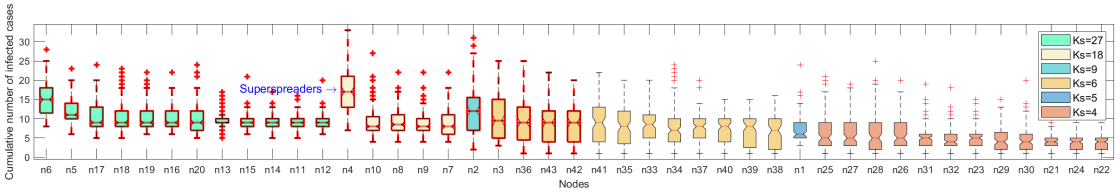

(b)

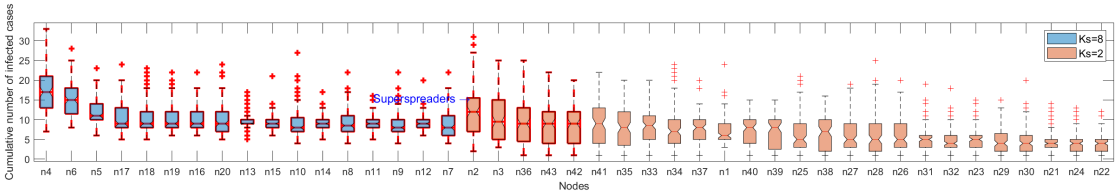

(c)

Figure 7.8: Cumulative number of infected cases on the 4th day predicted by stochastic epidemic models in the hierarchical network where nodes are analysed with: (a) conventional K-shell decomposition; (b) weighted K-shell decomposition; and (c) generalized K-shell decomposition.

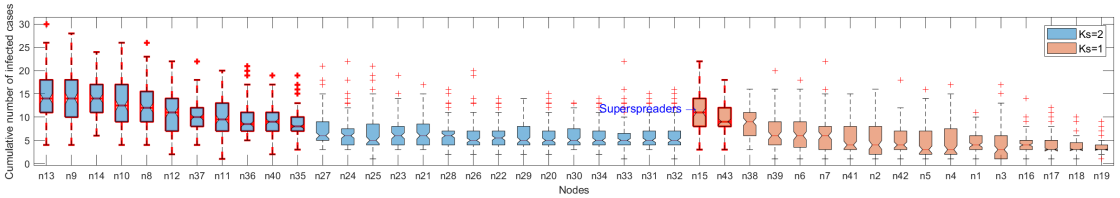

(a)

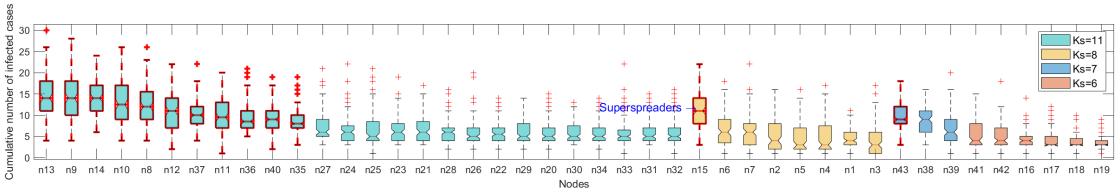

(b)

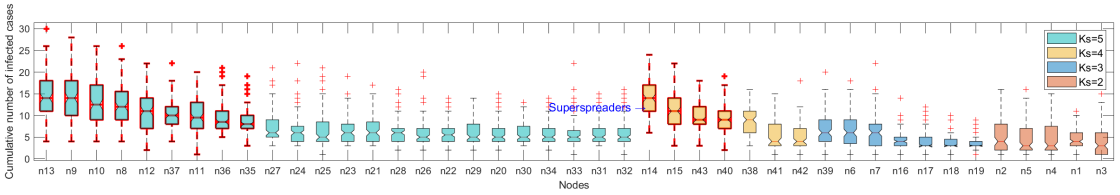

(c)

Figure 7.9: Cumulative number of infected cases on the 4th day predicted by stochastic epidemic models in the matrix network where nodes are analysed with: (a) conventional K-shell decomposition; (b) weighted K-shell decomposition; and (c) generalized K-shell decomposition.

results, the predictive performance of the K-shell methods and the stochastic network-based epidemic model are shown in Table 7.7. In terms of the default $k_{s,thr}$, which is assumed to be 50%, there are 32 actual superspreaders which are included in the K-shell superspreader pool. The three K-shell decomposition methods exhibited the same performance. In terms of the numerically certified superspreader pool, the AR_{thr} is assumed to be 11% as indicated in Section 7.4.2. When the number of confirmed cases on the 4th day exceeds 34.87, the primary case will be regarded as a numerically certified superspreader. This study identified 81 numerically certified superspreaders, accounting for 25.5% of the total. In the results generated by the stochastic network-based epidemic model, these numerically certified superspreaders are able to generate 112.5-193.4 secondary cases within 4 days. There are 28 actual superspreaders from the empirical data that are correctly identified in the numerically certified superspreader pool. In total, there are 25 nodes which are both K-shell based and numerically certified superspreaders. There are 53 'FP' nodes, 10 'FN' nodes and 229 'TN' nodes in the numerically certified pool. There are 127 'FP' nodes, 6 'FN' nodes and 152 'TN" nodes in the K-shell superspreader pool. After validating the value of $k_{s,thr}$ as 28%, the number of 'FP' nodes decreases from 127 to 57 and the accuracy increases from 58.04% to 80.13%. In the results generated by all three K-shell decomposition methods, these K-shell based superspreaders ($k_{s,thr}$: 28%) are able to generate 28.3-193.4 secondary cases within 4 days.

Table 7.7: Predictive performance of K-shell methods and Stochastic Epidemic Models as compared to empirical results

Method		Confusion Matrix		Precision	Recall	F1 Score	Accuracy
Conventional K-shell decomposition analysis	$K_{s,thr} = 50\%$	32	6	20.13%	84.21%	32.49%	58.04%
		127	152				
	$K_{s,thr} = 28\%$	32	6	35.96%	84.21%	50.39%	80.13%
		57	222				
Weighted K-shell decomposition analysis	$K_{s,thr} = 50\%$	32	6	20.13%	84.21%	32.49%	58.04%
		127	152				
	$K_{s,thr} = 28\%$	32	6	35.96%	84.21%	50.39%	80.13%
		57	222				
Generalized K-shell decomposition analysis	$K_{s,thr} = 50\%$	32	6	20.13%	84.21%	32.49%	58.04%
		127	152				
	$K_{s,thr} = 28\%$	32	6	35.96%	84.21%	50.39%	80.13%
		57	222				
Stochastic network-based epidemic model	$AR_{thr} = 11\%$	28	10	34.57%	73.68%	47.06%	80.13%
		53	229				

As shown in Figures7.10-7.10(c),the shell with the highest k_s according to all three K-shell decomposition methods consists of 'G12node$1-9' and 'G13node$2-9'. Only 'G12node$1' is

an actual superspreader listed in Table 7.4. In the outbreak from January 28 to March 24, 2022, there was a super-spreading event in G12, which was triggered by 'G12node$1'. All three K-shell decomposition methods successfully predicted this super-spreading event as well as all infected cases. All individuals in G12 are scaffolders who have cooperative behaviours. In addition, they have close interactions off-site as they are villagers living in the same village. Some of them are also relatives. Close interactions off-site are the major reason for this super-spreading event. G12node$1 is regarded as an actual superspreader as he/she is the primary case in this super-spreading event. Other members in G12 also exhibit a high probability of generating secondary cases based on their close interactions off-site. As described in Section 7.4.2.2, G13 has a similar structure to G12. When analysing their structures, G13 also exhibits a high probability of triggering a super-spreading event like G12. In reality, G12 has an intra-subcontractor interaction with G2 by a pair of nodes ('G2node$14' and G12node$1'). 'G2node$14' is an actual superspreader as well. As for G13, there are no intra-interactions, which hindered the spread of infection. The other two pairs of groups (i.e., G2 and G3; G9 and G14) also have a similar situation. Like G13, if there is any infected case in G3 and G14, a majority of individuals would likely get infected due to their close interactions. However, the outbreak in G3 and G14 would be consistently limited to a particular region since there are no intra-interactions.

As shown in Table SI.3.1, there are 9 groups containing superspreaders. More than half of the 38 actual superspreaders are from the main contractor "G1", with a prediction accuracy of 98.77% (TP:19, FN:1, FP:0, TN:61). Within the first 4 days, each superspreader in G1 could generate 48.40 secondary cases on average. Notably, the first case in many subcontractors was infected by contagious individuals from G1. For example, the outbreak in G25 was triggered by two infector–infectee pairs (i.e., "G1node$35" & "G25node$1" and "G1node$35" & "G25node$2"). Similarly, "G15node$2", the only superspreader in G15, was caused by infected cases from G1 (i.e., G1node$3-13). If all predicted superspreaders from G1 were detected through regular rapid antigen tests (RATs), the spread of COVID-19 in the following 4 groups (i.e., G9, G17, G15, and G25) could have been mitigated. By using contact tracing (Adam et al., 2020; Y. Liu et al., 2021; Yuan et al., 2023), up to 68.77% of infected cases could have been averted. Thus, this study recommends that all potential superspreaders, especially if they are employed by the main contractor, should take RATs regularly. If all potential superspreaders were detected through regular RATs and all potential secondary cases were detected through contact tracing, up to 82.35% of infected cases could have been prevented.

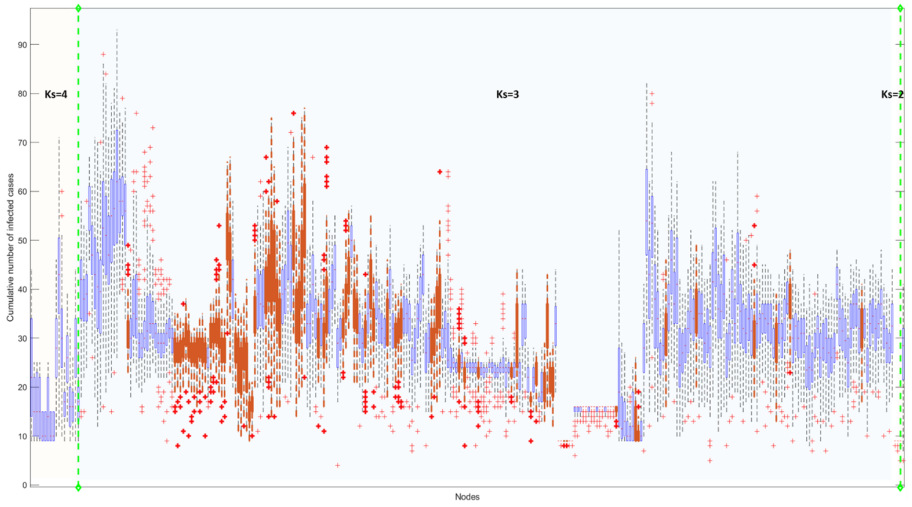

(a)

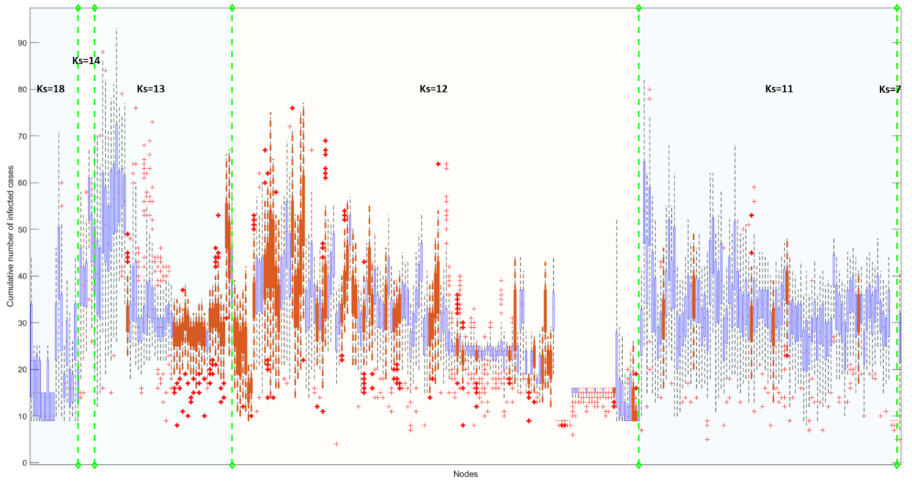

(b)

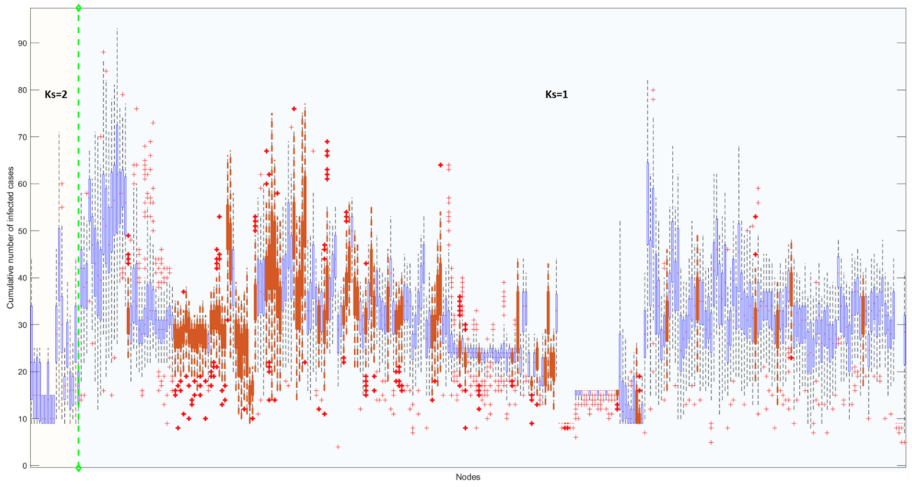

(c)

Figure 7.10: Cumulative number of infected cases on the 4th day predicted by stochastic epidemic models in the interaction network of the construction project in Hong Kong where nodes are analyzed with (a) conventional K-shell decomposition analysis; (b) weighted K-shell decomposition analysis; and (c) generalized K-shell decomposition analysis.

7.6 Chapter summary

7.6.1 Conclusions and Implications

This study introduced a network-based computational framework for identifying superspreaders for airborne infectious diseases (in Figure 7.1). With the input of the on-site interaction network data, this study uses K-shell decomposition methods to estimate the K-shell index of each node to identify K-shell based superspreaders based on K-shell ($k_{s,thr}$) threshold as shown in Figure7.1(a). The possible course of the epidemic spread is predicted based on stochastic network-based epidemic models (as shown in Figure7.1(b)). Given the first case in the network, when the attack rate within a serial interval is larger than the threshold of the attack rate (AR_{thr}), this specific first case is regarded as a numerically certified superspreader. Both K-shell based and numerically certified superspreaders can be potential superspreaders. If a potential superspreader gets infected, all his/her downstream, potentially infected cases who are predicted by stochastic models should be excluded from the workplace to prevent further adverse impacts.

In the case study of COVID-19 spreading through two sample networks, the proposed framework helped identify superspreaders in a hierarchical network with an average accuracy of 98.4% (AR_{thr} : 20%; $k_{s,thr}$: 50%) and in a matrix network with an average accuracy of 92.25% (AR_{thr} : 20%; $k_{s,thr}$: 26%). After considering the impacts caused by connected nodes with weighted or generalized K-shell decomposition methods, the accuracy can be further improved to nearly 100%. Specifically, if the primary case is located in the shell with the highest ks value, he/she has an almost 100% possibility of becoming a superspreader.

Based on the COVID-19 outbreak in the Hong Kong construction project examined in our case study, the total attack rate (i.e., the percentage of confirmed cases from the total population) is 11.48%. This outbreak lasted 56 days, from January 28 to March 24, 2022. By considering both inter-subcontractor and intra-subcontractor interactions, 317 participants from 12 subcontractors were inputted into the proposed framework (including 121 COVID-19 cases). K-shell decomposition helped identify superspreaders with an average accuracy of 80.13% when the value of $k_{s,thr}$ is set to 28%, which is close to the prediction accuracy of the stochastic network-based epidemic model (80.31%). If all potential superspreaders were detected through regular RATs and all potential secondary cases were detected by contact tracing, up to 82.35% of infected cases could be averted.

7.6.2 Limitations and Directions for Future Research

This study is an exploratory attempt to inform efforts in boosting the resilience of construction projects in the face of airborne infectious disease. As such, this research could be improved through various avenues. For instance, the prediction accuracy of K-shell decomposition methods could be further fine-tuned if more detailed information could be collected, such as the topology of interaction networks. A more reliable topology of interaction networks can help predict the possible sequence of the epidemic spread more accurately. Theoretically, individuals in the numerically certified superspreader pool should be included in the list of the K-shell based superspreader pool. In this study, the topology of interaction networks was established based on people's occupations, frequency of contact with others, and a small-world assumption. After performing K-shell decomposition, in some cases the majority of nodes have the same or close ks value, which means that the core and the periphery of the network cannot be significantly distinguished from each other. In addition, this limitation prevented further discussion on the threshold of ks values ($k_{s,thr}$). According to three numerical cases, the values of $k_{s,thr}$ are validated as 50% in the hierarchical network, 26% in the matrix network, and 28% in the empirical case. To enhance the practical application of the developed framework, more empirical data should be collected and analyzed to more accurately determine the range of $k_{s,thr}$ values for superspreaders.

Chapter 8
Conclusion

This chapter summarizes the major findings, theoretical implications, practical implications, limitations, and potential directions for future research contained in this dissertation.

8.1 Summary of major findings

This study explores the epidemiological evidence of the spread of COVID-19 in the construction industry in Hong Kong (see Chapter 4 and 5) and investigated potential strategies for the construction industry (see Chapter 6 and 7). By applying epidemic models in epidemiology, this interdisciplinary study describes the transmission dynamics of COVID-19 among the population in the construction industry with considerations on the relationship between main contractors and subcontractors, different construction activities among different construction workers, and their cooperative and management behaviours from the knowledge body of construction management. The major findings are as follows:

In Chapter 4, the transmissibility of COVID-19 and the effectiveness of macro-level NPIs (such as gathering restrictions and quarantine orders) in Hong Kong were evaluated via a modified SEIHR model using time-series data from the period between 24th January 2020 and 13th April 2021. The phenomenon of "pandemic fatigue" demonstrated gradually decreasing adherence to these NPIs among people living in Hong Kong. At the same time, the possibility of "backward bifurcation" indicated that, even if the $\mathcal{R}_0$ value is reduced below one, this disease still cannot be controlled. It is thus critical to further explore the specific transmission patterns of COVID-19 in order to develop targeted response strategies for individual industries.

In Chapter 5, the transmission patterns of COVID-19 throughout the construction industry of Hong Kong was explored through spatiotemporal connectivity analysis based on five COVID-19 case clusters associated with construction sites in Hong Kong. Each outbreak had three to five generations and lasted 25.8 days on average. On average, 46.61%, 37.56%, and 15.84% of offspring cases were infected at the workplace, in a household, or through social activities, respectively. The percentage of superspreaders (confirmed cases producing more than five offspring cases) within each cluster was 6.33% on average. The spatial distribution of each cluster was scattered, and the majority of confirmed cases were not located in areas immediately near the primary case (i.e., surrounding the construction sites), but rather in residential areas

where infected construction workers live.

In Chapter 6, the effectiveness of NPIs (e.g., contact restrictions, a ban on visitors onsite and disinfection) and vaccine programs were estimated using a dual-community compartment-based epidemic model. The findings indicated that, when the first case of COVID-19 was introduced to the construction site, in the absence of any interventions, infections spread rapidly among both construction workers and their close contacts, reaching its peak within 10 days. In terms of contact restrictions, controlling the exposure of individuals among the close contacts of construction workers was recommended, given the estimated ability of such controls to reduce DO by 1.8 days and TAR with an AE of 25%. In addition to NPIs, the model demonstrated that vaccination of construction workers alone would not be sufficient to curb an outbreak. In addition to construction workers, approximately 67–79% of their close contacts should also be given a vaccine.

In Chapter 7, to reduce the probability of superspreading events, a network-based computational framework based on a K-shell decomposition approach was developed with the input of the topological interaction network of project participants to identify potential superspreaders in construction projects. The feasibility of the developed framework is evaluated with three case studies: one sample case with a hierarchical structure with an average accuracy of 98.45%, one sample case with a matrix structure with an average accuracy of 92.25%, and an empirical case related to a COVID-19 outbreak in a construction project in Hong Kong with an accuracy of over 80.13%. This study recommends that all potential superspreaders, especially if they are employed by the main contractor, take RATs regularly. If all potential superspreaders are detected through regular RATs and all potential secondary cases were detected by contract tracing, up to 82.35% of infected cases could be prevented.

These findings hold both theoretical and practical implications, as previous studies relevant to COVID-19 in the construction industry [5, 15, 18, 105] have rarely discussed the transmission patterns of the virus–a gap in the literature filled by this present study. On the practical side, the epidemiological foundation of this study allows the development targeted NPIs designed to mitigate the spread of COVID-19 within the construction industry specifically.

8.2 Limitations and directions for future research

The main limitation of this study is due to the uncertainties of data collection. For some of the epidemiological information, the date of symptom onset cannot be identified for every asymptomatic infectious individual. There was also potential recall bias regarding the identification of symptom onset among patients with COVID-19. In addition, the COVID-19 surveillance system for tracing close contacts in Hong Kong is based on the application "LeaveHomeSafe", which does not collect Geographic Information System (GIS) data automatically. When tracing back the list of venues visited during the incubation period of each confirmed case, spatial connectivity appears to be mostly concentrated in highly frequented locations (residential buildings, workplaces, and restaurants), and so some random contacts may be missing from the analysis. This may be significant, according to Sneppen et al. (2021) [197], because random contacts might be a driver of repetitive waves. At the same time, however, the topology of an interaction network is established in this study using contact tracing data, which allows the determination of the possible sequence of the epidemic spread. The interactions of two sample networks (as shown in Figure 7.3) were established based on the occupations of individuals and their frequency of contact. The interaction network of the construction project in Hong Kong that experienced an outbreak was linked to attempts by management to increase coordination among different groups of workers on the site (as shown in Figure 7.5). While this model establishes the broad outlines of the spread of COVID-19, if better contact tracing data can capture even more real-time interactions, a more detailed picture of the epidemic's spread can be drawn.

In addition to the contact tracing data, the transmission possibility of each interaction between people is also important to consider. The transmission possibility can be influenced by many factors (proximity, face coverings, vaccination, and environment). In Chapter 5, the weight of each edge in the transmission network (as shown in Figure 5.3) was classified into one of five groups based on the relationship identified between each pair of confirmed cases [3, 120, 131]. In Chapter 7, the transmission possibility P_e was assumed based on the relationship established between each pair of confirmed cases [109], as shown in Table 7.2. More precise data would enable more accurate weighting of the transmission possibility, and more closely mimic the actual spread of the virus.

Due to the limitations of current data, this study did not consider different working environments. It is well established that the working environment has a significant impact on the infection risks of COVID-19. Prior studies have indicated that sharing indoor spaces with infected

individuals ia a major infection risk for SARS-CoV-2 [175, 190]. During the research period of this study, many construction sites confronted more than one outbreak. The TKO-LT Tunnel construction site, which had an especially poorly ventilated working environment, experienced at least three COVID-19 outbreaks. The infection risk in different working environments should be investigated further using other methods (e.g., Computational Fluid Dynamics (CFD) analysis [149]) to supplement the current research.

In addition to the identification of potential superspreaders, the supply and demand of construction labour should also be considered. In epidemiology, the operation threshold is defined by different percentiles of a Poisson distribution with a reproduction number $\mathcal{R}_0$ [1]. For example, if $\mathcal{R}_0$ is 2, when a seed case generates 6 secondary cases [99% percentile], that individual will be regarded as a superspreader. If contact tracing is implemented, close contacts of each infected case might have to accept a quarantine. Given the vulnerability of construction environments, a larger number of workers will be on sick leave than those who are infected. Negative labor supply shocks are frequently associated with public health crises [32], and the main objective for managers and public authorities will be to balance the continuation of construction activities while protecting workers from health risks. The relationship between construction labour supply and demand, which is likely to fluctuate during epidemics, also demands further research.

Bibliography

[1] Dillon C Adam, Peng Wu, Jessica Y Wong, Eric HY Lau, Tim K Tsang, Simon Cauchemez, Gabriel M Leung, and Benjamin J Cowling. 2020. Clustering and superspreading potential of SARS-CoV-2 infections in Hong Kong. *Nature Medicine* 26, 11 (2020), 1714–1719. https://doi.org/10.1038/s41591-020-1092-0

[2] Kofi Agyekum, Augustine Senanu Kukah, and Judith Amudjie. 2021. The impact of COVID-19 on the construction industry in Ghana: the case of some selected firms. *Journal of Engineering, Design and Technology* 20, 1 (2021), 222–244. https://doi.org/10.1108/JEDT-11-2020-0476

[3] Tetsuya Akaishi, Shigeki Kushimoto, Yukio Katori, Shigeo Kure, Kaoru Igarashi, Shin Takayama, Michiaki Abe, Junichi Tanaka, Akiko Kikuchi, Ko Onodera, et al. 2021. COVID-19 transmission in group living environments and households. *Scientific reports* 11, 1 (2021), 1–12.

[4] Manabu Akazawa, Jody L Sindelar, and A David Paltiel. 2003. Economic costs of influenza-related work absenteeism. *Value in Health* 6, 2 (2003), 107–115. https://doi.org/10.1046/j.1524-4733.2003.00209.x

[5] MKS Al-Mhdawi, Mario P Brito, Mohamad Abdul Nabi, Islam H El-Adaway, and Bhakti Stephan Onggo. 2022. Capturing the impact of COVID-19 on construction projects in developing countries: A case study of Iraq. *Journal of Management in Engineering* 38, 1 (2022), 05021015. https://doi.org/10.1061/(ASCE)ME.1943-5479.0000991

[6] Réka Albert, Hawoong Jeong, and Albert-László Barabási. 2000. Error and attack tolerance of complex networks. *nature* 406, 6794 (2000), 378–382. https://doi.org/10.1038/35019019

[7] Dipo Aldila, Herningtyas Padma, Khusnul Khotimah, Bevina Desjwiandra, and Hengki Tasman. 2018. Analyzing the MERS disease control strategy through an optimal control problem. *International Journal of Applied Mathematics and Computer Science* 28, 1 (2018).

[8] Muluneh Alene, Leltework Yismaw, Moges Agazhe Assemie, Daniel Bekele Ketema, Wodaje Gietaneh, and Tilahun Yemanu Birhan. 2021. Serial interval and incubation

period of COVID-19: a systematic review and meta-analysis. *BMC Infectious Diseases* 21, 1 (2021), 1–9. https://doi.org/10.1186/s12879-021-05950-x

[9] Yousef Alimohamadi, Maryam Taghdir, and Mojtaba Sepandi. 2020. Estimate of the basic reproduction number for COVID-19: a systematic review and meta-analysis. *Journal of Preventive Medicine and Public Health* 53, 3 (2020), 151. https://doi.org/10.3961/jpmph.20.076

[10] Abdullah Alsharef, Siddharth Banerjee, SM Uddin, Alex Albert, and Edward Jaselskis. 2021. Early impacts of the COVID-19 pandemic on the United States construction industry. *International journal of environmental research and public health* 18, 4 (2021), 1559. https://doi.org/10.3390/ijerph18041559

[11] Christopher Amoah and Fredrick Simpeh. 2020. Implementation challenges of COVID-19 safety measures at construction sites in South Africa. *Journal of Facilities Management* 19, 1 (2020), 111–128. https://doi.org/10.1108/JFM-08-2020-0061

[12] Roy M Anderson, Carolin Vegvari, James Truscott, and Benjamin S Collyer. 2020. Challenges in creating herd immunity to SARS-CoV-2 infection by mass vaccination. *The Lancet* 396, 10263 (2020), 1614–1616. https://doi.org/10.1016/S0140-6736(20)32318-7

[13] Roumen Anguelov, Salisu M Garba, and Salisu Usaini. 2014. Backward bifurcation analysis of epidemiological model with partial immunity. *Computers & Mathematics with Applications* 68, 9 (2014), 931–940.

[14] Chimay J Anumba, Catherine Baugh, and Malik MA Khalfan. 2002. Organisational structures to support concurrent engineering in construction. *Industrial management & data systems* 102, 5 (2002), 260–270. https://doi.org/10.1108/02635570210428294

[15] Felipe Araya. 2021. Modeling the spread of COVID-19 on construction workers: An agent-based approach. *Safety science* 133 (2021), 105022. https://doi.org/10.1016/j.ssci.2020.105022

[16] Felipe Araya and Leonardo Sierra. 2021. Influence between COVID-19 impacts and project stakeholders in chilean construction projects. *Sustainability* 13, 18 (2021), 10082. https://doi.org/10.3390/su131810082

[17] Sima Asadi, Nicole Bouvier, Anthony S Wexler, and William D Ristenpart. 2020. The coronavirus pandemic and aerosols: Does COVID-19 transmit via expiratory particles? , 635–638 pages. https://doi.org/10.1080/02786826.2020.1749229

[18] Rayan Assaad and Islam H El-adaway. 2021. Guidelines for Responding to COVID-19 Pandemic: Best Practices, Impacts, and Future Research Directions. *Journal of Management in Engineering* 37, 3 (2021), 06021001. https://doi.org/10.1061/(ASCE)ME.1943-5479.0000906

[19] Thomas Avice. 2020. COVID-19: Lessons from a construction site, can we apply one industry safety protocol to another? *Journal of Pediatric Rehabilitation Medicine* 13, 3 (2020), 433–437. https://doi.org/10.3233/PRM-200808

[20] Parham Azimi, Zahra Keshavarz, Jose Guillermo Cedeno Laurent, Brent Stephens, and Joseph G Allen. 2021. Mechanistic transmission modeling of COVID-19 on the Diamond Princess cruise ship demonstrates the importance of aerosol transmission. *Proceedings of the National Academy of Sciences* 118, 8 (2021), e2015482118. https://doi.org/10.1073/pnas.2015482118

[21] Jantien A Backer, Dirk Eggink, Stijn P Andeweg, Irene K Veldhuijzen, Noortje van Maarseveen, Klaas Vermaas, Boris Vlaemynck, Raf Schepers, Susan van den Hof, Chantal BEM Reusken, et al. 2022. Shorter serial intervals in SARS-CoV-2 cases with Omicron BA. 1 variant compared with Delta variant, the Netherlands, 13 to 26 December 2021. *Eurosurveillance* 27, 6 (2022), 2200042. https://doi.org/10.2807/1560-7917.ES.2022.27.6.2200042

[22] Shweta Bansal, Jonathan Read, Babak Pourbohloul, and Lauren Ancel Meyers. 2010. The dynamic nature of contact networks in infectious disease epidemiology. *Journal of biological dynamics* 4, 5 (2010), 478–489. https://doi.org/10.1080/17513758.2010.503376

[23] Albert-László Barabási and Réka Albert. 1999. Emergence of scaling in random networks. *science* 286, 5439 (1999), 509–512. https://doi.org/10.1126/science.286.5439.509

[24] Sarah M Bartsch, Kelly J O'Shea, Marie C Ferguson, Maria Elena Bottazzi, Patrick T Wedlock, Ulrich Strych, James A McKinnell, Sheryl S Siegmund, Sarah N Cox, Peter J

Hotez, et al. 2020. Vaccine efficacy needed for a COVID-19 coronavirus vaccine to prevent or stop an epidemic as the sole intervention. *American journal of preventive medicine* 59, 4 (2020), 493–503. https://doi.org/10.1016/j.amepre.2020.06.011

[25] Mathieu Bastian, Sebastien Heymann, and Mathieu Jacomy. 2009. Gephi: an open source software for exploring and manipulating networks. 3, 1 (2009), 361–362.

[26] Adnane Belout and Clothilde Gauvreau. 2004. Factors influencing project success: the impact of human resource management. *International journal of project management* 22, 1 (2004), 1–11. https://doi.org/10.1016/S0263-7863(03)00003-6

[27] Daniel Bernoulli. 1760. Essai d'une nouvelle analyse de la mortalité causée par la petite vérole, et des avantages de l'inoculation pour la prévenir. *Histoire de l'Acad., Roy. Sci.(Paris) avec Mem* (1760), 1–45.

[28] Ankan Biswas, Abhinandan Ghosh, Adrish Kar, Tuhin Mondal, Buntee Ghosh, and Prasanta Kumar Bardhan. 2021. The impact of COVID-19 in the construction sector and its remedial measures. In *Journal of Physics: Conference Series*, Vol. 1797. IOP Publishing, 012054.

[29] Stephen P Borgatti. 2005. Centrality and network flow. *Social networks* 27, 1 (2005), 55–71. https://doi.org/10.1016/j.socnet.2004.11.008

[30] Harold Brenner and William Ahern. 2000. Sickness absence and early retirement on health grounds in the construction industry in Ireland. *Occupational and environmental medicine* 57, 9 (2000), 615–620. https://doi.org/10.1136/oem.57.9.615

[31] Byram W. Bridle. 2021. 5 factors that could dictate the success or failure of the COVID-19 vaccine rollout. https://theconversation.com/5-factors-that-could-dictate-the-success-or-failure-of-the-covid-19-vaccine-rollout-152856. Accessed April 3,2021.

[32] Pedro Brinca, Joao B Duarte, and Miguel Faria-e Castro. 2021. Measuring labor supply and demand shocks during COVID-19. *European Economic Review* 139 (2021), 103901. https://doi.org/10.1016/j.euroecorev.2021.103901

[33] Tom Britton, Frank Ball, and Pieter Trapman. 2020. A mathematical model reveals the influence of population heterogeneity on herd immunity to SARS-CoV-2. *Science* 369, 6505 (2020), 846–849. https://doi.org/10.1126/science.abc6810

[34] Jack H Buckner, Gerardo Chowell, and Michael R Springborn. 2021. Dynamic prioritization of COVID-19 vaccines when social distancing is limited for essential workers. *Proceedings of the National Academy of Sciences* 118, 16 (2021), e2025786118. https://doi.org/10.1073/pnas.2025786118

[35] Tommaso Celeste Bulfone, Mohsen Malekinejad, George W Rutherford, and Nooshin Razani. 2021. Outdoor transmission of SARS-CoV-2 and other respiratory viruses: a systematic review. *The Journal of infectious diseases* 223, 4 (2021), 550–561. https://doi.org/10.1093/infdis/jiaa742

[36] Greg Burkhart, Paul A Schulte, Cynthia Robinson, William K Sieber, Pamela Vossenas, and Knut Ringen. 1993. Job tasks, potential exposures, and health risks of laborers employed in the construction industry. *American journal of industrial medicine* 24, 4 (1993), 413–425. https://doi.org/10.1002/ajim.4700240407

[37] Ewen Callaway. 2021. Heavily mutated coronavirus variant puts scientists on alert. *Nature* (2021). Access 27 November, 2021.

[38] Finlay Campbell, Brett Archer, Henry Laurenson-Schafer, Yuka Jinnai, Franck Konings, Neale Batra, Boris Pavlin, Katelijn Vandemaele, Maria D Van Kerkhove, Thibaut Jombart, et al. 2021. Increased transmissibility and global spread of SARS-CoV-2 variants of concern as at June 2021. *Eurosurveillance* 26, 24 (2021), 2100509.

[39] Shai Carmi, Shlomo Havlin, Scott Kirkpatrick, Yuval Shavitt, and Eran Shir. 2007. A model of Internet topology using k-shell decomposition. *Proceedings of the National Academy of Sciences* 104, 27 (2007), 11150–11154. https://doi.org/10.1073/pnas.0701175104

[40] Census and Hong Kong Statistics Department. 2013. Statistics on Domestic Households. https://data.gov.hk/en-data/dataset/hk-censtatd-tablechart-statistics-on-domestic-households.

[41] Albert Chan. 2018. Pilot medical examination scheme for construction workers:research summary. Accessed 15 October,2021.

[42] Albert Chan. 2021. Good practice on preventive measures against COVID-19 for construction sites. Accessed 15 October,2021.

[43] Oliver KY Chau, Chun-Ho Liu, and Michael KH Leung. 2006. CFD analysis of the performance of a local exhaust ventilation system in a hospital ward. *Indoor and Built Environment* 15, 3 (2006), 257–271. https://doi.org/10.1177/1420326X06066123

[44] Wen-Hsiang Chen, Ulrich Strych, Peter J Hotez, and Maria Elena Bottazzi. 2020. The SARS-CoV-2 vaccine pipeline: an overview. *Current tropical medicine reports* 7, 2 (2020), 61–64. https://doi.org/10.1007/s40475-020-00201-6

[45] Ying-Yi Chih, Cody Yu-Ling Hsiao, Ali Zolghadr, and Nader Naderpajouh. 2022. Resilience of Organizations in the Construction Industry in the Face of COVID-19 Disturbances: Dynamic Capabilities Perspective. *Journal of Management in Engineering* 38, 2 (2022), 04022002. https://doi.org/10.1061/(ASCE)ME.1943-5479.0001014

[46] Matteo Chinazzi, Jessica T Davis, Marco Ajelli, Corrado Gioannini, Maria Litvinova, Stefano Merler, Ana Pastore y Piontti, Kunpeng Mu, Luca Rossi, Kaiyuan Sun, et al. 2020. The effect of travel restrictions on the spread of the 2019 novel coronavirus (COVID-19) outbreak. *Science* 368, 6489 (2020), 395–400. https://doi.org/10.1126/science.aba9757

[47] Gerardo Chowell, Fatima Abdirizak, Sunmi Lee, Jonggul Lee, Eunok Jung, Hiroshi Nishiura, and Cécile Viboud. 2015. Transmission characteristics of MERS and SARS in the healthcare setting: a comparative study. *BMC medicine* 13, 1 (2015), 1–12.

[48] Gary KK Chung, Siu-Ming Chan, Yat-Hang Chan, Jean Woo, Hung Wong, Samuel Y Wong, Eng Kiong Yeoh, Michael Marmot, and Roger Y Chung. 2021. Socioeconomic Patterns of COVID-19 Clusters in Low-Incidence City, Hong Kong. *Emerging Infectious Diseases* 27, 11 (2021). https://doi.org/10.3201/eid2711.204840

[49] Benjamin J Cowling, Sheikh Taslim Ali, Tiffany WY Ng, Tim K Tsang, Julian CM Li, Min Whui Fong, Qiuyan Liao, Mike YW Kwan, So Lun Lee, Susan S Chiu, et al. 2020. Impact assessment of non-pharmaceutical interventions against coronavirus disease 2019 and influenza in Hong Kong: an observational study. *The Lancet Public Health* 5, 5 (2020), e279–e288. https://doi.org/10.1016/S2468-2667(20)30090-6

[50] Aaqib Bashir Dar, Auqib Hamid Lone, Saniya Zahoor, Afshan Amin Khan, and Roohie Naaz. 2020. Applicability of mobile contact tracing in fighting pandemic (COVID-19): Issues, challenges and solutions. *Computer Science Review* 38 (2020), 100307. https://doi.org/10.1016/j.cosrev.2020.100307

[51] Marco D'Arienzo and Angela Coniglio. 2020. Assessment of the SARS-CoV-2 basic reproduction number, R0, based on the early phase of COVID-19 outbreak in Italy. *Biosafety and Health* 2, 2 (2020), 57–59. https://doi.org/10.1016/j.bsheal.2020.03.004

[52] R Maria del Rio-Chanona, Penny Mealy, Anton Pichler, Francois Lafond, and J Doyne Farmer. 2020. Supply and demand shocks in the COVID-19 pandemic: An industry and occupation perspective. *Oxford Review of Economic Policy* 36, Supplement_1 (2020), S94–S137. https://doi.org/10.1093/oxrep/graa033

[53] Xiuwen Dong and James W Platner. 2004. Occupational fatalities of Hispanic construction workers from 1992 to 2000. *American journal of industrial medicine* 45, 1 (2004), 45–54. https://doi.org/10.1002/ajim.10322

[54] Nicole Doria-Rose, Mehul S Suthar, Mat Makowski, Sarah O'Connell, Adrian B McDermott, Britta Flach, Julie E Ledgerwood, John R Mascola, Barney S Graham, Bob C Lin, et al. 2021. Antibody persistence through 6 months after the second dose of mRNA-1273 vaccine for Covid-19. *New England Journal of Medicine* 384, 23 (2021), 2259–2261. https://doi.org/10.1056/NEJMc2103916

[55] Kaitano Dube, Godwell Nhamo, and David Chikodzi. 2021. COVID-19 cripples global restaurant and hospitality industry. *Current Issues in Tourism* 24, 11 (2021), 1487–1490. https://doi.org/10.1080/13683500.2020.1773416

[56] Andrew Ebekozien and Clinton Aigbavboa. 2021. COVID-19 recovery for the Nigerian construction sites: The role of the fourth industrial revolution technologies. *Sustainable Cities and Society* 69 (2021), 102803. https://doi.org/10.1016/j.scs.2021.102803

[57] Steffen E Eikenberry, Marina Mancuso, Enahoro Iboi, Tin Phan, Keenan Eikenberry, Yang Kuang, Eric Kostelich, and Abba B Gumel. 2020. To mask or not to mask: Modeling the potential for face mask use by the general public to curtail the COVID-19 pandemic. *Infectious Disease Modelling* 5 (2020), 293–308. https://doi.org/10.1016/j.idm.2020.04.001

[58] Shereen Mohamed Elnaggar and Hosam Elhegazy. 2022. Study the impact of the COVID-19 pandemic on the construction industry in Egypt. *Structures* 35 (2022), 1270–1277. https://doi.org/10.1016/j.istruc.2021.09.028

[59] Helen R Fielding, Trevelyan J McKinley, Richard J Delahay, Matthew J Silk, and Robbie A McDonald. 2021. Characterization of potential superspreader farms for bovine tuberculosis: A review. *Veterinary Medicine and Science* 7, 2 (2021), 310–321. https://doi.org/10.1002/vms3.358

[60] Paul EM Fine. 2003. The interval between successive cases of an infectious disease. *American journal of epidemiology* 158, 11 (2003), 1039–1047. https://doi.org/10.1093/aje/kwg251

[61] Seth Flaxman, Swapnil Mishra, Axel Gandy, H Juliette T Unwin, Thomas A Mellan, Helen Coupland, Charles Whittaker, Harrison Zhu, Tresnia Berah, Jeffrey W Eaton, et al. 2020. Estimating the effects of non-pharmaceutical interventions on COVID-19 in Europe. *Nature* 584, 7820 (2020), 257–261. https://doi.org/10.1038/s41586-020-2405-7

[62] Organisation for Economic Co-operation and Development. 2020. *Productivity gains from teleworking in the post COVID-19 era: How can public policies make it happen?* OECD Publishing, Paris, France.

[63] Centre for Health Protection. [n. d.]. Latest Situation of Coronavirus Disease (COVID-19) in Hong Kong. https://chp-dashboard.geodata.gov.hk/covid-19/en.html. Accessed April 14, 2021.

[64] Centre for Health Protection. [n. d.]. Latest Situation of Coronavirus Disease (COVID-19) in Hong Kong. https://chp-dashboard.geodata.gov.hk/covid-19/en.html. Accessed August 16, 2022.

[65] Brody H Foy, Brian Wahl, Kayur Mehta, Anita Shet, Gautam I Menon, and Carl Britto. 2021. Comparing COVID-19 vaccine allocation strategies in India: A mathematical modelling study. *International Journal of Infectious Diseases* 103 (2021), 431–438. https://doi.org/10.1016/j.ijid.2020.12.075

[66] Noah E Friedkin. 1991. Theoretical foundations for centrality measures. *American journal of Sociology* 96, 6 (1991), 1478–1504. https://doi.org/10.1086/229694

[67] Wee Hoe Gan and David Koh. 2021. COVID-19 and return-to-work for the construction sector: lessons from Singapore. *Safety and Health at Work* 12, 2 (2021), 277–281. https://doi.org/10.1016/j.shaw.2021.04.001

[68] Daozhou Gao, Yijun Lou, Daihai He, Travis C Porco, Yang Kuang, Gerardo Chowell, and Shigui Ruan. 2016. Prevention and control of Zika as a mosquito-borne and sexually transmitted disease: a mathematical modeling analysis. *Scientific reports* 6, 1 (2016), 1–10.

[69] Zhiru Gao, Yinghui Xu, Chao Sun, Xu Wang, Ye Guo, Shi Qiu, and Kewei Ma. 2021. A systematic review of asymptomatic infections with COVID-19. *Journal of Microbiology, Immunology and Infection* 54, 1 (2021), 12–16. https://doi.org/10.1016/j.jmii.2020.05.001

[70] Jawa Anak Gara, Rozana Zakaria, Eeydzah Aminudin, Khairulzan Yahya, Abdul Rahman Mohd Sam, Vikneswaran Munikanan, Muhamad Azani Yahya, Noraziah Wahi, and Siti Mazzuana Shamsuddin. 2022. Effects of the COVID-19 Pandemic on Construction Work Progress: An On-Site Analysis from the Sarawak Construction Project, Malaysia. *Sustainability* 14, 10 (2022), 6007. https://doi.org/10.3390/su14106007

[71] Antonios Garas, Frank Schweitzer, and Shlomo Havlin. 2012. A k-shell decomposition method for weighted networks. *New Journal of Physics* 14, 8 (2012), 083030. https://doi.org/10.1088/1367-2630/14/8/083030

[72] Marino Gatto, Enrico Bertuzzo, Lorenzo Mari, Stefano Miccoli, Luca Carraro, Renato Casagrandi, and Andrea Rinaldo. 2020. Spread and dynamics of the COVID-19 epidemic in Italy: Effects of emergency containment measures. *Proceedings of the National Academy of Sciences* 117, 19 (2020), 10484–10491. https://doi.org/10.1073/pnas.2004978117

[73] Indrajit Ghosh, Pankaj Kumar Tiwari, and Joydev Chattopadhyay. 2019. Effect of active case finding on dengue control: Implications from a mathematical model. *Journal of theoretical biology* 464 (2019), 50–62. https://doi.org/10.1016/j.jtbi.2018.12.027

[74] Alberto Gómez-Carballa, Jacobo Pardo-Seco, Xabier Bello, Federico Martinón-Torres, and Antonio Salas. 2021. Superspreading in the emergence of COVID-19 variants. *Trends in Genetics* 37, 12 (2021), 1069–1080. https://doi.org/10.1016/j.tig.2021.09.003

[75] Nicolò Gozzi, Paolo Bajardi, and Nicola Perra. 2021. The importance of non-pharmaceutical interventions during the COVID-19 vaccine rollout. *PLoS computational biology* 17, 9 (2021), e1009346. https://doi.org/10.1371/journal.pcbi.1009346

[76] Simon Gregson, Constance A Nyamukapa, Geoffrey P Garnett, Peter R Mason, Tom Zhuwau, Michel Caraël, Stephen K Chandiwana, and Roy M Anderson. 2002. Sexual mixing patterns and sex-differentials in teenage exposure to HIV infection in rural Zimbabwe. *The Lancet* 359, 9321 (2002), 1896–1903. https://doi.org/10.1016/S0140-6736(02)08780-9

[77] John Griffin, Miriam Casey, Áine Collins, Kevin Hunt, David McEvoy, Andrew Byrne, Conor McAloon, Ann Barber, Elizabeth Ann Lane, and SImon More. 2020. Rapid review of available evidence on the serial interval and generation time of COVID-19. *BMJ open* 10, 11 (2020), e040263. https://doi.org/10.1136/bmjopen-2020-040263

[78] Gerrit Großmann, Michael Backenköhler, and Verena Wolf. 2021. Heterogeneity matters: Contact structure and individual variation shape epidemic dynamics. *Plos one* 16, 7 (2021), e0250050.

[79] Yoshiaki Gu, Nobuhiro Komiya, Hajime Kamiya, Yoshinori Yasui, Kiyosu Taniguchi, and Nobuhiko Okabe. 2011. Pandemic (H1N1) 2009 transmission during presymptomatic phase, Japan. *Emerging infectious diseases* 17, 9 (2011), 1737. https://doi.org/10.3201/eid1709.101411

[80] Wei-jie Guan, Zheng-yi Ni, Yu Hu, Wen-hua Liang, Chun-quan Ou, Jian-xing He, Lei Liu, Hong Shan, Chun-liang Lei, David SC Hui, et al. 2020. Clinical characteristics of coronavirus disease 2019 in China. *New England journal of medicine* 382, 18 (2020), 1708–1720. https://doi.org/10.1056/NEJMoa2002032

[81] Abba B Gumel. 2012. Causes of backward bifurcations in some epidemiological models. *J. Math. Anal. Appl.* 395, 1 (2012), 355–365. https://doi.org/10.1016/j.jmaa.2012.04.077

[82] Thomas Hale, Noam Angrist, Rafael Goldszmidt, Beatriz Kira, Anna Petherick, Toby Phillips, Samuel Webster, Emily Cameron-Blake, Laura Hallas, Saptarshi Majumdar, et al. 2021. A global panel database of pandemic policies (Oxford COVID-19 Government

Response Tracker). *Nature Human Behaviour* 5, 4 (2021), 529–538. https://doi.org/10.1038/s41562-021-01079-8

[83] Seng Hansen. 2020. Does the COVID-19 outbreak constitute a force majeure event? A pandemic impact on construction contracts. *Journal of the civil engineering forum* 6, 1 (2020), 201–214. https://doi.org/10.22146/jcef.54997

[84] William S Hart, Elizabeth Miller, Nick J Andrews, Pauline Waight, Philip K Maini, Sebastian Funk, and Robin N Thompson. 2022. Generation time of the alpha and delta SARS-CoV-2 variants: an epidemiological analysis. *The Lancet Infectious Diseases* (2022). https://doi.org/10.1016/S1473-3099(22)00001-9

[85] Nils Haug, Lukas Geyrhofer, Alessandro Londei, Elma Dervic, Amélie Desvars-Larrive, Vittorio Loreto, Beate Pinior, Stefan Thurner, and Peter Klimek. 2020. Ranking the effectiveness of worldwide COVID-19 government interventions. *Nature human behaviour* 4, 12 (2020), 1303–1312. https://doi.org/10.1038/s41562-020-01009-0

[86] Chuanni He, Min Liu, YuXiang Zhang, Zhigao Wang, Simon M Hsiang, Gongfan Chen, and Jiang Chen. 2022. Exploit Social Distancing in Construction Scheduling: Visualize and Optimize Space–Time–Workforce Tradeoff. *Journal of Management in Engineering* 38, 4 (2022), 04022027. https://doi.org/10.1061/(ASCE)ME.1943-5479.0001037

[87] Xi He, Eric HY Lau, Peng Wu, Xilong Deng, Jian Wang, Xinxin Hao, Yiu Chung Lau, Jessica Y Wong, Yujuan Guan, Xinghua Tan, et al. 2020. Temporal dynamics in viral shedding and transmissibility of COVID-19. *Nature medicine* 26, 5 (2020), 672–675. https://doi.org/10.1038/s41591-020-0869-5

[88] Niel Hens, Marc Aerts, Christel Faes, Ziv Shkedy, O Lejeune, P Van Damme, and P Beutels. 2010. Seventy-five years of estimating the force of infection from current status data. *Epidemiology & Infection* 138, 6 (2010), 802–812. https://doi.org/10.1017/S0950268809990781

[89] Herbert W Hethcote. 2000. The mathematics of infectious diseases. *SIAM review* 42, 4 (2000), 599–653. https://doi.org/10.1137/S0036144500371907

[90] Clifford K Ho. 2021. Modelling airborne transmission and ventilation impacts of a COVID-19 outbreak in a restaurant in Guangzhou, China. *International Journal of*

Computational Fluid Dynamics 35, 9 (2021), 708–726. https://doi.org/10.1080/10618562.2021.1910678

[91] Jeremy Howard, Austin Huang, Zhiyuan Li, Zeynep Tufekci, Vladimir Zdimal, Helene-Mari van der Westhuizen, Arne von Delft, Amy Price, Lex Fridman, Lei-Han Tang, et al. 2020. Face masks against COVID-19: an evidence review. (2020).

[92] Bisong Hu, Jingyu Qiu, Haiying Chen, Vincent Tao, Jinfeng Wang, and Hui Lin. 2020. First, second and potential third generation spreads of the COVID-19 epidemic in mainland China: an early exploratory study incorporating location-based service data of mobile devices. *International Journal of Infectious Diseases* 96 (2020), 489–495. https://doi.org/10.1016/j.ijid.2020.05.048

[93] Maogui Hu, Hui Lin, Jinfeng Wang, Chengdong Xu, Andrew J Tatem, Bin Meng, Xin Zhang, Yifeng Liu, Pengda Wang, Guizhen Wu, et al. 2021. Risk of coronavirus disease 2019 transmission in train passengers: an epidemiological and modeling study. *Clinical Infectious Diseases* 72, 4 (2021), 604–610. https://doi.org/10.1093/cid/ciaa1057

[94] Nafiu Hussaini, Kamaldeen Okuneye, and Abba B Gumel. 2017. Mathematical analysis of a model for zoonotic visceral leishmaniasis. *Infectious Disease Modelling* 2, 4 (2017), 455–474. https://doi.org/10.1016/j.idm.2017.12.002

[95] Akiko Iwasaki. 2021. What reinfections mean for COVID-19. *The Lancet Infectious Diseases* 21, 1 (2021), 3–5. https://doi.org/10.1016/S1473-3099(20)30783-0

[96] Haddy Jallow, Suresh Renukappa, and Subashini Suresh. 2020. The impact of COVID-19 outbreak on United Kingdom infrastructure sector. *Smart and Sustainable Built Environment* 10, 4 (2020), 581–593. https://doi.org/10.1108/SASBE-05-2020-0068

[97] Thayyil Jayakrishnan, Bina Thomas, Bhaskar Rao, and Biju George. 2013. Occupational health problems of construction workers in India. *International Journal of Medicine and Public Health*| 3, 4 (2013). https://doi.org/10.4103/2230-8598.123415

[98] JungHo Jeon, Suyash Padhye, Arkaprabha Bhattacharyya, Hubo Cai, and Makarand Hastak. 2022. Impact of COVID-19 on the US Construction Industry as Revealed in the Purdue Index for Construction. *Journal of Management in Engineering* 38, 1 (2022), 04021082. https://doi.org/10.1061/(ASCE)ME.1943-5479.0000995

[99] Terry C Jones, Barbara Mühlemann, Talitha Veith, Guido Biele, Marta Zuchowski, Jörg Hoffmann, Angela Stein, Anke Edelmann, Victor Max Corman, and Christian Drosten. 2020. An analysis of SARS-CoV-2 viral load by patient age. *MedRxiv* (2020). https://doi.org/10.1101/2020.06.08.20125484

[100] Masayasu Kanno. 2021. Assessing the impact of COVID-19 on major industries in Japan: A dynamic conditional correlation approach. *Research in International Business and Finance* 58 (2021), 101488. https://doi.org/10.1016/j.ribaf.2021.101488

[101] Matt J Keeling and Ken TD Eames. 2005. Networks and epidemic models. *Journal of the royal society interface* 2, 4 (2005), 295–307. https://doi.org/10.1098/rsif.2005.0051

[102] William Ogilvy Kermack and Anderson G McKendrick. 1927. A contribution to the mathematical theory of epidemics. *Proceedings of the royal society of london. Series A, Containing papers of a mathematical and physical character* 115, 772 (1927), 700–721. https://doi.org/10.1098/rspa.1927.0118

[103] Daniel Fu Keung Wong, Chang Ying Li, and He Xue Song. 2007. Rural migrant workers in urban China: living a marginalised life. *International Journal of Social Welfare* 16, 1 (2007), 32–40. https://doi.org/10.1111/j.1468-2397.2007.00475.x

[104] Jerome H Kim, Florian Marks, and John D Clemens. 2021. Looking beyond COVID-19 vaccine phase 3 trials. *Nature medicine* 27, 2 (2021), 205–211. https://doi.org/10.1038/s41591-021-01230-y

[105] Sungchul Kim, Minjin Kong, Jinwoo Choi, Seungwoo Han, Hoyoung Baek, and Taehoon Hong. 2021. Feasibility Analysis of COVID-19 Response Guidelines at Construction Sites in South Korea Using CYCLONE in Terms of Cost and Time. *Journal of Management in Engineering* 37, 5 (2021), 04021048. https://doi.org/10.1061/(ASCE)ME.1943-5479.0000957

[106] Maksim Kitsak, Lazaros K Gallos, Shlomo Havlin, Fredrik Liljeros, Lev Muchnik, H Eugene Stanley, and Hernán A Makse. 2010. Identification of influential spreaders in complex networks. *Nature physics* 6, 11 (2010), 888–893. https://doi.org/10.1038/nphys1746

[107] David Koh. 2020. Occupational risks for COVID-19 infection. *Occupational Medicine (Oxford, England)* 70, 1 (2020), 3. https://doi.org/10.1093/occmed/kqaa036

[108] Florian Krammer. 2020. SARS-CoV-2 vaccines in development. *Nature* 586, 7830 (2020), 516–527. https://doi.org/10.1038/s41586-020-2798-3

[109] Vesa Kuikka. 2022. Modelling epidemic spreading in structured organisations. *Physica A: Statistical Mechanics and its Applications* (2022), 126875. https://doi.org/10.1016/j.physa.2022.126875

[110] Kai Kupferschmidt and Meredith Wadman. 2021. Delta variant triggers new phase in the pandemic.

[111] John A Kuprenas. 2003. Implementation and performance of a matrix organization structure. *International Journal of Project Management* 21, 1 (2003), 51–62. https://doi.org/10.1016/S0263-7863(01)00065-5

[112] Jasmin S Kutter, Monique I Spronken, Pieter L Fraaij, Ron AM Fouchier, and Sander Herfst. 2018. Transmission routes of respiratory viruses among humans. *Current opinion in virology* 28 (2018), 142–151. https://doi.org/10.1016/j.coviro.2018.01.001

[113] Kin On Kwok, Kin Kit Li, Henry Ho Hin Chan, Yuan Yuan Yi, Arthur Tang, Wan In Wei, and Samuel Yeung Shan Wong. 2020. Community responses during early phase of COVID-19 epidemic, Hong Kong. *Emerging infectious diseases* 26, 7 (2020), 1575. https://doi.org/10.3201/eid2607.200500

[114] Kin On Kwok, Wan In Wei, Ying Huang, Kai Man Kam, Emily Ying Yang Chan, Steven Riley, Ho Hin Henry Chan, David Shu Cheong Hui, Samuel Yeung Shan Wong, and Eng Kiong Yeoh. 2021. Evolving epidemiological characteristics of COVID-19 in Hong Kong from January to August 2020: retrospective study. *Journal of medical Internet research* 23, 4 (2021), e26645. https://doi.org/10.2196/26645

[115] Keun-Sang Kwon, Jung-Im Park, Young Joon Park, Don-Myung Jung, Ki-Wahn Ryu, and Ju-Hyung Lee. 2020. Evidence of long-distance droplet transmission of SARS-CoV-2 by direct air flow in a restaurant in Korea. *Journal of Korean medical science* 35, 46 (2020). https://doi.org/10.3346/jkms.2020.35.e415

[116] Hien Lau, Veria Khosrawipour, Piotr Kocbach, Agata Mikolajczyk, Hirohito Ichii, Maciej Zacharski, Jacek Bania, and Tanja Khosrawipour. 2020. The association between international and domestic air traffic and the coronavirus (COVID-19) outbreak. *Journal of Microbiology, Immunology and Infection* 53, 3 (2020), 467–472. https://doi.org/10.1016/j.jmii.2020.03.026

[117] Max SY Lau, Bryan Grenfell, Michael Thomas, Michael Bryan, Kristin Nelson, and Ben Lopman. 2020. Characterizing superspreading events and age-specific infectiousness of SARS-CoV-2 transmission in Georgia, USA. *Proceedings of the National Academy of Sciences* 117, 36 (2020), 22430–22435. https://doi.org/10.1073/pnas.2011802117

[118] Quentin J Leclerc, Naomi M Fuller, Lisa E Knight, Sebastian Funk, Gwenan M Knight, cmmid covid 19 Working Group, et al. 2020. What settings have been linked to SARS-CoV-2 transmission clusters? *Wellcome open research* 5 (2020). https://doi.org/10.12688/wellcomeopenres.15889.2

[119] Kelley Lee, Catherine Z Worsnop, Karen A Grépin, and Adam Kamradt-Scott. 2020. Global coordination on cross-border travel and trade measures crucial to COVID-19 response. *The Lancet* 395, 10237 (2020), 1593–1595. https://doi.org/10.1016/S0140-6736(20)31032-1

[120] Hao Lei, Xiaolin Xu, Shenglan Xiao, Xifeng Wu, and Yuelong Shu. 2020. Household transmission of COVID-19-a systematic review and meta-analysis. *The Journal of infection* 81, 6 (2020), 979. https://doi.org/10.1093/cid/ciaa450

[121] Nancy HL Leung, Daniel KW Chu, Eunice YC Shiu, Kwok-Hung Chan, James J McDevitt, Benien JP Hau, Hui-Ling Yen, Yuguo Li, Dennis KM Ip, JS Peiris, et al. 2020. Respiratory virus shedding in exhaled breath and efficacy of face masks. *Nature medicine* 26, 5 (2020), 676–680. https://doi.org/10.1038/s41591-020-0843-2

[122] Qun Li, Xuhua Guan, Peng Wu, Xiaoye Wang, Lei Zhou, Yeqing Tong, Ruiqi Ren, Kathy SM Leung, Eric HY Lau, Jessica Y Wong, et al. 2020. Early transmission dynamics in Wuhan, China, of novel coronavirus–infected pneumonia. *New England journal of medicine* (2020). https://doi.org/10.1056/NEJMoa2001316

[123] Yuguo Li, Hua Qian, Jian Hang, Xuguang Chen, Pan Cheng, Hong Ling, Shengqi Wang, Peng Liang, Jiansen Li, Shenglan Xiao, et al. 2021. Probable airborne transmission of

SARS-CoV-2 in a poorly ventilated restaurant. *Building and Environment* 196 (2021), 107788. https://doi.org/10.1016/j.buildenv.2021.107788

[124] Yang-Kai Li, Shu Peng, Le-Qun Li, Qi Wang, Wei Ping, Ni Zhang, and Xiang-Ning Fu. 2020. Clinical and transmission characteristics of Covid-19—a retrospective study of 25 cases from a single thoracic surgery department. *Current medical science* 40, 2 (2020), 295–300. https://doi.org/10.1007/s11596-020-2176-2

[125] Shaohong Liang, Hapuarachchige Chanditha Hapuarachchi, Jayanthi Rajarethinam, Carmen Koo, Choon-Siang Tang, Chee-Seng Chong, Lee-Ching Ng, and Grace Yap. 2018. Construction sites as an important driver of dengue transmission: implications for disease control. *BMC infectious diseases* 18, 1 (2018), 1–10. https://doi.org/10.1186/s12879-018-3311-6

[126] Yunping Liang, Anil Baral, Mohsen Shahandashti, and Baabak Ashuri. 2022. Availability Heuristic in Construction Workforce Decision-Making amid COVID-19 Pandemic: Empirical Evidence and Mitigation Strategy. *Journal of Management in Engineering* 38, 5 (2022), 04022046. https://doi.org/10.1061/(ASCE)ME.1943-5479.0001077

[127] Qianying Lin, Shi Zhao, Daozhou Gao, Yijun Lou, Shu Yang, Salihu S Musa, Maggie H Wang, Yongli Cai, Weiming Wang, Lin Yang, et al. 2020. A conceptual model for the coronavirus disease 2019 (COVID-19) outbreak in Wuhan, China with individual reaction and governmental action. *International journal of infectious diseases* 93 (2020), 211–216. https://doi.org/10.1016/j.ijid.2020.02.058

[128] Florence YY Ling, Zhe Zhang, and Aurelia YR Yew. 2022. Impact of COVID-19 Pandemic on Demand, Output, and Outcomes of Construction Projects in Singapore. *Journal of Management in Engineering* 38, 2 (2022), 04021097. https://doi.org/10.1061/(ASCE)ME.1943-5479.0001020

[129] Hui Liu, Miroslaw J Skibniewski, and Mengjun Wang. 2016. Identification and hierarchical structure of critical success factors for innovation in construction projects: Chinese perspective. *Journal of Civil Engineering and Management* 22, 3 (2016), 401–416. https://doi.org/10.3846/13923730.2014.975739

[130] Xingchun Liu, Meng Zhang, Qu Cheng, Yingtao Zhang, Guoqiang Ye, Xiqing Huang, Zeyu Zhao, Jia Rui, Qingqing Hu, Roger Frutos, et al. 2021. Dengue fever transmission

between a construction site and its surrounding communities in China. *Parasites & Vectors* 14, 1 (2021), 1–14. https://doi.org/10.1186/s13071-020-04463-x

[131] Yang Liu, Rosalind M Eggo, and Adam J Kucharski. 2020. Secondary attack rate and superspreading events for SARS-CoV-2. *The Lancet* 395, 10227 (2020), e47. https://doi.org/10.1016/S0140-6736(20)30462-1

[132] Yang Liu, Zhonglei Gu, and Jiming Liu. 2021. Uncovering transmission patterns of COVID-19 outbreaks: A region-wide comprehensive retrospective study in Hong Kong. *EClinicalMedicine* 36 (2021), 100929. https://doi.org/10.1016/j.eclinm.2021.100929

[133] Yuan Liu, Zhi Ning, Yu Chen, Ming Guo, Yingle Liu, Nirmal Kumar Gali, Li Sun, Yusen Duan, Jing Cai, Dane Westerdahl, et al. 2020. Aerodynamic analysis of SARS-CoV-2 in two Wuhan hospitals. *Nature* 582, 7813 (2020), 557–560. https://doi.org/10.1038/s41586-020-2271-3

[134] Ying Liu, Ming Tang, Tao Zhou, and Younghae Do. 2015. Core-like groups result in invalidation of identifying super-spreader by k-shell decomposition. *Scientific reports* 5, 1 (2015), 1–8.

[135] Ying Liu, Ming Tang, Tao Zhou, and Younghae Do. 2015. Improving the accuracy of the k-shell method by removing redundant links: From a perspective of spreading dynamics. *Scientific reports* 5, 1 (2015), 1–11.

[136] James O Lloyd-Smith, Sebastian J Schreiber, P Ekkehard Kopp, and Wayne M Getz. 2005. Superspreading and the effect of individual variation on disease emergence. *Nature* 438, 7066 (2005), 355–359. https://doi.org/10.1038/nature04153

[137] Jianyun Lu, Jieni Gu, Kuibiao Li, Conghui Xu, Wenzhe Su, Zhisheng Lai, Deqian Zhou, Chao Yu, Bin Xu, and Zhicong Yang. 2020. COVID-19 outbreak associated with air conditioning in restaurant, Guangzhou, China, 2020. *Emerging infectious diseases* 26, 7 (2020), 1628. https://doi.org/10.3201/eid2607.200764

[138] Yalin Lu, Majeed Oladokun, and Zhang Lin. 2020. Reducing the exposure risk in hospital wards by applying stratum ventilation system. *Building and Environment* 183 (2020), 107204. https://doi.org/10.1016/j.buildenv.2020.107204

[139] Lei Luo, Dan Liu, Xinlong Liao, Xianbo Wu, Qinlong Jing, Jiazhen Zheng, Fanghua Liu, Shigui Yang, Hua Bi, Zhihao Li, et al. 2020. Contact settings and risk for transmission in 3410 close contacts of patients with COVID-19 in Guangzhou, China: a prospective cohort study. *Annals of internal medicine* 173, 11 (2020), 879–887. https://doi.org/10.7326/M20-2671

[140] Xia Ma, Yicang Zhou, and Hui Cao. 2013. Global stability of the endemic equilibrium of a discrete SIR epidemic model. *Advances in Difference Equations* 2013, 1 (2013), 1–19.

[141] Macrotrends. [n. d.]. Hong Kong Life Expectancy 1950-2020. https://www.macrotrends.net/countries/HKG/hong-kong/life-expectancy. Retrieved 2020-12-16.

[142] Elisabeth Mahase. 2021. Covid-19: Is it safe to lift all restrictions in England from 21 June? *BMJ* 373 (2021). https://doi.org/10.1136/bmj.n1399 arXiv:https://www.bmj.com/content/373/bmj.n1399.full.pdf

[143] Siu Shing Man, Saad Alabdulkarim, Alan Hoi Shou Chan, and Tingru Zhang. 2021. The acceptance of personal protective equipment among Hong Kong construction workers: An integration of technology acceptance model and theory of planned behavior with risk perception and safety climate. *Journal of safety research* 79 (2021), 329–340. https://doi.org/10.1016/j.jsr.2021.09.014

[144] CJ Mann. 2003. Observational research methods. Research design II: cohort, cross sectional, and case-control studies. *Emergency medicine journal* 20, 1 (2003), 54–60. https://doi.org/10.1136/emj.20.1.54

[145] Baichuan Mo, Kairui Feng, Yu Shen, Clarence Tam, Daqing Li, Yafeng Yin, and Jinhua Zhao. 2021. Modeling epidemic spreading through public transit using time-varying encounter network. *Transportation Research Part C: Emerging Technologies* 122 (2021), 102893. https://doi.org/10.1016/j.trc.2020.102893

[146] Seyed M Moghadas, Affan Shoukat, Meagan C Fitzpatrick, Chad R Wells, Pratha Sah, Abhishek Pandey, Jeffrey D Sachs, Zheng Wang, Lauren A Meyers, Burton H Singer, et al. 2020. Projecting hospital utilization during the COVID-19 outbreaks in the United States. *Proceedings of the National Academy of Sciences* 117, 16 (2020), 9122–9126. https://doi.org/10.1073/pnas.2004064117

[147] Fatemeh Mohammadi-Nasrabadi, Yeganeh Salmani, Nasrin Broumandnia, and Fatemeh Esfarjani. 2021. A mixed-method study on COVID-19 prevention in Iranian restaurants. *Frontiers in Public Health* 8 (2021), 585290. https://doi.org/10.3389/fpubh.2020.585290

[148] Sam Moore, Edward M Hill, Michael J Tildesley, Louise Dyson, and Matt J Keeling. 2021. Vaccination and non-pharmaceutical interventions for COVID-19: a mathematical modelling study. *The Lancet Infectious Diseases* 21, 6 (2021), 793–802. https://doi.org/10.1016/S1473-3099(21)00143-2

[149] Lidia Morawska, Julian W Tang, William Bahnfleth, Philomena M Bluyssen, Atze Boerstra, Giorgio Buonanno, Junji Cao, Stephanie Dancer, Andres Floto, Francesco Franchimon, et al. 2020. How can airborne transmission of COVID-19 indoors be minimised? *Environment international* 142 (2020), 105832. https://doi.org/10.1016/j.envint.2020.105832

[150] Xiaoyan Mu, Anthony Gar-On Yeh, and Xiaohu Zhang. 2020. The interplay of spatial spread of COVID-19 and human mobility in the urban system of China during the Chinese New Year. *Environment and Planning B: Urban Analytics and City Science* (2020), 2399808320954211. https://doi.org/10.1177/2399808320954211

[151] Christopher JL Murray and Peter Piot. 2021. The potential future of the COVID-19 pandemic: will SARS-CoV-2 become a recurrent seasonal infection? *Jama* 325, 13 (2021), 1249–1250.

[152] Salihu Sabiu Musa, Shi Zhao, Hei-Shen Chan, Zhen Jin, Daihai He, et al. 2019. A mathematical model to study the 2014–2015 large-scale dengue epidemics in Kaohsiung and Tainan cities in Taiwan, China. *Mathematical biosciences and engineering* (2019). https://doi.org/10.3934/mbe.2019190

[153] Salihu Sabiu Musa, Shi Zhao, Hei-Shen Chan, Zhen Jin, Daihai He, et al. 2019. A mathematical model to study the 2014–2015 large-scale dengue epidemics in Kaohsiung and Tainan cities in Taiwan, China. *Mathematical Biosciences and Engineering* (2019). https://doi.org/10.3934/mbe.2019190

[154] Salihu S Musa, Shi Zhao, Daozhou Gao, Qianying Lin, Gerardo Chowell, and Daihai He. 2020. Mechanistic modelling of the large-scale Lassa fever epidemics in Nigeria

from 2016 to 2019. *Journal of theoretical biology* 493 (2020), 110209. https://doi.org/10.1016/j.jtbi.2020.110209

[155] Samuel Mwalili, Mark Kimathi, Viona Ojiambo, Duncan Gathungu, and Rachel Mbogo. 2020. SEIR model for COVID-19 dynamics incorporating the environment and social distancing. *BMC Research Notes* 13, 1 (2020), 1–5. https://doi.org/10.1186/s13104-020-05192-1

[156] Mark EJ Newman and Duncan J Watts. 1999. Scaling and percolation in the small-world network model. *Physical review E* 60, 6 (1999), 7332. https://doi.org/10.1103/PhysRevE.60.7332

[157] Calistus N Ngonghala, Enahoro Iboi, Steffen Eikenberry, Matthew Scotch, Chandini Raina MacIntyre, Matthew H Bonds, and Abba B Gumel. 2020. Mathematical assessment of the impact of non-pharmaceutical interventions on curtailing the 2019 novel Coronavirus. *Mathematical biosciences* 325 (2020), 108364. https://doi.org/10.1016/j.mbs.2020.108364

[158] Long H Nguyen, David A Drew, Mark S Graham, Amit D Joshi, Chuan-Guo Guo, Wenjie Ma, Raaj S Mehta, Erica T Warner, Daniel R Sikavi, Chun-Han Lo, et al. 2020. Risk of COVID-19 among front-line health-care workers and the general community: a prospective cohort study. *The Lancet Public Health* 5, 9 (2020), e475–e483. https://doi.org/10.1016/S2468-2667(20)30164-X

[159] Bjarke Frost Nielsen, Lone Simonsen, and Kim Sneppen. 2021. COVID-19 superspreading suggests mitigation by social network modulation. *Physical Review Letters* 126, 11 (2021), 118301.

[160] Annett Nold. 1980. Heterogeneity in disease-transmission modeling. *Mathematical biosciences* 52, 3-4 (1980), 227–240. https://doi.org/10.1016/0025-5564(80)90069-3

[161] Cortney L Norris, Scott Taylor Jr, and D Christopher Taylor. 2021. Pivot! How the restaurant industry adapted during COVID-19 restrictions. *International Hospitality Review* (2021). https://doi.org/10.1108/IHR-09-2020-0052

[162] Mercy Ogunnusi, Temitope Omotayo, Mansur Hamma-Adama, Bankole Osita Awuzie, and Temitope Egbelakin. 2021. Lessons learned from the impact of COVID-19 on the

global construction industry. *Journal of engineering, design and technology* 20, 1 (2021), 299–320. https://doi.org/10.1108/JEDT-05-2021-0286

[163] World Health Organization. 2021. World Health Organization (WHO) Coronavirus Disease (COVID-19) Dashboard. https://covid19.who.int/. Accessed March 15, 2021.

[164] World Health Organization. 2022. World Health Organization (WHO) Coronavirus Disease (COVID-19) Dashboard. https://covid19.who.int/. Accessed August 22, 2022.

[165] Apurva Pamidimukkala and Sharareh Kermanshachi. 2021. Impact of Covid-19 on field and office workforce in construction industry. *Project Leadership and Society* 2 (2021), 100018. https://doi.org/10.1016/j.plas.2021.100018

[166] Remy F Pasco, Spencer J Fox, S Claiborne Johnston, Michael Pignone, and Lauren Ancel Meyers. 2020. Estimated association of construction work with risks of COVID-19 infection and hospitalization in Texas. *JAMA network open* 3, 10 (2020), e2026373–e2026373. https://doi.org/10.1001/jamanetworkopen.2020.26373

[167] Romualdo Pastor-Satorras, Claudio Castellano, Piet Van Mieghem, and Alessandro Vespignani. 2015. Epidemic processes in complex networks. *Rev. Mod. Phys.* 87 (Aug 2015), 925–979. Issue 3. https://doi.org/10.1103/RevModPhys.87.925

[168] Romualdo Pastor-Satorras, Claudio Castellano, Piet Van Mieghem, and Alessandro Vespignani. 2015. Epidemic processes in complex networks. *Reviews of modern physics* 87, 3 (2015), 925.

[169] Roengrudee Patanavanich and Stanton A Glantz. 2020. Smoking is associated with COVID-19 progression: a meta-analysis. *Nicotine and Tobacco Research* 22, 9 (2020), 1653–1656.

[170] Vincent Pestre, Bruno Morel, Nathalie Encrenaz, Amandine Brunon, FréDéric Lucht, Bruno Pozzetto, and Philippe Berthelot. 2012. Transmission by super-spreading event of pandemic A/H1N1 2009 influenza during road and train travel. *Scandinavian journal of infectious diseases* 44, 3 (2012), 225–227. https://doi.org/10.3109/00365548.2011.631936

[171] Vanessa Piechotta and Thomas Harder. 2022. Waning of COVID-19 vaccine effectiveness: individual and public health risk. *The Lancet* 399, 10328 (2022), 887–889. https://doi.org/10.1016/S0140-6736(22)00282-3

[172] Payam Pirzadeh and Helen Lingard. 2021. Working from Home during the COVID-19 Pandemic: Health and Well-Being of Project-Based Construction Workers. *Journal of Construction Engineering and Management* 147, 6 (2021), 04021048. https://doi.org/10.1061/(ASCE)CO.1943-7862.0002102

[173] Fernando P Polack, Stephen J Thomas, Nicholas Kitchin, Judith Absalon, Alejandra Gurtman, Stephen Lockhart, John L Perez, Gonzalo Pérez Marc, Edson D Moreira, Cristiano Zerbini, et al. 2020. Safety and efficacy of the BNT162b2 mRNA Covid-19 vaccine. *New England journal of medicine* (2020). https://doi.org/10.1056/NEJMoa2034577

[174] Kiesha Prem, Yang Liu, Timothy W Russell, Adam J Kucharski, Rosalind M Eggo, Nicholas Davies, Stefan Flasche, Samuel Clifford, Carl AB Pearson, James D Munday, et al. 2020. The effect of control strategies to reduce social mixing on outcomes of the COVID-19 epidemic in Wuhan, China: a modelling study. *The Lancet Public Health* 5, 5 (2020), e261–e270. https://doi.org/10.1016/S2468-2667(20)30073-6

[175] Hua Qian, Te Miao, Li Liu, Xiaohong Zheng, Danting Luo, and Yuguo Li. 2021. Indoor transmission of SARS-CoV-2. *Indoor Air* 31, 3 (2021), 639–645. https://doi.org/10.1111/ina.12766

[176] Stella R Quah and Lee Hin-Peng. 2004. Crisis prevention and management during SARS outbreak, Singapore. *Emerging infectious diseases* 10, 2 (2004), 364.

[177] Hong Kong Special Administrative Region. [n. d.]. Government further strengthens compulsory testing. https://www.info.gov.hk/gia/general/202102/03/P2021020300018.htm?fontSize=1. Accessed 1 March,2021.

[178] Hong Kong Special Administrative Region. [n. d.]. Data in Coronavirus Disease (COVID-19). https://data.gov.hk/en-data/dataset/hk-dh-chpsebcddr-novel-infectious-agent. Accessed 1 October,2021.

[179] Hong Kong Special Administrative Region. 2020. 7 Ways to Fight the Virus under the New Normal: 3. Maintain social distancing. https://www.coronavirus.gov.hk/eng/7-ways-fight.html. Accessed 16 December,2020.

[180] Hong Kong Special Administrative Region. 2020. Stepping up testing and continuation of targeted group testing scheme. https://www.info.gov.hk/gia/general/202009/19/P2020091900029.htm. Accessed May 12, 2021.

[181] Hong Kong Special Administrative Region. 2021. Free COVID-19 testing service provided for targeted groups at community testing centres. https://www.info.gov.hk/gia/general/202105/15/P2021051500504.htm?fontSize=1. Accessed May 20,2021.

[182] Mathilde Richard, Adinda Kok, Dennis de Meulder, Theo M Bestebroer, Mart M Lamers, Nisreen MA Okba, Martje Fentener van Vlissingen, Barry Rockx, Bart L Haagmans, Marion PG Koopmans, et al. 2020. SARS-CoV-2 is transmitted via contact and via the air between ferrets. *Nature communications* 11, 1 (2020), 1–6. https://doi.org/10.1038/s41467-020-17367-2

[183] Julien Riou and Christian L Althaus. 2020. Pattern of early human-to-human transmission of Wuhan 2019 novel coronavirus (2019-nCoV), December 2019 to January 2020. *Eurosurveillance* 25, 4 (2020), 2000058.

[184] Myrto Rizou, Ioannis M Galanakis, Turki MS Aldawoud, and Charis M Galanakis. 2020. Safety of foods, food supply chain and environment within the COVID-19 pandemic. *Trends in food science & technology* 102 (2020), 293–299. https://doi.org/10.1016/j.tifs.2020.06.008

[185] Daniel J Rosenkrantz, Anil Vullikanti, SS Ravi, Richard E Stearns, Simon Levin, H Vincent Poor, and Madhav V Marathe. 2022. Fundamental limitations on efficiently forecasting certain epidemic measures in network models. *Proceedings of the National Academy of Sciences* 119, 4 (2022).

[186] RStudio Team. 2015. *RStudio: Integrated Development Environment for R*. RStudio, Inc., Boston, MA. http://www.rstudio.com/

[187] Mohammad A Safi and Abba B Gumel. 2013. Dynamics of a model with quarantine-adjusted incidence and quarantine of susceptible individuals. *Journal of mathematical*

analysis and applications 399, 2 (2013), 565–575. https://doi.org/10.1016/j.jmaa.2012.10.015

[188] Jonathan Schwartz, Chwan-Chuen King, and Muh-Yong Yen. 2020. Protecting healthcare workers during the coronavirus disease 2019 (COVID-19) outbreak: lessons from Taiwan's severe acute respiratory syndrome response. *Clinical Infectious Diseases* 71, 15 (2020), 858–860. https://doi.org/10.1093/cid/ciaa255

[189] Muhammed Semakula, FranÇois Niragire, Angela Umutoni, Sabin Nsanzimana, Vedaste Ndahindwa, Edison Rwagasore, Thierry Nyatanyi, Eric Remera, and Christel Faes. 2021. The secondary transmission pattern of COVID-19 based on contact tracing in Rwanda. *BMJ global health* 6, 6 (2021), e004885. https://doi.org/10.1136/bmjgh-2020-004885

[190] Vincenzo Senatore, Tiziano Zarra, Antonio Buonerba, Kwang-Ho Choo, Shadi W Hasan, Gregory Korshin, Chi-Wang Li, Mohamed Ksibi, Vincenzo Belgiorno, and Vincenzo Naddeo. 2021. Indoor versus outdoor transmission of SARS-COV-2: environmental factors in virus spread and underestimated sources of risk. *Euro-Mediterranean journal for environmental integration* 6, 1 (2021), 1–9. https://doi.org/10.1007/s41207-021-00243-w

[191] Nima Gerami Seresht. 2022. Enhancing resilience in construction against infectious diseases using stochastic multi-agent approach. *Automation in Construction* 140 (2022), 104315. https://doi.org/10.1016/j.autcon.2022.104315

[192] Natasha Shaukat, Daniyal Mansoor Ali, and Junaid Razzak. 2020. Physical and mental health impacts of COVID-19 on healthcare workers: a scoping review. *International journal of emergency medicine* 13, 1 (2020), 1–8. https://doi.org/10.1186/s12245-020-00299-5

[193] Zhuang Shen, Fang Ning, Weigong Zhou, Xiong He, Changying Lin, Daniel P Chin, Zonghan Zhu, and Anne Schuchat. 2004. Superspreading sars events, Beijing, 2003. *Emerging infectious diseases* 10, 2 (2004), 256. https://doi.org/10.3201%2Feid1002.030732

[194] Shivkumar Vishnempet Shridhar, Marcus Alexander, and Nicholas A Christakis. 2021. Characterizing super-spreaders using population-level weighted social networks in rural

communities. *Philosophical Transactions of the Royal Society A* 380, 2214 (2021), 20210123.

[195] Fredrick Simpeh and Christopher Amoah. 2021. Assessment of measures instituted to curb the spread of COVID-19 on construction site. *International Journal of Construction Management* (2021), 1–19. https://doi.org/10.1080/15623599.2021.1874678

[196] Mark K Slifka and Lina Gao. 2020. Is presymptomatic spread a major contributor to COVID-19 transmission? *Nature Medicine* 26, 10 (2020), 1531–1533. https://doi.org/10.1038/s41591-020-1046-6

[197] Kim Sneppen, Bjarke Frost Nielsen, Robert J Taylor, and Lone Simonsen. 2021. Overdispersion in COVID-19 increases the effectiveness of limiting nonrepetitive contacts for transmission control. *Proceedings of the National Academy of Sciences* 118, 14 (2021).

[198] Ilya M Sobol. 2001. Global sensitivity indices for nonlinear mathematical models and their Monte Carlo estimates. *Mathematics and computers in simulation* 55, 1-3 (2001), 271–280. https://doi.org/10.1016/S0378-4754(00)00270-6

[199] The Standard. [n. d.]. K11 diner cluster grows to 34 as HK logs 33 new cases. https://www.thestandard.com.hk/breaking-news/section/4/166385/K11-diner-cluster-grows-to-34-as-HK-logs-33-new-cases. Accessed 1 March,2021.

[200] Juliette Stehlé, Nicolas Voirin, Alain Barrat, Ciro Cattuto, Vittoria Colizza, Lorenzo Isella, Corinne Régis, Jean-François Pinton, Nagham Khanafer, Wouter Van den Broeck, et al. 2011. Simulation of an SEIR infectious disease model on the dynamic contact network of conference attendees. *BMC medicine* 9, 1 (2011), 1–15.

[201] Richard A Stein. 2011. Super-spreaders in infectious diseases. *International Journal of Infectious Diseases* 15, 8 (2011), e510–e513. https://doi.org/10.1016/j.ijid.2010.06.020

[202] Biao Tang, Xia Wang, Qian Li, Nicola Luigi Bragazzi, Sanyi Tang, Yanni Xiao, and Jianhong Wu. 2020. Estimation of the transmission risk of the 2019-nCoV and its implication for public health interventions. *Journal of clinical medicine* 9, 2 (2020), 462. https://doi.org/10.3390/jcm9020462

[203] Song Tang, Yixin Mao, Rachael M Jones, Qiyue Tan, John S Ji, Na Li, Jin Shen, Yuebin Lv, Lijun Pan, Pei Ding, et al. 2020. Aerosol transmission of SARS-CoV-2? Evidence, prevention and control. *Environment international* 144 (2020), 106039. https://doi.org/10.1016/j.envint.2020.106039

[204] Xiujuan Tang, Salihu S Musa, Shi Zhao, and Daihai He. 2021. Reinfection or reactivation of severe acute respiratory syndrome coronavirus 2: a systematic review. *Frontiers in Public Health* 9 (2021).

[205] Xiujuan Tang, Salihu S Musa, Shi Zhao, Shujiang Mei, and Daihai He. 2021. Using proper mean generation intervals in modeling of COVID-19. *Frontiers in public health* 9 (2021).

[206] Moosa Tatar, Jalal Montazeri Shoorekchali, Mohammad Reza Faraji, and Fernando A Wilson. 2021. International COVID-19 vaccine inequality amid the pandemic: Perpetuating a global crisis? *Journal of Global Health* 11 (2021). https://doi.org/10.7189/jogh.11.03086

[207] Census and Statistic Department. [n. d.]. Population Estimates. https://www.censtatd.gov.hk/hkstat/sub/sp150.jsp?tableID=001&ID=0&productType=8. Accessed 10 November, 2020.

[208] Department of Health. 2021. Latest situation of cases of COVID-19 (as of 23 March 2021). https://www.chp.gov.hk/files/pdf/local_situation_covid19_en.pdf. Accessed March 23, 2021.

[209] Dimsum Daily Hong Kong. [n. d.]. COVID-19 cluster outbreaks at Ho Man Tin construction site of the Central Kowloon Route and the T2 Trunk Road project site. https://www.dimsumdaily.hk/covid-19-cluster-outbreaks-at-ho-man-tin-construction-site-of-the-central-kowloon-route-and-the-t2-trunk-road-project-site/. Accessed 8 June,2022.

[210] European Centre for Disease Prevention and Control. 2020. COVID-19 situation update for the EU and the UK (as of 20 November 2020). https://www.ecdc.europa.eu/en/cases-2019-ncov-eueea. Accessed November 21, 2020.

[211] Immigration Department. [n. d.]. Statistics on Passenger Traffic (January 2020). https://www.immd.gov.hk/eng/message_from_us/stat2.html. Accessed November 15, 2020.

[212] Kelly Outram. 2020. Five Ways COVID-19 Has Impacted Construction Companies. https://www.marsh.com/hk/en/insights/risk-in-context/five-ways-covid-19-has-impacted-construction-companies.html. Accessed April 5, 2021.

[213] Mass Transit Railway (MTR). [n. d.]. Historic patronage figues from Jan. 2020 to Dec. 2020. https://www.mtr.com.hk/en/corporate/investor/patronage.php#search. Accessed January 18, 2022.

[214] Phil Mercer. [n. d.]. Hotel Quarantine Under Scrutiny as Australian State Races to Contain COVID-19 Outbreak. https://www.voanews.com/covid-19-pandemic/hotel-quarantine-under-scrutiny-australian-state-races-contain-covid-19-outbreak. Accessed March 5,2021.

[215] The Lancet. 2020. COVID-19: protecting health-care workers. *Lancet (London, England)* 395, 10228 (2020), 922. https://doi.org/10.1016/S0140-6736(20)30644-9

[216] The MathWorks, Inc. 2021. SimBiology: SimBiology Model Builder and SimBiology Model Analyzer. https://www.mathworks.com/products/simbiology.html.

[217] Victor Ting. [n. d.]. Hong Kong fourth wave: sewage tests for coronavirus to be expanded, aim for 'gold standard'. https://www.scmp.com/news/hong-kong/health-environment/article/3117041/hong-kong-fourth-wave-sewage-tests-coronavirus-be?utm_source=copy_link&utm_medium=share_widget&utm_campaign=3117041. Accessed 1 March,2021.

[218] World Health Organization. [n. d.]. WHO Coronavirus (COVID-19) Dashboard. https://covid19.who.int/. Accessed 1 November,2021.

[219] World Health Organization. 2021. WHO validates Sinovac COVID-19 vaccine for emergency use and issues interim policy recommendations. https://www.who.int/news/item/01-06-2021-who-validates-sinovac-covid-19-vaccine-for-emergency-use-and-issues-interim-policy-recommendations. Accessed July 01, 2021.

[220] World Health Organization et al. 2020. *Contact tracing in the context of COVID-19: interim guidance, 10 May 2020*. Technical Report.

[221] World Health Organization and others. 2020. *Pandemic fatigue: reinvigorating the public to prevent COVID-19: policy framework for supporting pandemic prevention and management: revised version November 2020*. Technical Report. World Health Organization. Regional Office for Europe. Accessed April 3, 2021.

[222] Huaiyu Tian, Yonghong Liu, Yidan Li, Chieh-Hsi Wu, Bin Chen, Moritz UG Kraemer, Bingying Li, Jun Cai, Bo Xu, Qiqi Yang, et al. 2020. An investigation of transmission control measures during the first 50 days of the COVID-19 epidemic in China. *Science* 368, 6491 (2020), 638–642. https://doi.org/10.1126/science.abb6105

[223] Juliana Tolles and ThaiBinh Luong. 2020. Modeling Epidemics With Compartmental Models. *JAMA* 323, 24 (06 2020), 2515–2516. https://doi.org/10.1001/jama.2020.8420 arXiv:https://jamanetwork.com/journals/jama/articlepdf/2766672/jama_tolles_2020_gm_200010.pdf

[224] John S Tregoning, Katie E Flight, Sophie L Higham, Ziyin Wang, and Benjamin F Pierce. 2021. Progress of the COVID-19 vaccine effort: viruses, vaccines and variants versus efficacy, effectiveness and escape. *Nature Reviews Immunology* 21, 10 (2021), 626–636. https://doi.org/10.1038/s41577-021-00592-1

[225] Tim K Tsang, Li-Qun Fang, Anran Zhang, Fa-Chun Jiang, Shi-Man Ruan, Lan-Zheng Liu, Benjamin J Cowling, Wei Liu, and Yang Yang. 2022. Variability in Transmission risk of SARS-CoV-2 in close contact settings: a contact tracing study in Shandong Province, China. *Epidemics* 39 (2022), 100553. https://doi.org/10.1016/j.epidem.2022.100553

[226] Dimitrios Tsilingiris, Margarita Papatheodoridi, and Chris J Kapelios. 2020. Providing evidence on the ongoing health care workers' mask debate. *Internal and Emergency Medicine* 15, 5 (2020), 773–777. https://doi.org/10.1007/s11739-020-02382-4

[227] Pauline Van den Driessche and James Watmough. 2002. Reproduction numbers and sub-threshold endemic equilibria for compartmental models of disease transmission. *Mathematical biosciences* 180, 1-2 (2002), 29–48. https://doi.org/10.1016/S0025-5564(02)00108-6

[228] Srinivasan Venkatramanan, Bryan Lewis, Jiangzhuo Chen, Dave Higdon, Anil Vullikanti, and Madhav Marathe. 2018. Using data-driven agent-based models for forecasting emerging infectious diseases. *Epidemics* 22 (2018), 43–49. https://doi.org/10.1016/j.epidem.2017.02.010

[229] Rachel M Wake, Matthew Morgan, Jenny Choi, and Simon Winn. 2020. Reducing nosocomial transmission of COVID-19: implementation of a COVID-19 triage system. *Clinical Medicine* 20, 5 (2020), e141–e145. https://doi.org/10.7861/clinmed.2020-0411

[230] Jacco Wallinga, Peter Teunis, and Mirjam Kretzschmar. 2006. Using data on social contacts to estimate age-specific transmission parameters for respiratory-spread infectious agents. *American journal of epidemiology* 164, 10 (2006), 936–944. https://doi.org/10.1093/aje/kwj317

[231] Haiying Wang, Jack Murdoch Moore, Michael Small, Jun Wang, Huijie Yang, and Changgui Gu. 2022. Epidemic dynamics on higher-dimensional small world networks. *Appl. Math. Comput.* 421 (2022), 126911. https://doi.org/10.1016/j.amc.2021.126911

[232] Jingxuan Wang, Xiao Chen, Zihao Guo, Shi Zhao, Ziyue Huang, Zian Zhuang, Eliza Lai-yi Wong, Benny Chung-Ying Zee, Marc Ka Chun Chong, Maggie Haitian Wang, et al. 2021. Superspreading and heterogeneity in transmission of SARS, MERS, and COVID-19: A systematic review. *Computational and structural biotechnology journal* 19 (2021), 5039–5046. https://doi.org/10.1016/j.csbj.2021.08.045

[233] Yuanyuan Wang, Zhishan Hu, Yi Feng, Amanda Wilson, and Runsen Chen. 2020. Changes in network centrality of psychopathology symptoms between the COVID-19 outbreak and after peak. *Molecular psychiatry* 25, 12 (2020), 3140–3149. https://doi.org/10.1038/s41380-020-00881-6

[234] Duncan J Watts and Steven H Strogatz. 1998. Collective dynamics of 'small-world'networks. *nature* 393, 6684 (1998), 440–442. https://doi.org/10.1038/30918

[235] Kim A. Weeden and Benjamin Cornwell. 2020. The small-world network of college classes: implications for epidemic spread on a university campus. *Sociological science* 7, 9 (2020), 222–241. https://doi.org/10.15195/v7.a9

[236] Bo Wei, Jie Liu, Daijun Wei, Cai Gao, and Yong Deng. 2015. Weighted k-shell decomposition for complex networks based on potential edge weights. *Physica A: Statistical Mechanics and its Applications* 420 (2015), 277–283. https://doi.org/10.1016/j.physa.2014.11.012

[237] W Joost Wiersinga, Andrew Rhodes, Allen C Cheng, Sharon J Peacock, and Hallie C Prescott. 2020. Pathophysiology, transmission, diagnosis, and treatment of coronavirus disease 2019 (COVID-19): a review. *Jama* 324, 8 (2020), 782–793. https://doi.org/10.1001/jama.2020.12839

[238] David WS Wong and Yun Li. 2020. Spreading of COVID-19: Density matters. *Plos one* 15, 12 (2020), e0242398. https://doi.org/10.1371/journal.pone.0242398

[239] SCY Wong, RT-S Kwong, TC Wu, JWM Chan, MY Chu, SY Lee, HY Wong, and DC Lung. 2020. Risk of nosocomial transmission of coronavirus disease 2019: an experience in a general ward setting in Hong Kong. *Journal of Hospital Infection* 105, 2 (2020), 119–127. https://doi.org/10.1016/j.jhin.2020.03.036

[240] Shuk-Ching Wong, Hong Chen, David Christopher Lung, Pak-Leung Ho, Kwok-Yung Yuen, and Vincent Chi-Chung Cheng. 2021. To prevent SARS-CoV-2 transmission in designated quarantine hotel for travelers: Is the ventilation system a concern? *Indoor air* 31, 5 (2021), 1295. https://doi.org/10.1111/ina.12870

[241] Mark EJ Woolhouse, C Dye, J-F Etard, T Smith, JD Charlwood, GP Garnett, P Hagan, JLK Hii, PD Ndhlovu, RJ Quinnell, et al. 1997. Heterogeneities in the transmission of infectious agents: implications for the design of control programs. *Proceedings of the National Academy of Sciences* 94, 1 (1997), 338–342.

[242] Joseph T Wu, Kathy Leung, and Gabriel M Leung. 2020. Nowcasting and forecasting the potential domestic and international spread of the 2019-nCoV outbreak originating in Wuhan, China: a modelling study. *The Lancet* 395, 10225 (2020), 689–697. https://doi.org/10.1016/S0140-6736(20)30260-9

[243] Joseph T Wu, Edward SK Ma, Cheuk Kwong Lee, Daniel KW Chu, Po-Lai Ho, Angela L Shen, Andrew Ho, Ivan FN Hung, Steven Riley, Lai Ming Ho, et al. 2010. The infection attack rate and severity of 2009 pandemic H1N1 influenza in Hong Kong. *Clinical Infectious Diseases* 51, 10 (2010), 1184–1191.

[244] Zhonglan Wu, David Harrich, Zhongyang Li, Dongsheng Hu, and Dongsheng Li. 2021. The unique features of SARS-CoV-2 transmission: Comparison with SARS-CoV, MERS-CoV and 2009 H1N1 pandemic influenza virus. *Reviews in Medical Virology* 31, 2 (2021), e2171.

[245] Yue Xiang, Yonghong Jia, Linlin Chen, Lei Guo, Bizhen Shu, and Enshen Long. 2021. COVID-19 epidemic prediction and the impact of public health interventions: A review of COVID-19 epidemic models. *Infectious Disease Modelling* 6 (2021), 324–342. https://doi.org/10.1016/j.idm.2021.01.001

[246] Han Xiao, Yan Zhang, Desheng Kong, Shiyue Li, and Ningxi Yang. 2020. The effects of social support on sleep quality of medical staff treating patients with coronavirus disease 2019 (COVID-19) in January and February 2020 in China. *Medical science monitor: international medical journal of experimental and clinical research* 26 (2020), e923549–1. https://doi.org/10.12659/MSM.923549

[247] Yao Xiao, Mofeng Yang, Zheng Zhu, Hai Yang, Lei Zhang, and Sepehr Ghader. 2021. Modeling indoor-level non-pharmaceutical interventions during the COVID-19 pandemic: a pedestrian dynamics-based microscopic simulation approach. *Transport Policy* 109 (2021), 12–23. https://doi.org/10.1016/j.tranpol.2021.05.004

[248] Chaojun Xie, Hongjun Zhao, Kuibiao Li, Zhoubin Zhang, Xiaoxiao Lu, Huide Peng, Dahu Wang, Jin Chen, Xiao Zhang, Di Wu, et al. 2020. The evidence of indirect transmission of SARS-CoV-2 reported in Guangzhou, China. *BMC public health* 20, 1 (2020), 1–9. https://doi.org/10.1186/s12889-020-09296-y

[249] Jinying Xu, Zhongze Yang, Weisheng Lu, and Fan Xue. 2021. Impacts of the COVID-19 Pandemic on construction industry: a comparison between Hong Kong and Singapore. In *26th International Symposium on Advancement of Construction Management and Real Estate*. CRIOCM.

[250] Yang Yang, Albert PC Chan, Ming Shan, Ran Gao, Fengyu Bao, Sainan Lyu, Qingwen Zhang, and Junfeng Guan. 2021. Opportunities and Challenges for Construction Health and Safety Technologies under the COVID-19 Pandemic in Chinese Construction Projects. *International Journal of Environmental Research and Public Health* 18, 24 (2021), 13038. https://doi.org/10.3390/ijerph182413038

[251] Zimo Yang, Ai-Xiang Cui, and Tao Zhou. 2011. Impact of heterogeneous human activities on epidemic spreading. *Physica A: Statistical Mechanics and its Applications* 390, 23-24 (2011), 4543–4548. https://doi.org/10.1016/j.physa.2011.06.068

[252] Annalee Yassi, Jennifer M Grant, Karen Lockhart, Stephen Barker, Stacy Sprague, Arnold I Okpani, Titus Wong, Patricia Daly, William Henderson, Stan Lubin, et al. 2021. Infection control, occupational and public health measures including mRNA-based vaccination against SARS-CoV-2 infections to protect healthcare workers from variants of concern: A 14-month observational study using surveillance data. *PLoS One* 16, 7 (2021), e0254920. https://doi.org/10.1371/journal.pone.0254920

[253] Zhongnan Ye, Kuangly Cheng, Shu-Chien Hsu, Hsi-Hsien Wei, and Clara Man Cheung. 2021. Identifying critical building-oriented features in city-block-level building energy consumption: A data-driven machine learning approach. *Applied Energy* 301 (2021), 117453. https://doi.org/10.1016/j.apenergy.2021.117453

[254] Ziyue YUAN. 2020. Local data related COVID-19 in Hong Kong (updated till 30th November 2020). https://github.com/YUANZIYUE1997/covid19.

[255] Ziyue Yuan, Shu-Chien Hsu, Clara Man Cheung, and Vahid Asghari. 2022. Effectiveness of Interventions for Controlling COVID-19 Transmission between Construction Workers and Their Close Contacts. *Journal of Management in Engineering* 38, 3 (2022), 04022010. https://doi.org/10.1061/(ASCE)ME.1943-5479.0001033

[256] Ziyue Yuan, Salihu Sabiu Musa, Shu-Chien Hsu, Clara Man Cheung, and Daihai He. 2022. Post Pandemic Fatigue: What are Effective Strategies? *Scientific reports* 12, 1 (2022), 1–15. https://doi.org/10.1038/s41598-022-13597-0

[257] Ziyue Yuan, Shi Zhao, Shu-Chien Hsu, and Clara Man Cheung. 2023. Uncovering Construction Site–Specific Transmission Patterns of COVID-19: A Spatiotemporal Connectivity Analysis in Hong Kong. *Journal of Management in Engineering* 39, 1 (2023), 04022067. https://doi.org/10.1061/(ASCE)ME.1943-5479.0001100

[258] X-Y Zhang, Mirjam N Trame, Lawrence J Lesko, and Stephan Schmidt. 2015. Sobol sensitivity analysis: a tool to guide the development and evaluation of systems pharmacology models. *CPT: pharmacometrics & systems pharmacology* 4, 2 (2015), 69–79. https://doi.org/10.1002/psp4.6

[259] Shi Zhao, Qianyin Lin, Jinjun Ran, Salihu S Musa, Guangpu Yang, Weiming Wang, Yijun Lou, Daozhou Gao, Lin Yang, Daihai He, et al. 2020. Preliminary estimation of the basic reproduction number of novel coronavirus (2019-nCoV) in China, from 2019 to 2020: A data-driven analysis in the early phase of the outbreak. *International journal of infectious diseases* 92 (2020), 214–217. https://doi.org/10.1016/j.ijid.2020.01.050

[260] Zian Zhuang, Shi Zhao, Qianying Lin, Peihua Cao, Yijun Lou, Lin Yang, Shu Yang, Daihai He, and Li Xiao. 2020. Preliminary estimates of the reproduction number of the coronavirus disease (COVID-19) outbreak in Republic of Korea and Italy by 5 March 2020. *International Journal of Infectious Diseases* 95 (2020), 308–310. https://doi.org/10.1016/j.ijid.2020.04.044

Supplementary Information

SI.1 Supplementary information in Chapter 4

SI.1.1 The Proof of the Existence of EE

Given the model (4.1), we obtain

$$N_q^* = \frac{m_{N_q} + \theta_1 S^*}{q_0 + \theta_3 \lambda^*} \tag{SI.1.1}$$

$$E_m^* = \frac{(\theta_3 \lambda^{*2} + (q_0 + \theta_1 \theta_3)\lambda^*) S^* + \theta_3 m_{N_q} \lambda^*}{q_1 (q_0 + \theta_3 \lambda^*)} \tag{SI.1.2}$$

$$I_a^* = \frac{\sigma_1 (\theta_3 \lambda^{*2} + (q_0 + \theta_1 \theta_3)\lambda^*)}{q_3 q_1 (q_0 + \theta_3 \lambda^*)} S^* + \frac{\sigma_1 (\theta_3 \lambda^{*2} + (q_0 + \theta_1 \theta_3)\lambda^*)}{q_3 q_1 (q_0 + \theta_3 \lambda^*)} \tag{SI.1.3}$$

$$I_m^* = \frac{\sigma_2 (\theta_3 \lambda^{*2} + (q_0 + \theta_1 \theta_3)\lambda^*)}{q_4 q_1 (q_0 + \theta_3 \lambda^*)} S^* + \frac{\sigma_2 \theta_3 m_{N_q} \lambda^*}{q_4 q_1 (q_0 + \theta_3 \lambda^*)} \tag{SI.1.4}$$

$$H_a^* = \frac{\epsilon_3 \sigma_1 (\theta_3 \lambda^{*2} + (q_0 + \theta_1 \theta_3)\lambda^*)}{q_3 q_6 q_1 (q_0 + \theta_3 \lambda^*)} S^* + \frac{\epsilon_3 \sigma_1 \theta_3 m_{N_q} \lambda^*}{q_3 q_6 q_1 (q_0 + \theta_3 \lambda^*)} \tag{SI.1.5}$$

$$E_q^* = \frac{\theta_1 q_1 (1 - \theta_2 - \theta_3) + \theta_4 (\theta_3 \lambda^{*2} + (q_0 + \theta_1 \theta_3)\lambda^*)}{q_2 q_1 (q_0 + \theta_3 \lambda^*)} S^* + \frac{m_{N_q} q_1 (1 - \theta_2 - \theta_3) + \theta_4 \theta_3 m_{N_q} \lambda^*}{q_2 q_1 (q_0 + \theta_3 \lambda^*)} \tag{SI.1.6}$$

$$\begin{aligned} H_s^* = & [\frac{(\epsilon_1 q_5 + \epsilon_2 \theta_5)\sigma_2 (\theta_3 \lambda^{*2} + (q_0 + \theta_1 \theta_3)\lambda^*)}{q_4 q_5 q_7 q_1 (q_0 + \theta_3 \lambda^*)} + \frac{\theta_1 q_1 \epsilon_2 \sigma_3 (1 - \theta_2 - \theta_3) + \epsilon_2 \sigma_3 \theta_4 (\theta_3 \lambda^{*2} + (q_0 + \theta_1 \theta_3)\lambda^*)}{q_2 q_7^2 q_1 (q_0 + \theta_3 \lambda^*)}] S^* \\ & + [\frac{(\epsilon_1 q_5 + \epsilon_2 \theta_5)\sigma_2 \theta_3 m_{N_q} \lambda^*}{q_4 q_5 q_7 q_1 (q_0 + \theta_3 \lambda^*)} + \frac{\epsilon_2 \sigma_3 [q_1 (1 - \theta_2 - \theta_3) m_{N_q} + \theta_4 \theta_3 m_{N_q} \lambda^*}{q_2 q_7^2 q_1 (q_0 + \theta_3 \lambda^*)}] \end{aligned} \tag{SI.1.7}$$

$$I_q^* = \frac{\theta_1\sigma_3 q_1 q_4(1-\theta_2-\theta_3)+\sigma_3\theta_4 q_4(\theta_3\lambda^{*2}+(q_0+\theta_1\theta_3)\lambda^*)+\theta_2\sigma_2 q_2(\theta_3\lambda^{*2}+(q_0+\theta_1\theta_3)\lambda^*)}{q_2 q_4 q_5 q_1(q_0+\theta_3\lambda^*)} S^* + \frac{\sigma_3 q_1 q_4 m_{N_q}(1-\theta_2-\theta_3)+\sigma_2\theta_5 q_2\theta_3 m_{N_q}\lambda^*}{q_2 q_4 q_5 q_1(q_0+\theta_3\lambda^*)} \tag{SI.1.8}$$

From above, we can easily get N_q^*... ,I_q^* are positive with a non-negative S^*.

Substitute Eq. (SI.1.1), (SI.1.3), (SI.1.4), (SI.1.8), (SI.1.7) and (SI.1.5) into (1), $\frac{dR}{dt}$ can be rewritten as below:

$$R^* = \frac{\gamma_1 I_a^* + \gamma_2 I_m^* + \gamma_3 I_q^* + \gamma_4 H_s^* + \gamma_5 H_a^*}{q_8} \tag{SI.1.9}$$

Obviously, R^* is larger than zero when I_a^*... ,H_a^* are positive. Hence, the EE exits in terms of a positive solution of model (1).

SI.1.2 The initial variables and estimated parameters for four phases

All parameter descriptions and ranges are described in Table 4.5. Based on the force of infections in Eqns. (4.2), Table SI.1.1 describe the initial values of variables and estimated values of some parameters (i.e., β_1, β_2, θ_3, a_1, a_2, a_3, a_4, and a_5) for each phase.

Table SI.1.1: The initial variables and estimated parameters for four phases (Phase 1: 24th Jan.-24th Mar., Phase 2: 25th May.-19th Jul., Phase 3: 20th Jul.-29th Jul. and Phase 4: 30th Jul.-31st Oct.).

	Phase 1	**Phase 2**	**Phase 3**	**Phase 4**
Initial values of variables				
S	7181657	7181657	8019956	8014725
N_q	162336	162336	34584	18185
E_m	300	1000	71	2527
E_q	15	20	8313	8779
I_a	16	270	557	748
I_m	5	170	108	2096
I_q	2	100	575	588
H_a	1	100	517	695
H_s	1	50	1419	2384
R	5	15	1313	1685
Estimated values of parameters				
β_1	0.6779	0.3856	1.0058	0.1518
β_2	0.1472	1.5234	0.9399	0.4864
θ_3	0.1596	0.4114	0.3134	0.3274
a_1	0.0298	0.0735	0.1981	0.1800
a_2	0.1076	0.1280	0.1912	0.1738
a_3	0.0575	0.1329	0.1968	0.1898
a_4	0.0445	0.1752	0.1049	0.1423
a_5	0.1072	0.1971	0.1208	0.1615

SI.2 Supplementary information in Chapter 6

There are 28 NPIs interventions described in Table SI.2.1.

Table SI.2.1: Scenario Performance

Scenario No.	$max(AR^c)$	$max(AR^s)$	TAR	$max(AE)$	$max(RE)$
Scenario 1	0.51392	0.52367	0.51555	0	0
Scenario 2	0.51233	0.52188	0.51392	0.163%	0.317%
Scenario 3	0.036658	0.019904	0.033866	48.168%	14.22
Scenario 4	0.38772	0.48959	0.4047	11.085%	27.391%
Scenario 5	0.48238	0.51443	0.48772	2.783%	5.706%
Scenario 6	0.5013	0.51858	0.50418	1.137%	2.255%
Scenario 7	0.45969	0.5113	0.46829	4.726%	10.092%
Scenario 8	0.50268	0.51908	0.50542	1.013%	2.004%
Scenario 9	0.5023	0.51872	0.50504	1.051%	2.081%
Scenario 10	0.43243	0.40096	0.42718	8.837%	20.687%
Scenario 11	0.49571	0.50351	0.49701	1.854%	3.730%
Scenario 12	0.50504	0.51539	0.50677	0.878%	1.733%
Scenario 13	0.48961	0.49251	0.49009	2.546%	5.195%
Scenario 14	0.5063	0.51643	0.50798	0.757%	1.490%
Scenario 15	0.50541	0.51603	0.50718	0.837%	1.650%
Scenario 16	0.25758	0.29543	0.26389	25.166%	95.365%
Scenario 17	0.46025	0.49142	0.46544	5.011%	10.766%
Scenario 18	0.49278	0.51123	0.49585	1.970%	3.973%
Scenario 19	0.43067	0.47129	0.43744	7.811%	17.856%
Scenario 20	0.49597	0.51309	0.49882	1.673%	3.354%
Scenario 21	0.49419	0.51205	0.49717	1.838%	3.697%
Scenario 22	0.13346	0.13314	0.1334	38.215%	286.469%
Scenario 23	0.43218	0.47327	0.43903	7.652%	17.429%
Scenario 24	0.46751	0.49643	0.47233	4.322%	9.150%
Scenario 25	0.44943	0.38533	0.43874	7.681%	17.507%
Scenario 26	0.035261	0.026888	0.033866	48.168%	14.22
Scenario 27	0.19351	0.35191	0.21991	29.564%	1.34
Scenario 28	0.2406	0.14982	0.22547	29.008%	1.29

SI.3 Supplementary information in Chapter 7

Table SI.3.1: Description of actual superspreaders in the empirical case

Superspreaders	**Occupation**
G2node$5	Assistant Engineer
G12node$1	Scaffolder
G15node$1	Electrical Fitter
G15node$2	Carpenter
G15node$3	Labourer
G15node$5	Senior Site Engineer
G15node$8	Labourer
G17node$1	Construction Plant Technician
G1node$10	Assistant Forman
G1node$11	Quantity Surveyor
G1node$12	Electrical Fitter
G1node$13	Assistant Foreman
G1node$14	Quantity Surveyor
G1node$15	Graduate Engineer
G1node$16	Manager
G1node$23	Assistant General Foreman
G1node$24	Senior Safety Officer
G1node$25	Assistant Foreman
G1node$3	Clerk
G1node$32	Labourer
G1node$33	Carpenter
G1node$34	Carpenter
G1node$35	Security
G1node$4	Engineer
G1node$6	Assistant Foreman
G1node$7	Site Engineer
G1node$8	Assistant Engineer
G1node$9	Assistant Engineer
G25node$1	Building Service Engineer
G25node$2	Building Service Engineer
G2node$14	Plumber
G4node$3	Labourer
G4node$4	Foreman
G8node$1	Associate Foreman
G9node$1	Building Service Engineer
G2node$6	Electrical Fitter
G2node$16	Worker
G4node$12	Worker